UNIVERSITY OF BIRMINGHAM

Advanced Studies of Catalytic Upgrading of Heavy Oils

By

Abarasi Hart

A thesis submitted to
The University of Birmingham
for the degree of
DOCTOR OF PHILOSOPHY

School of Chemical Engineering
College of Engineering and Physical Science
University of Birmingham
April 2014

Abstract

As light crude oil production approaches peak, attention has been shifted to vast deposits of heavy oil and bitumen to offset the rising fuels demand. However, heavy oil and bitumen are known to constitute high-boiling molecules which gives them characteristic high viscosity, high density/low API gravity, low yields of low-boiling fuel distillates, and high heteroatom content compared to light oil. The main challenges are: low fluidity through the reservoir and pipeline because of its high viscosity, high processing cost, and low market value. Upgrading therefore refers to the breaking down of heavy oil into oil with similar characteristics as light crude oil. The toe-to-heel air injection (THAI) and its catalytic add-on CAPRI (i.e., CAtalytic upgrading PRocess *In-situ*) were developed to achieve this objective down-hole. In this study, the CAPRI process was explored with the objective of controlling catalyst deactivation due to coking while increasing the extent of upgrading. The CAPRI section was replicated with a fixed-bed reactor using Co-Mo/γ-Al_2O_3, Ni-Mo/γ-Al_2O_3, activated carbon, and Al_2O_3 support. The effects of reaction temperature and weight hourly space velocity (WHSV) on the extent of upgrading were studied in the range of 350-425 ^oC and 9.1-28 h^{-1}, respectively. Control experiments for thermal cracking upgrading were carried out at the same temperature range (350-425 ^oC) and condition to evaluate the effectiveness of the catalyst. In order to control premature deactivation of the catalysts due to coke and metal deposition, the following were investigated activated carbon guard-bed on top of the catalyst bed, hydrogen-addition, steam environment as a source of hydrogen-donor, and nanoparticulate catalyst. It was found that high reaction temperature of 425 ^oC and lower WHSV (9.1 h^{-1}) improved the cracking as well as increase API gravity (~3-7^o), viscosity reduction of (81.9 %), demetallisation (9.3-12.3 %), desulphurisation (5.3-6.6 %), and higher yield of fuel distillates, respectively compared to upgrading at 350 and 400 ^oC. In spite of the

improvement in produced oil at 425 ^{o}C, the carbon-rejection was high (51-56.6 wt.%) compared to (42-47.8 wt.%) and (48-50.3 wt.%) when reaction was carried out at 350 and 400 ^{o}C for 25 hours time-on-stream operations. Reactions carried out under different environments showed that after 6 hours time-on-stream, the spent catalyst contained 6 and 3 wt.% less coke under hydrogen and methane/THAI-gas reaction gases compared to 23.5 wt.% coke content under nitrogen atmosphere. Additionally, the API gravity and viscosity reduction increased further by ~2^{o} and 6.2% under hydrogen-addition compared to nitrogen environment. However, with steam-addition the viscosity reduction range from 88-92% depending on the steam/oil ratio (0.02-0.1) compared to 85.5% (nitrogen). It was also observed that the coke content of the spent catalyst reduced from 17.02 to 11.3 wt % as the steam/oil ratio increased from 0.02 to 0.1 mL·mL^{-1} compared to 27.53 wt % (nitrogen) after 15 h time-on-stream. The API gravity and viscosity reduction achieved using dispersed particulate Co-Mo/γ-Al_2O_3 catalyst was 3^{o} points and 2 % above that obtained with pelleted fixed-bed catalyst (5.6 ^{o}API and 97.1%). A significant reduction of sulphur and metals was also noted. The synergistic effect of thermal-catalysis caused the cleavage of C-C, C-H, and C-heteroatom bonds with large number of reactions occurring. This produces significant upgrade and enhances oil production, benefits pipeline transportation through viscosity reduction, and most of the impurities such as sulphur and metals are left behind in the reservoir, lowering impact on downstream processes and the environment. The yield of fuel distillates significantly improved compared to the original heavy oil.

Dedication

In memoriam: My Father Mr Israel Joseph Abbey-Hart

And

King Edward Asimini William Dappa Pepple (Perekule XI), the Amayanabo of Grand Bonny Kingdom, Rivers State, Nigeria

Acknowledgement

Thanks to God's grace and mercy in my life. I would like to especially acknowledge the Petroleum Technology Development Fund (PTDF), Nigeria, School of Chemical Engineering, University of Birmingham, Ms Ama I. Pepple, and King Edward Asimini William Dappa Pepple (Perekule XI), the Amayanabo of Grand Bonny Kingdom, Rivers State, Nigeria for funding this project.

My deepest appreciation to: Prof. Joseph Wood for his leadership in supervising this study with patience, constructive comments and support, Dr. Gary A. Leeke for his co-supervision and encouraging comments, Emeritus Prof. Malcolm Greaves, University of Bath, for valuable comments and discussion, Dr. Amjad A. Shah, and Dr. Jiawei Wang for their contributions. Thanks to Mr Jacob Omajali who manufactured the bioPd catalyst used in this study.

The Chemical Engineering and Biosciences Workshop teams Mr David Boylin and Mr Andrew Tanner for their technical contribution towards the maintenance of the CAPRI experimental rig, Mr John Wedderburn for his technical assistance with the nitrogen sorption measurement, Petrobank, Canada for supplying the heavy oils used in this study, and Intertek Laboratories for sulphur and metals analyses of oil samples.

My dearest family members, they invested in me and the Catalysis and Reaction Engineering Research Group at School of Chemical Engineering, University of Birmingham for their support in the successful completion of this study.

Table of Contents

List of Figures

List of Tables

Nomenclature

CAPRI	CAtalytic upgrading PRocess In situ
DTG	Differential Thermal Gravimetric
HDS	Hydrodesulphurization
HDT	Hydrotreating
HDA	Hydrodeasphaltization
HDS	Hydrodesulphurization
HDM	Hydrodemetalisation
OOIP	Original Oil In Place
SARA	Saturates, Aromatics, Resins and Asphaltenes
TGA	Thermogravimetric Analysis
THAI	Toe-to-Heel Air Injection
WHSV	Weight Hourly Space Velocity

Chapter 1

Introduction

1. Background and Motivation

World oil demand is expected to increase by more than 40% by 2025 (USEIA, 2005). The global society needs fuel for heating, cooking, and transportation. Also, the world's chemical industries depend majorly on hydrocarbon as primary feedstock. The demand is therefore ever increasing swiftly as a result of population growth at an average annual growth rate of 1.6% (OECD/IEA, 2005), industrialisation, and developing economies. As the world's conventional light crude oil approaches its peak, exploitation of vast deposits of heavy oil and bitumen remains one of the mitigating options to off-set the rise in demand (Hirsch, et al., 2006). The heavy crude oil and tar sands (i.e., non-conventional oil) reserve globally is estimated by the International Energy Agency (IEA) to be about 6 trillion barrels, with major reserves found in Canada and Venezuela (OECD/IEA, 2005; Das and Butler, 1998). This amount could fill the gap between world energy supply and demand in future. According to Zhang et al. (2012) heavy oil, extra heavy oil, and bitumen make up about 70% of the world's total oil resources of about 9-13 trillion barrels. In this respect, the reserve of non-conventional oil resources outweighs that of conventional light crude oil reserve which is about 1.02 trillion barrels (Hein, 2006). Hence, non-conventional oils could potentially meet global energy needs for the next five decades. The global distribution of non-conventional oil in place as estimated is presented in Figure 1.1.

Figure 1.1 World heavy oil distribution (modified from Smalley, 2000).

Although Canada and Venezuela have extraction and upgrading industries in place, very little has been done by other nations to exploit non-conventional oil resources. For instance in Africa, there are large heavy crude oil and bitumen deposits onshore in Egypt, Nigeria, Angola, etc., but there are no firm plans and technology to extract them at the moment (Atkins, 2011). The major hurdles being issues such as greenhouse gas emissions from production, the cost of upgrading heavy crude oil by refining is double that of conventional crude oil, technical challenges associated with transportation, and their extraction is energy and capital intensive. Also, the market value of non-conventional oil is low compared to light crude oil.

On the other hand, heavy crude oil and bitumen are characterised by high viscosity (i.e., resistance to flow), high density/low API gravity, high asphaltenes and heteroatom content, which is the reason for the high cost and technical challenges associated with their extraction and refining. The key factors controlling the commercial development of heavy

crude oil resources are therefore world crude oil price, the capital expense and the technology (Focus, 2006; Atkins, 2011). Unlike the light crude oil, the heavy oil/bitumen requires further processing by upgrading, that is the process that converts heavy oil/bitumen into synthetic oil with API gravity, viscosity, and heteroatom characteristics similar to light crude oil, before being subjected to further refining processes (Carrillo and Corredor, 2012). Parenthetically, surface upgrading of heavy crude oil/bitumen to light crude oil is cost-effective when the deviation between the light and heavy crude oil prices is enough to cover the cost of production and upgrading (Focus, 2006). A combination of different surface upgrading processes such as delayed coking, hydroconversion processes, catalytic cracking, solvent deasphalting, etc. are required to produce synthetic crude (or syncrude) suitable for refining. However, these surface upgrading processes significantly impact the environment with the emission of greenhouse gases (GHG). Additionally, the use of surface upgrading processes like visbreaking and delayed coking have been characterised by low conversion and high yield of undesirable by-product coke (Furimsky, 2009). In this respect, effort is being focused on *in situ* upgrading technologies, that is, converting the heavy crude oil to light oil prior to reaching the surface.

With regard to the economics, the major cost associated with heavy oil and bitumen exploitation is the additional cost incurred for the surface upgrading facility (Atkins, 2011; Hart, et al., 2014a). Therefore, the development of efficient *in situ* upgrading technologies could substantially improve the economics of production of heavy oil and bitumen resources. Conventional light oil is produced by primary and secondary methods before the declining of the reservoir energy, but the production of heavy crude oil/bitumen requires thermal and/or solvent stimulation of the reservoir, which are termed Enhanced Oil Recovery, (EOR) techniques. Thermal EOR processes can be classified as steam-based and in-situ combustion

techniques. The steam-based methods includes: steam flooding, Steam Assisted Gravity Drainage (SAGD), and Cyclic Steam Stimulation (CSS), and the in-situ combustion processes are namely conventional *in Situ* Combustion (ISC) and the novel Toe-to-Heel Air Injection (THAI) and its add-on catalytic upgrading process in-situ (CAPRI). These processes all rely on viscosity reduction through heating to improve oil fluidity and production. However, for steam processes such as SAGD and CSS for every 2-5 barrels of water injected as steam a barrel of oil is produced, which makes it very energy-intensive with a large environmental burden (Gates and Chakrabarty, 2006). This implies that large volumes of water and natural gas are needed for steam generation adding to the capital and operational cost. Additionally, the produced oil from steam EOR processes requires the addition of expensive diluents to aid pipeline transportation to refineries as well as further surface upgrading to meet refinery feedstock specification. In-situ combustion processes however require less amount of water and also the heat provided by the combustion reactions aid oil recovery.

In situ upgrading of heavy oil/bitumen downhole could present a number of advantages, such as use of available heat and gases, reduced requirement for surface upgrading and production of low-viscosity oil that can be transported without diluent addition (Xia and Greaves, 2001; Xia, et al., 2002). THAI and its catalytic add-on CAPRI have been developed over the last 10-15 years as techniques for thermal heavy oil recovery and in situ upgrading. In CAPRI the horizontal producer well is incorporated with an annular packed-bed of refinery catalyst. As the mobilized heavy oil flow through the packed-bed of catalyst it undergoes further upgrading reactions. The yardstick for measuring the extent of heavy crude oil upgrade is the improvement in API gravity, viscosity, and the reduction of asphaltenes and hetero-atoms (Ovalles and Rodriguez, 2008). Xia and Greaves (2001) reported a 3-D physical model study of catalytic upgrading of Wolf lake heavy oil using THAI-CAPRI. They found

that thermal cracking upgrading alone by THAI achieved about 9^{o} increase in the API gravity of the produced oil, while the API gravity of the produced oil by incorporating CAPRI increased upgrading further by 3-7 ^{o} API with 85 % recovery of original oil in place (OOIP). This result indicates that it can be possible to convert heavy oil to light oil in a single step down-hole process. Subsequent work by Shah and co-workers (2011) gave a detailed optimisation of process variables such as reaction temperature, pressure, oil flow rate, and gas-to-oil ratio to be used in the CAPRI process. They found an optimum reaction temperature of 425^{o}C, oil flow rate of 1 $mL.min^{-1}$, and that the deposited coke and metals on the catalyst during reaction rapidly deactivate the catalyst. In this study therefore the central objective is extending the lifetime of the catalyst by controlling coke formation while improving upgrading by performing the reaction under hydrogen, steam, and methane environments and also activated carbon guard-bed. However, CAPRI conventionally requires the packing of the well with commercial pelleted hydrodesulphurisation catalyst prior to start-up, and has been associated with catalyst deactivation issues during production. So, the hurdles of packing the horizontal producer well as well as the catalyst deactivation problems could potentially be solved by the use of dispersed once-through nano-catalytic particles injection ahead of the combustion front during THAI-CAPRI process. Coke formation is minimised, because nanosized catalyst exposes more active sites and possess short diffusion routes, rather than diffusion limitation of large molecules experienced in their pelleted counterpart (Xuhong, et al., 2013). The upgrading levels achieved in the fixed-bed process are compared with the dispersed nanoparticulate catalyst. The objectives of the study and thesis layout are detailed in Sections 1.2 and 1.3, respectively.

1.2 Aim and Objectives of the Study

The aim of the THAI-CAPRI process was not only to improve API gravity and viscosity of the oil to promote pipeline transportation, but also to remove impurities and provide a feedstock that meet downstream processing and refinery specification. The specific objectives investigated in the current study were:

1. To investigate the effectiveness and performance of catalyst under different conditions, by evaluation of;

    a. The extent of thermal versus catalytic cracking upgrading.

    b. Effect of reaction temperature and weight hourly space velocity (WHSV).

    c. Effect of catalyst type, shape and mono/bi-metallic catalysts.

    d. Effect of different heavy oil feedstocks.

2. To obtain an understanding of the role of reaction gas environment on the chemistry of the in situ catalytic upgrading process, namely to investigate;

    a. The effect of hydrogen, methane, blend of gases (CO, CO_2, CH_4 and N_2), and nitrogen on the upgrading chemistry and coke formation.
    b. Comprehend the role of hydrogen and methane in hydroconversion of macromolecules, olefin saturation, and heteroatom removal.
    c. Performance evaluation of ex situ regenerated catalyst against fresh catalyst.

3. To understand the magnitude of upgrading and coke deposition reduction in controlling catalyst deactivation.

a. Investigate the influence of a guard bed installed prior to the catalyst bed upon the extent of upgrading, impurities removal and coke reduction.
b. Investigate the role of hydrogen-addition in reducing coke formation and hydrogenation.
c. Evaluate the role of steam environment in reducing coke deposition as well as removing sulphur and metals.
d. To evaluate the potential of water-gas-shift reaction in providing hydrogen for *in situ* hydrocracking and hydrogenation reactions in steam atmosphere.

4. To evaluate the effect of alternative contacting pattern using dispersed nanoparticulate catalyst as compared to conventional fixed-bed catalyst CAPRI process. Also, the performance of biomanufactured and refinery catalyst was tested.

1.3 Thesis Organisation and Overview

The eight technical Chapters in this thesis demonstrated the experimental technique of catalytic upgrading of heavy crude oil in-situ. The study explores the CAPRI concept of down-hole catalytic upgrading of heavy oils with emphasis on controlling coke formation and catalyst deactivation while maximising the level of upgrading. The extent of upgrading was evaluated in terms of change in API gravity, viscosity, true boiling point (TBP) distribution, sulphur and metals removal, and change in asphaltenes content.

Chapter 1 provides an in-depth introduction to the study and motivation. It also identified the need to sustain petroleum-based fuels, provides an overview of world heavy oil distribution, and identified considerable areas of challenges from previous studies that require further investigation. In Chapter 2, the different EOR technologies available for heavy oil and

bitumen extraction as well as the upgrading is reviewed. The Chapter provides the fundamental knowledge of CAPRI on which the entire thesis was built. The experimental set-up and procedures used in this study are detailed in Chapter 3. Also, the instrumental techniques used to measure changes in upgraded oil samples properties; produced gas composition, characterised fresh and spent catalysts after reactions are described in this Chapter.

Chapter 4 is devoted to finding the optimum reaction temperature and WHSV for upgrading. The emphasis is on effects of reaction temperature, WHSV, catalyst type, and feedstock on the extent of upgrading and performance of CAPRI. Subsequent experimental runs were based on the optimum temperature and WHSV obtained.

The impact of reaction gas environments on the chemistry of upgrading reactions and coke formation is the subject of Chapter 5. In this Chapter, different media such as hydrogen, methane, blend of gases (i.e., CO, CO_2, CH_4, and N_2), and nitrogen are reported. In addition, hydrogen-addition route to heavy oil upgrading was further explored. Understanding the role of hydrogen in the conversion of poly-aromatic compounds was treated using anthracene. Ex situ regenerated spent catalyst was also evaluated against fresh catalyst in terms of upgrading level obtainable.

Catalytic upgrading process deals with cracking of heavy molecules into lighter ones. However, these molecules contribute to high coking and catalyst deactivation as they impact directly on the catalyst bed. In this regard, the aspect of this study that deals with controlling coke formation by introducing guard-bed on top of the catalytic bed is described and reported in Chapter 6. Consequently, the impacts of the guard-bed on upgrading, asphaltenes as well as sulphur and metals removal are also explored.

In Chapter 7, analysis of the spent catalysts recovered from the CAPRI reactor after upgrading reactions for coke content, elemental composition, surface morphology, and micro-structural changes before and after reaction are reported. Chapter 8 is concerned with the effect of steam environment on the extent of upgrading and coke formation.

Chapter 9 is concerned with a comparative study of alternative contacting pattern by dispersing nanoparticulate catalyst at the mobile oil zone (MOZ) beyond the combustion front during THAI process and the conventional CAPRI which involves packing of the horizontal well with pelleted refinery catalyst prior to start-up. Also, biomanufactured Pd are compared with its chemical counterpart.

Finally, Chapter 10 presents some concluding remarks on the results of the studies and highlights various aspects of this study that still need further investigation.

Chapter 2

Review of Heavy Oils Recovery and Upgrading Processes

2. Introduction

Crude oil is a fossil fuel formed from the remains of plants and animals which have accumulated at sediment bottoms. Over time, pressure, heat, and bacterial action transformed the deposits into hydrocarbons, water, carbon dioxide, hydrogen sulphides, etc. (Robinson, 2006). Geologically, crude oil becomes heavy via biological, chemical and physical degradation processes during migration and after entrapment inside the pore-space of the rocky reservoir. Hence, heavy oil and bitumen is formed from the residue of formerly light oil whose light molecular weight hydrocarbons components have been lost through microbial degradation, water-washing and evaporation (Meyer and Attanasi, 2003). The U.S. Geological Survey (USGS) Energy Resource Program has classified crude oils depending on their API (i.e., American Petroleum Institute) gravity and viscosity (i.e., the resistance flow) as shown in Figure 2.1.

It is clear that the API gravity of heavy oil is several points lower than that of light oil. Similarly, the viscosity of heavy oil is extremely high in magnitude compared with that of light oil. Natural bitumen (or tar sands) is more dense, has poor mobility, and extremely low viscosity. The photographs in Figure 2.2 illustrate the physical characteristics of light oil, heavy oil and oilsand.

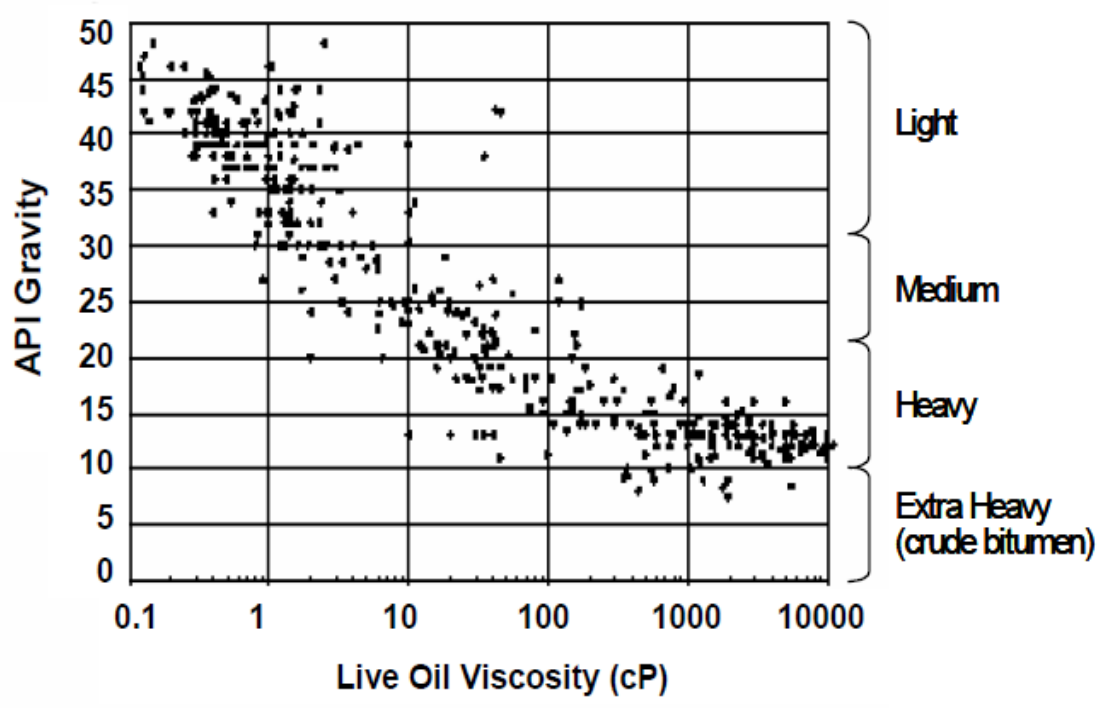

Figure 2.1 Crude oil classification based on API gravity and viscosity (Smalley, 2000).

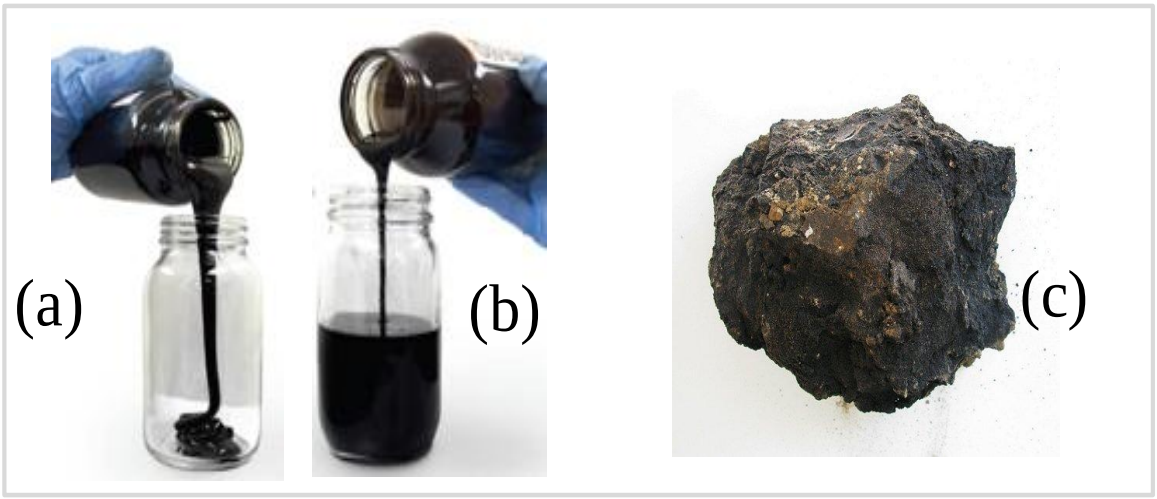

Figure 2.2 Photograph of (a) heavy oil; (b) light oil and (c) oilsand.

While light crude oils are produced easily by the natural reservoir pressure and water flooding, heavy oil and bitumen rely on Enhanced Oil Recovery (EOR) technologies for their

exploitation. This Chapter provides an in-depth description of the different methods of extracting and upgrading heavy oils and bitumen into light oil.

2.1 Composition of Heavy Oils

The crude oil composition and properties vary with location, origin and type. Heavy crude oil and bitumen are a complex mixture of about 10^5-10^6 different hydrocarbon components (Wiehe, 1999). Notwithstanding, heavy crude oil components can be classified into four components: saturates, aromatics, resins, and asphaltenes collectively called SARA, as illustrated in Figure 2.3.

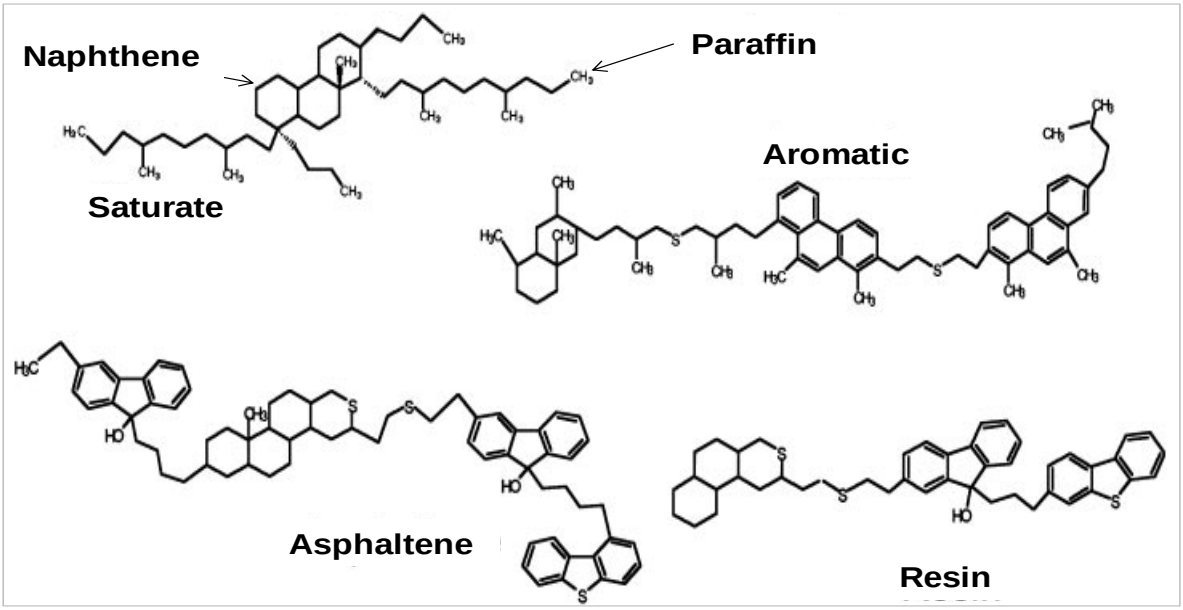

Figure 2.3 Molecular structures illustrating SARA components of heavy oil (Strauz and Lown, 2003).

A micro-emulsion model involving the above four components present in the crude oil was proposed by Wiehe and Liang (1996). In the model, asphaltenes occupy the core of micelles dispersed by the surfactant-like properties of resin that have been adsorbed on their

surface, which are held in solution by aromatic, as shown in Figure 2.4 (Wiehe and Liang, 1996; Leyva, et al., 2007).

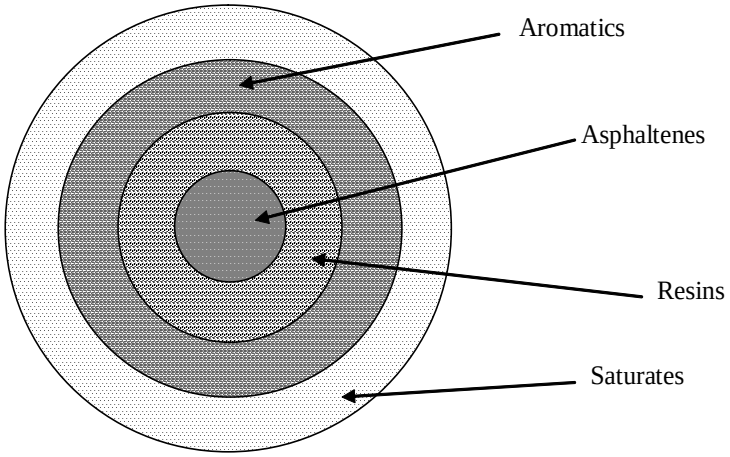

Figure 2.4 Micro-emulsion of crude oil SARA components.

Saturates are a fraction of the heavy oil consisting of non-polar hydrocarbons with linear, branched, and cyclic structures saturated with hydrogen. They include paraffins (i.e., saturated straight and/or branched chains hydrocarbon) and naphthenes (i.e., cyclic saturated hydrocarbon with one or more rings and in some case with paraffin side chains, as shown in Figure 2.3). Moreover, a high proportion of saturates in the crude oil indicates an increase in the yield of lower molecular weight or lower boiling point fractions.

Aromatics are hydrocarbons with one or more unsaturated benzene rings fused together. They may be linked with paraffinic side chains and/or a naphthenic ring as shown in Figure 2.3. However, saturates and aromatics are light components compared to resins and asphaltenes, which implies that light crude oil contains high percentage of these components.

Asphaltenes and resins are the heaviest components of the crude oil; as such the heaviness of crude oil can be linked to the high proportion of asphaltenes compared to light crude oil (Alvarez-Ramirez, et al., 2006). Resins are polar poly-aromatic molecules often

containing heteroatoms such as nitrogen, oxygen, or sulphur. They are soluble in light alkanes such as n-pentane, n-heptane, etc. with molecular weight less than 1000 $g.mol^{-1}$. Asphaltenes are composed of aromatic polycyclic clusters linked with one or more aliphaltic (or naphthenic) structure (Alvarez-Ramirez, et al., 2006; Montel, et al., 2008). The model of asphaltene molecular structure from California, Venezuela and Maya crude oils, respectively, obtained from the literature are shown in Figure 2.5.

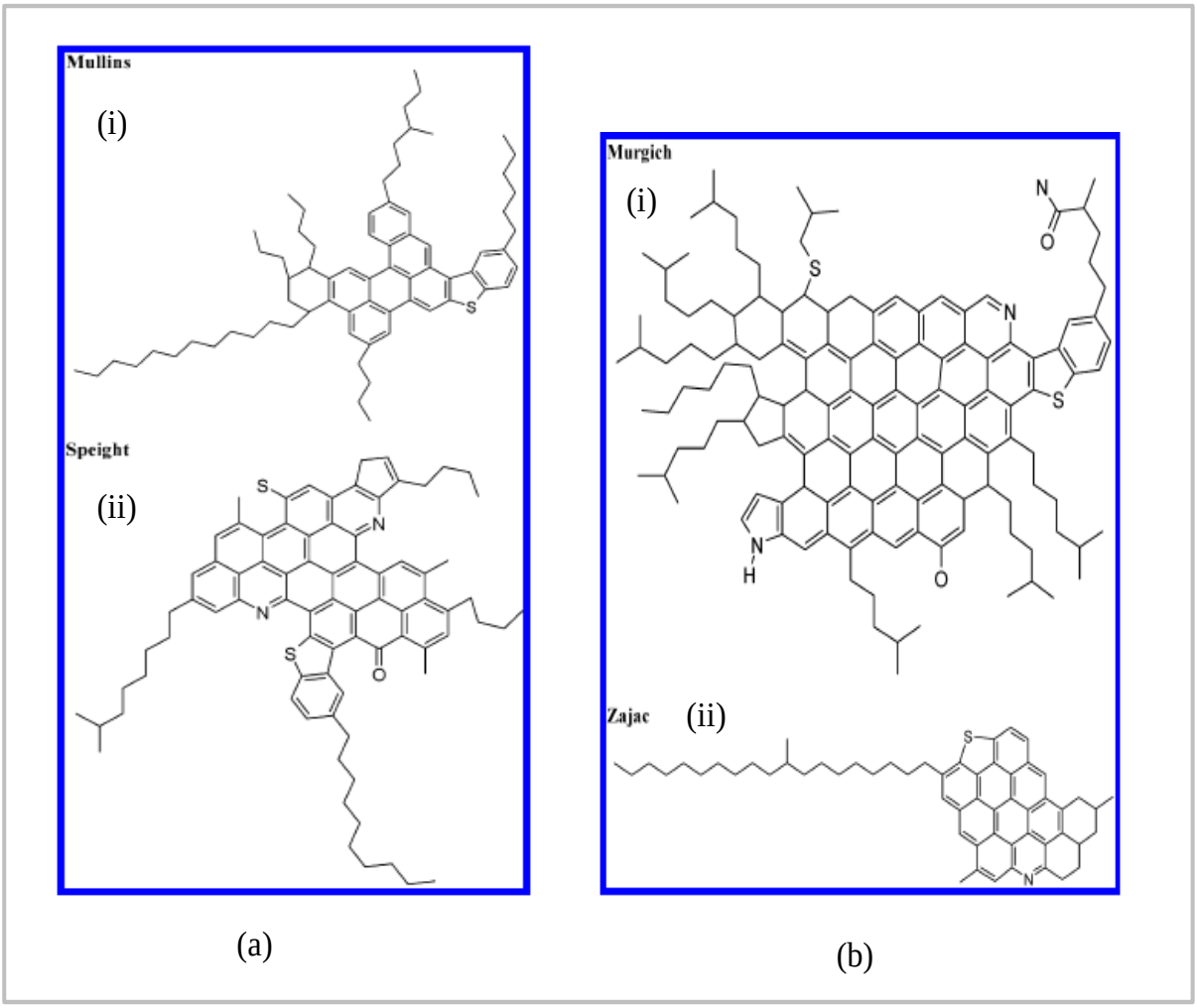

Figure 2.5 Four asphaltenes molecular structures (a) i. Obtained from California crude oil by Groenzin and Mullins (2000), ii. Obtained from Venezuela crude oil by Speight and Moschopedis (1979) (b) i. Obtained from Mayan crude oil by Zajac et al. (1994) and ii. Obtained from Venezuela crude oil by Murgich et al. (1996).

The constituents of the heavy oil/bitumen that are soluble in n-alkanes are referred to as maltenes/petrolenes (i.e., saturates, aromatics and resins). Whilst the asphaltene components of the crude oil are insoluble in low-molecular weight n-alkanes (e.g., n-C_5 to n-C_7), they are soluble in aromatic solvents such as toluene (Pacheco-Sanchez, et al., 2004). Also, their molecular weight ranges from 3000 to 5000 g.mol^{-1} (Jacob, 1971). Mansur et al. (2012) used Photo Correlation Spectroscopy (PCS) to study the size of asphaltene macromolecules. They found the average size of the asphaltene particles ranging from 12 to 22 nm, which is too large to pass through micro-pores or even some meso-pores in the catalyst. This component of the oil has the tendency to agglomerate due to temperature, pressure, and composition changes during extraction, transport, and upgrading stages. Additionally, asphaltenes possess a high content of Conradson Carbon Residue, CCR (i.e., the coking tendency) more than the other components. The coke formation during upgrading is a consequence of a series of multiple reactions that proceeds from saturates to aromatics, then resins to asphaltenes and finally to coke, as the conversion to light hydrocarbon oil occurs (Sawarkar, et al., 2007). The asphaltene cores (i.e., aromatics) are suspended in the oil by paraffinic side chains that interact with the other components. Upon reaction, the aromatic cores are separated from the asphaltene and the cracked paraffin form gas or liquid product while the aromatic core polymerises to coke (Chianelli, et al., 2013).

Heavy metals (e.g., Ni, V, etc.) and other heteroatoms (e.g., S, N, and O) are known to be more concentrated in the heavier components of the crude oil such as asphaltenes and resins, and less linked with saturates and aromatics. The organometallic compounds readily poison and shorten catalyst lifetime during catalytic upgrading. These heavy metals such as nickel and vanadium exist in chelating complexes in the form of porphyyrinic or nonporphyrinic structures (Yin, et al., 2009; Leyva, et al., 2007), as shown in Figure 2.6.

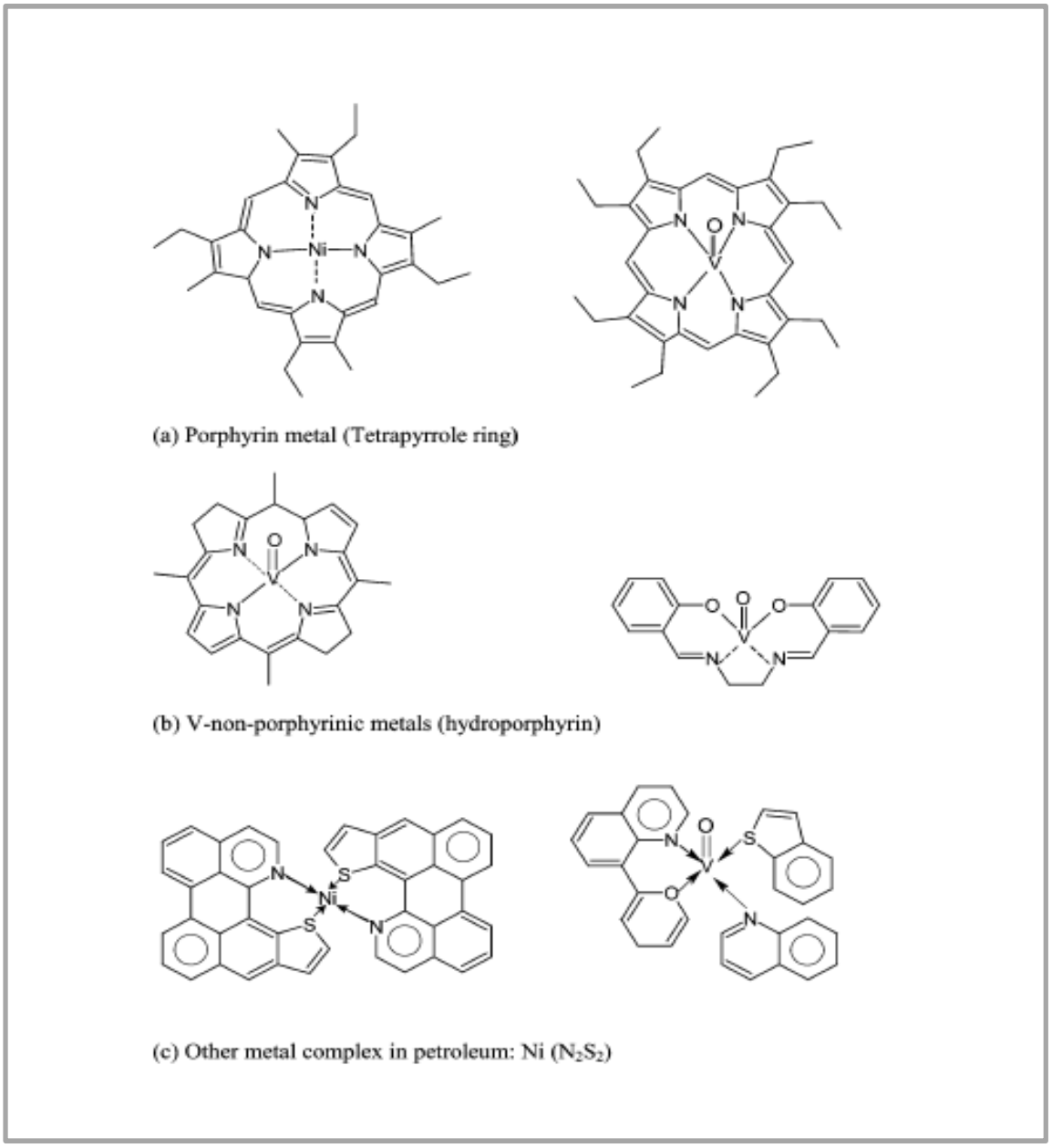

Figure 2.6 Organo-metallic compounds in heavy oil as porphyrinic, non porphyrinic, and other form of complex (Leyva, et al., 2007).

Moreover, both porphyrin and non-porphyrin form of the metals can result from the presence of rock minerals in the oil reservoir induced by temperature and pressure changes within the reservoir during crude oil formation.

2.2 Enhanced Oil Recovery (EOR) Technologies

With heavy oil having viscosities in the range of 1 to more than 50 Pa.s, primary (i.e., by natural reservoir pressure) and secondary recovery methods such as water flooding are limited to 5-10% recovery of the original oil in place (OOIP), due to unfavourable mobility ratio between oil and water phases, leaving a considerable amount of oil (about 80-95%) in the reservoir (Liu, et al., 2007; Dong, et al., 2009). EOR is therefore regarded as a tertiary recovery or Improved Oil Recovery (IOR) technique. EOR techniques are mainly applied to recover trapped residual oils retained in the reservoir after secondary recovery, owing to capillary forces and immobility of oils as a result of high viscosity at reservoir conditions of temperature and pressure (Thomas, 2008). EOR techniques typically involve increasing the temperature of the oil-bearing formation (i.e., heating) or reducing interfacial tension to improve oil mobility. Heavy oil recovery technologies are generally classified into two main groups the thermal and non-thermal recovery methods as shown in Figure 2.7 (page 18).

After laboratory assessment of the various EOR methods, ExxonMobil classified the applicability of the various EOR technologies based on the grade of oil: light oil – gas injection (miscible and immiscible) and chemical processes, heavy oil – thermal processes and mining, and viscous oil – polymer flooding, cold flow (ExxonMobil, 2009). However, reservoir geology and thickness plays a significant role in the choice of technique in addition to the oil properties (Shah, et al., 2011). In the following Sections the various types of EOR techniques are reviewed in detail and compared.

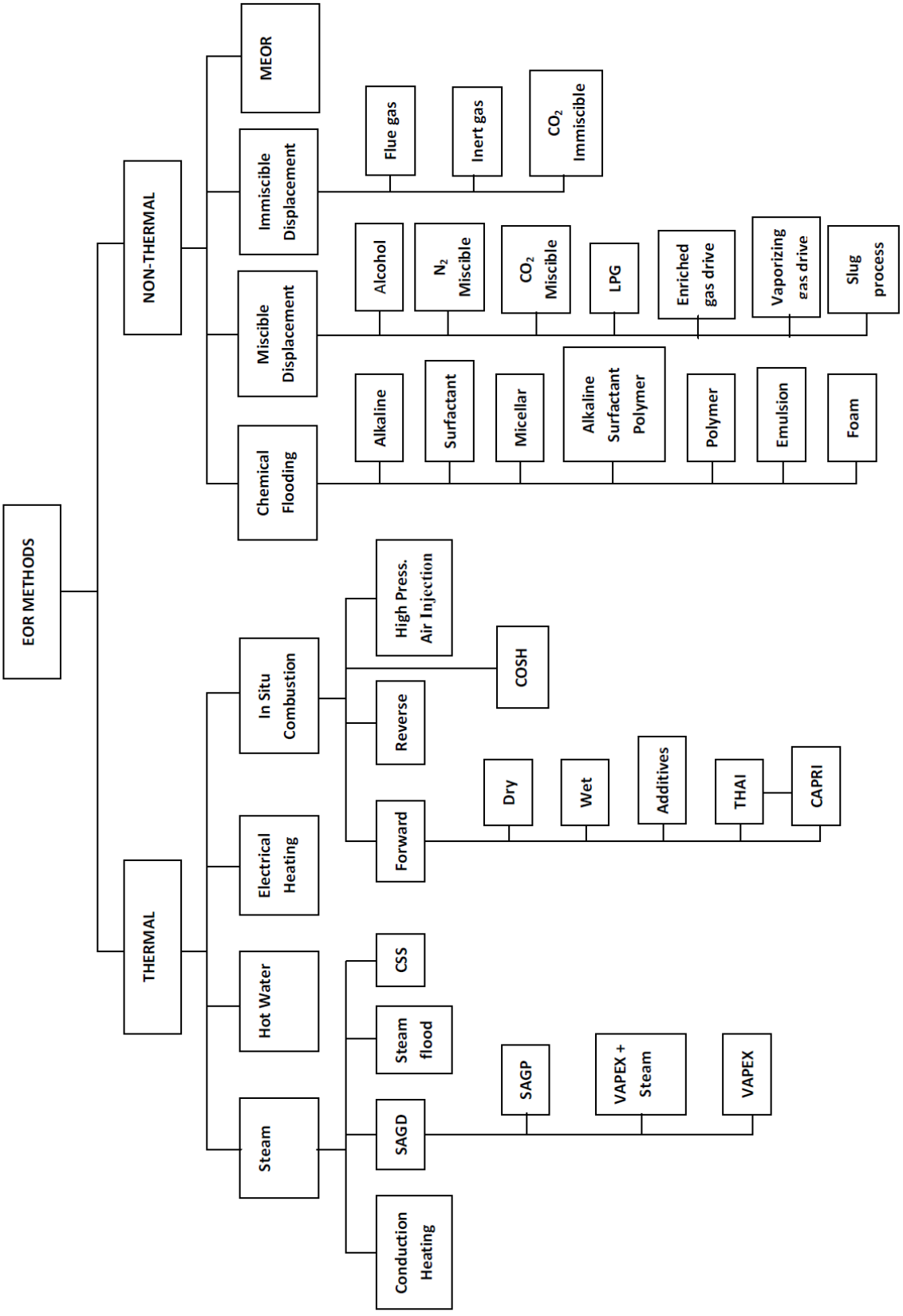

Figure 2.7 Heavy oil recovery technologies.

2.3 Chemical Flooding

Chemical flooding involves the injection of chemical formulation as the displacing fluid into the reservoir to reduce interfacial tension between the oil and water, decrease mobility ratio, increase capillary number and improve sweep efficiency (Shah, et al., 2011; Thomas, 2008; Greaves, et al., 2000; Thomas and Farouq, 2009). Chemical flooding requires higher reservoir permeability compared to gas injection, however it offers an environmental benefit as it produces no green house gases. The technique has a typical recovery factor (i.e., the ratio of produced oil to the initial oil in place) up to 40% OOIP; it is limited by the high cost of chemicals and its application to large reservoirs (Thomas, 2008; Shah, et al., 2011).

2.3.1 Polymer Flooding

Polymer flooding involves the injection of water soluble polymer solutions such as polysaccharides and polyacrylamides into the oil-bearing formation to improve the water-oil mobility ratio, increase viscosity of water, reduce the permeability of the aqueous phase, and improves displacement sweep efficiency in order to enhance oil recovery (Thomas, 2008; Hou, 2007). In the light of this, the method is sometimes referred to as polymer-augmented water flooding, applied as a slug process and driven using dilute brine. The technique has considerably higher oil recovery potentials than water flooding, typically about 6-12% higher, which gives a 40-50% recovery factor of initial oil in place (IOIP) after application (Hou, 2007).

Following this recovery level, polymer flooding has been found to be suitable for reservoirs with high mobile oil saturation and moderate reservoir heterogeneity, and not recommended for oil with viscosity greater than 200 mPa.s (Wang and Dong, 2009).

However, the technique is limited by polymer degradation in the reservoir, loss of polymer to porous matrix of the reservoir, and for heavy oils higher concentration of polymer solution is required to reduce the mobility ratio, which may cause injection difficulty and more cost (Sheng, 2011 and 2013).

2.3.2 Surfactant Flooding

Surfactants are a blend of surface active substances which are usually amphiphilic compounds (e.g., petroleum sulfonates). The blend of these surface active materials has the potential to reduce interfacial tension between oil and water because of its amphiphilic character, boosting the dispersion of oil in water, making oil droplets more readily deformed and easing the flow through pores, lowering the threshold pressure and residual oil saturation in the oil-bearing formation upon injection, thereby increasing the oil production rate (Bryan and Kantzas, 2007; Dai-yin and Hui, 2008). In some cases, co-surfactants such as alcohol and water-soluble polymers are injected to improve the interactions between surfactant and sandstone rocks. However, the porous medium geology in addition to the reservoir pore wettability greatly influences the performance of surfactant-based flooding for EOR (Jamaloei, et al., 2011). Besides, the slug size and surfactant concentration are limited by cost. Additional difficulties facing surfactant flooding are: excessive surfactant loss to the porous medium of the reservoir incurring more cost, treatment and disposal of emulsions, and also the adsorption and reactions of surfactant with rock and sandstones in the reservoir in some cases (Krumrine and Falcone, 1983).

2.3.3 Alkaline Flooding

Alkaline flooding involves the injection of an aqueous alkaline solution such as sodium hydroxide, sodium orthosilicate, potassium hydroxide, sodium carbonate, ammonium hydroxide, etc. in slug form into the oil-bearing formation. The improved recovery depends on the chemical reaction between the alkaline agent and the organic acid constituents (i.e., saponifiable component) of the crude oil to produce in situ surfactant (i.e., soap) that has the ability of reducing interfacial tension between oil, water and rock in the reservoir (Thomas, 2008; Sheng, 2011; Mayer, et al., 1983).

It has been reported that the fundamental recovery mechanisms of the alkaline flooding process include *in situ* formation of water-in-oil (O/W) emulsions, penetration of the alkaline solution into the oil and the formation of water drops inside the crude oil phase. This implies that the crude oil should have a significant amount of saponifiable components (i.e. organic acid) for its effectiveness and formation of *in situ* surfactants. The method is suitable for reservoirs with oil viscosity less than 100 cP (Sheng, 2011).

Despite its simplicity, low cost of chemicals and operation in comparison to other chemical methods, there has been little field application, as most of them have been unsuccessful. This is because of the complex reactions between the alkaline solution and the rocks and reservoir fluids, the technique not being suitable for reservoirs of carbonate formation, and the cost of treating produced emulsion and fluids recovered from the reservoir. Other challenges associated with the method for heavy oil recovery includes channelling of injected alkaline solution, the formed water-in-oil emulsion may block the high permeability zone, and poor volumetric sweep efficiency (Sheng, 2013; Chen, et al., 2013).

2.3.4 Micellar Flooding

In this process, a slug solution containing surfactant, co-surfactant, alcohol, brine and oil are formulated to form surfactant-stabilised microemulsions slug with droplet sizes of 10^{-4} to 10^{-6} mm composed of micelles that are miscible with reservoir oil as well as water (Thomas, 2008). The micellar solutions injected into the oil-bearing formation lowers the interfacial tension between the oil, aqueous phase and rocks, to release and improve the mobility of trapped oil in the pores of the formation of the reservoir. This is immediately followed by the injection of a polymer buffer for mobility control, and subsequent injection of a buffer of fresh water to prevent contamination.

Notwithstanding the recorded field successes compared to other chemical methods (Gogarty and Tosch, 1968), the geology and conditions of the reservoir such as high salinity, high temperature and clay content have limited its applications (Thomas, 2008). Moreover, the design and formulation of the micellar solution is expensive and complex due to the multiple phase behaviour. However, investigations have shown that micellar flooding has the potential to recover 35-50% of the oil in place after water flooding (Thomas, 2008).

2.3.5 Alkaline-Surfactant-Polymer (ASP) Flooding

ASP flooding was developed in the 1980's and its oil recovery potential is based on the combined mechanisms of alkaline, surfactant and polymer flooding in a single unit. In the light of this, an aqueous solution containing alkali, surfactant and polymer is injected into the oil-bearing strata of the reservoir to drive the crude oil out of the formation and enhance production rate. It has been found that the EOR potential of the technology is over 20% OOIP (Deng, et al., 2005). The ASP flooding method has had several field trials especially in China,

such as Daqing and Shengli oilfields with some satisfactory increase in oil production (Kang, 2001; Hong, et al., 2009).

The drawbacks identified during field application of ASP flooding method are severe scaling in the injection lines and the produced water contains large amounts of residual chemicals, which forms a complex and stable emulsion, therefore making it difficult to treat (Hong, et al., 2009; Wang, et al., 2011). Furthermore, no effective treatment technique has been developed to treat the produced waste water from ASP flooding, which makes it a potential environmental pollutant and therefore limited further field applications (Wang, et al., 2011).

2.4 Miscible Displacement

The two main reasons of using a fluid that is miscible with the oil residue include: firstly, it eliminates the effects of interfacial intensions. Secondly, if the miscible fluid has lower viscosity than the oil, upon solubilising with the oil it creates a mixture which has a lower viscosity than that of the OOIP, thus aiding recovery with low pressure gradient to displace the oil mix from the porous medium. The technique therefore involves the injection of common driving fluids such as carbon dioxide, light hydrocarbon, nitrogen or liquefied petroleum gas (LPG) into a separate injection well to drive the oil into another well called the production well.

As the displacing fluid advances, a mixing zone develops with spreading profile as the solvent front advances. The miscibility of the process is however governed by the temperature, pressure, composition of the oil in the reservoir as well as the composition of the displacing fluid. Thus, the key parameter for designing a miscible displacement system for

EOR is the minimum miscibility pressure (MMP), which depends on the reservoir temperature, oil composition and the displacing fluid (Zuo, et al., 1993).

The various miscible drive methods are miscible slug process, enriched gas drive, vaporizing gas drive and high pressure gas (e.g., CO_2, N_2, etc.) injection. The fluids that are used for miscible displacement have lower density than the reservoir oil, as the greater density difference between the fluid and oil increases the sweep efficiency (Thomas, 2008). However, channelling and viscous fingering can decrease efficiency of the process. Hence, miscible displacement is only economical for enhanced recovery of low viscosity crude oil with API gravity greater than 20^o API (Zuo, et al., 1993).

2.4.1 Carbon dioxide Miscible Displacement

Carbon dioxide miscible displacement for enhanced oil recovery was first implemented in 1964 at the Mead-Strawn Oilfield and in 1972 at the Collie-Schneider Oilfield in the United States (PingPing, et al., 2010). Carbon dioxide can become a supercritical fluid at relatively low temperatures (31.1^oC) and pressures (73.8 bar), and is less viscous than oil. The use of carbon dioxide for EOR process is based on its properties which are ability to reduce the viscosity of the oil, decreasing the residual oil saturation; its low minimum miscibility pressure for a wide range of crude oils, and swelling the oil phase in the reservoir formation (Mehos and Ramirez, 1989). It has the ability to vaporise heavier components (C_5-C_{30}), leading to reduction in surface tension and viscosity of the oil which improves miscible displacement through multiple contact extraction of the C_5-C_{30} hydrocarbons. Carbon dioxide miscible flooding is suitable for light and medium crude oils, low temperature and shallow reservoir.

After oil recovery has been completed the CO_2 is left behind in the reservoir. Therefore, its use for EOR would be of potential importance in reducing greenhouse gas emission, due to the increasing concern about global warming. Also, CO_2 flooding is applicable to both sandstones and carbonate reservoirs. However, due to its low viscosity, mobility control is poor and the gas tends to channel and bypass the producer well, leaving most areas of the oil reservoir unswept. In addition, severe reservoir heterogeneity can lead to excessive channelling and bypassing of the injected CO_2, because it is less dense and therefore tends to move upwards through the reservoir. Other problems encountered on the use of CO_2 miscible displacement includes low reservoir volumetric sweep efficiency due to viscous fingering and gravity override, which is not suitable for heavy oil and bitumen as high miscibility pressure is required. Also, it requires laboratory and field evaluation to acquire adequate information for planning and implementation of a full scale project, in addition it is expensive compared to water flooding (Matthews, 1989). Additionally, dissolved CO_2 could induce asphaltene precipitation, which upon deposition onto the porous matrix, plugs and reduces the amount of oil recovery.

Regardless of the above limitations, the CO_2 miscible displacement technique can achieve up to 30-35% recovery factor of IOIP (Matthews, 1989). Tuzunoglu and Bagci (2000) reported that in continuous CO_2 injection mechanism, the highest recovery factor (15.1% OOIP) was obtained using Vertical Injection Horizontal Production (VIHP) well arrangement and water-alternating-gas (WAG) injection mechanism yield a higher recovery factor of about 34.5% OOIP. The main problem of the process is severe corrosion of the injection well.

2.4.2 Nitrogen Miscible Displacement

Nitrogen has been used successfully as the injection fluid for EOR, in the following oilfields; Jay field, FL (Exxon), Painter field, WY (Chevron), East Binger field, OK (Phillips), and Lake Barre field, LA (Texaco) (Hudgins, et al., 1990). The fundamental principle and mechanisms of nitrogen miscible displacement is similar to that of CO_2 miscible flooding, except that the MMP for nitrogen miscible displacement is higher. The extent of miscibility is affected by the temperature and pressure of the oil reservoir. The conditions that improve miscibility of nitrogen with crude oil in the reservoir include high reservoir pressure and light crude oil containing intermediate hydrocarbon components C_2-C_5 (Hudgins, et al., 1990). In this regard, the reservoir that will satisfy this condition must be deep enough to withstand this high pressure.

Subsequently, the advantages of nitrogen EOR include the ready availability of nitrogen gas which makes the process more economical, cheaper than the use of CO_2 or LPG, environmentally friendly, completely inert even in the presence of water and not corrosive. The estimation of MMP of nitrogen is one of the major limitations to its application.

2.4.3 Hydrocarbon Miscible Displacement

Hydrocarbon flooding is becoming a viable means of EOR; it involves the injection of short-chain hydrocarbon fluids such as methane, propane or liquefied petroleum gas (LPG) through an injection well into the oil-bearing formation to aid dilution of the heavy oil. As a result of mixing through diffusion and/or dispersion of the LPG into the residue/heavy oil, the heavy oil viscosity reduces and the fluidity improves, which causes a displacement towards the production well. This is because the short-chain hydrocarbons are considerably less

viscous than the oil in place. The rate of oil recovery is affected by several factors such as mass transfer, viscous forces and gravity drainage (Salama and Kantzas, 2006). The molecules of the injected hydrocarbon fluid may continue to mix with the oil in the reservoir until a saturation concentration is reached at the reservoir temperature and pressure.

Moreover, when the mobility ratio M (i.e., the ratio hydrocarbon mobility/oil mobility) is less than 1 it favours dispersion, mixing and displacement. If M > 1, it causes instability in the displacement front leading to viscous fingering or channelling. This will therefore lead to early breakthrough of the fluid and poor sweep efficiency, as most portions of the porous medium remain unswept by the displacing fluid. Therefore, the main challenges to the process are ensuring sufficiently high rock permeability to gain access to a large fraction of the oil in the reservoir (Salama and Kantzas, 2006). Hydrocarbon fluid is expensive to use. Another limitation of using hydrocarbon fluids is their propensity to precipitate asphaltenes from the crude oil (Mehran, et al., 2008).

2.5 Microbial Enhanced Oil Recovery (MEOR)

The MEOR was first proposed by Bechman in 1926, but the laboratory work of ZoBell in the 1940s brought a serious consideration of the technology (Zobell, 1947). MEOR techniques rely on the inoculation of the oil reservoir with mixed anaerobic or facultative hydrocarbon degrading microbes such as clostridium, bacillus, micrococcus, arthrobacterium, or xanthomonous. The enhancement of recovery is based on their ability to generate bio-surfactants (to help reduce interfacial tension between oil and rock/water surface), biopolymers, gases, acids, and solvents as they multiply exponentially. The modes of injecting the microorganisms into the oil-bearing formation include cyclic microbial recovery

(single well stimulation), microbial flooding recovery and selective plugging recovery (Lazar, et al., 2007).

Over 400 patents have been issued on MEOR technology, however it has not gained wide acceptance by the oil industries because most of the literature reports are on laboratory scale and field trials lack convincing proof (Brown, 2010). Additionally, the physical and environmental constraints within the oil reservoir such as temperature, pressure, the pore size and geometry, chemical and biological factors, and salinity level limits microbial activities in the oil-bearing formation. In the view of this, attention has been turned to anaerobic extremophiles such as thermophiles, barophiles and halophiles that can withstand extreme conditions in the oil reservoir (Sen, 2008). The microbes can reside and perform *in situ* conditions of temperature up to 94^{o}C, formation depth range 2400-3500 m, and water salinities as high as 140,000 ppm total dissolved solids (Govreau, et al., 2013). In contrast, microbial EOR offers the following advantages: the products are biodegradable and environmentally friendly, and the method is economical since no energy is required.

2.6 Thermal Methods

Cold production of heavy oil typically achieves oil recovery factors of less than 20% OOIP (Greaves, et al., 2000; Tuzunoglu and Bagci, 2000). In such situations, reducing the viscosity of the heavy oil is the most efficient and immediate means to produce the oil left in the reservoir after cold production. In order words, thermal EOR is a potential candidate for secondary recovery as it supplies heat to the reservoir, which induces temperature rise in the oil-bearing matrix, reducing the viscosity of the heavy oil *in situ* by several orders of magnitude, vaporising the lighter components of the oil and thus mobilising the oil. In

essence, compared with other methods of in EOR, thermal methods for heavy oil recovery are the most efficient and successful owing to their high oil recovery following the field reports (Xia and Greaves, 2006; Greaves, et al., 2000b; Nare, et al., 2007).

Thermal methods include hot fluid injection, *in situ* combustion (i.e. heat generated *in situ* by burning small fraction of the reservoir crude) and use of electrical heaters. The high cost of energy and thermal efficiency influences the choice of thermal EOR.

2.6.1 Steam Flooding

It is well known that heavy oil and bitumen viscosity decreases steadily with increasing temperatures. In this respect, high temperature steam is used to convey heat to the oil-bearing matrix. Steam flooding is one of the most commonly used thermal EOR techniques that have been studied extensively over the past 40 years and as a result of these trials is considered suitable for medium and heavy oil reservoirs, with many commercial successes from field projects reported in the literature (Bagci, et al., 1998). The continuous injection of steam into the oil-bearing formation via the injection well induces heat energy, thereby improving the fluidity of the oil towards the producer well, as shown in Figure 2.8 (Shah, et al., 2010).

Steam flooding is a complex EOR process involving heat, mass and momentum transport in the porous media, leading to viscosity reduction, phase change, thermal expansion, steam distillation, gas drive, solvent extraction and capillary variations to improve oil fluidity and production (Jabbour, et al., 1996; Liu and Ramirez, 1994).

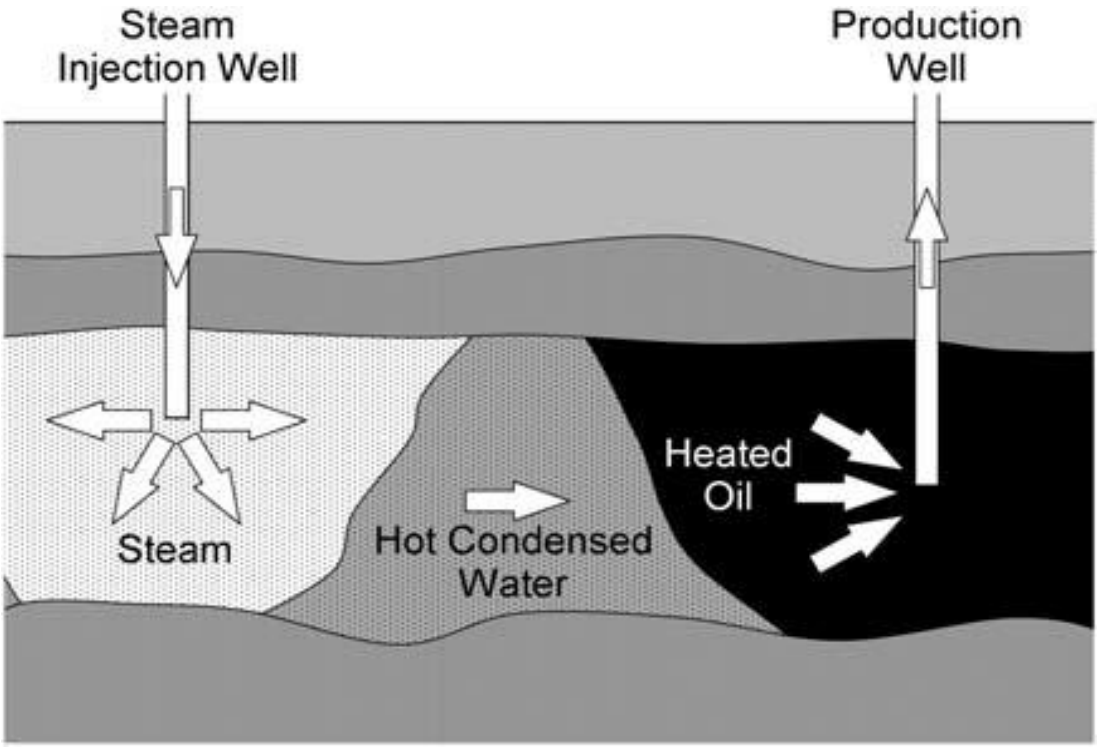

Figure 2.8 Steam flooding EOR method.

However, reports have shown that oil recovery by steam flooding is greater for lighter oil reservoirs, because they contained a larger fraction of steam-distillable components than heavy oil (Jabbour, et al., 1996).

Furthermore, conventional steam flooding (CSF) uses Vertical Injection and Vertical Production wells (VIVP) (see Figure 2.8), which is categorised as a Long-Distance Oil Displacement (LDOP) process based on the fact that the mobilized oil travels over long distance hundreds of meters from the injection to the producer well, and is mainly applied to relatively shallow oil reservoirs. This VIVP well arrangements are prone to gravity override or channelling, leading to extremely low volumetric sweep efficiency (Xia and Greaves, 2001; Fatemi and Jamaloei, 2011). However, the advent of horizontal producer well, a 'toe-to-heel' steam flooding (THSF) arrangement in the same fashion as the THAI technique has been proposed, which uses a VIHP well in direct line drive as illustrated in Figure 2.9 (Xia

and Greaves, 2000 & 2001; Fatemi and Jamaloei, 2011). This arrangement achieves high steam front sweeping efficiency compared to the VIVP well, as the mobilised oil and the steam condensate ahead of the steam front is drained into the exposed section of the horizontal producer well immediately. Therefore, the VIHP well is called a short distance oil displacement (SDOD) method.

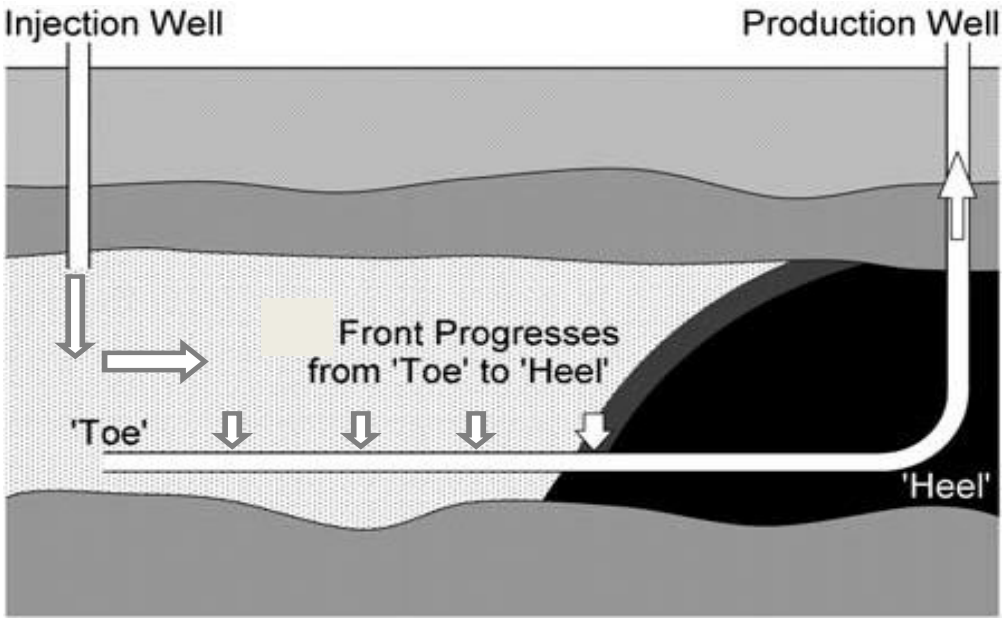

Figure 2.9 Toe-to-heel steam flooding (THSF).

Typical oil recovery factors in steam flooding are in the range 50-60% of oil in place (Thomas, 2008). Research on steam flooding EOR has identified factors such as rock properties, crude oil composition, steam quality, steam/oil ratio and steam injection rate as the key variables that determine the performance and success of the process (Bagci, et al., 1998). The amount of water required depends on the steam/oil ratio. For instance, a steam/oil of 2 means that two barrels of water converted to steam are required to produce one barrel of the heavy oil. Additionally, gravity override and excessive heat loss to adjacent formations occur,

steam generation is energy intensive and expensive, and steam breakthroughs are other common factors that impede the process efficiency.

2.6.2 Cyclic Steam Stimulation (CSS)

Cyclic steam stimulation was discovered accidentally by Shell in Venezuela during production of heavy crude oil by steam flooding of the Mene Grande field (Butler and Stephens, 1980). The process is also known by the 'steam soak' and 'huff and puff'. The CSS method of heavy oil recovery has been used to produce 14,500 m^3 per day bitumen from Cold Lake, Alberta, Canada by Imperial Oil Limited for over ten years (Label and Moriyama, 1997). In CSS technology, the heavy oil recovery mechanism is similar to other steam flooding techniques which include heating oil-bearing matrix, steam distillation, viscosity reduction, gas drive and mobilisation of oil towards the well.

The CSS technique involves alternating cycles of injecting steam and producing oil from the same well, involving a three stage process (i.e., injection, soak and production) as illustrated in Figure 2.10. The first stage involves the injection high pressure and high temperature steam into the oil reservoir for several weeks depending on the formation thickness, oil saturation and number of previously performed injection cycles. Then in the second stage (see Figure 2.10), the well is temporally shut for a period (some weeks) to allow the steam to heat or "soak" the oil-bearing formation, reduce oil viscosity and improve mobility towards the well. After an adequate soaking period, the injection well is then opened for oil production. The oil production rate continues until the rate of oil recovery becomes uneconomical due to heat losses to rock formations. At this stage, the cycle of soak-and-produce or huff-and-puff is then repeated. However, the oil production rates tend to reduce

with each successive cycle and require an increasing amount of injection steam (Fanaritis and Chilingarian, 1989). The steam to oil ratios starts from 2:1, and increases as the cycles are repeated in the range 3:1 to 4:1.

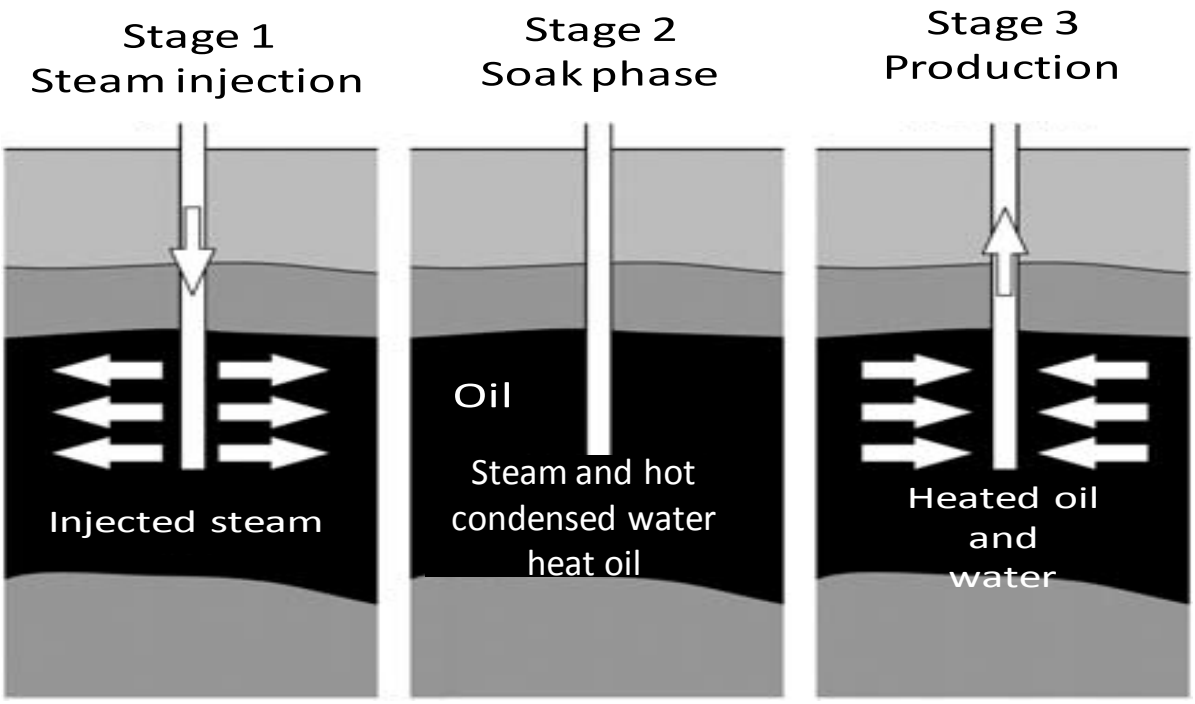

Figure 2.10 The 3 stages of cyclic steam stimulation (CSS).

The temperature of the heated zone with time and the radius of the heated zone determines the stimulation ratio (or percentage increase in oil production), that is, the ratio of oil production rate following steam stimulation to oil production rate prior to steam stimulation (Fanaritis and Chilingarian, 1989). Although, there is a faster production response and lower capital cost initially using CSS than steam flooding, it is challenging to estimate the stimulation ratio due to factors such as steam bypassing through fractures in the formation, well-bore heat loss and gravity segregation (Razavi and Kharrat, 2009). Thus, due to its discontinuous manner, the typical recovery factor is 10-40% of oil in place.

2.6.3 Steam Assisted Gravity Drainage (SAGD)

The advent of horizontal wells in the 1980s, led to the development of SAGD. It is another steam injection technique, with greater superiority compared to other steam processes because its gravity-assisted mechanism allows the expansion of a stable steam chamber and the short distance oil displacement (Greaves, et al., 2000a). The concept of SAGD technology for heavy oil recovery was developed by Roger Butler with Imperial Oil, and the technique was first trialled at Cold Lake for the recovery of heavy oil in the 1980s (Butler and Stephens, 1980; Butler, 1985). Presently, there are many of the SAGD process projects in progress for the recovery of heavy oils, bitumen and tar sands in operations in Canada.

SAGD uses two parallel horizontal wells which are about 4-6 meters apart into the oil-bearing formation, as illustrated schematically in Figure 2.11. The top is the steam injection well and the bottom horizontal well serves as the producer well. The heated heavy oil or bitumen drains down by gravity with condensed steam into the producer well immediately below.

The technique is described as a short distance oil displacement process, since the mobilised oil flows into the producer well in the shortest distance (a few metres) compared to the long distance displacement encountered with the VIVP well configuration of conventional steam-flooding. The driving force is therefore the gravity force (Xia, et al., 2003; Greaves, et al., 2000a). The continuous injection of steam creates a rising high-temperature steam chamber, which then spreads vertically and horizontally in the oil reservoir reducing viscosity and enhancing fluidity (Thomas, 2008).

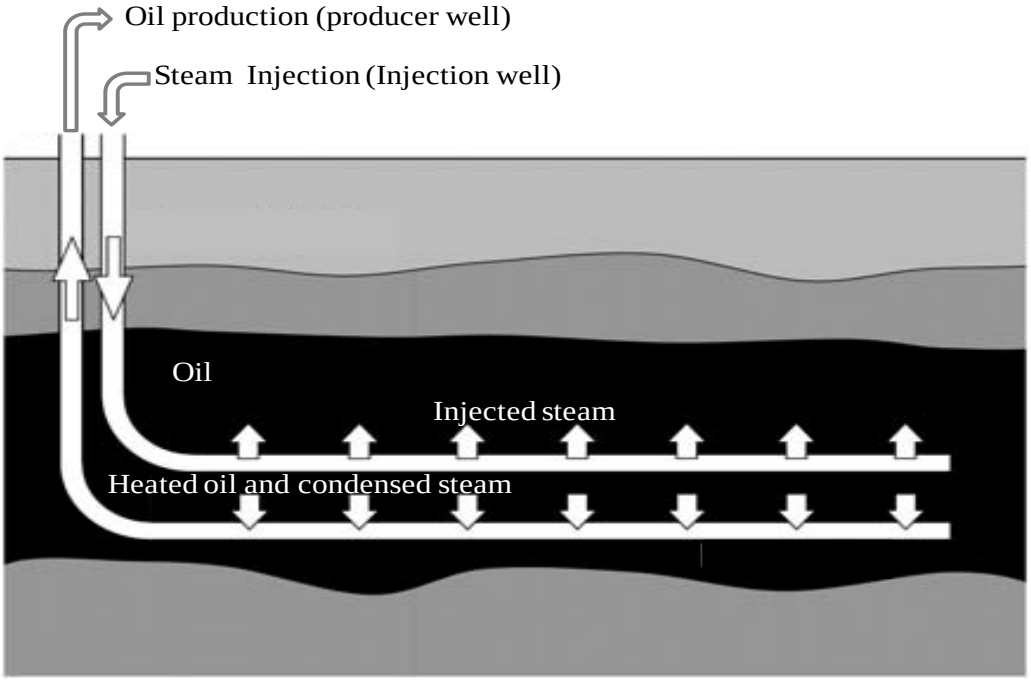

Figure 2.11 Steam Assisted Gravity Drainage (SAGD) process.

However, the counter-current flow between the rising steam and the draining oil, limits the efficiency and the utilisation of the reservoir energy (i.e., natural drive) and the gravity drive; therefore, SAGD is mainly recommended for reservoirs with low reservoir energy (i.e., low pressure and low solution-gas oil ratio) such as exist in tar sands (Greaves, et al., 2000a; Batycky, 1997).

Furthermore, the SAGD process is faced with challenges such as the cost and the large volume of water and natural gas required for steam generation, the applicability is demanding in terms of large formation thickness and permeability greater than 5000 mD (Batycky, 1997; Farouq, 1997). The process is complex and labour intensive (Greaves, et al., 2000a), not suitable for thin reservoirs, and it is also sensitive to operational and reservoir parameters such as steam injection rate and duration, well separation, reservoir heterogeneity, and rock permeability. Additionally, at the early stage efficiency is higher, but lowers significantly with

time due to heat losses to the formation. The oil recovery factor ranges from 40-70% of OOIP.

These limitations and the quest to improve the economics of SAGD, led to the development of alternative processes such as vapour-assisted petroleum extraction (VAPEX), expanding solvent steam assisted gravity drainage (ES-SAGD), and steam and gas push (SAGP). VAPEX process is the solvent analogue of SAGD for heavy oil recovery, it was proposed by Butler and Mokrys (Mokrys and Butler, 1993; Butler and Mokrys, 1989 & 1991). VAPEX is therefore non-thermal version of SAGD, in which mixture fluids such as ethane, propane, butane, etc., are injected alongside a carrier gas (e.g., nitrogen, carbon dioxide, etc. used to raise the dew point of the solvent to keep it in vapour phase) into the upper horizontal well instead of steam (Mokrys and Butler, 1993). The vaporising solvents forms a vapour chamber, which spread through diffusion and dispersion into the oil-bearing formation, reducing the viscosity of the heavy oil by dilution, and the diluted and reduced-viscosity oil is drained down by gravity into the lower production well, as shown in Figure 2.12 (Swapan and Butler, 1997).

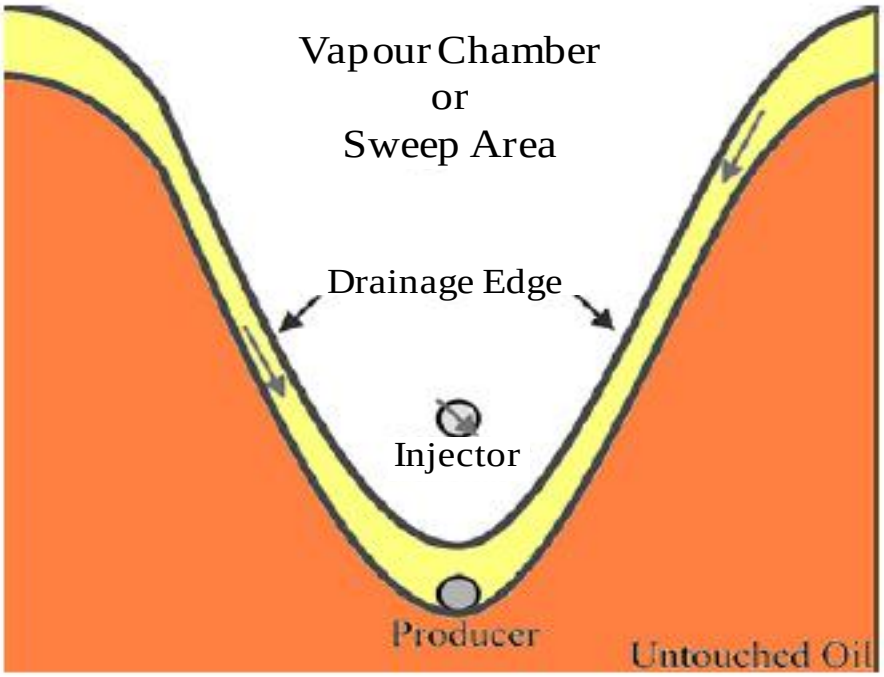

Figure 2.12 Mechanism of VAPEX process (Swapan and Butler, 1997).

The process offers some benefits such as lower energy cost, in situ upgrading attributed to deasphalting, less energy consumption, and less environmental pollution (i.e., reduction greenhouse gas emission) compared to SAGD (Swapan and Butler, 1997). However, the mechanisms of viscosity reduction and upgrading are slow compared to SAGD. Because of the large difference between molecular and thermal diffusivities thermal processes tend to be faster than solvent methods. The basic mechanisms of viscosity reduction by VAPEX are dispersion and diffusion, which are relatively less efficient than the application of heat for viscosity reduction (Thomas, 2008). Additionally the cost of solvent adds to its capital and operational cost.

ES-SAGD process is a combination of VAPEX and SAGD process (Nasr and Isaac, 2001), in which small amount of solvent is injected with steam. The solvent and steam enters into the vapour chamber and flows to the edge of the chamber, with the steam delivering its

latent heat to the heavy oil and the solvent diffusing and dissolving into the heavy oil, lowering viscosity via dilution, the mobilised oil and condense steam with solvent drained down by gravity into the producer well (Gates, 2007 & 2010). However, using solvent and steam incur an additional cost. The steam and gas push (SAGP) was proposed in which a non-condensable gas (natural gas or nitrogen) is injected with steam. This therefore reduces the amount of steam used, increases the thermal efficiency, oil/steam ratio is improved and the steam chamber expands faster laterally (Liu, et al., 2011; Butler, 1999). However, the SAGP process is still at the developmental stages.

2.6.4. In Situ Combustion (ISC)

In situ combustion (fire flooding) is a thermal EOR technology, in which an oxidizing gas (e.g., air) is injected into the oil-bearing formation to generate heat as it combusts with a small fraction of the oil in the reservoir. The generated coke supports continuous combustion with air. The released heat increases the temperature of the oil-bearing formation, which causes viscosity reduction by several orders of magnitude and mobilises the flow of the unburned oil fraction (Xia and Greaves, 2000; Xia, et al., 2003; Castanier and Brigham, 2003). The conventional in-situ combustion technique for heavy oil recovery uses vertical injection well and vertical production well (VIVP) arrangement, as illustrated in Figure 2.13. Therefore, the mobilised oil in conventional ISC builds up in the colder region of the oil reservoir before getting to the producer well.

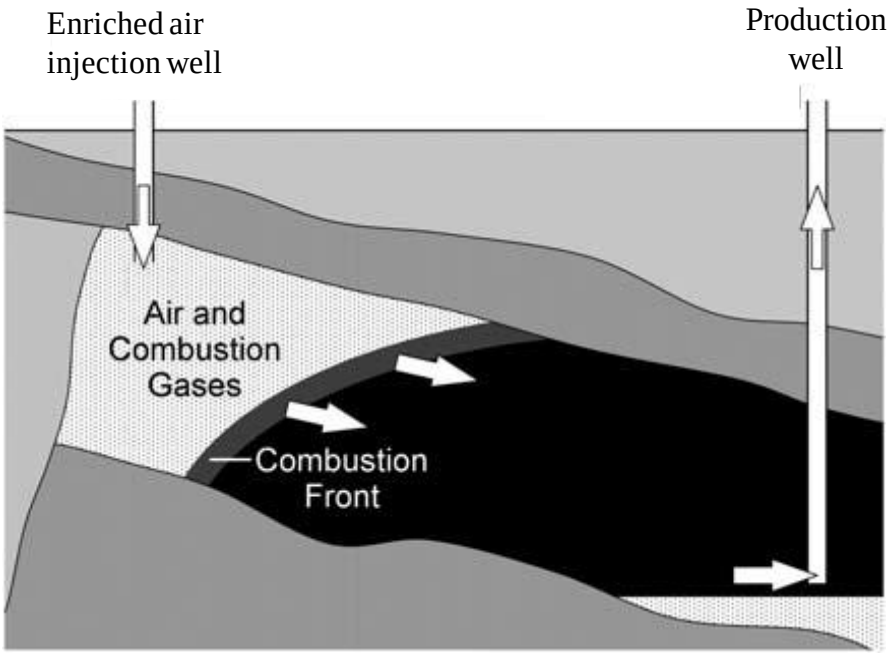

Figure 2.13 Schematics conventional In Situ Combustion (ISC).

The progression of this combustion front in the oil reservoir creates several zones between the injection well and the producer well, in this order: burned zone, combustion zone, cracking region, evaporation and visbreaking region, steam plateau, water bank, oil bank and initial zone, the details of each zones can be found in Castanier and Brigham (2003). An exothermic oxidation reaction is believed to occur between the hydrocarbons and oxygen, while pyrolysis takes at higher temperature. Because of these reactions, the temperature of the oil-bearing formation in the combustion zone can increase in the range of 500-700^{o}C, which is significantly higher compared to steam flooding 150-250^{o}C (Xia and Greaves, 2000). High temperature is favourable for heavy oil as it lowers the oil viscosity drastically and aids pyrolysis of the heavy oil to lighter oil. However, when ISC is operated in high temperature oxidation (HTO), the reactions occurring are (Xia and Greaves, 2001 & 2006):

(a) Thermal cracking (pyrolysis):

Heavy residue → Light oil + Coke (2.1)

(b) Oxidation of coke (HTO):

Coke + Oxygen → CO + CO_2 + H_2O (2.2)

(c) Oxidation of heavy residue:

Heavy residue + Oxygen → CO + CO_2 + H_2O (2.3)

According to Moore et al. (1997), ISC offers many advantages over other EOR methods, because the generation of thermal energy in situ in the reservoir offers: high thermal efficiency in terms of heat utilisation, highly efficient displacement drive mechanism, less environmental impact, and subsequently upgrades the heavy crude oil (Xia, et al., 2002). Despite the extensive laboratory and field studies, the conventional ISC technique has not gained wide acceptance because the process has not achieved the success predicted by the theory (Xia and Greaves, 2006), due to poor control of the process and the challenges associated with the use of VIVP wells for heavy oil recovery.

Nonetheless, the continuous supply of sufficient air flux is necessary to maintain the process in HTO mode. However, a very high gas flux leads to gas overriding and oxygen breakthrough at the production well (Xia and Greaves, 2003). The methods of operating ISC include:

- Forward combustion;
    - dry combustion.
    - wet combustion.
- Reverse combustion;
- High pressure air injection.

In the forward combustion technique, the combustion front moves in the same direction as the air flow towards the production well from the injection well. It is the most widely practiced in the field. The forward combustion is further categorised as "dry" when only enriched air is injected and "wet" when water and air are co-injected (Castanier and Brigham, 2003), while the reverse combustion operation occurs when the combustion front advances in opposite direction to the flow of air. The high pressure air injection is a low temperature oxidation (LTO) process that occurs below 300^{o}C, which does not support combustion leading to the production of oxidized hydrocarbons (Greaves, et al., 2000b; Thomas, 2008).

2.6.5 Toe-to-Heel Air Injection (THAI)

The limitations of the VIVP wells of the conventional ISC process led to the concept of THAI. The THAI technology was developed by the Improved Oil Recovery group at the University of Bath, in collaboration with the Petroleum Recovery Institute, Calgary, Canada in the 1990's (Greaves, 2004). The technology has been field trialled at Christina Lake, Alberta, Canada. It integrates ISC and horizontal production well(s) to create a stable propagation of combustion front, as illustrated in Figure 2.14. The fundamental principles of operations of THAI process are same with conventional ISC process. However, the mobilised oil travels a short distance to the producer well in a region called the mobile oil zone (MOZ). The coke for combustion is produced ahead of the combustion front by thermal cracking of heavy oil (Xia, et al., 2003; Xia and Greaves, 2006).

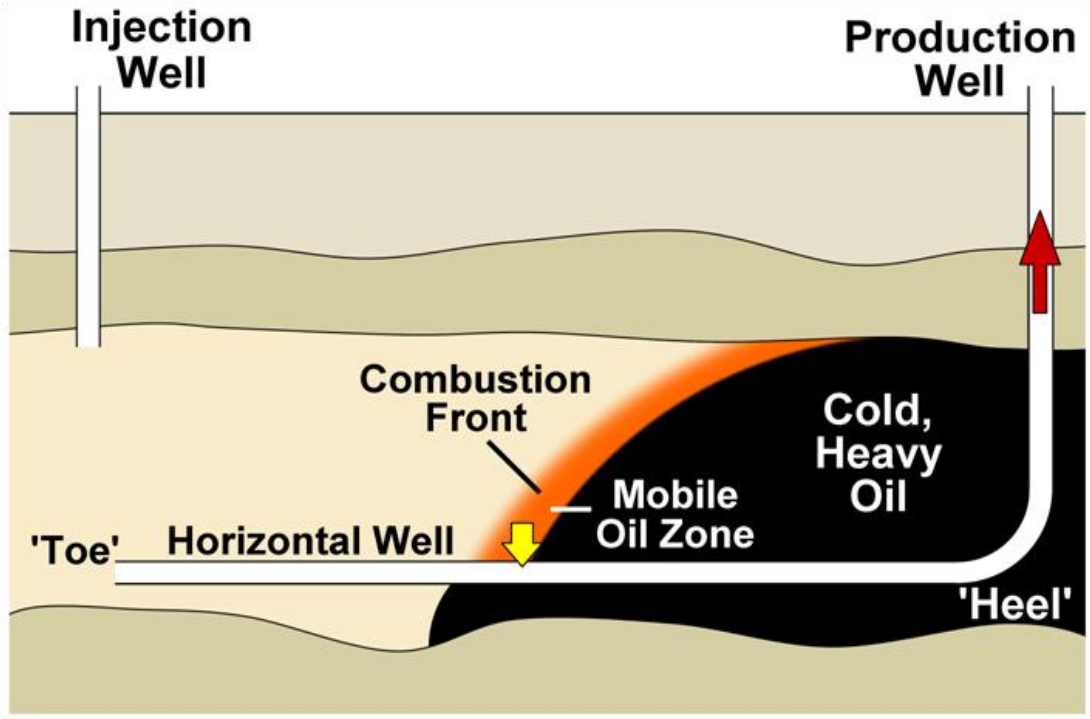

Figure 2.14 Schematic presentation of THAI process.

One of the basic prerequisites for in situ combustion is fuel (i.e., coke material that is rich in carbon) availability in the reservoir, sufficient to support the propagation of the combustion front (Greaves, et al., 2008, 2012; Jinzhong, et al., 2012; Wenlong, et al., 2011). The fuel accessibility is a function of thermal cracking of high molecular weight hydrocarbon molecules. This complex process is primarily a function of: oil composition, porous matrix properties, cracking temperature, reservoir pressure, fluid flow, and temperature (Greaves, et al., 2008; Wenlong, et al., 2011). The main distinguishing feature between THAI process and conventional ISC process is that THAI uses a horizontal producer well(s) instead of vertical producer well as in conventional ISC process (Greaves and Xia, 2004). The propagation of the combustion front from toe-to-heel due to continuous injection of air creates different zones namely: burned zone, combustion front, coke zone, mobile oil zone (MOZ), and cold oil zone, as shown in Figure 2.15, further details can be found in Xia et al. (2002).

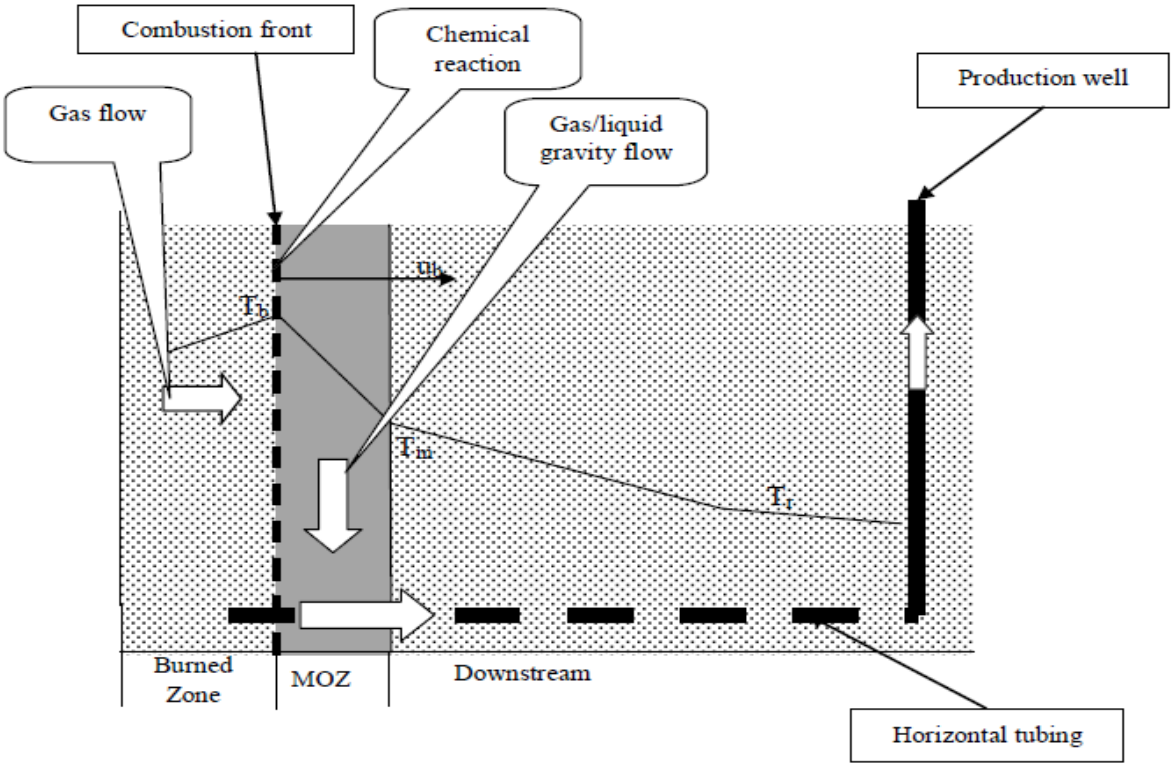

Figure 2.15 Illustration of the recovery and upgrading process in THAI.

The temperature ranges from 500-600 ^{o}C in the combustion zone, to aid thermal cracking (or pyrolysis) of high molecular weight hydrocarbons (see Eq. 2.1). A mobile oil zone (MOZ) is created ahead of the combustion front (see Figure 2.15) where most of the thermal upgrading reactions are occurring. The mobilised and thermally upgraded oil in MOZ does not pass through the cold region as in conventional ISC process, but rather are drawn downward into the horizontal production well(s) via the shortest pathway. This VIHP however eliminates the problem of gas overriding and bypass, as the horizontal well seals as a result of coke formation during the propagation of the combustion front (Shah, et al., 2010; Xia, et al., 2003). However, the recovery factor of THAI process ranges from 70-80% of oil in place (Greaves, et al., 2012; Thomas, 2008). Table 2.1 summarizes the main benefits of THAI process for the recovery of heavy oil and bitumen.

Table 2.1 Benefits of THAI process for recovery and upgrading of heavy oil (Xia, et al., 2003).

1. controlled gas override, resulting in a quasi-upright in situ combustion front
2. High sweep efficiency due to the absence of gas channelling in the producer
3. Less environmental impact due to the removal of sulphur and heavy metals
4. Maintain process in HTO mode, avoiding LTO mode as a result of high air flux
5. Unique enhanced mobile oil zone (MOZ) ahead of the combustion front reduces sensitivity to reservoir heterogeneity in the virgin zone.
6. Front tracking capability through its 'toe-to-heel' propagation with tight control of propagation.
7. Create ideal condition for downhole catalytic upgrading, through CAPRI^{TM} process.

According to the available results from 3D combustion cell (0.6 x 0.4 x 0.1 m) experiment and study carried out by Greaves et al. (2012), the propagating front average temperature of 500-550 ^{o}C, and *in situ* upgrading up to 16-17^{o} API gravity compared to 10.9^{o} for the feedstock was reported. The API gravity increment was the result of thermal cracking of the heavy fractions into lighter component in MOZ. In addition to the oil undergoing pyrolysis, upgrading reactions could also result from the natural catalytic activity of the host rock. In another study of THAI fire-flooding process by Jinzhong et al. (2012) and Wenlong et al. (2011) using 3D sand-pack cell (0.4 x 0.4 x 0.15 m) consisting of injection, production, and measuring and control systems. The experiment was performed for heavy oil viscosity of 12,090 mPa.s at 50 ^{o}C, sand-pack porosity of 39%, injected air/oil ratio 1400 m^3/m^3, and oil saturation of 84%. They found that the combustion front could reach temperature as high as 600 ^{o}C with average in the range of 450-550 ^{o}C, with 70 % recovery of OOIP.

2.7 Heavy Crude Oil Upgrading Technologies

The need to upgrade heavy oil into cleaner and more valuable light oil is increasing continuously, in order to sustain future fuel needs. However, heavy oils and bitumen properties such as high viscosity/low fluidity, high density/low API gravity, high asphaltenes, sulphur, and metal does meet refinery feedstock specifications. Therefore, the objectives of upgrading are 1) to reduce the viscosity to aid production and pipeline transportation without diluents addition and 2) to produce synthetic crude oil that meets the qualities of refinery feedstock (see Figure 2.16).

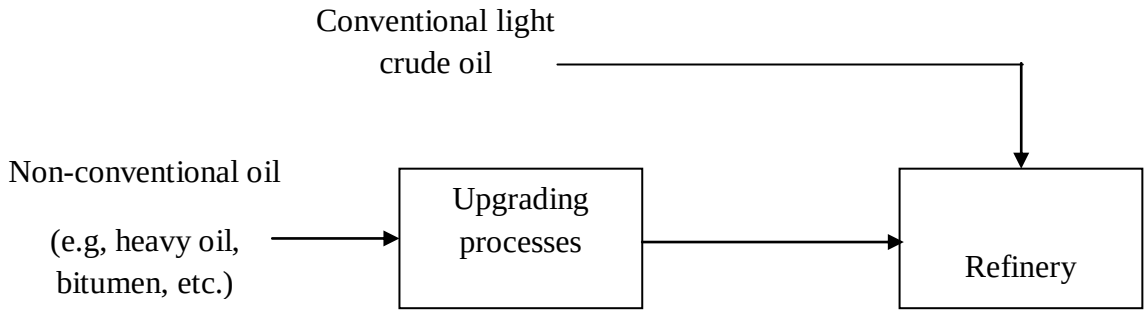

Figure 2.16 Route to refinery for conventional and non-conventional oils.

Consequently, upgrading heavy oil and bitumen is pivotal to the economics of their exploitation, as it adds to the total capital cost of making them commercially viable (Hedrick, et al., 2006). In addition, the profitability of heavy crude oil/bitumen upgrading is a function of the market value, i.e., the price differential between the heavy oil and the upgraded oil (Leyva, et al., 2007). Thus, the rising price of crude oil globally favours heavy oil exploitation. The upgrading technologies are generally classified under two headings, namely surface upgrading and in-situ upgrading (Speight, 2009). The different technologies used in upgrading heavy oil and bitumen are presented in Figure 2.17.

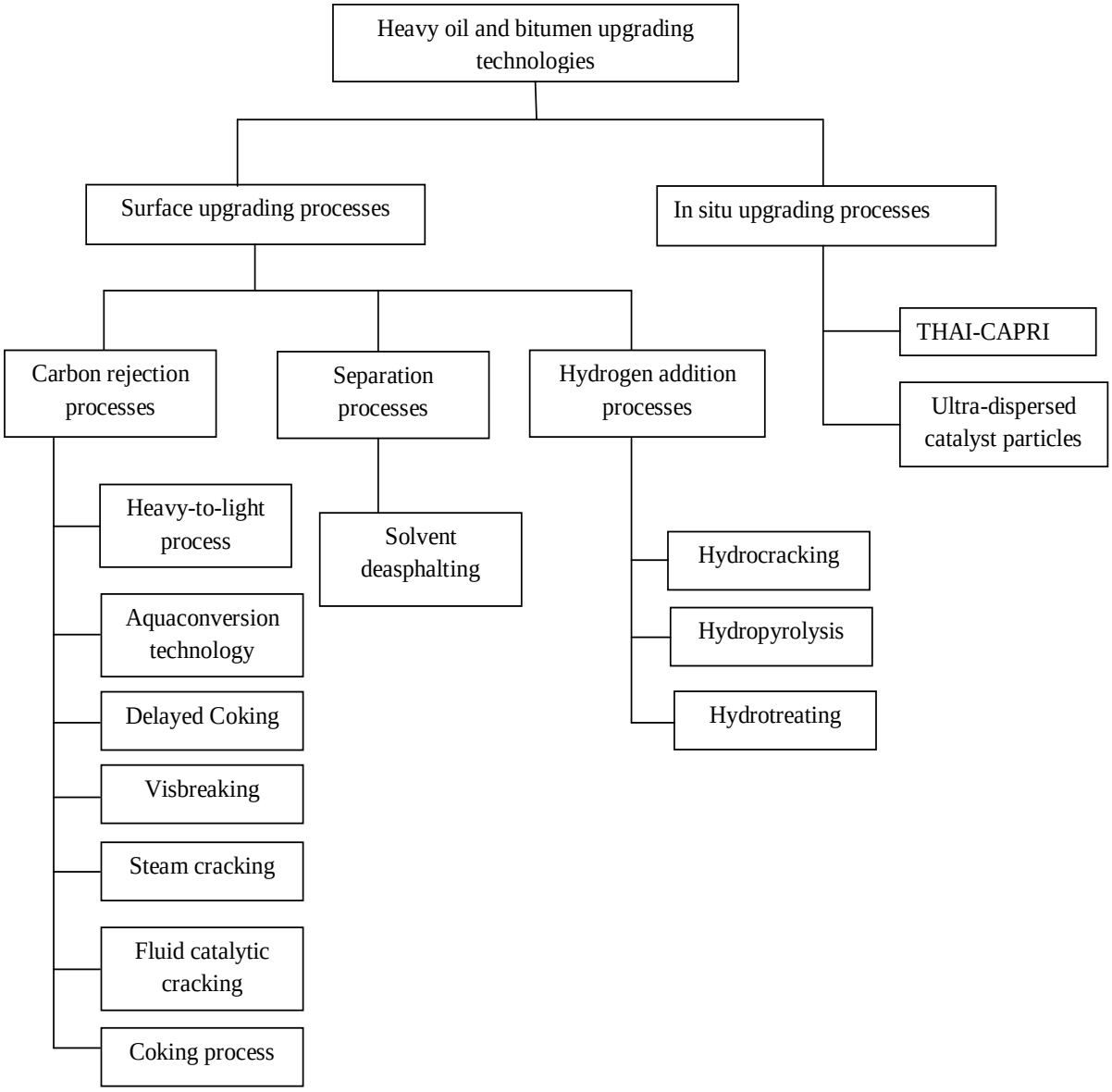

Figure 2.17 Classification of heavy oil upgrading processes.

The conversion of heavy crude oil to synthetic light crude oil is either accomplished by carbon-rejection (i.e., thermal cracking reducing carbon content), hydrogen-addition (i.e., hydroprocessing increasing hydrogen content), and/or solvent deasphalting.

2.8 Surface Upgrading Processes

Existing refineries can be modified to accommodate heavy oil/bitumen or a stand-alone upgrading facility can be used convert the heavy oil into synthetic light crude suitable for conventional refineries. A surface upgrading facility is an integrated collection of two or more unit processes mentioned in Figure 2.17. However, surface upgrading is cost and energy intensive and also faced with environmental pollution problems associated with emissions (Shen, et al., 2008).

2.8.1. Coking Processes

The coking process was first used by Great Canadian Oil Sands (now Suncor) in 1967, to upgrade heavy crude oil (Flores, 2010). Coking is the generic term for thermal conversion (i.e., carbon-rejection process) used to upgrade heavy crude oils, bitumen or atmospheric/vacuum distillation residues to light oils, with coke as by-product. However, the coking process is a severe thermal cracking of high molecular weight hydrocarbons into light weight hydrocarbons performed at high temperature range of 450-520^{o}C. There are three main coking processes, namely delayed coking, fluid coking and flexicoking (Hsu and Robinson, 2006; Sawarkar, et al., 2007).

Delayed coking is a semi-continuous process in which the heavy crude oil is heated in a furnace to initiate thermal cracking and charged into a large coking drum. The coking drum provides a sufficient residence time necessary for the cracking reactions to proceed to completion (Sawarkar, et al., 2007). The produced coke accumulates at the bottom of the drum. To aid continuous upgrading two coking drums are used. The cracked product is sent to

a hydrocracking/hydrotreating unit to improve stability and H/C atomic ratios, as shown in Figure 2.18.

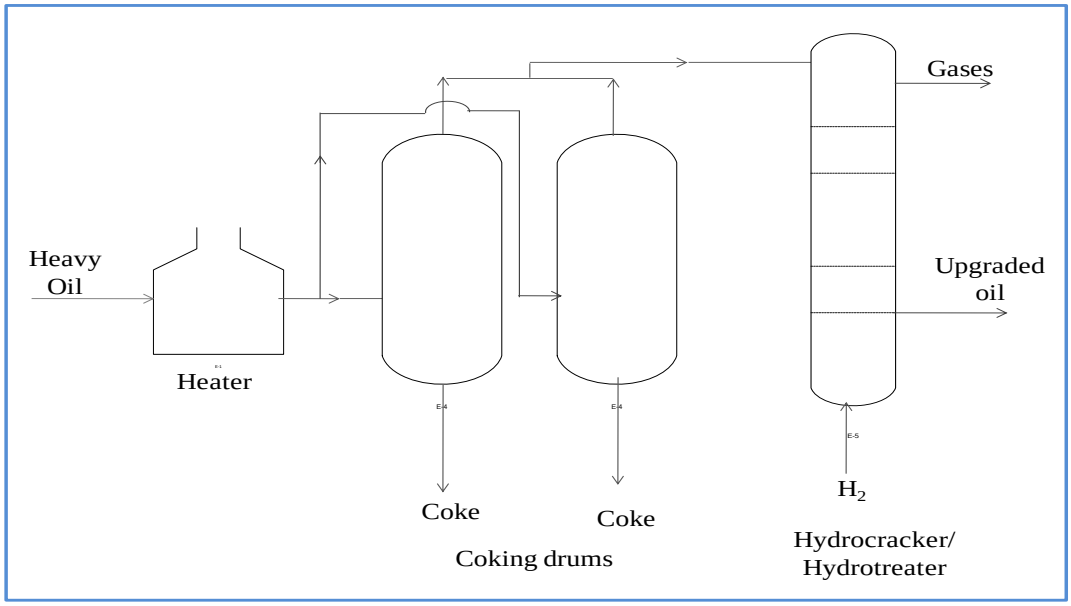

Figure 2.18 Schematic diagram of delayed coking upgrading process.

The coking process is capable of accounting for up to 30 wt% of the product as produced coke, making it challenging in term of handling the coke stockpiles generated (Hsu and Robinson, 2006). Despite the fact that it is the most preferred surface upgrading technology by refiners, high coke formation and low liquid product are some of the demerits of the process. In addition, the emissions of greenhouse gas (GHG) have been a major environmental concern regarding the use.

Meanwhile, fluid coking (continuous coking) involves the use of a fluidized-bed of hot coke particles to convert the heavy crude oil into light oil, as it is atomised into the fluid bed. The hot coke particles aid the thermal cracking reactions in the reactor. The fluid coking

process consists of a reactor and a burner. The cokes deposited on the particles are burned-off in the burner and the particles recycled. However, the operating temperature is higher than that of delayed coking, while the contact is time for cracking reactions is short. This condition therefore reduces the amount of coke generated in fluid coking process.

2.8.2. Hydroprocessing

Hydroprocessing of heavy crude oil includes hydrocracking and hydrotreating, respectively. In this process, cracking of the heavy crude is accompanied by hydrogen-addition reactions, which facilitates the termination of many of the coke forming reactions in the course of the cleavage of C-C bond. Hydroprocessing does not only upgrade the heavy crude oil, but also produce synthetic oil of lower heteroatom and metal content (Leyva, et al., 2007). While coking processes lower the carbon content, hydroprocessing increases the hydrogen content with little carbon-rejection. In addition to dealkylation of aromatic rings and C-C bond cleavage are hydrodesulphurisation (HDS), hydrodenitrogenation (HDN), hydrodemetallisation (HDM), and hydrodeasphaltenization (HDAs), which are reactions occurring simultaneously with hydrocracking during the process (Hsu and Robinson, 2006; Leyva, et al., 2007).

Hydroprocessing reactors used to upgrade heavy oil or residues are typically operated as fixed-bed, slurry phase, ebullating-bed, or moving bed of catalysts (Scherzer and Gruia, 1996). The commonly used catalysts are combinations of the following transition metals such as Ni, Co, Mo, W, Pd, etc. (e.g., Ni-Mo, Co-Mo, Ni-W, Co-Pd, etc.) supported on solid acidic silica, alumina (i.e., Al_2O_3), or zeolites (Leyva, et al., 2007). The profitability of the process is a function of the catalyst lifetime. In spite of decreased coke formation, high hydrogen

partial pressure is required (Batholomew, 1993). Moreover, the reaction conditions of temperature, pressure (or hydrogen partial pressure) and space velocity influences the process (Sanchez and Ancheyta, 2007). On the other hand, when impurities and heteroatoms are to be removed from the crude oil/distillates, the process is called non-destructive (i.e., hydrotreating)

2.8.3. HTL (Heavy-to-Light) Upgrading Technology

The Rapid Thermal Processing, RTP (now HTL) was developed by Ivanhoe Energy Inc. in the 1980s. The HTL process is similar to the fluidized catalytic cracking (FCC) unit, however it is non-catalytic. The technology uses a circulating transport bed of hot sand to rapidly induce thermal cracking of the heavy crude oil/bitumen in the absence of air to convert them to a synthetic light crude oil, as shown in Figure 2.19 (Silverman, et al., 2011). The HTL begins with atmospheric and vacuum pre-fractionation process as illustrated in Figure 2.19. These initial fractionations add to the cost of the process. Also, the extent of upgrading depends on sand-to-oil ratio and contact time, and it is a stand-alone upgrading facility. Details of the HTL process can be found in Silverman et al. (2011), Koshka, et al. (2008) and Veith, et al. (2007), respectively.

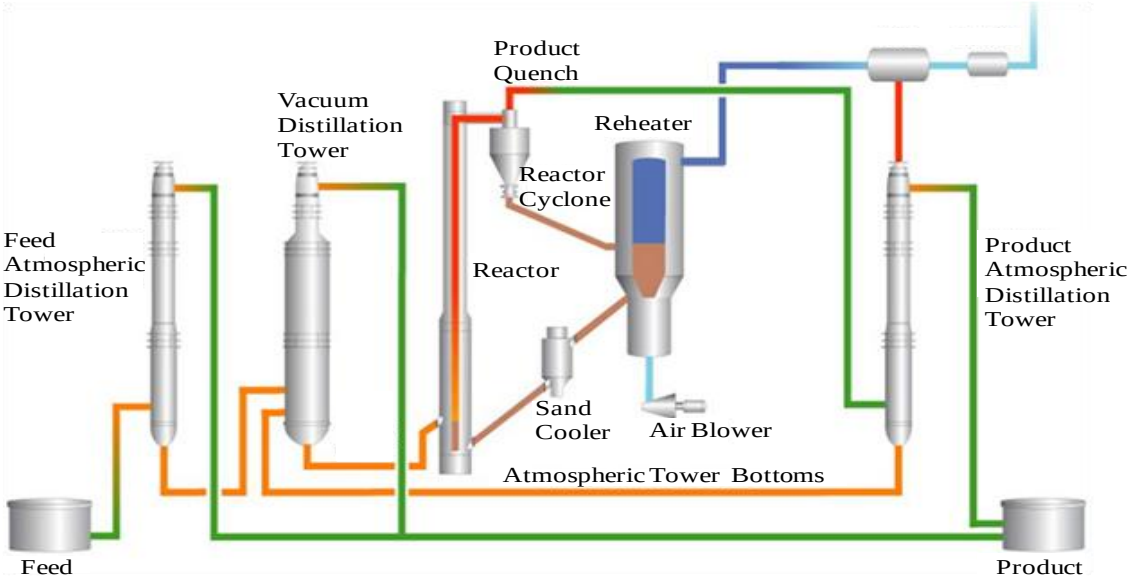

Figure 2.19 HTL process flow diagram (Silverman, et al., 2011).

Subsequently, the cost of HTL surface upgrading process ranges from USD $12,000-$20,000 per installed barrel of capacity, which depends on the scale, configuration and heavy crude oil properties (Silverman, et al., 2011).

2.8.4. Visbreaking

Visbreaking (viscosity breaking) is a non-catalytic mild thermal cracking process used to upgrade heavy crude oil with the aim of reducing viscosity as well as pour point (Ogbuneke, et al., 2009; Joshi, et al., 2008). The process is mainly used in the petroleum industry to upgrade heavy residue from atmospheric and vacuum distillation, to enhance the production of naphtha and light distillate, respectively. The heavy crude oil is heated to a temperature of about 480^{o}C and transferred to a soaker at a pressure range of 140-300 psig (Hsu and Robinson, 2006). Most of the thermal cracking and viscosity reduction occur in the soaker.

The residence time in the soaker is short compared to delayed coker process. Thus, the stability of the visbroken product depends on the heavy crude oil characteristics such as paraffin, aromatic, asphaltenes, and heteroatom content (Kataria, et al., 2004). However, during visbreaking, some C-C bonds split leading to reduction in carbon number, aromatics and resins undergo dealkylation reaction, and asphaltenes also condensation reactions (Fainberg, et al., 1996).

2.8.5. Solvent Deasphalting

This involves selective removal of asphaltenes from the heavy oil. In this respect, the solvent deasphalting process makes use of the fact that asphaltene compounds are insoluble in light hydrocarbons such as n-alkanes or paraffin, e.g., propane, butane, heptane, etc. to selectively precipitate the asphaltenes present in the heavy crude oil (Hsu and Robinson, 2006). The process separation is achieved by molecular weight (i.e., density) rather than boiling point.

The blend is heated slightly above the critical temperature of the used solvent, and pumped into a rotating-disc solvent extraction tower at a temperature range of 65-120 ^{o}C and pressure of 350-600 psig (Hsu and Robinson, 2006). The product is charged into a solvent evaporator and steam stripped to recover used solvent. The deasphalted oil (DAO) has a relatively low content of metals (Speight, 2009). A typical solvent deasphalting scheme is shown in Figure 2.20.

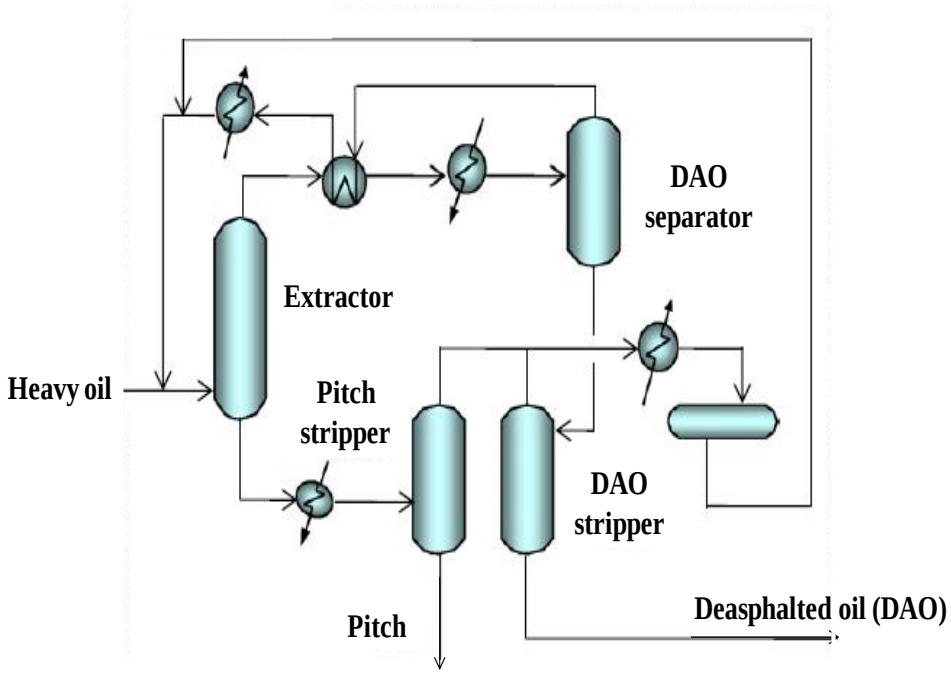

Figure 2.20 Deasphalting scheme for heavy oil

The choice of solvent and solvent-to-oil ratio is crucial to the performance of the deasphalting process in terms of DAO quality and yield. The critical temperature influences the extraction temperature, which directly affects the extent of viscosity reduction. Dual solvents such as a mixture of butane and heptane can provide some extent of flexibility. However, the process is limited by high cost of energy and light hydrocarbon solvents (Sawarkar, et al., 2007). The recovery of used solvent may account for most of the energy requirement.

2.8.6. Aquaconversion (or aquathermolysis)

Aquathermolysis is an *in situ* catalytic upgrading process carried out under a steam environment. In this process, the high temperature steam reacts with the oil in the presence of

catalyst; this was first studied by Hyne et al. (1982). The heat released by the steam pyrolyzes the large molecular weight hydrocarbons present in the heavy oil in the presence of catalyst into light hydrocarbon components (Wang, et al., 2010). The chemical reaction detail for aquathermolysis proposed by Hyne et al. (1982) is:

$$RCH_2\text{-}CH_2S\text{-}CH_3 + 2H_2O \rightarrow RCH_3 + CO_2 + H_2 + H_2S + CH_4$$

Notably, the breaking of C-S bond and the generation of hydrogen gas from water are the main mechanism of aquathermolysis. Nevertheless, the produced hydrogen improves the stability of the liquid product. The process has the potential of converting heavy crude oil into synthetic crude oil (syncrude) with reduced viscosity and high API gravity. In addition, aquathermolysis does not yield much solid-byproduct such as coke nor does it require external hydrogen, as the hydrogen-donor is steam (Speight, 2009). With the aid of catalysis, the pyrolysis of the heavy oil is enhanced, its viscosity reduced significantly to enhance the extraction of the oil (Wang. et al., 2010).

Though steam reduces viscosity by some order of magnitude, the issue of viscosity regression with time remains a concern. The viscosity regression is attributed to the interaction between the heteroatoms in the oil and other groups through hydrogen bonding or van der Waals forces which lead to the formation larger molecules that cause viscosity regression (Wang, et al., 2010). Furthermore, steam acts as a hydrogen-donor to support hydrogenation, hydrodesulphurisation, hydrodenitrogenation, and hydrodemetallisation reactions, respectively. Another limitation of the method is that the generation of steam is expensive, as it requires large amount of water and natural gas.

2.9. In-situ Upgrading Processes

Commonly used surface upgrading processes, have shown to be environmentally unfriendly, in addition to the costs of building stand-alone facilities and emission of gaseous pollutants such as CO_2, H_2S and other pollutants. The petroleum industries are presently focusing attention on *in situ* upgrading of heavy oil. In-situ upgrading of heavy oil/bitumen in the reservoir presents a number of advantages, such as production of low-viscosity oil that can be transported without diluent addition, and that some of the impurities in the heavy oil are left behind in the reservoir during extraction and upgrading process in-situ.

Furthermore, *in situ* upgrading of heavy oil prior to reaching the surface in the reservoir offers significant economic and environmental advantages over surface upgrading techniques, because it is less capital intensive, can be applied on a well by well basis, produces valuable product, and reduces demanding downstream processing (Moore, et al., 1999). Subsequently, the reservoir serves as the reactor which implies that there is no need to build a large costly pressure vessel as in the case of surface upgrading technology (Weissman, et al., 1996). Weissman et al. (1996) and Moore et al. (1999) have outlined the requirements for a successful down-hole or in situ catalytic upgrading of heavy oil in the reservoir, which are: provision and placement of a down-hole catalyst bed in the oil-bearing formation, creating appropriate reaction conditions of temperature and pressure at the catalyst bed and process, mobilisation of heavy oil and co-reactants such as hydrogen, water, or carbon monoxide over the catalyst in order to achieve adequate catalytic upgrading and produce upgraded oil. The *in situ* upgrading processes include ISC, THAI and THAI-CAPRI.

2.9.1 CAtalytic upgrading PRocess In-situ (CAPRI)

In 1998 the Improved Oil Recovery group at the University of Bath, UK, in collaboration with the Petroleum Recovery Institute (PRI), Calgary, Canada, developed the CAPRI^{TM} process. The concept is based on THAI process, by placing an active catalyst layer between the concentric slotted liners of the horizontal production well(s), as illustrated in Figure 2.21. This creates a down-hole catalytic reactor aimed at achieving further upgrading of the heavy crude as it flows across the catalyst layer, in addition to thermal upgrading occurring (Xia and Greaves, 2001b; Shah, et al., 2011). The produced oil possesses improved fluidity for pipeline transport and decreased impurities.

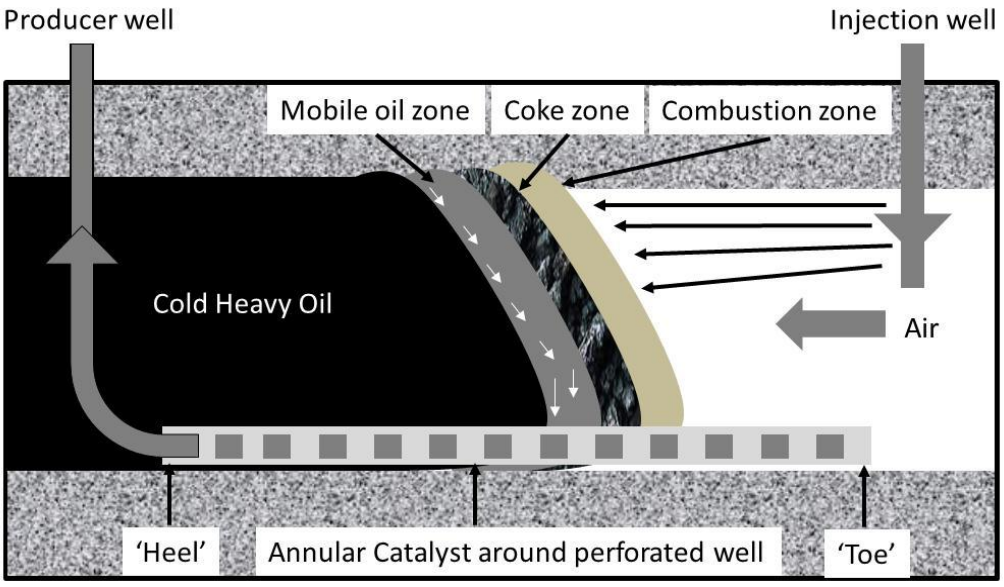

Figure 2.21 Schematic of the THAI-CAPRI process

Xia and Greaves (2001) experimentally demonstrated the potential of THAI-CAPRI using Wolf Lake heavy oil. The result showed that THAI alone achieves roughly 10^{o}

increment of API gravity in the produced oil, with a further increase in the range of 4-7^{o} API points upon the addition of CAPRI. The produced oil had a low viscosity of 10 mPa.s at 20^{o}C. In another investigation Xia, et al. (2002) carried out a series of 3-D combustion cell experiments, using Lloydminster heavy crude oil (11.9^{o}API) and Co-Mo/alumina HDS catalyst at a temperature of 500-550^{o}C. They found that the oil recovery factor was 79% OOIP and upgraded oil was 23^{o} compared to 11.9^{o}API initially, with low viscosity of 20-30 mPas. These results show that THAI-CAPRI process has the potential to convert heavy crude oil to almost light crude oil in a single step and with a recovery factor in a range 79-85% OOIP, without resorting to expensive surface upgrading process.

On September 22nd 2008, Petrobank Energy and Resources Ltd. announced the first THAI-CAPRI^{TM} production (Petrobank, 2008). The well (P-3B) located at Whitesands near Conklin, Alberta, Canada, commenced production in August, 2008. The P-3B well demonstrated the additional upgrading ability of the CAPRI section, as reported in the laboratory scale experiments of Xia, et al. (2002). Subsequently, the P-3B well has been in continuous production, with oil production level up to 400 barrels per day on low air injection rate and limited sand produced from the sandstone reservoir encountered at Whitesands (Petrobank, 2008).

The hydroprocessing catalyst used for *in situ* catalytic upgrading are derived from oxides of transition metals of group VIB such as Mo, W, and group VIII such as Co, Ni, supported on high-surface-area alumina, silica, or silica-alumina. Examples are: Ni-Mo/Al_2O_3, Co-Mo/Al_2O_3, Ni-W/Al_2O_3, Pd-Rh promoted Co/HPS (high porous saponite) (Hossian, et al., 2004), and active carbon (Fukuyama, et al., 2004). In the work of Shah et al. (2011), it was found that coke and metals are deposited on the catalyst during reaction and rapidly deactivate the catalyst in the CAPRI section within a short time period (typically a few

hours). Though, catalyst deactivation is inevitable, extending the catalyst lifespan could improve the process economy. In this study, various means of extending catalyst lifetime while improving upgrading will be explored by using hydrogen-addition, guard bed on top of the catalyst, in-situ steam generation and its impact on coke reduction, and alternative contacting pattern with nanoparticulate catalyst.

The cracking functions are provided by the acidic alumina support, whereas the Co, Ni, and Mo metals perform the hydrogenation function. It is imperative to maintain rapid molecular transfer between the acid sites and the hydrogenation sites in order to avoid undesirable coke formation reaction. Coke formation suppression due to hydrogen-addition is widely thought of as capping of free radical coke precursors, formed when carbon-carbon and carbon-heteroatoms bonds split, leading to lower molecular weight compounds than the original feed oil molecules (Benito and Martinez, 1996; Galarraga, et al., 2012). Active hydrogen is released from the dissociation of hydrogen molecules on the metal sites of the catalyst, and then subsequently reacts with coke precursors to form a stable molecule (Liu, et al., 2003; Rezaei, et al., 2012).

Comparing THAI-CAPRI with SAGD, the most commonly used thermal EOR method, it is obvious that SAGD projects are capital intensive in line with rising oil prices, with some projects built at ~C$30,000-35,000/bbl/day five years ago, with a large amount of natural gas and water is required to create steam for SAGD or CSS (Macquarie, 2010). A surface upgrading plant was recently proposed for the UK at a cost of $2-3 billion, while the THAI-CAPRI process could potentially cost a fraction of the surface upgrading process because standard hydrotreating (HDT) catalysts are relatively cheap (Shah, et al., 2010). Additionally, CAPRI uses the in-situ generated energy via combustion to drive the upgrading

reactions, from which produced oil has enough fluidity for pipeline transport with little or no diluents required.

The conventional CAPRI fixed-bed horizontal production well presented in Figure 2.21 stand the risks of well plugging as a result of asphaltenes and coke deposition, which can cause possible shutdown as well as loss of production stability (Hashemi, et al., 2013). In this respect attention has been turned to slurry-phase *in situ* catalytic upgrading with nanoparticules. Dispersed nanoparticulate catalysts display several advantages over their pelleted counterpart such as high metal utilisation due to the absence of diffusion limitation, more active sites per unit mass, reduces the chances of pore plugging experienced in fixed-bed, and high moderation of coke formation and deactivation (Alkhaldi and Husein, 2014; Galarraga and Pereira-Almao, 2010; Hashemi, et al., 2013; Angeles, et al., 2013). The formulation of nanoparticulate catalysts is similar to that of conventional pelleted catalysts in which soluble precursors or water-in-oil emulsions containing metallic precursors such as Mo, W, Co, Ni, or mixture thereof is used (Galarraga, et al., 2012). Galarraga and Pereira-Almao (2010) tested trimetallic (Ni-W-Mo) submicronic catalyst in a batch reactor for dispersed-phase upgrading at 380^{o}C, a stirring speed of 500 rpm, and reaction time 3-70 h. After upgrading reactions, they found that the produced oil sample (API gravity 16o and viscosity at 40^{o}C, 60 cP) compared to the Athabasca bitumen (API gravity 9.5^{o} and viscosity 7,680 cP). However, it is challenging to recover and reuse the catalyst powder after reaction.

2.10 Chemistry of Heavy Oil Upgrading

Heavy crude oil and bitumen are complex mixtures of about 10^5-10^6 different hydrocarbon components (Wiehe, 1999). Therefore, the chemistry of heavy crude oil

upgrading is complicated, because of the many complex reaction mechanisms involved in the thermal and catalytic upgrading to syncrude. The two main reaction routes to upgrade heavy crude oil to synthetic light crude oil either carbon-rejection and/or hydrogen-addition, with or without catalyst, basically driven by thermal energy (Heck and Diguiseppi, 1994). The overall aim is to improve H/C atomic ratio, decrease heteroatom (e.g., S, N, etc.) and metals (e.g., Ni, V, Fe, etc.), lower the viscosity, and increase the yield of distillates. Consequently, upgrading occurs as a result of bond breaking. The most significant bond dissociation that leads to upgrading is the cleavage of C-C bonds. The dissociation energies of the common bonds found in the crude oil is presented in Table 2.2.

Table 2.2 Bond dissociation energy (Rahimi and Gentzi, 2006)

Bonds	**Kcal/mol**
H-H	103
C-C	83-85
C-H	96-99
N-H	93
S-H	82
O-H	110-111
C=C	146-151
C-N	69-75
C-S	66
Ar-CH_2-CH_2-Ar	71
Ar-H	111

* Ar is an aromatic hydrocarbon

Furthermore, Hsu and Robinson (2006) outlined the numerous possible chemical reactions that occur during upgrading, they include: homolytic cleavage of C-C bonds, side chain fragmentation (or cleavage), ring growth, hydrogen shuttling, hydrogenation of

aromatic/dehydrogenation of cycloparaffins, ring opening, heteroatom and heavy metals removal. It is believed that the reaction mechanism during upgrading proceeds via the formation of free radicals, as a result of the cleavage of C-C bond through free radical chain reactions (Gray, 1994). Other reactions that take place in upgrading include thermal and catalytic cleavage of C-C, C-S, and C-N bond dissociation (McMillan, et al., 1994; Rahimi and Gentzis, 2006). From Table 2.2, it is clear that C-S has the lowest bond dissociation energy; therefore it will easily break at low temperatures.

2.11 The Mechanism of Catalytic Upgrading

The mechanisms of catalytic upgrading are discussed in this section, in order to later explain the observed experimental results. The catalytic upgrading reactions proceed through the carbonium ion intermediate and beta-scission (Jian-hong, et al., 2008). The carbonium ions are hydrocarbon ions having a positive charge on a carbon atom. This mechanism is similar to the chain reaction mechanism in thermal cracking. However it has three basic stages: initiation step, chain propagation, and termination. The initiation step begins with formation of carbenium ion generated by paraffin cracking over the acid sites of the catalyst, which was initiated by the direct attack of the Brønsted acid sites on C-C and/or abstraction of a hydride ion (H^-) from C-H bonds. Additionally, the other routes through which carbenium ions may be generated include: 1) protolytic cracking, 2) hydride abstraction of paraffins, or 3) protonation of olefins by Brønsted acid sites (Lee, et al., 2011).

Thereafter, a series of hydride ion transfers from the hydrocarbon molecules to carbocations takes place in the chain propagation stage, yielding carbenium ions steadily. In some cases, the generated carbenium ions undergo isomerisation to stable secondary or

tertiary carbenium ion through hydride shift or alkyl shift (Lee, et al., 2011). However, the produced carbenium ions could split to various smaller hydrocarbons through β-scission, hydride transfer, isomerisation, cracking, alkylation/dealkylation, protonation/deprotonation, ring opening (i.e., naphthenic), cyclisation, etc. In the termination stage the carbonium ions are depronated from the catalyst, collapse to give light hydrocarbons and/or hydrogen, and tri-co-ordinated carbenium ions (Jian-hong, et al., 2008). In Figures 2.22 and 2.23, the cracking pathways for paraffins, naphthenes, and aromatics are illustrated, respectively.

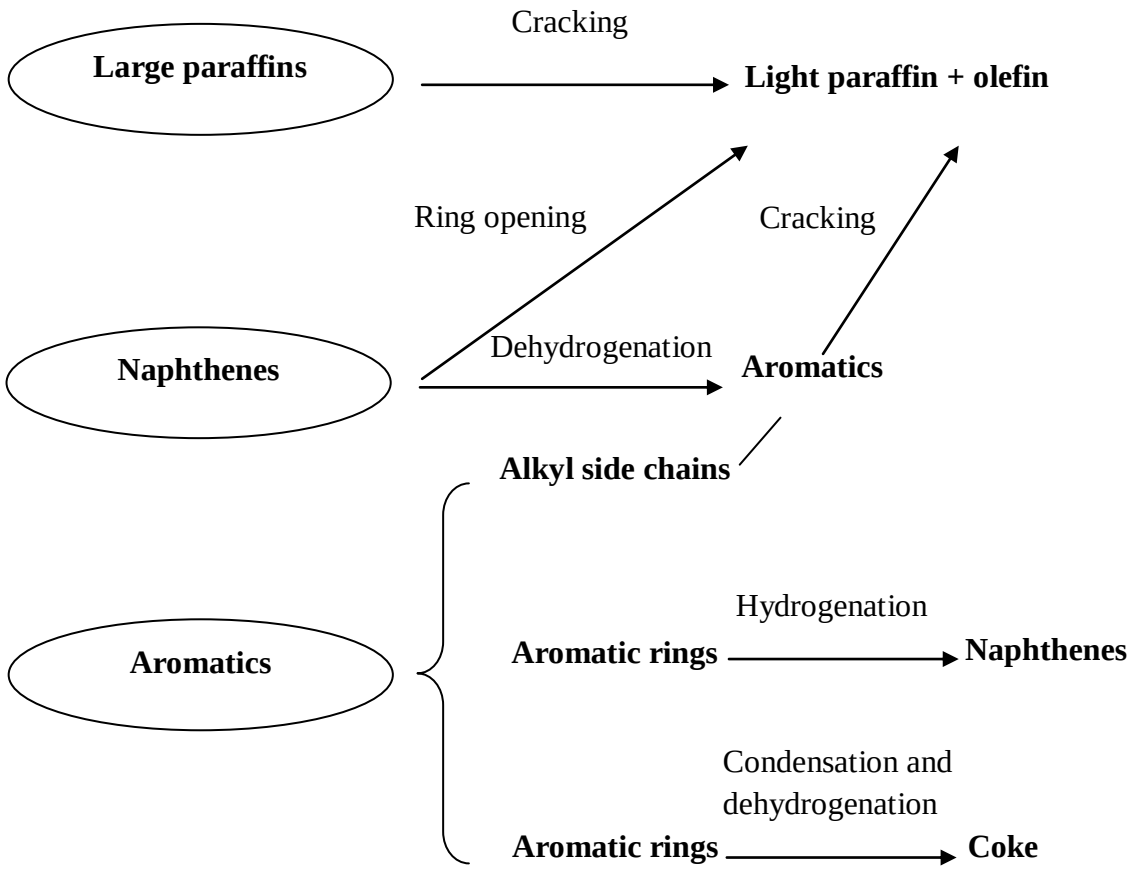

Figure 2.22 Reaction pathways for paraffins, naphthenes, and aromatics.

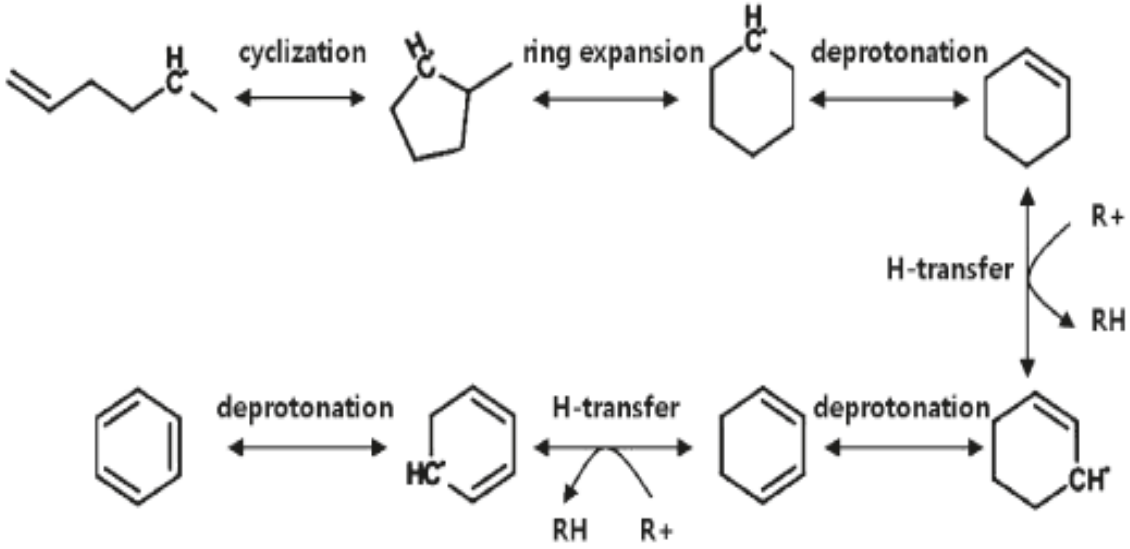

Figure 2.23 Aromatic cracking mechanisms (Lee, et al., 2011).

The several classes of reactions occurring are illustrated in Table 2.3. These reactions may be responsible for the occurrence of low-boiling components in the upgraded oil (Pashikanti and Liu, 2011).

Table 2.3 Key classes of catalytic upgrading reactions during CAPRI process.

Description	**Reactants and products**
Class 1: Cracking reactions	
Paraffin cracked to smaller paraffin and olefins:	$C_{m+n}H_{2[(m+n)+2]} \rightarrow C_mH_{2m+2} + C_nH_{2n+2}$ $C_nH_{2n+2} \rightarrow C_mH_{2m+2} + C_{n-m}H_{2(n-m)}$ $n > m$
Olefins cracked to smaller olefins:	$C_{(m+n)}H_{2(m+n)} \rightarrow C_mH_{2m} + C_nH_{2n}$
Aromatics side-chain cracked:	$Ar\text{-}C_{(m+n)}H_{2(m+n)+1} \rightarrow Ar\text{-}C_mH_{2m-1} + C_nH_{2n+2}$
Naphthenes (cycloparaffins) cracked to olefins and smaller naphthenes:	$C_{(m+n)}H_{2(m+n)}$ (naphthene) $\rightarrow$ C_mH_{2m} (naphthene) + C_nH_{2n} (olefin)
Class 2: Dehydrogenation and hydrogenation	
Paraffin dehydrogenated to olefin:	$n\text{-}C_nH_{2n+2} \rightarrow C_nH_{2n} + H_2$
Naphthenes dehydrogenated to aromatics:	Naphthene $\rightarrow$ Aromatic + $3H_2$

Olefin to paraffin:	$C_nH_{2n} + H_2 \rightarrow C_nH_{2n+2}$ or $C_nH_m + H_2 \rightarrow C_nH_{m+2}$
Class 3: Hydrogen transfer	
Paraffins and olefins converted to aromatics and paraffins:	C_nH_{2n} (naphthene) C_mH_{2m} (olefin) $\rightarrow$ Ar-C_xH_{2x+1} (aromatic) + C_pH_{2p+2} (paraffin) where $x = m + n - 6 - p$
Class 4: Isomerisation	
Normal paraffin to isoparaffin:	n-$C_nH_{2n+2} \rightarrow$ i-C_nH_{2n+2}
Normal olefin to iso-olefin:	n-$C_nH_{2n} \rightarrow$ i-C_nH_{2n}
Class 5: Polymerisation and condensation of aromatics rings	
Condensation of mono-, di-, and tri-aromatics to poly-aromatics:	Ar-$CHCH_2$ + R_1CH-$CHR_2 \rightarrow$ Ar – Ar + H_2
where; Ar is aromatic compound, and R_1, R_2 are alkyl group	

2.12. Conclusion

In this Chapter, various heavy oil recovery and upgrading technologies were reviewed. The advantages and limitations of each process were highlighted. Findings showed that combining extraction and upgrading in-situ has several advantages over surface upgrading. Also, thermal extraction process has superior advanatages nonthermal processes. The review of the CAPRI process for in-situ downhole upgrading of heavy oil revealed that rapid catalyst deactivation as result of asphaltenes, coke and heavy metals deposition impact adversely on the economy and operations. Therefore, in subsequent Chapters extending catalyst lifetime by minimising coke and metals deposition will be explored. Alternatively, contacting the heavy oil via nanoparticles application to THAI-CAPRI technology was investigated and reported.

Chapter 3

Materials and Method

3.1 Introduction

Crude oil remains a major provider of not only transportation fuels, but also feedstock for paint, plastics, fertilizer and related industries. It is well known that light and heavy crude oils have outstanding differences. Upgrading therefore is aimed at producing oil with similar characteristics as light oil.

The in-situ catalytic upgrading process (CAPRI) starts with in-situ combustion to supply thermal energy to the reservoir by heating the heavy oil and the rocks to high temperature (400-550 ^{o}C). This will induce cracking reactions as well as drive catalytic conversion incorporated to the horizontal well to reduce viscosity, remove impurities and produce upgraded oil. The overview of the CAPRI experimental method and analytical schemes used in this study is presented in Figure 3.1. The presence of hundreds of component undergoing different reactions and competing for active sites of the catalysts contribute to the complexity of the CAPRI. Details of the feed oil properties, experimental procedures, catalyst characteristics, and assay of crude oil used to evaluate the level of upgrading relative to the feedstock are presented in the following Sections. The catalyst performance assessment was based on their ability to crack heavy fraction of the feed oils with boiling point above 343 ^{o}C into lighter fractions, increase API gravity, decrease viscosity, remove impurities, and less prone to coking.

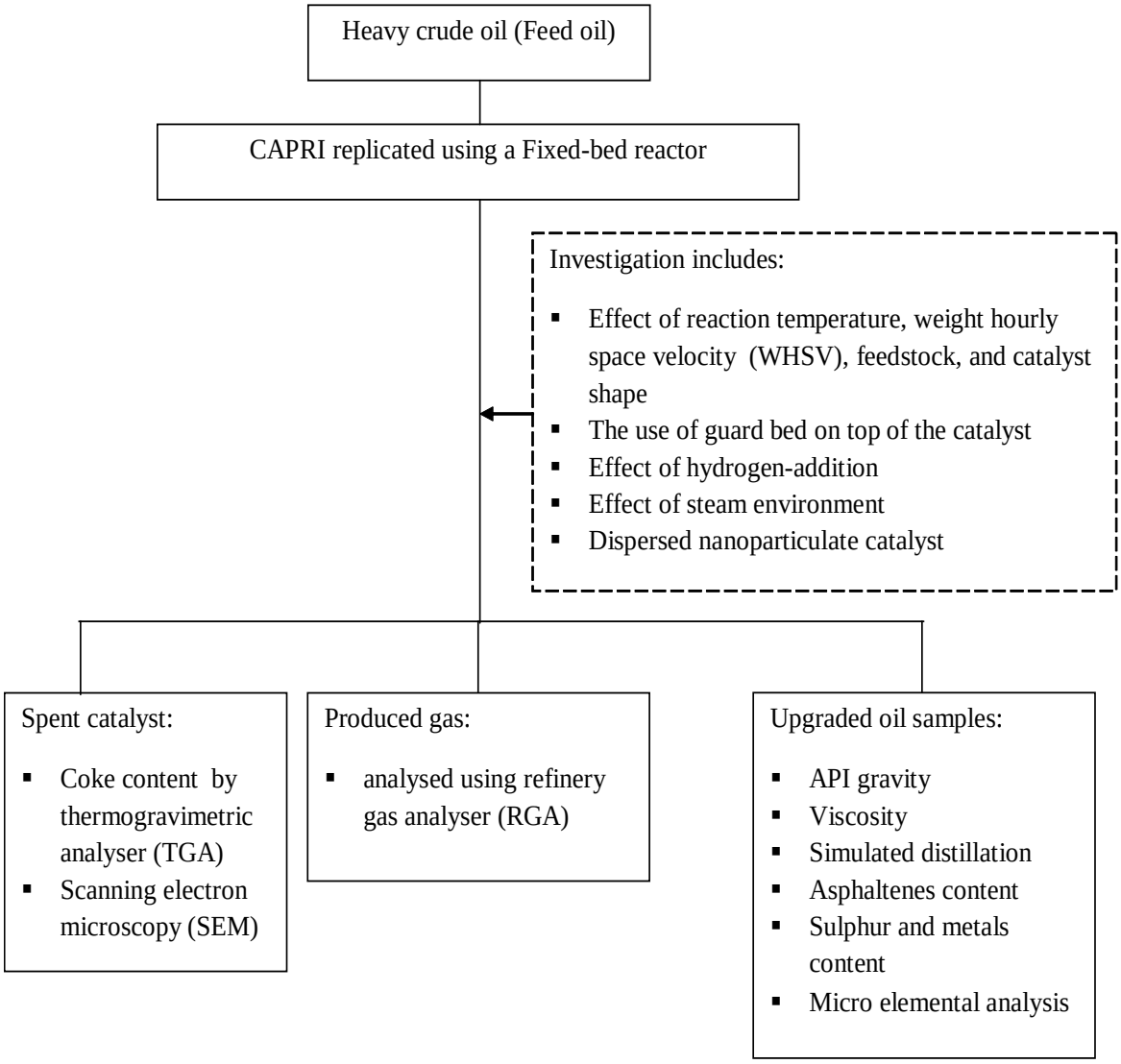

Figure 3.1 Experimental method and analytical schemes of the study.

3.2 Feedstock Properties

The heavy crude oil used in this study was supplied by Petrobank Energy and Resources Ltd. from its WHITESANDS THAI pilot trial at Christina Lake, Alberta, Canada. The feedstocks have been partially upgraded during thermal recovery by the THAI process alone. The physical and chemical properties of the feedstocks are presented in Table 3.1. The first denoted feed oil-A, was produced by THAI from a single well and the second is a blend

of partially upgraded oil produced by THAI trials obtained from eight different wells, denoted feed oil-B. The feed oil-B displayed 1°API greater than feed oil-A, but its viscosity is two times that of feed oil-A. It is clearly seen from the simulated distillation that feed oil-B contains more distillable fraction than THAI feed oil-A.

Table 3.1 Properties of the THAI heavy feed oils.

Parameter	**Feed oil-A**	**Feed oil-B**
API gravity (°)	~13	14.1
Viscosity at 20°C (Pa.s)	0.49	1.091
Density at 15°C (g.cm^{-3})	0.9801	0.972
Sulphur (wt.%)	3.8	3.52
Ni (ppm)	56	41
V (ppm)	150	108
Ni + V (ppm)	206	149
Asphaltene (wt.%)	11.1	10.4
ASTM D2887 Distillation, °C		
10 vol.%	105	104
30 vol.%	151	145
50 vol.%	208	177
70 vol.%	293	240
90 vol.%	405	336

3.3 Experimental Set-Up and Procedure

In the THAI process, air (and initially steam for raising temperature) is injected and once the combustion is started the oil flows downwards in the mobile oil zone (MOZ) into the perforated horizontal production well (Figure 3.2). This is the area where most of the thermal

cracking is believed to be happening. Hence the process moves from the 'Toe' position to the 'Heel'. The oil in the MOZ remains hot upon reaching the horizontal production well due to heat gained from the combustion zone. In the CAPRI section, the horizontal production well has been packed with annular catalyst layer. As the hot oil passes through the catalytic layer, catalytic upgrading is believed to occur. The CAPRI section was replicated by a cylindrical core of 1 cm taken in a radial direction through the layer of the catalyst surrounding well as represented in Figure 3.2.

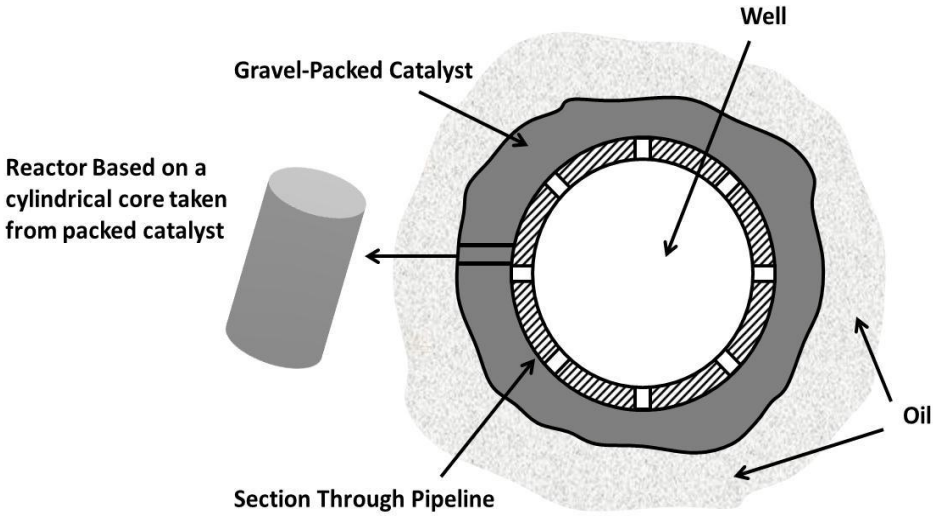

Figure 3.2 Scaling the field CAPRI section to laboratory model representation with catalyst bed volume of 12.86 cm^3.

A flow diagram of the experimental rig used in this study is shown in Figure 3.3. The experimental set-up was built and commissioned at the School of Chemical Engineering, University of Birmingham, UK. A down flow micro reactor was used to ensure the complete wetting of the catalytic bed with the help of gravity. The experiment was initiated by turning on the furnace (Baskerville Ltd., UnK) and the trace heating (Omega, UK) and setting the

controls to the desired temperatures and pressures. Once the operating conditions of temperatures and pressures were achieved in the reactor, the oil flow metering valve was opened manually to initiate the oil flow from a feed tank pressurised by nitrogen gas. The flow metering valve was adjusted until the desired flow rate of 1mL.min^{-1} was achieved.

The pressure in the feed tank was kept 5-10 barg higher than the packed microreactor inside the furnace to ensure oil flow through the reactor. The feed oil (i.e., heavy crude oil) was delivered to the packed catalyst bed in down flow mode to ensure flow by gravity and complete wetting of the catalytic bed.

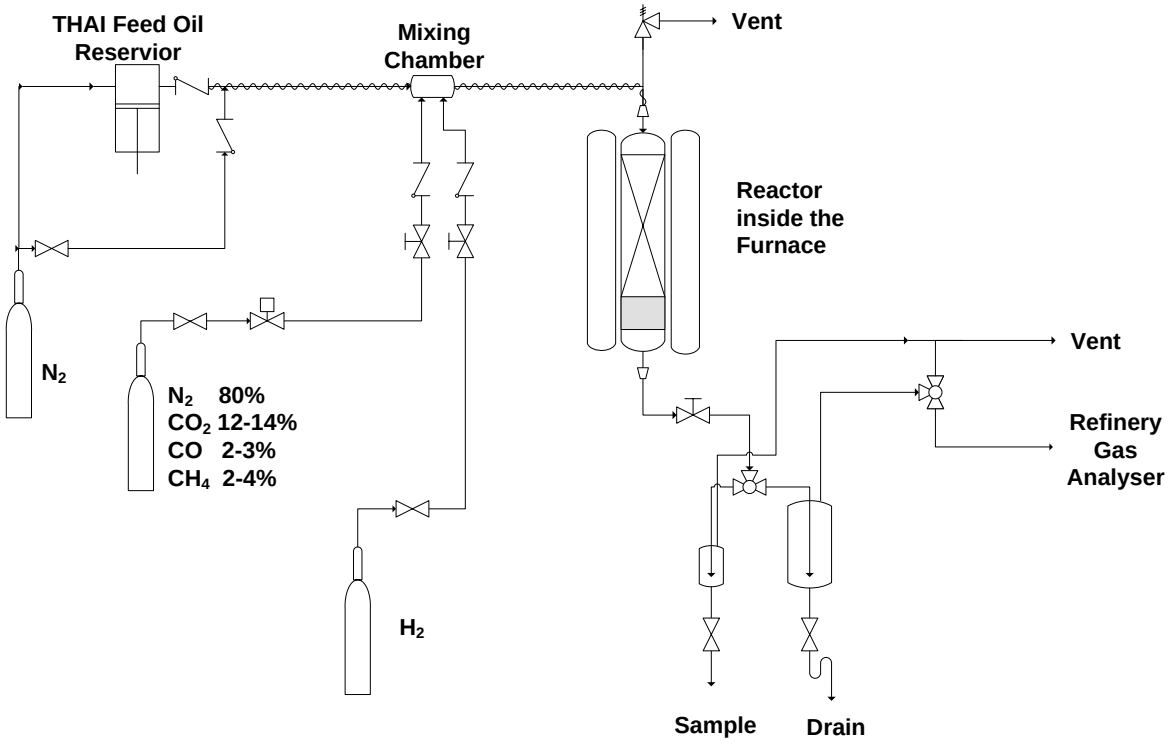

Figure 3.3 Schematic diagram of the CAPRI experimental setup (Hart, et al., 2013).

The feed oil was fed into trace heated lines having a set temperature of 280^{o}C and into the furnace after achieving the desired experimental temperature. The furnace provides isothermal conditions along the active section of micro-reactor. Four gases, N_2, H_2, CH_4, or THAI gas (comprising 80% N_2, 13-14% CO_2, 3% CO, 4% CH_4) were used as the reaction

media to simulate the combustion gases expected in a real THAI-CAPRI reservoir. These gases were mixed with the THAI feed oil in the mixing chamber and the gas-oil mixture passed through the reactor in co-current flow. The gas-oil mixture of the partially vaporised THAI feed oil flowed downward through the voids of the packed catalyst bed where it undergoes cracking reactions aided by heat consumption.

The product stream coming out of the reactor passed through a back pressure regulator (Swagelok Co. UK), which regulated and maintained a constant pressure of 20 barg in the reactor. The upgraded products which include light oil and gases were passed to the gas-liquid separator, where the light oil was collected. While the gaseous products are flashed off, and either vented or sent to refinery gas analyser (RGA) for concentration and compositional analysis by gas chromatography. The analyses were performed every 20 minutes during each experimental run. The light oil sample was drained from the gas-oil separator initially every 20 minutes for the first hour, every 30 minutes for 4 hours and thereafter every 40 minutes, and the collected oil was analysed using techniques listed in next section. The experimental conditions used in this study are listed in Table 3.2.

Table 3.2 Operating conditions in the experiments.

Feed flowrate (mL.min^{-1})	1
Catalyst inventory (g)	2.5 – 6
Pressure (barg)	10 – 40
Reaction temperature (^{o}C)	350 – 425
WHSV (h^{-1})	9 – 21.8
Gas-to-oil ratio (mL.mL $^{-1}$)	50 – 500
Steam-to-oil ratio (mL.mL^{-1})	0.02 – 0.1

The micro-reactors each consist of a fixed catalytic bed of 1 cm diameter and length 41 cm. The reactors have three distinct zones: preheating, catalyst bed and post reaction zones. The first zone was packed with inert glass beads 3 mm in diameter to a length of 9.3 cm to ensure homogeneous flow distribution of the feed oil and gas, to enhance the radial contact and prevent axial mixing. The middle zone contains the catalyst bed comprised of catalyst pellets, with a volume of 9.11 cm^3 for 6 g catalyst (see Figure 3.4). This section is intended to represent a cylindrical core of 1 cm diameter and 11.6 cm height taken in the radial direction of the annular CAPRI section of the well. Finally, the post reaction zone of the reactor was also packed with an inert glass beads to facilitate the disengagement of the gas-oil mixture by the impingement of oil droplets upon the beads. However, when guard-bed was introduced, the reactor was loaded in four zones: preheating, guard-bed (Activated Carbon (AC) or alumina), catalyst-bed, and post reaction zones, as illustrated in Figure 3.5. The weight ratio of the guard-bed material to the catalysts is 2:6 (w/w).

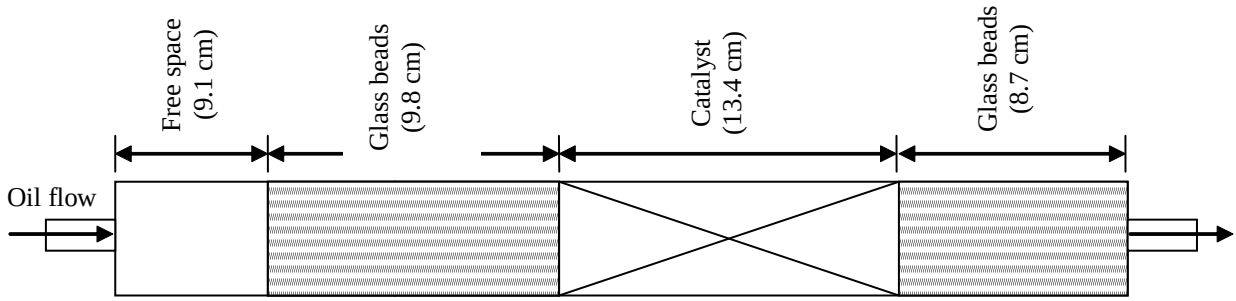

Figure 3.4 Reactor packing for 6 g of catalyst microreactor loading with catalyst only (Actual bed is vertical in orientation).

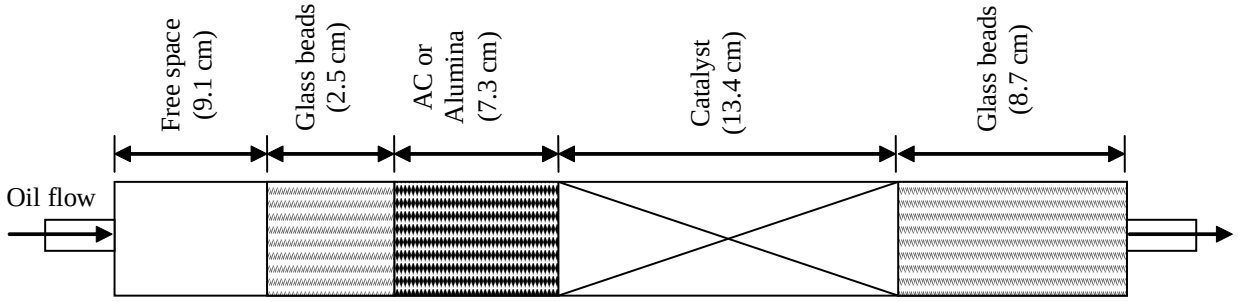

Figure 3.5. Microreactor loading for catalyst with guard-bed (Actual bed is vertical in orientation).

In order to understand the influence of the generated gases of the THAI process on the CAPRI upgrading effect, a laboratory bottled gas mixture representing the typical combustion gases released by in-situ combustion in the THAI process, consisting of 13% CO_2, 3% CO, 4% CH_4, and 80% N_2, was used as gas feed in selected experiments. In some experiments the catalyst was reduced with hydrogen prior to the experiments at 425 °C for 45 minutes. The catalysts used for the experiments were industrial hydrotreating catalysts.

3.3.1 Characteristics of the Packed-Bed Reactor

The bed void fraction was determined by the volume of water displaced by 6 g of catalyst and the volume of bed from the height of the same catalyst in the reactor. The porosity, bulk density, surface area of particles, and residence time of the fixed bed therefore calculated using equation 3.1 to 3.4.

$$\varepsilon_B = 1 - \frac{V_p}{V_B} \quad (3.1)$$

$$\rho_B = \rho_p(1 - \varepsilon_B) \quad (3.2)$$

$$a_v = \frac{6(1-\varepsilon_B)}{d_{peq}} \quad (3.3)$$

$$\tau = \frac{V_B \varepsilon_B}{F_i} \quad (3.4)$$

where; ε_B is the bed porosity, V_B, V_p are volume of the fixed bed and catalyst particles (cm^3), ρ_B, ρ_p are density of bed and particles ($kg.m^{-3}$), a_v, surface area of particles per unit volume ($cm^2.cm^{-3}$), d_{peq} is the equivalent particle diameter (cm), τ, is the residence in the catalyst bed (min), F_i is the flow rate of the oil or gas phase.

The weight hourly space velocity (WHSV) is the ratio of the hourly mass flow rate of oil charged to the mass of catalyst in the reactor. The WHSV is calculated using equation 3.5.

$$\text{WHSV } (h^{-1}) = \frac{\text{Feed oil weight per hour } \left(\frac{g}{h}\right)}{\text{Catalyst weight loaded in the reactor (g)}} \quad (3.5)$$

The pressure drops for both the oil and gas phase were calculated using Ergun's equation (see equation 3.6). The calculated pressure drop does account for build up due to coke deposition on the catalyst. The liquid and gas hold up are calculated using equations 3.7 to 3.9.

$$\frac{\Delta P_i}{L_B} = \frac{150(1-\varepsilon_B)^2}{\varepsilon_B{}^3} \frac{u_i \mu_i}{d_{peq}{}^2} + \frac{1.75(1-\varepsilon_B)}{\varepsilon_B{}^3} \frac{u_i{}^2 \rho_i}{d_{peq}} \quad (3.6)$$

$$\chi = \left(\frac{\Delta P_L}{\Delta P_g}\right)^{0.5} \quad (3.7)$$

$$H_L = 0.185\, \varepsilon_B a_v{}^{0.333} \chi^{0.22} \quad \text{(Ramachandran and Chaudhari, 1983)} \quad (3.8)$$

$$\varepsilon_g = \varepsilon_B - H_L \quad (3.9)$$

where; L_B is the catalyst bed height, ΔP_i is the pressure drop (Pa), μ_i is the fluid viscosity (Pa.s), the fraction of the catalysts bed occupied by the gas phase (ε_g), H_L, is liquid hold up ($cm^3.cm^{-3}$) is a measure of the extent of contacting between the oil and the catalyst.

The pressure drop over the reactor is a vital fixed-bed reactor characteristic, as it influences operation cost. The liquid holdup is a function of the gas and oil flow rates, the oil properties (e.g., density, viscosity, etc.), and the catalyst characteristics (e.g., size, shape, etc.). Therefore, using the above equations 3.1 to 3.9 the characteristics of the packed-bed catalyst was estimated for 6 g of catalyst and presented in Table 3.3.

Table 3.3 Packed bed characteristics for 6 g of catalyst; gas flow rate of 500 $mL.min^{-1}$; oil flow rate 1 $mL.min^{-1}$.

Parameter	**Value**
Reactor dimension	
Inner diameter, ID (cm)	1
Outer diameter, OD (cm)	1.3
Packed Characteristics for 6 g catalyst	
Bed height (cm)	12.6 – 13.2
Bed porosity, ε_B	0.45
Equivalent particle diameter, d_{peq} (cm)	3.55
Oil residence time in catalyst-bed, τ_o (min)	5.1
Gas residence time in catalyst-bed, τ_g (min)	0.01
WHSV (h^{-1})	9.1
Oil pressure drop, ΔP_o (kPa)	12.6
Gas pressure drop, ΔP_g (kPa)	7.64
Liquid holdup, H_L ($cm^2.cm^{-3}$)	0.36
Total oil residence time in the 3-zones of fixed-bed reactor (min)	9.8

3.3.2 Mass Balance

During the reactions gases are liberated and coke deposited in the bed as heavy oil gets converted into light oil. The mass of gas evolved therefore was calculated as the mass remaining after subtracting the masses of produced liquid and solid deposits in the reactor

from a known mass of heavy oil fed. The mass balances of the three products liquid, gas and coke were calculated as percentage of the mass of feed oil fed using equations 3.10 and 3.11:

$$\text{Yield (wt.\%)} = \frac{W_i}{W_{Feed}} \times 100 \quad (3.10)$$

Gas (wt. %) = 100 – liquid yield (wt. %) – coke yield (wt. %) (3.11)

where w_i is the weight of component i and w_{Feed} is the overall weight of the THAI feed oil.

3.4 Characteristics of Catalyst

Hydrotreating (HDT) catalysts of Co-Mo/Al_2O_3 and Ni-Mo/Al_2O_3 quadra-lobe shaped extrudate (AkzoNobel) were used in this study. The microstructural properties of the catalysts such as specific surface area, pore volume, and pore diameter were determined by Brunauer – Emmett – Teller (BET) technique of nitrogen adsorption-desorption experiment and mercury porosimetry. The compositions as well as the properties of the used catalysts are presented in Table 3.4. The size and shape of the catalyst pellets (see Figure 3.6) are important parameters that require quantification; therefore the dimensions of the catalyst were measured using Mitutoyo, CD-6″ Cp calliper. The nitrogen adsorption-desorption isotherm of the catalysts are presented in Appendix A.

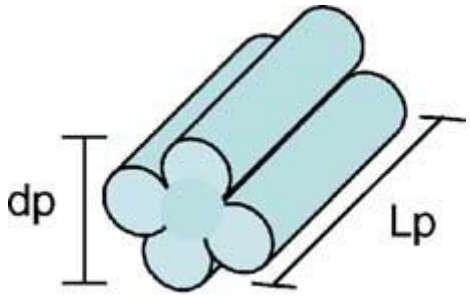

Figure 3.2 Quadra-lobe catalyst sample.

Table 3.4 Composition and properties of used catalysts.

Co-Mo/Al_2O_3 catalyst		**Ni-Mo/Al_2O_3-SiO_2 catalyst**	
Component	Value	Component	Value
Cobalt (II) oxide, CoO (wt. %)	1-10	Nickel (II) oxide, NiO (wt. %)	1-10
Molybdenum (VI) oxide, MoO_3 (wt. %)	10-20	Molybdenum (VI) trioxide, MoO_3 (wt. %)	10-20
Aluminium oxide (or alumina, Al_2O_3) as support (wt. %)	> 50	Aluminium oxide (or alumina, Al_2O_3) as support (wt. %)	20-70
Boron oxide, B_2O_3 (wt. %)	10-20	Silicon dioxide (or silica, SiO_2) as support (wt. %)	20-70
Aluminium orthophosphate, AlO_4P (wt. %)	< 2		
Pellet dimension and BET characteristics			
Diameter, (a, b) (mm)	1.5 ± 0.03, 1.3 ± 0.02		1.40 ± 0.03, 1.21 ± 0.02
Length (mm)	6 ± 3		5 ± 2
Specific surface area, ($m^2.g^{-1}$)	214.1± 0.4		195.4 ± 2.1
Micropore volume, ($cm^3.g^{-1}$)	0.004		0.011
Micropore area, ($m^2.g^{-1}$)	12.73		22.7
External surface area, ($m^2.g^{-1}$)	201.4		175.8
Pore diameter, (nm)	63.7		34
Bulk density ($g.cm^{-3}$)	1.27		1.05
Acid sites and strength			
Moderate at 320 ^oC, (mmol adsorbed $(CH_3)_3CNH_2$/g sample)	2.86	Moderate at 280 ^oC, (mmol adsorbed $CH_3)_3CNH_2$/g sample)	0.62
Strong at 500 ^oC, (mmol adsorbed $(CH_3)_3CNH_2$/g sample)	0.45	Strong at 480 ^oC, (mmol adsorbed $(CH_3)_3CNH_2$/g sample)	0.11

The surface area and pore size of the catalysts were measured using the BET method according to ASTM C1274 by physical adsorption. This was accomplished by performing nitrogen adsorption and desorption on the catalysts pellets at a temperature of 77K, using a Micromeritics Analytical Instrument ASAP® 2010, to measure an adsorption isotherm. Prior to the analysis, the catalyst samples weighing about 1.27 g were degassed at elevated

temperature to remove contaminants. Analysis was performed using the BET equation (3.12) presented below, which describes the relationship between nitrogen adsorbed at a given partial pressure and the volume adsorbed at monolayer coverage. The formation of monolayer (i.e., a layer of adsorbed gas one molecule thick) of gas molecules on the surface of the catalyst is used to estimate the specific surface area, while the principle of capillary condensation of the N_2 gas enables the determination of pore size, pore volume and size distribution. However, nitrogen is commonly used as its molecular size is well established, available in high purity, cost-effective, and inert.

$$\frac{P}{V(P_o-P)} = \frac{1}{V_m C} + \frac{(C-1)P}{V_m C P_o} \qquad (3.12)$$

where p is the partial pressure of N_2, P_o is the saturation pressure at the experimental temperature, V volume adsorbed at P, V_m volume adsorbed at monolayer coverage, and C a constant. A sample of BET plot and calculation for fresh Co-Mo/Al_2O_3 is presented in Appendix A.

The BET surface area (S_{BET}) was then calculated using equation (3.13):

$$S_{BET} = \frac{v_m n_a a_m}{m_v} \qquad (3.13)$$

where n_a is the Avogadro's number (6.022 x 10^{23} mol^{-1}), a_m is the cross-sectional area occupied by each adsorbate molecule at 77 K (0.162 nm^2) and m_v is the gram-molecule volume (22.414 mL).

The catalysts used in the experiments reported here was pre-sulphided ex-situ using carbon disulphide (CS_2). This was carried in two steps; firstly the fresh catalyst was contacted with sulphur containing CS_2, and dried in inert atmosphere as described by Eijsbouts et al. (2008). Additionally, the feed oil contains sulphur that could promote activation and sulphiding during reaction (Barman, et al., 1997).

A mercury porosimeter (AutoPore^{TM} IV 9500, Micromeritics) was used to measure the pore size and distribution, pore volume, and other porosity related characteristics of the catalysts. The technique uses the Washburn equation (see equation 3.14) to describe the intrusion of mercury into the catalyst pellets as a function of applied pressure. Therefore, the pressure required to force mercury into the pores of the catalyst pellets is inversely proportional to the size of the pores.

$$\Delta P = \frac{4\sigma Cos\theta}{D_p} \qquad (3.14)$$

where ΔP is differential pressure, σ is surface tension of mercury 485 dynes.cm^{-1} (or 0.480 N.m^{-1}), θ is the contact angle 130^o and D_p is the pore diameter. Notably, the Washburn equation assumes cylindrical pores.

Nevertheless, prior to the start of analysis all the penetrometers were calibrated without sample to obtain the baseline error due to compressibility and thermal effects of mercury and the penetrometer. The penetrometer with sample was then transferred to the high pressure chamber, where the intrusion of mercury into the sample under controlled pressure from 15 to 30000 psia takes place. As pressure increases during the analysis, the pore size is calculated for each equilibrium pressure point, the volume of mercury required to fill the

pores is recovered and was used to estimate the catalyst characteristics such as pore size and distribution, total pore volume and area, and surface area.

The temperature programmed desorption (TPD) of the fresh catalysts samples were carried out in a Micromeritics AutoChem II 2920 analyser (Micromeritics Instrument Corporation). This was performed to determine the number, the relative strength and distribution of the acid sites based on the adsorption-desorption of tert-butylamine ($(CH_3)_3CNH_2$). The acid sites possessed by the solid catalysts play a vital role in catalytic cracking reactions and also provide some understanding about their catalytic activity. For the TPD analysis about 0.158 g of the catalyst sample was loaded into a U-shaped quartz tube which was placed in a sample port located in an enclosed furnace. Prior to the TPD, the catalyst sample was degassed at temperature ramp of 25 to 500 ^{o}C at 10 ^{o}C.min^{-1} for 60 minutes under argon flow of 50 mL.min^{-1}. The catalyst sample was saturated with tert-butylamine by the flow of a mixture of gas containing tert-butylamine and helium (He). Thus, the physically adsorbed tert-butylamine was removed by flowing helium gas at the rate of 50mL.min^{-1} for 30 minutes. In order to determine the strength of the acid sites, tert-butylamine desorption was conducted at temperature range of 25-500 ^{o}C at the rate of 15 ^{o}C.min^{-1} under flowing helium gas. The thermal conductivity detector (TCD) analysed the He gas leaving from the catalyst sample. The strength of the acid sites was determined from the area, position and shape of the peak produced by the tert-butylamine adsorbed and desorbed. The temperature at which a given peak occurs indicates the strength of the acid site. Both catalysts have two acid sites (see Table 3.4).

3.4.1 Oxidative Regeneration of Spent Catalyst

The spent catalyst from upgrading reaction with nitrogen atmosphere was regenerated at high temperature using 14.4 g of the spent catalyst in a Carbolite® furnace (Keison Products, UK) under air atmosphere. Thereafter, reduction was performed in the CAPRI reactor using hydrogen gas at a flow rate of 50 $mL.min^{-1}$ for 45 minutes, before being retested for catalytic activity. The oxidative regeneration furnace was programmed as follows: ramp increase in temperature in range of 25 – 600 ^{o}C at a heating rate of 20 $^{o}C.min^{-1}$, followed by holding at 600 ^{o}C for a total of four hours to avoid sintering. This temperature is typical of the regeneration temperature used in fluidised-bed catalytic cracker reactors in the petroleum industry. At the end of the reaction, 24.5 wt.% of the carbonaceous deposits were burned-off upon thermal oxidative regeneration. Nonetheless, oxidative-regeneration removes mostly the asphaltene and coke deposits, whilst the metal sulphides of Mo and Co are transformed into their oxides, which was reduced with hydrogen before reuse.

3.4.2 Preparation of Ni-based Zeolite Catalyst

It has been reported that by modifying the catalyst support it is possible to improve its activity, stability, and selectivity as the surface properties are manipulated (Biswas, et al., 2011). In this regard, a zeolite Ni-based catalyst was prepared by the incipient wetness impregnation method. 12 g of $Ni(NO_3)_2.6H_2O$ was dissolved in 20 mL ethanol and 10 g HY-zeolite was added. The mixture was stirred vigorously for 2 hours using a magnetic stirrer. After impregnation, the samples were filtered and dried at room temperature overnight, followed by calcinations at 500 ^{o}C for 4 hours in a muffle furnace. Furthermore, dry phase

mixing of 50 wt.% of Ni/HY-zeolite and 50 wt.% of commercial alumina boehmite, was followed by peptization with 5% (v/v) acetic acid (CH_3COOH). Extrusion was performed and the extrudates were subsequently dried at 100^oC for 5 hours and calcined at 500^oC for 5 hours. The flowchart for the catalyst preparation is shown in Figure 3.7. The detailed properties and composition of the synthesised zeolite Ni-based catalyst was determined by X-ray fluorescent (XRF) analyser and BET analysis, respectively. Zeolite was considered because of its use in the oil refining processes such as catalytic cracking (e.g., FCC).

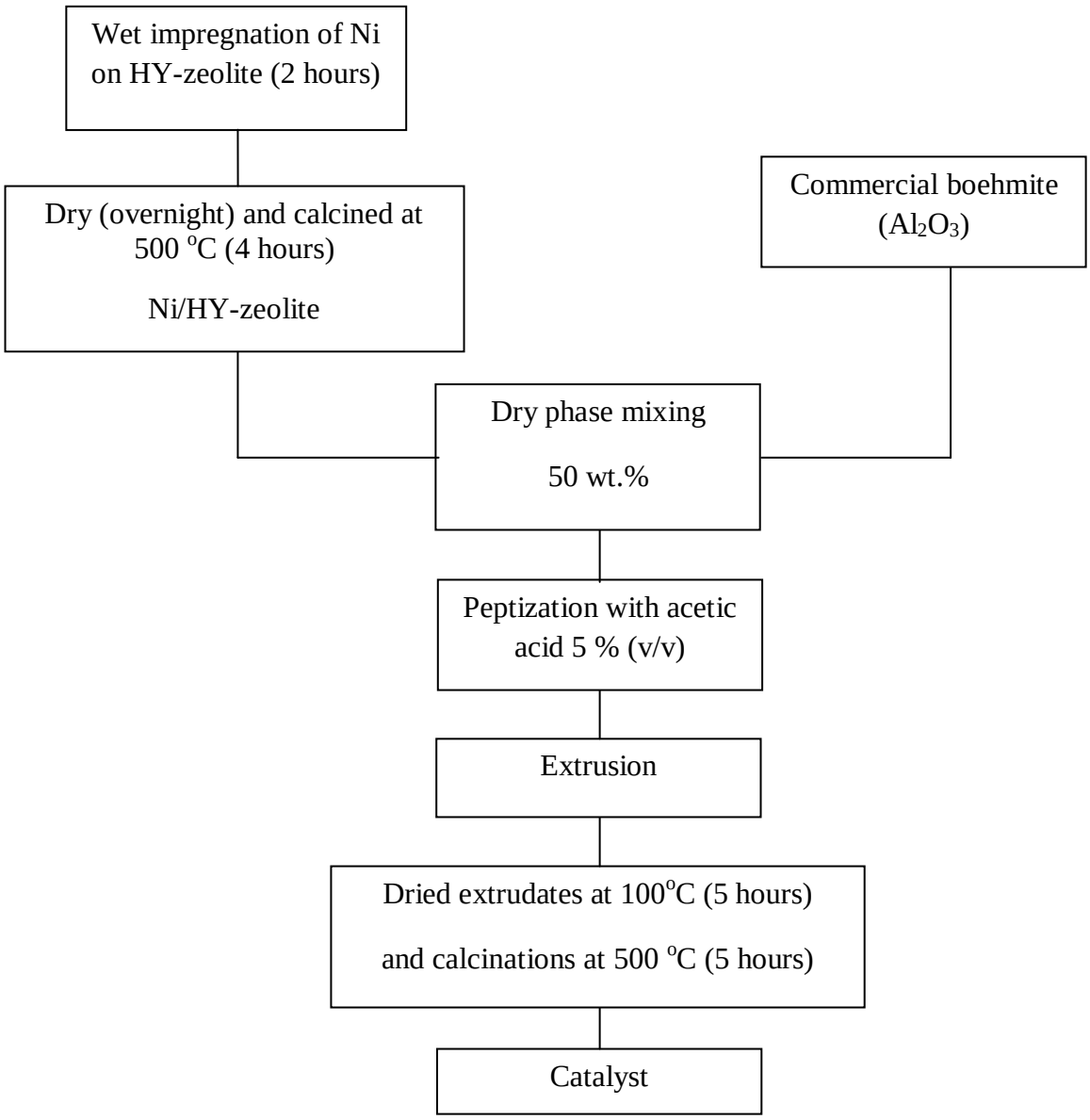

Figure 3.3 Flowchart of the zeolite Ni-based on alumina catalyst synthesis.

3.4.3 Analysis of Surface Morphology using SEM

The external morphology and texture of the fresh Co-Mo and Ni-Mo catalyst as well as the spent catalysts were studied using a Philips XL 30 Scanning Electron Microscope (XL 30 ESEM-FEG) equipped with a LaB5 emission source. Energy-Dispersive X-ray spectroscopy (EDX) was used for elemental composition analysis of the catalyst before and after upgrading reactions. The XL 30 ESEM-FEG was used because of its ability to examine the natural state of oily materials without preparation or modification. This technique was useful for detecting changes affecting the catalyst morphology due to coke deposition before and after reactions. The SEM photomicrographs was collected over a selected area of the surface of the catalyst, which is 2 μm in width and magnification of 35000X.

3.5 Analytical Instruments

The following instruments were used to analyse the produced oils, evolved gas and coke deposited upon the used catalyst. The extent of upgrading in the oil produced from catalytic upgrading process relative to the feed oil was evaluated in terms on viscosity, API gravity, true boiling distribution, asphaltenes content, sulphur and metals content before and after reactions.

3.5.1 Density and API Gravity Measurement

The density and American Petroleum Institute (API) gravity (i.e., how heavy or light a crude oil is compared to water) of the feed and produced oils was determined using digital Anton Paar DMA 35 portable density meter density meter (Anton Paar GmbH, Austria) at

15°C and reported in $g.cm^{-1}$. The crude oil is introduced into the U-shaped glass tube through the pump lever as shown in Figure (3.8). The filled U-shaped tube is agitated and the density measurement is based on oscillating U-tube principle. A temperature sensor measures the oil temperature right at the measuring cell. The API gravity and increment was calculated using equations (3.15) and (3.16):

Figure 3.4 Photograph of Anton Paar digital density and API gravity meter.

$$\text{API gravity} = \frac{141.5}{\text{SG}} - 131.5 \qquad (3.15)$$

Change in API gravity (^{o}) = API of feedstock – API of produced oil (3.16)

where *SG* represents specific gravity.

3.5.2 Viscosity Measurement

The oil viscosity is a measure of its internal resistance to flow. Advanced rheometer AR 1000 (TA Instruments Ltd, United Kingdom) was used to measure the viscosity of the

feed and produced oils. An aluminium plate of parallel geometry with diameter 40 mm and a polished surface was used as shown in Figure 3.9. Firstly, the viscometry mode that measures the viscosity of the crude oil as a function of shear stress versus shear rate was carried out to assess the rheological behaviour of the oil with parallel plate gap size set at 150 µm.

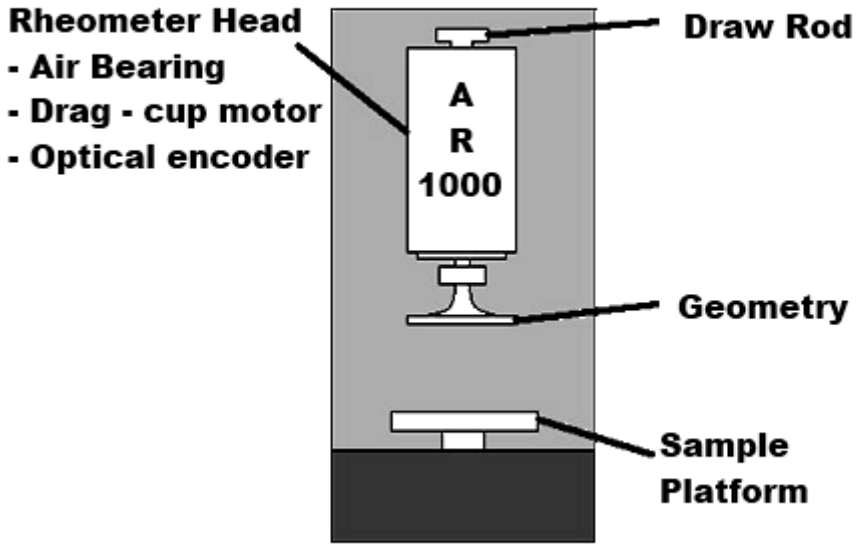

Figure 3.5 Advanced rheometer AR 1000 (Rodger, et al., 2008).

All the analysed samples showed Newtonian fluid behaviour before and after upgrading reactions, that is, the viscosity of the oil is constant with increasing shear rate ranging from 0.5 to 600s^{-1}. This therefore implies that the viscosity of the crude oil is independent of shear rate. Subsequently, the viscosity measurements were performed using a shear rate of 100 s^{-1}. All viscosity measurements were performed at 20 ± 0.1 ^{o}C. The reported data were averages of duplicate measurements, each of which are averaged from five data points. The degree of viscosity reduction (DVR) is calculated using equation (3.17):

$$DVR\ (\%) = (\mu_o - \mu) / \mu_o \times 100 \qquad (3.17)$$

where; μ_o and μ viscosity of the THAI feed oil and produced oils (Pa.s), respectively.

3.5.3 Asphaltene Measurement

Asphaltenes are the heaviest component of the heavy crude oil generally separated by collecting its precipitate from the diluted heavy oil with straight chain alkanes such as n-pentane or n-heptane, as shown in Figure 3.10. The remaining portion thereafter is known as maltene (mixture of saturates, aromatics, and resins). In this study, the asphaltene fraction was precipitated from the corresponding THAI feed oils and produced upgraded oils using n-heptane in accordance to the ASTM D2007-80.

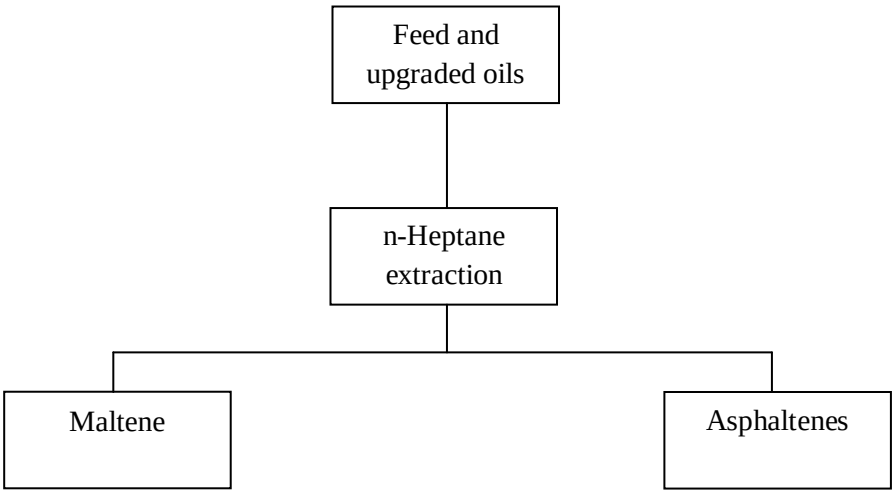

Figure 3.6 Asphaltene precipitation from feed and produced oils using n-heptane as solvent.

Specifically, 1 g of the samples was mixed with 40 mL of n-C_7H_{16}, which was used as a precipitant. The oil plus n-C_7H_{16} mixture was agitated for 4 hours using a magnetic stirrer.

Thereafter, the mixture was left for 24 hours to allow the asphaltenes precipitate and settled. The precipitated fraction was vacuum filtered using a Whatman 1 filter paper with 11 µm pore size and 4.25 cm diameter to separate the n-C_7H_{16} soluble portion (i.e., maltene) from the asphaltene portion (i.e., n-C_7H_{16} insoluble). The filtered asphaltenes were washed with n-C_7H_{16} until a colourless liquid was observed from the filter. The filter paper and precipitate were dried under an inert gas flow (N_2) in the hood for 24 hours to remove any residual n-C_7H_{16}, and then the precipitated asphaltenes was weighed. The weight percent of the asphaltenes content was calculated as follows:

$$\text{wt.\% Asphaltene content} = \frac{\text{Weight of dried precipitated asphaltene (g)}}{\text{Weight of heavy oil (g)}} \times 100 \qquad (3.18)$$

3.5.4 Sulphur and Metals Content

The extent of catalytic upgrading process was also evaluated in terms of impurities removals. The sulphur and metals content of the crude oil before and after upgrading reactions was performed by Intertek Laboratories Sunbury Technology Centre, UK, using ICP-OES (Inductively Coupled Plasma Optical Emission Spectrometry). The results were analysed as percentage of impurities removed through desulphurization, demetalization, and deasphaltenization and calculated using equation 3.19:

$$\text{\% Removal} = \frac{(C_{\text{Feed oil}} - C_{\text{Oil produced}})}{C_{\text{Feed oil}}} \times 100 \qquad (3.19)$$

where $C_{feed\ oil}$ and $C_{oil\ produced}$ are the amount of sulphur, metals and asphaltenes in the feed oil and produced oils, respectively.

3.5.5 True Boiling Point (TBP) Distribution

Method ASTM-D2887 provides a comprehensive TBP distribution range of carbon numbers of petroleum and its distillates. For this reason simulated distillation (SIMDIS) based on an Agilent 6850N gas chromatography (GC) and calibrated in accordance with the ASTM-D2887 was used to characterize the feed and produced oils. The Agilent 6850N GC (Agilent Technologies, Inc., Germany) was fitted with a J&W 125-10 DB-1 10m length, 530 µm ID and 2.65 µm film thickness capillary column. Before injection, the feed and produced oil samples were diluted with carbon disulphide (CS_2) in a ratio of 1 to 10. CS_2 was chosen as the dilution solvent due to its miscibility with crude oil, low response factor in the Flame Ionization Detector (FID) as well as the low boiling point (BP). Thereafter, 1 µL of the blend was taken by means of a syringe and injected into the GC; each run was performed in duplicate. The FID was maintained at 260 ^{o}C, provided with 450 mL.min^{-1} air, hydrogen flow 40mL.min^{-1} and nitrogen as make up gas with flow 32.3 mL.min^{-1}, respectively. The column was eluted with helium at a flow 20 mL.min^{-1}. The analyses were performed at a programmed column temperature of 20 ^{o}C.min^{-1} from 40 to 260 ^{o}C. However, the maximum oven temperature of the GC is 280 ^{o}C. The GC was calibrated with a hydrocarbon standard mixture containing C_5 – C_{40}. The conversion of high-boiling-point (or high molecular weight) fractions to lighter fractions (BP < 343 ^{o}C) was defined as the conversion of the 343 ^{o}C+ hydrocarbons (HCs) that are found in the feed oil to the produced upgraded oils. The thermal and catalytic cracking during CAPRI can simply be expressed by equation (3.20):

$$\text{heavy fractions (343 }^{o}\text{C+)} \rightarrow \text{distillable (< 343 }^{o}\text{C)} + \text{coke} + \text{gas} \qquad (3.20)$$

The distillables consist of light and medium oil fractions in the produced oil. Therefore, the calculation is made by first determining the weight of the BP greater than 343^{o}C HCs in the feed oil and the liquid products, then using equation 3.21 to calculate the conversion (Ortiz-Moreno, et al., 2012).

$$\text{Conversion} = \frac{(343\ ^{o}\text{C}+)\text{HC in feed} - (343\ ^{o}\text{C})\text{HC in products}}{(343\ ^{o}\text{C})\text{HC in feed}} \quad (3.21)$$

The above conversion equation only accounts for materials that elute the GC column. This is the definition that is utilised throughout the thesis for conversion; this is a typical way of measuring conversion (Ortiz-Moreno, et al., 2012). However, the maximum temperature attainable using the previous column is 280^{o}C, the Agilent 6850N GC was modified to the ASTM-2887-08 method. The new column details are as follows: DB-HT 5 m length, 0.53 mm internal diameter and 0.15 µm film thickness capillary. This was fitted with a Programmed Temperature Vaporisation (PTV) injector which rapidly heats the sample to 355 ^{o}C to vaporise the sample before been introduced into the GC. The integrated PTV injector reduces the effect of large volume of sample that causes column and detector overload.

3.5.6 Thermogravimetric Analysis (TGA)

A thermogravimetric analyser (TGA) was used to determine the amount of coke deposit on the spent catalysts. In this study, TGA was carried out with NETZSCH-Geratebau GmbH, TG 209 F1 Iris®. 15-18 mg of the spent catalyst sample was recovered from the reactor and placed on alumina crucible above the microbalance. The micro-furnace is programmed as follows: ramp temperature in range of 25 – 1000 ^{o}C and a heating rate of 20 ^{o}C.min^{-1}. At 1000^{o}C an isothermal condition was maintained for 20 min to enable total burn-

off of the materials deposited on the spent catalysts. An air flow rate of 50 mL.min^{-1} was used. The mass change of the sample in percent (wt.%) due to burn-off as the temperature rises was registered in the TG 209 F1 Iris® which runs under Proteus® software. The vacuum-tight thermo-microbalance, works based on the principles of electromagnetic power compensation as illustrated in Figure 3.11. The sample is heated by a micro-furnace enclosed by a cooling jacket. Typically, the loss of the weight of the sample due to burn-off on heating and exposure to air is measured by the TGA sensitive microbalance.

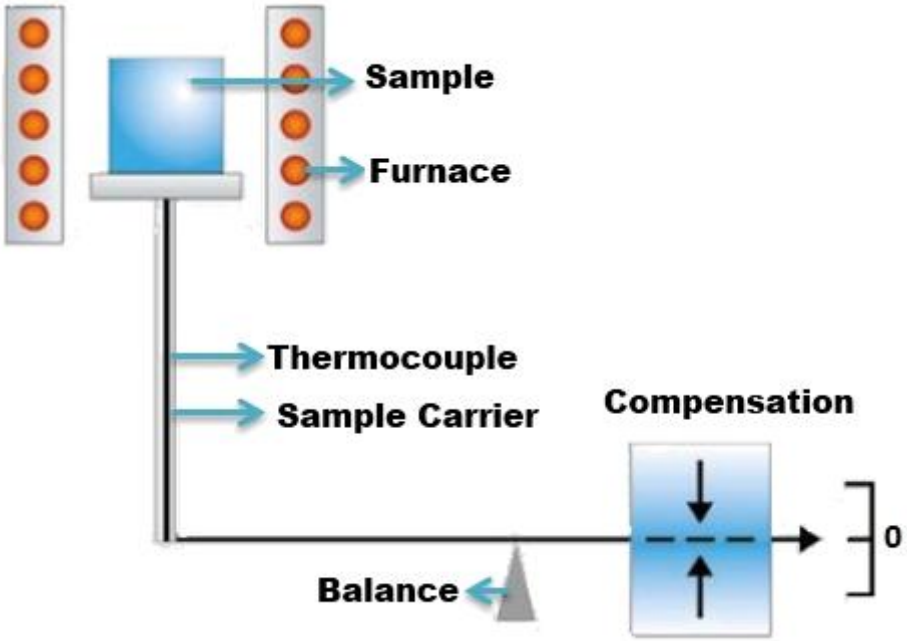

Figure 3.7 The working principle of the thermo-microbalance of the TGA.

The issue of corrosion and coke at high temperature led to the use of platinum crucible with lid top. The method was then modified as follows: firstly a ramp temperature in range of 25 – 900 ^{o}C at a heating rate of 10 ^{o}C.min^{-1} with the same air flow rate of 50 mL.min^{-1}. At 900 ^{o}C an isothermal condition was maintained for 20 minutes to enable total burn-off of the materials deposited on the spent catalysts.

3.5.7 Refinery Gas Analyser (RGA)

The composition of gas produced during the catalytic upgrading process was analysed using an Agilent 7890A RGA-GC to determine the volume percentage of H_2, H_2S, CO, CO_2, and C_1-C_5 hydrocarbons. This is in accordance to the method ASTM D1945-03. The RGA three channels include FID and two thermal conductivity detectors (TCD). The light hydrocarbon components in the gas stream are determined by the FID channel column HP-PLOT Al_2O_3S capable of separating C_1 to nC_5 including their isomers based on the calibrated table, whilst components heavier than nC_5 are back flushed through the pre-column. One of the TCD with helium carrier gas is used for permanent gases analysis such as N_2, CO, CO_2, O_2, and H_2S. The other TCD with nitrogen as carrier gas determines gases like hydrogen and helium in the gas stream. The oven column dimension is 27 m x 320 µm x 8 µm at temperature of 200 ^oC. The operating conditions of the channels are as follows: FID channel H_2 flow (45 mL.min^{-1}), air flow (400 mL.min^{-1}), reference flow (45 mL.min^{-1}) and makeup flow N_2 (25 mL.min^{-1}); TCD channel conditions, reference flow (45 mL.min^{-1}), and makeup flow, He (2 mL.min^{-1}); and the third TCD channel, reference flow (45 mL.min^{-1}) and makeup flow, N_2 (2 mL.min^{-1}). The gas samples were injected online during the catalytic upgrading reactions. The calibration mix consists of the following gases presented in Table 3.5.

Table 3.5 RGA calibration gas composition.

Gas	**Amount (vol. %)**	**Gas**	**Amount (vol.%)**
Hydrogen	1	Methane	1
Ethane	1	Propane	1
Carbon dioxide	3	Propene	1

i-butane	1	n-butane	1
Trans-2-butene	1	1-butene	1
Cis-2-butene	1	i-pentane	1
n-pentane	1	Carbon monoxide	4
Nitrogen	1	Hydrogen sulphide	0.0005

3.6 Fine Particulate Catalyst

The Co-Mo/Al_2O_3 and Ni-Mo/Al_2O_3 catalysts pellets were crushed using a Tema laboratory disc mill model T 750K (TEMA Machinery Ltd, UK). The size of the catalyst particles after pulverization was measured by laser diffraction particle size analyser (Helos-Rodos T4.1, Sympatec, Germany). The particle size distribution and BET result is presented in Table 3.6. The mean size is approximately 2.6 ± 1.08 µm.

Table 3.6 Catalyst fine particles size distribution and surface area.

Particle size (µm)	**Value**
< 10	62 %
10 – 30	24.3 %
> 30	13.7 %
BET surface area ($m^2.g^{-1}$)	196.2

3.6.1 Experimental Procedure for Dispersed Nano-particulate Catalysts

The dispersed micro-catalyst experiments were performed in batch autoclave reactor. The schematics diagram of the batch autoclave reactor used for the dispersed catalyst experiments is shown in Figure 3.12.

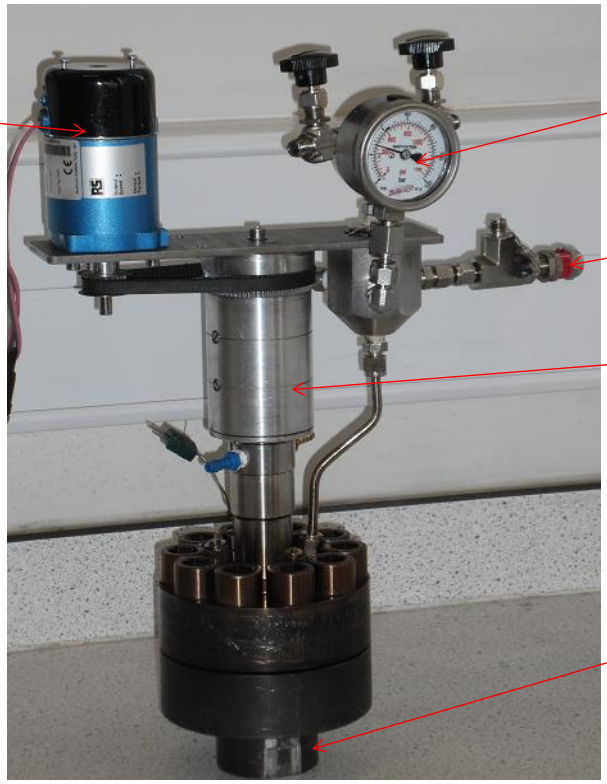

Figure 3.8 Photograph of the batch autoclave reactor 100 mL used in dispersed catalyst experiments.

0.4 to 2 g of micro-particulate catalyst was placed in 20 g heavy oil in the batch autoclave reactor (100 mL). Agitation was performed by a two blade impeller. The upgrading reaction was performed at the optimised reaction temperature 425 ^{o}C in fixed-bed reactor, stirring speed of 133 rpm that gives the same Reynolds number as the fixed-bed; detailed experimental conditions are presented in Table 3.7. It is generally accepted that the reaction time starts when the heavy oil and reactants are confined in the reactor and operating conditions have been reached. Thus, zero time was taken when the temperature inside reached 425 ^{o}C.

Table 3.7 Operating conditions for dispersed nano-catalyst experiments.

Parameter	**Value**
Catalyst weight (g)	0.4 – 2
Catalyst-to-oil ratio (w/w)	0.03 – 0.1
Feed oil (g)	20
Stirring speed (rpm)	133 – 500
Reaction time (minutes)	10
Temperature (^{o}C)	425
Pressure (barg)	20

The spare space of the reactor was purged with nitrogen to remove air and pressurised to 20 bar. After a reaction time of 10 minutes (to replicate the same residence time as the fixed-bed reactor) had elapsed the heating was stopped and the reactor cooled to room temperature. The composition of the produced gas was determined using RGA-GC. In order to evaluate the effect of dispersed micro-catalyst, the experiment was also conducted without catalyst as control.

Chapter 4

Effects of Reaction Conditions, Catalyst and Feedstock on Upgrading

4.1 Introduction

In any heavy oil upgrading process, the main characteristics of the produced liquid product of interest are: the total liquid yield, the API gravity and viscosity of the produced oil, the conversion of high boiling heavy fractions, and the removal impurities.

In this chapter therefore, the effects of reaction conditions such as temperature on thermal cracking and catalytic CAPRI upgrading are presented in Sections 4.2 and 4.3. The effect of Weight Hourly Space Velocity (WHSV) is presented in Section 4.4, catalyst type, mono- vs. bi-metallic catalyst in Section 4.5 to 4.6, and feedstock on the extent of upgrading in Section 4.7.

4.2 Thermal Cracking Effect

In this Section, the thermal cracking upgrading was evaluated using inert 3 mm glass beads. The extent of non-catalytic reactions on API gravity, viscosity and conversion was evaluated. The investigation was carried out in the temperature range 350-425 ^{o}C, at 20 bar reactor pressure, 1 mL.min^{-1} oil flow rate, and 6 hours time-on-stream operation. The change in API gravity, viscosity and the conversion of 343 ^{o}C+ heavy fractions of the produced oil samples as a function of reaction temperature are presented in Table 4.2 and Table 4.2 shows the results from catalytic upgrading counterpart at the same conditions.

Table 4.1 Thermal effect on API gravity, viscosity, and conversion of heavy oil using 3 mm glass beads as a function of temperature under nitrogen medium (feedstock: 13 ^{o}API, 0.49Pa.s, and 59.5 % 343 ^{o}C+).

Reaction temperature (^{o}C)	**Change in API gravity (^{o})**	**Viscosity (Pa.s)**	**Conversion 343^{o}C+ (%)**
350	0.7 ± 0.2	0.3683	6.5
400	1.1 ± 0.18	0.2931	8.8
425	1.7 ± 0.18	0.226	16.8

Table 4. 2 Viscosity and change in API gravity of CAPRI produced oil at 350, 400 and 425 °C; Reaction Media (N_2), Pressure 20 barg, Oil flow rate 1mL.min^{-1}, Gas flow rate 500 mL.mL^{-1} and Catalysts: Co-Mo, Ni-Mo and Co-Mo on top Ni-Mo.

Temperature (^{o}C)	**Co-Mo/Al_2O_3**	**Ni-Mo/Al_2O_3**	**Co-Mo + Ni-Mo**
	Absolute viscosity (Pa.s)		
350	0.282 ± 0.05	0.261 ± 0.09	0.245 ± 0.08
400	0.170 ± 0.03	0.160 ± 0.06	0.155 ± 0.06
425	0.094 ± 0.03	0.089 ± 0.04	0.151 ± 0.03
	Change in API gravity of upgraded oil (^{o})		
350	1.97 ± 0.24	1.69 ± 0.91	1.72 ± 0.66
400	2.63 ± 0.76	2.21 ± 0.86	2.21 ± 0.71
425	3.75 ± 0.93	3.73 ± 0.66	2.74 ± 0.62

As noticed in Table 4.1, thermal cracking effect causes an average of 0.7, 1.1, and 1.7^{o} API points increased in the produced oil at 350, 400 and 435 ^{o}C above 13^{o} API gravity (feed oil). Conversely, the degrees of viscosity reduction (DVR) as the temperature increases from 350 to 400 then 425 ^{o}C are 24, 40 and 51%. Clearly, thermal cracking becomes significant as the reaction temperature increases, promoting the splitting of heavy molecules into smaller molecules. This is in line with the results of thermal cracking effect reported in the literature for fixed and fluidized bed cracking of residue at similar temperatures (Kressmann, et al.,

1998; Lee, et al., 2011; Kim, et al., 1998). However, at 350 and 400 ^{o}C visbreaking may have been the means of viscosity and API gravity improvement.

On the other hand, the conversion of heavy fractions with BP 343 ^{o}C+ into low-boiling fractions at 350, 400, and 425 ^{o}C, are 6.5, 8.8 and 16.8 %, respectively. The results of the SIMDIS analysis shows that the low-boiling range fractions increased as the temperature increased. Thermal upgrading generally occurs via free radical chain reaction mechanism. This involves a series of chemical reaction steps, illustrated with the following examples (Speight, 2011):

1. **Initiation reaction**, where some components of the heavy oil molecules splits into two free radicals by the breaking the C – C bonds, rather than C – H bond, as shown below:

$$CH_3CH_3 \rightarrow 2CH_3^{\bullet} \quad (4.1)$$

2. **Hydrogen abstraction reaction** in which a free radical abstracts a hydrogen atom from another hydrocarbon molecule:

$$CH_3^{\bullet} + CH_3CH_3 \rightarrow CH_4 + CH_3CH_2^{\bullet} \quad (4.2)$$

3. **Radical decomposition reaction** involves the splitting of a free radical into olefin:

$$CH_3CH_2^{\bullet} \rightarrow CH_2 = CH_2 + H^{\bullet} \quad (4.3)$$

4. **Radical addition reaction** involves the reaction of free radical react with an olefin to form a single and larger free radical

$$CH_3CH_2^{\bullet} + CH_2 = CH_2 \rightarrow CH_3CH_2CH_2CH_2^{\bullet} \quad (4.4)$$

5. **Termination reaction** involves the recombination reaction between two free radicals to form a molecule and/or disproportionation reaction in which a free radical transfers a hydrogen atom to the other to form an alkane and an olefin:

$$CH_3^{\bullet} + CH_3CH_2^{\bullet} \rightarrow CH_3CH_2CH_3 \quad (4.5)$$

$$CH_3CH_2^{\bullet} + CH_3CH_2^{\bullet} \rightarrow CH_2 = CH_2 + CH_3CH_3 \quad (4.6)$$

The smallest free radicals in the reacting system are hydrogen, methyl, and ethyl radicals which are more stable than higher ones. These free radicals form saturated hydrocarbon when they capture hydrogen from another hydrocarbon molecule or radical. These cracking reactions break the higher molecular weight hydrocarbons into lower molecular weight fractions. The rate of these reactions is a function of temperature. The following gases where determined by the RGA which are typical products of thermal cracking: hydrogen, methane, ethane, n-butane, n-pentane, i-pentane, trans-2-butene, ciss-2-butene, carbon dioxide, and carbon monoxide.

4.3 CAPRI Process

In this Section, catalytic cracking upgrading is reported. The effect of temperature upon the yield of liquid, gas and coke deposited upon the used catalyst was studied, together with the extent of upgrading of the produced oil as measured by viscosity, API gravity and true boiling point (TBP) distribution.

4.3.1 Effect of Temperature: Thermal vs Catalytic Cracking

Thermal and catalytic cracking are routes of upgrading heavy oils driven by temperature. However, for accurate evaluation of catalyst role and performance, CAPRI results were compared with thermal cracking counterpart (see Section 4.2 and Table 4.1 & 4.2), at the same experimental conditions. For the thermal reactions only, average change in API gravities at 350, 400 and 425 °C were 0.7, 1.1 and 1.7^{o} API, respectively. This compares less favourably with the catalytic upgrading counterpart where an average upgrading of 3.8, 2.5 and 1.7° API gravity occurred at 425, 400 and 350 °C, respectively. In the same vein, the absolute viscosity was measured as 0.22, 0.29 and 0.37 Pa.s for thermal compared to the catalytic runs viscosities of 0.09, 0.18 and 0.24 Pa.s at temperature 425, 400 and 350 °C, respectively. This represented a 2.4, 1.6 and 1.5 times viscosities reduction for CAPRI experiments compared to thermal cracking over glass beads, establishing the superiority of incorporating catalytic upgrading with THAI.

From Table 4.2, the conversion of residue fractions (BP > 343 ^{o}C) for thermal cracking reactions only was 16.8 % at 425 ^{o}C, whereas 36.6 and 34.6 % were obtained in CAPRI experiments using Ni-Mo/Al_2O_3 and Co-Mo/Al_2O_3, respectively. This represents 17-20% increase in residue fraction conversion. This observation is in conformity with that reported in literature (Panariti, et al., 2000). Similarly, the asphaltenes content of the produced oil using thermal cracking at 350, 400, and 425 ^{o}C were 9.9, 9.4, and 8.9 wt%, and upon catalytic upgrading at the same conditions the conversions were 9.6, 8.6, and 6.7 wt.%, respectively, relative to the feed oil (11.14 wt%). In all cases, the catalytic cracking effect over Co-Mo/Al_2O_3 and Ni-Mo/Al_2O_3 catalysts outweighs thermal cracking upgrading.

4.3.2 Effect of Temperature on Mass Balance

The liquid (i.e., produced oil), gas, and coke yields were calculated using equations 3.10 and 3.11 (see Chapter 3 and Section 3.3.2). Table 4.3 displays the yields, from which it can be observed that the lower temperature favours lesser production of gases and coke and more liquid products for both catalysts, suggesting a low degree of thermal and catalytic upgrading. The amount of coke produced at 350 °C was 0.64 wt.% compared to 1.86 wt.% at 425 °C, and the corresponding measured liquid yields were 97.4 and 93.8 wt.% respectively, for Co-Mo catalyst. The yield of gases was 1.96 wt.% at 350 °C and 4.34 wt.% at 425 °C. Whilst for Ni-Mo catalyst, the amount of coke and liquid produced at 350 ^{o}C 0.7 and 97.2 wt. %, 400 ^{o}C: 0.85 and 96.2 wt.%, and at 425 ^{o}C: 1.73 and 93.6 wt.%, respectively. The yields of gas were 2.1 wt.% at 350 °C and 4.4 wt.% for 425 °C.

Table 4.3 Mass balances; Catalysts Co-Mo/Al_2O_3 and Ni-Mo/Al_2O_3, Reaction Media (N_2), Pressure 20 barg, Oil flow rate 1 mL.min^{-1}, Gas flow rate 500 mL.mL^{-1}.

Reaction temperature (^{o}C)	**Gas (wt.%)**	**Liquid (wt.%)**	**Coke (wt.%)**
	Co-Mo/Al_2O_3		
350	1.96	97.4	0.64
400	2.96	95.87	1.17
425	4.34	93.8	1.86
Mean STDev*	0.2	1.20	0.91
	Ni-Mo/Al_2O_3		
350	2.1	97.18	0.72
400	2.77	96.2	0.85
425	3.81	93.56	1.73
Mean STDev*	0.32	0.98	0.74

**STDev is standard deviation*

A similar mass balance was reported by Krumm et al. (2011) and Fesharaki et al. (2013) they found that gas, coke and liquid yields were 5.49, 0.76, and 93.75% from upgrading using nanoporous catalyst on vacuum residue at 420 ^{o}C. The increase in yields of gas and coke at 425 ^{o}C temperature can be attributed to increased catalytic cracking reactions with temperature rise. Additionally, coke and gas are end products therefore expected to increase with reaction temperature.

4.3.3 Effect of Temperature on API gravity

The API gravity of the crude oil is one of the yardsticks for assessing the amount of distillate obtainable from the oil. In Figure 4.1 (a), (b), and (c), the API gravity of the produced oils at different processing temperatures as a function of time-on-stream for Co-Mo, Ni-Mo, and Co-Mo plus Ni-Mo (Co-Mo on top Ni-Mo in 3:3 w/w) catalysts are presented. For all the three scenarios, it is clear that the API gravity of the produced oil increased as the reaction temperature increases from 350 to 425 ^{o}C. At an experimental temperature of 425 ^{o}C, the API gravity for the oil produced with the three catalysts runs was roughly 19 to 21 ^{o}API at the early hours, which drastically fell shortly after the reaction started and reached its lowest value of about ~3° API (above 13 ^{o}API for feed oil) at about 200 minutes into the experiment and remained at a plateau of roughly 16 ^{o}API upgrading until the end of the experiment.

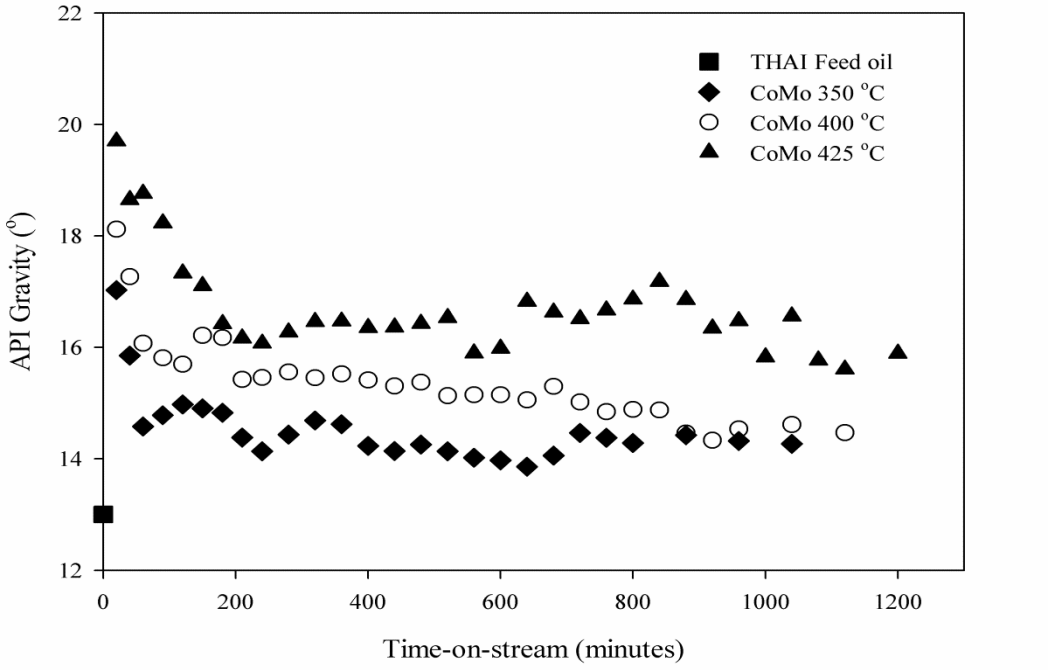
THAI Feed oil
CoMo 350 °C
CoMo 400 °C
CoMo 425 °C
API Gravity (°)
Time-on-stream (minutes)
22
20
18
16
14
12
0
200
400
600
800
1000
1200

(a)

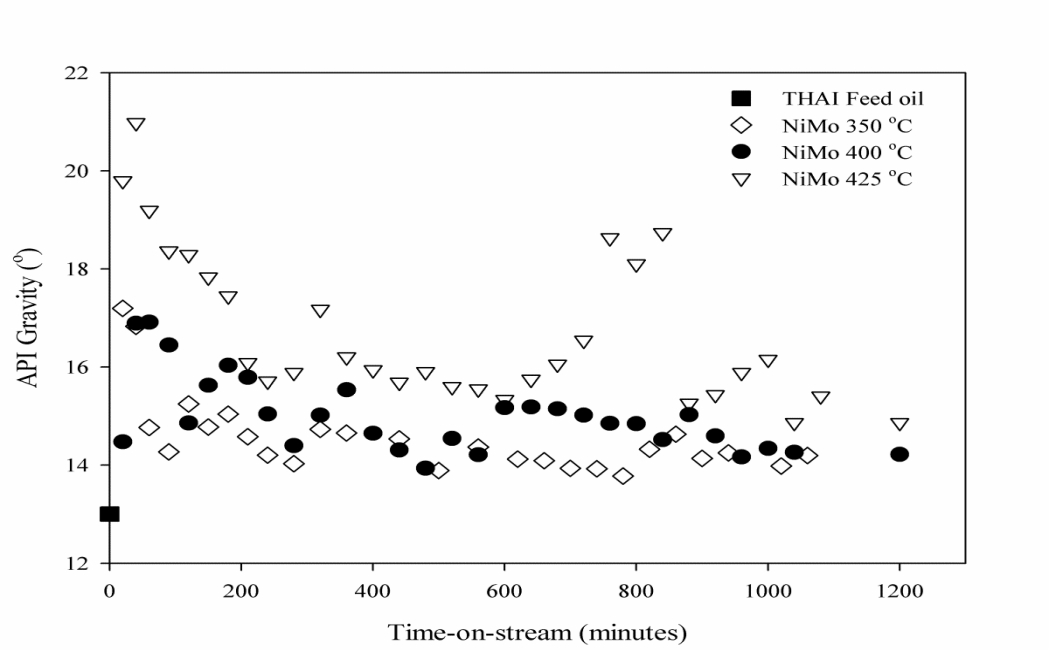
THAI Feed oil
NiMo 350 °C
NiMo 400 °C
NiMo 425 °C
API Gravity (°)
Time-on-stream (minutes)
22
20
18
16
14
12
0
200
400
600
800
1000
1200

(b)

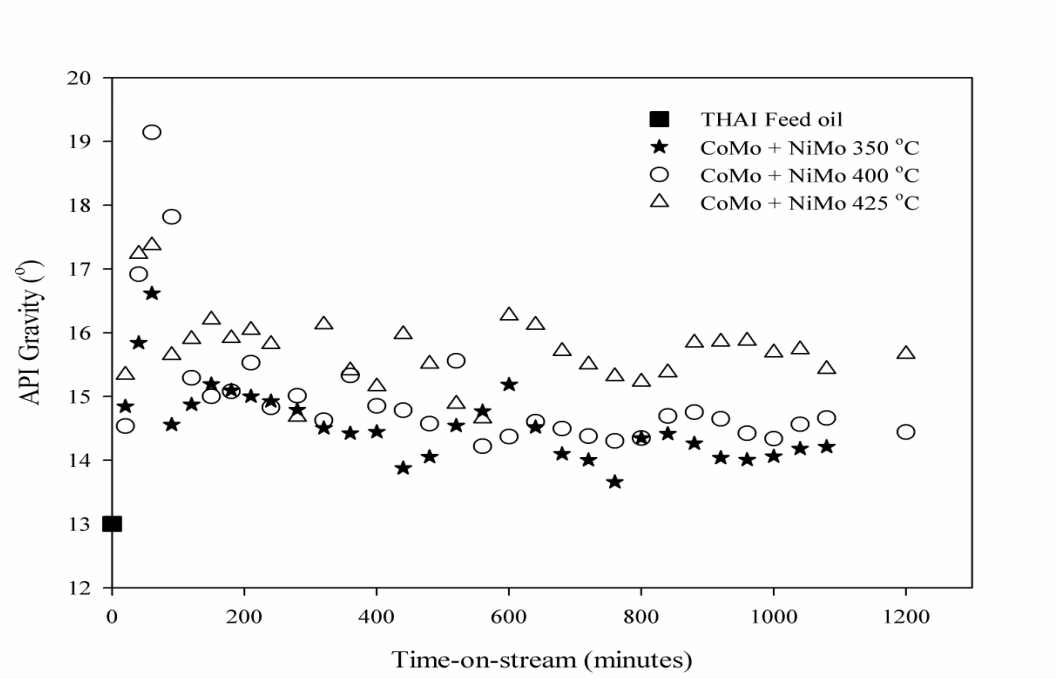

(c)

Figure 4.1 API gravity of CAPRI produced oil at 350, 400 and 425 °C; Reaction Media N_2, Pressure 20 barg, Oil flow rate 1 mL.min^{-1}, Gas flow rate 500 mL.mL^{-1} and Catalysts (a) Co-Mo (b) Ni-Mo and (c) Co-Mo on top Ni-Mo.

During the first 100 minutes, significant API gravity increase in the produced oil samples can be observed at all the three reaction temperatures and reaches a maximum value of 6.5° (Co-Mo/Al_2O_3), 8^o (Ni-Mo/Al_2O_3) and 6.3^o (Co-Mo + Ni-Mo), respectively at 425 °C. This is because at the earlier part of the reaction, the catalyst is still fresh, active and has not coked. At lower temperatures of 350 and 400 °C, an initial API increase in the range of 4 to 6°API can be noticed compared to the feed oil of 13 ^{o}API. At higher temperatures in the plateau region the level of upgrading also seems to depend on temperature, with about 1.7° increase at 350 °C and increasing up to ~4-5 °API upgrading at 425 °C. These trends in API gravity values were expected as reported earlier by Shah et al. (2011) that 425 °C was the optimum upgrading temperature for CAPRI, and further increase in temperature leads to

increased coke deposition which led to reactor shut down due to coke blockages. Also, the results are consistent with those reported by Kim et al. (1997) on upgrading of bitumen-derived heavy oils using commercial Ni-Mo/Al_2O_3 catalyst and also with the work of Ovalles and Rodriguez (2008) on upgrading of extra heavy oil down-hole under cyclic steam injection conditions. Comparing with the mass balance in Table 4.3, it can be observed that more liquid production occurs at lower temperature (350^{o}C), however, the level of upgrading at this temperature is not as significant as the previously optimized temperature of 425°C, suggesting a trade-off between liquid production and quality. Even so, it is clear that the catalyst activity decreased with time-on-stream, as can be observed in Figure 4.1 for all the experimental conditions and catalysts used. Xia and Greaves (2001) reported that coking of the catalyst with time-on-stream could reduce its activity.

The average API gravity of CAPRI produced oils at 350, 400, and 425 ^{o}C is presented in Table 4.4. These results however, establish the fact that even at lower temperatures of 350°C the average API gravity increase of 1.97° (Co-Mo), 1.69^o (Ni-Mo) and 1.72^o (Co-Mo + Ni-Mo) shows some measurable improvement compared to thermal cracking upgrading presented in Table 4.2 for all reaction temperatures.

Table 4.4 Average API gravity of CAPRI produced oil at 350, 400 and 425 °C; Reaction Media (N_2), Pressure 20 barg, Oil flow rate 1 mL.min^{-1}, Gas flow rate 500 mL.mL^{-1} and Catalysts: Co-Mo, Ni-Mo and Co-Mo on top Ni-Mo (feed: 13^{o}API).

Temperature (^{o}C)	**Co-Mo/Al_2O_3 (^{o})**	**Ni-Mo/Al_2O_3 (^{o})**	**Co-Mo + Ni-Mo (^{o})**
350	14.97 ± 0.24	14.69 ± 0.91	14.72 ± 0.66
400	15.63 ± 0.76	15.21 ± 0.86	15.21 ± 0.71
425	16.75 ± 0.93	16.73 ± 0.66	15.74 ± 0.62

The increase in API gravity as observed from Figure 4.1 and the averaged values presented in Table 4.4 shows improved quality of the produced oil as Greaves et al. (2000) noted that with a 5.9 °API increase needed only about 15% of diluent to meet pipeline transportation specifications, compared to 30–50% required for non-upgraded bitumen produced from SAGD and CSS operations.

4.3.4 Effect of Temperature on Viscosity

It is well known that high viscosity of heavy oils hinders their extraction and pipelining to refineries. The viscosities of the CAPRI produced oils as a function of time-on-stream at the reaction temperatures and for different catalysts are presented in Figure 4.2 (a), (b) and (c), respectively. As can be seen there is a substantial viscosity reduction of the upgraded oil samples observed compared to the feed oil, with higher viscosity reduction noticed at 425 ^{o}C. Additionally, the viscosity reduced from 0.5 Pa.s for the feed oil to 0.11 Pa.s (350 ^{o}C), 0.085 Pa.s (400 ^{o}C) and 0.022 Pa.s (425 ^{o}C) during the early hours of the reaction. After about 200 minutes the viscosity progressively increases with time-on-stream to settle in the range 0.245-0.282 Pa.s (350 ^{o}C), 0.155-0.17 Pa.s (400 ^{o}C) and 0.089-0.106 Pa.s (425 ^{o}C), respectively depending on the catalysts type. A similar trend was observed for the change in API gravity presented in Figure 4.1, which corresponds to the mirror trend of viscosity increase with time-on-stream as shown in Figure 4.2.

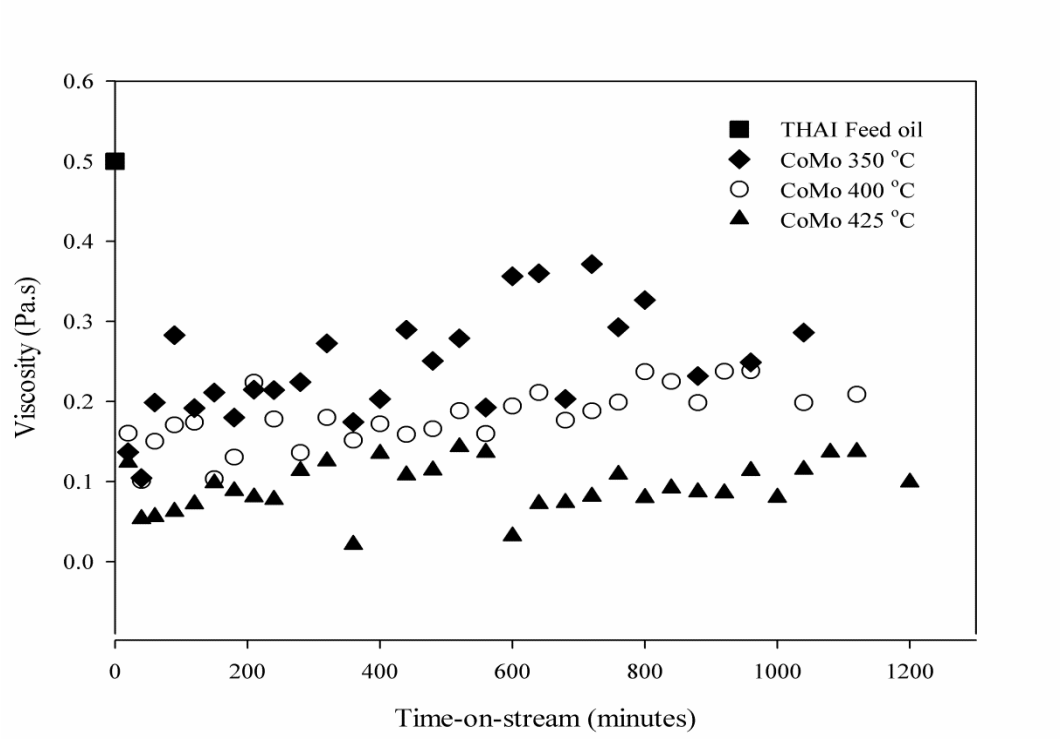
THAI Feed oil
CoMo 350 °C
CoMo 400 °C
CoMo 425 °C
Viscosity (Pa.s)
Time-on-stream (minutes)
0.0
0.1
0.2
0.3
0.4
0.5
0.6
0
200
400
600
800
1000
1200

(a)

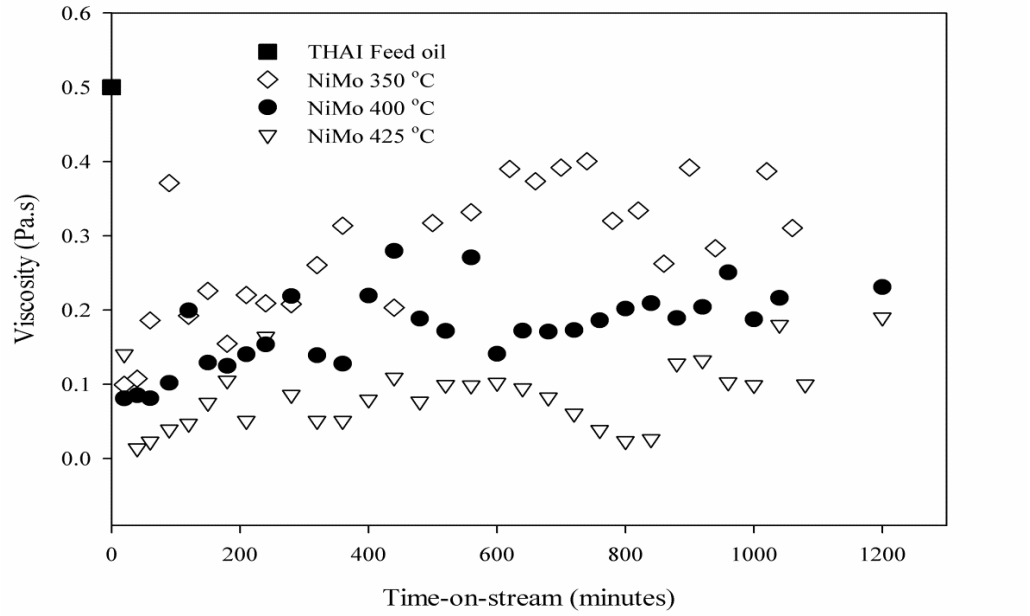
THAI Feed oil
NiMo 350 °C
NiMo 400 °C
NiMo 425 °C
Viscosity (Pa.s)
Time-on-stream (minutes)
0.0
0.1
0.2
0.3
0.4
0.5
0.6
0
200
400
600
800
1000
1200

(b)

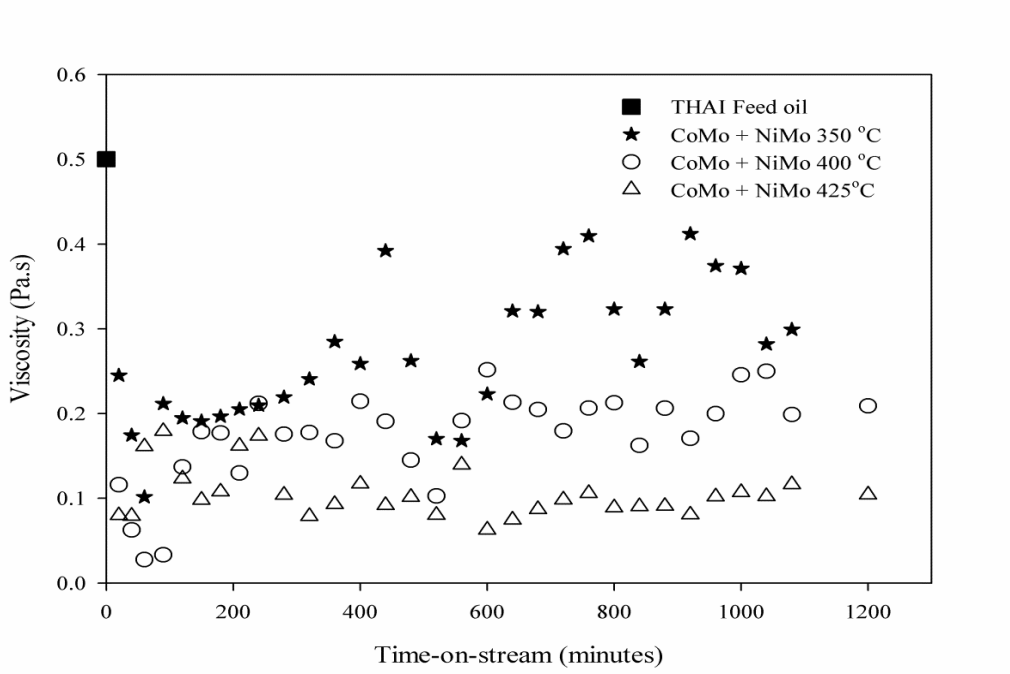

(c)

Figure 4.2 Viscosity of CAPRI produced oil at 350, 400 and 425 °C; Reaction Media N_2, Pressure 20 barg, Oil flow rate 1 mL.min^{-1}, Gas flow rate 500 mL.mL^{-1} and Catalysts: (a) Co-Mo (b) Ni-Mo and (c) Co-Mo on top Ni-Mo.

The absolute viscosity and DVR for the upgraded oil samples at the different reaction temperatures and catalyst types are presented in Table 4.5. Notably, at reaction temperatures of 350 and 400^{o}C, the use of Co-Mo + Ni-Mo catalyst further increased the DVR by 7.7 % (at 300 ^{o}C) and 3 % (at 400 °C) above that for Co-Mo and 3.3 and 0.9 % above that for Ni-Mo catalysts, respectively. This is due to the synergistic effect of the Co, Ni, and Mo metals upon the combined use of Co-Mo + Ni-Mo catalysts could be higher at 350 and 400 ^{o}C compared to 425 ^{o}C. This DVR is capable of improving the oil fluidity, quality and production index during the recovery as the oil viscosity is less than 0.2 Pa.s, the classical maximum viscosity for pipeline transport (Kessick, 1982). The viscosities of the produced oil obtained for reactions carried out at 400 and 425 ^{o}C for all three catalysts are below 0.2 Pa.s at 20^{o}C, the

expected range of viscosity for pipeline transport of crude oil (Ancheyta, et al., 2005). Additionally, they are lower than those reported in Table 4.1 for thermal upgrading only.

Table 4.5 Average viscosity and DVR of CAPRI produced oil at 350, 400 and 425 °C; Reaction Media (N_2), Pressure 20 barg, Oil flow rate 1mL.min^{-1}, Gas flow rate 500mL.mL^{-1} and Catalysts: Co-Mo, Ni-Mo and Co-Mo on top Ni-Mo (feed: 0.5 Pa.s).

Temperature (^{o}C)	**Co-Mo/Al_2O_3**	**Ni-Mo/Al_2O_3**	**Co-Mo + Ni-Mo**
	Absolute viscosity (Pa.s)		
350	0.282 ± 0.05	0.261 ± 0.09	0.245 ± 0.08
400	0.170 ± 0.03	0.160 ± 0.06	0.155 ± 0.06
425	0.094 ± 0.03	0.089 ± 0.04	0.151 ± 0.03
	Degree of viscosity reduction, DVR (%)		
350	42.3	46.7	50
400	65.3	67.4	68.3
425	88.9	81.9	78.5

Previously, the Saturates, Aromatics, Resins and Asphaltenes (SARA) analysis were carried out and reported by Shah et al. (2011) for experiments performed in the same reactor and under the same conditions as reported in this section. They found that saturates, aromatics, resins and asphaltene contents were 15.38, 57.04, 20.18 and 7.4 % for the feed oil and the values for the produced oil at 425 ^{o}C were 16.37, 67.62, 9.11 and 6.9 % respectively. They concluded that rise in API and viscosity reduction was due mainly to the increased amount of saturates and aromatics and the subsequent decrease in the resins and asphaltenes contents of the produced oil from the CAPRI process. This occurs as a result of the C-C bond cleavage in large hydrocarbons chains to lower molecular weight fractions (see Table 4.1), the occurrence is observed in the produced gas. In the course of reaction, the paraffinic side chains of the aromatic ring structures break while some portions of the aromatics undergo hydrogenation and/or polymerisation and condensation reactions to form coke (Chen and Cao,

1994). Notably, low viscosity oil has high API gravity; however there is no correlation between API gravity and viscosity of the produced oil after close examination of experimental data, because different factors influenced the viscosity and API gravity values differently (Ancheyta, et al., 2005).

Commercial HDS catalysts are low cost catalyst (Xia, et al., 2002). Shah et al. (2011) estimated that 20 tonnes of new HDS catalyst for 500 m horizontal producer well cost about $60– 100k. Early estimates from Petrobank suggested that the THAI-CAPRI process costs about one third per producing barrel of the equivalent SAGD process (Petrobank, 2010).

4.3.5 Effect of Temperature on TBP Distribution

Figure 4.3 provides the results of the TBP distribution curves of feed and produced oils at the different reaction temperatures and catalyst type. It can be observed that as the reaction temperature increased from 350 to 425 ^{o}C in the upgrading experiment; it favours a significant shift in TBP curves towards lighter distillate fractions in comparison to the feed oil. It has been demonstrated in Sections 4.3.2 and 4.3.3, that increasing upgrading temperature from 350-425 ^{o}C increases API gravity and DVR. It is clear therefore that upgraded oils that have high API gravity and low viscosity values present also the highest yields of distillates.

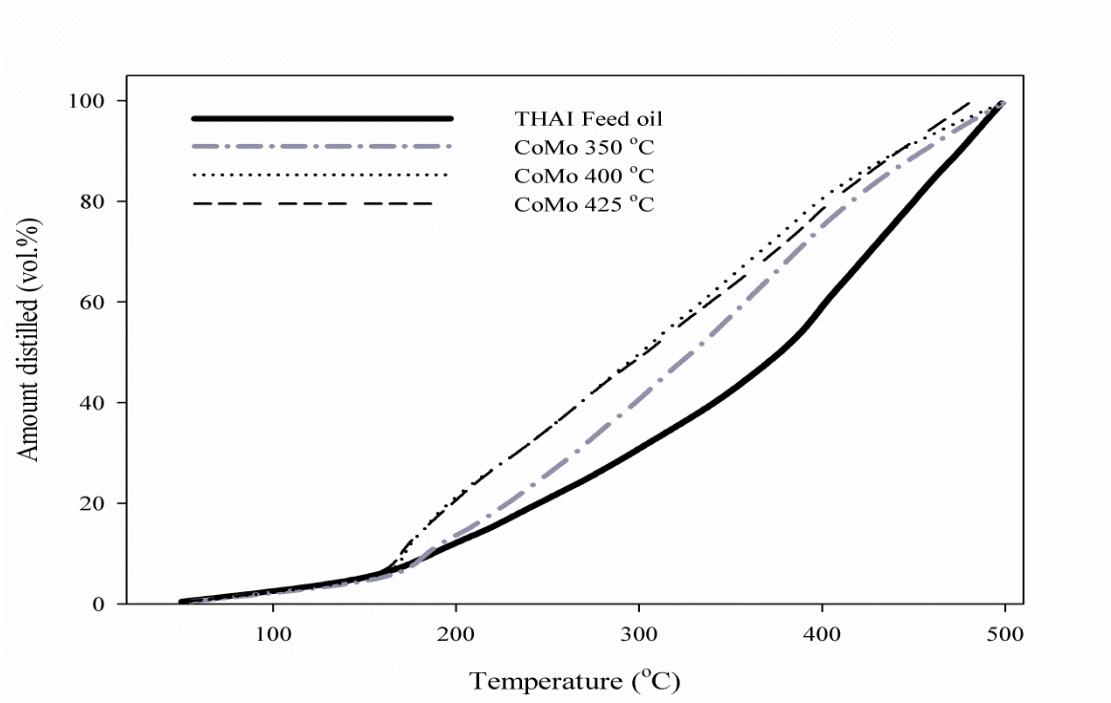
THAI Feed oil
CoMo 350 °C
CoMo 400 °C
CoMo 425 °C
Amount distilled (vol.%)
Temperature (°C)
0
20
40
60
80
100
100
200
300
400
500

(a)

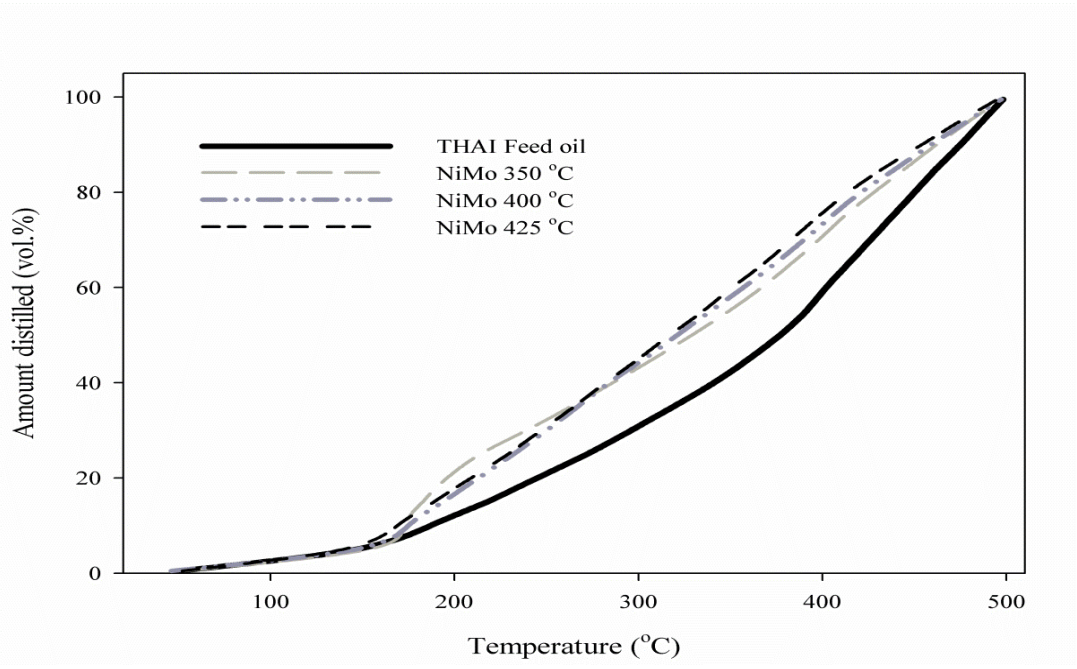
THAI Feed oil
NiMo 350 °C
NiMo 400 °C
NiMo 425 °C
Amount distilled (vol.%)
Temperature (°C)
0
20
40
60
80
100
100
200
300
400
500

(b)

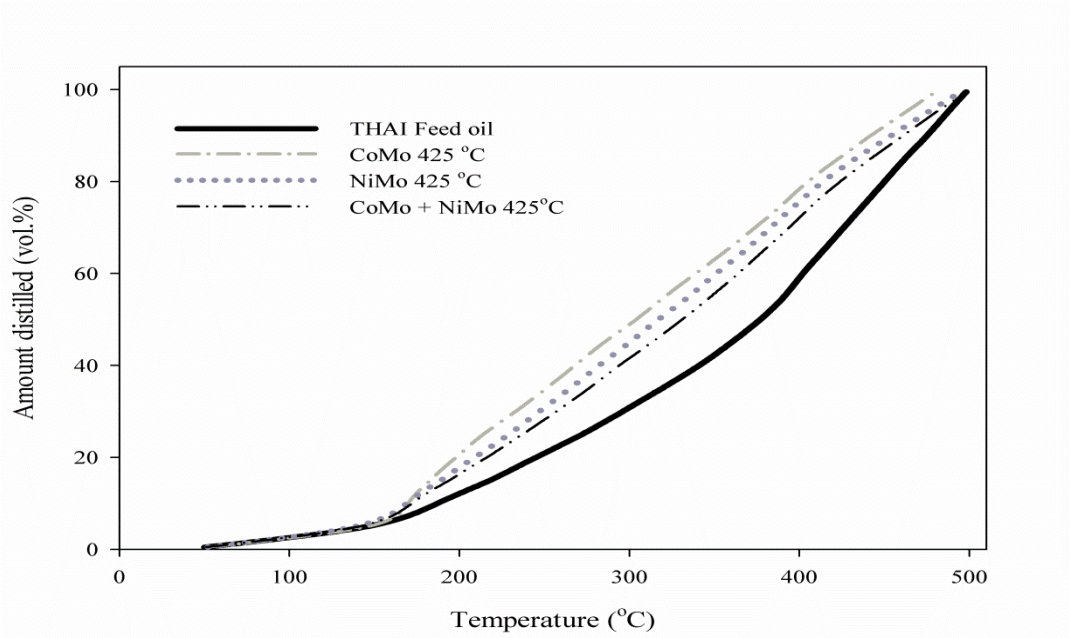

(c)

Figure 4.3 Viscosity of CAPRI produced oil at 350, 400 and 425 °C; Reaction Media N_2, Pressure 20 barg, Oil flow rate 1mL.min^{-1}, Gas flow rate 500 mL.min^{-1} and Catalysts: (a) Co-Mo at different temperatures (b) Ni-Mo at different temperatures and (c) different catalysts at the optimum temperature of 425 ^{o}C TBP curves.

For example in the TBP distribution curves for the use of Co-Mo/Al_2O_3 (Figure 4.3a), at the boiling point of 200 ^{o}C the cumulative percentage yields for reaction temperatures 350, 400, and 425 ^{o}C were 15, 22 and 23 %, respectively, relative to the feed oil (10 %). On the contrary, it can be seen in Figure 4.3 (a) that 10 % yield of distillate at 200 ^{o}C for the feed oil is obtained at lower temperatures for the produced upgraded oils depending on the reaction temperature, which explains the shift of curves to the left. This result is consistent with the literature (Fumoto, et al., 2009). They found that the yield of lighter distillates increased with reaction temperature on the cracking heavy oil using zirconia-alumina-iron oxide catalyst in a steam environment. Additionally, the increased yield of light distillates with reaction temperature is in line with the increased API gravity and reduced viscosity of the produced oil

relative to the feed oil presented in Figures 4.1 and 4.2. From Figure 4.3c, it is clear that Co-Mo/Al_2O_3 catalyst produced higher amount of low-boiling fractions than Ni-Mo/Al_2O_3 and Co-Mo + Ni-Mo catalysts at 425 ^oC. Consequently, the conversion of residue fraction (BP > 343 ^oC) was calculated and presented in Table 4.6.

Table 4.6 Conversion of 343 ^oC+ HCs at temperatures 350, 400, and 425^oC, pressure 20barg, N_2 reaction media, nitrogen-to-oil flow ratio 500 $mL.mL^{-1}$, oil flow rate 1 $mL.min^{-1}$ and Catalysts Co-Mo and Ni-Mo.

Catalyst	**Experimental temperature (^oC)**	**Conversion of 343^oC+ (%)**
Co-Mo	350	16.8
Co-Mo	400	28.7
Co-Mo	425	34.6
Ni-Mo	350	26.2
Ni-Mo	400	22.2
Ni-Mo	425	36.6

As the temperature increased from 350 to 425 ^oC the conversion of the heavy end fractions into lighter distillates increased with the highest conversion obtained at 425 ^oC. As expected the increase in the yield of distillates with boiling point less than 343 ^oC drastically lowers the viscosity of the produced oil (Ancheyta, et al., 2005). Evidence from Figures 4.1 and 4.2 and Table 4.6 showed that improved oil quality was obtained at 425 ^oC, however the magnitude of coke produced at 425 ^oC can not be ignored (see Table 4.3), as coke is known to drastically deactivate the catalyst and plug the bed.

4.3.6 Effect of Temperature on Asphaltenes, Sulphur and Metal content

Impurities such as sulphur and metals impact on the quality of the oil. The asphaltenes, sulphur and metals content of the feed oil and produced oils at 400 and 425 ^{o}C are presented in Table 4.7.

Table 4.7 Asphaltenes, sulphur and metal content of feed and produced oil at 400 and 425 °C; Reaction Media (N_2), Pressure 20 barg, Oil flow rate 1 mL.min^{-1}, Gas flow rate 500 mL.min^{-1}, Catalysts: Co-Mo and Ni-Mo.

Impurities	**Feedstock**	**Co-Mo/Al_2O_3**		**Ni-Mo/Al_2O_3**	
		400^{o}C	**425^{o}C**	**400^{o}C**	**425^{o}C**
Asphaltene (wt.%)	11.14	8.6	6.1	7.2	6.75
Aluminium (ppm)	6	7	7	7	0
Boron (ppm)	9	1.1	0.8	1	0
Calcium (ppm)	0.8	0.7	0	0.6	0
Cobalt (ppm)	< 1	< 1	0	< 1	0
Chromium (ppm)	0.4	0.3	0.3	0.2	0
Iron (ppm)	36	10	3	5	3
Molybdenum (ppm)	6	5	3	6	0
Sodium (ppm)	< 7	2	3	5	0
Nickel (ppm)	56	52	50	54	51
Vanadium (ppm)	150	144	131	146	136
Phosphorus (ppm)	0.3	0.6	0.1	0.5	0
Sulphur (wt.%)	3.8	3.7	3.55	3.6	3.6
Silicon (ppm)	0.4	2	1	2	0
Zinc (ppm)	2	0.6	0.3	0.7	1
Ni + V (ppm)	206	196	181	200	187

* Sulphur and metals content was performed by Intertek Laboratories Sunbury Technology Centre, UK, using ICP-OES (Inductively Coupled Plasma Optical Emission Spectrometry).

The content of the asphaltene in nC_7 was reduced from 11.14 to 8.6 and 7.2 wt.% (400 ^{o}C) and 6.1 and 6.75 wt.% (425 ^{o}C) for Co-Mo and Ni-Mo catalysts, respectively. It

shows that the cracking of asphaltenes increases as the reaction temperature increases. Notably, the decomposition of the asphaltene content of the feed oil as temperature increases was accompanied by the drop in viscosity, rise in API gravity and lower-boiling components in upgraded oil samples (see Figures 4.1, 4.2 and 4.3).

In the same reaction, sulphur content was reduced from 3.8 to 3.55 and 3.6 wt.% at 425 ^{o}C for Co-Mo and Ni-Mo catalysts. More so, the metal content of the produced oils was significantly lower than that of the feed oil mainly at 425 ^{o}C reported optimum by Shah et al. (2011). At 400 ^{o}C the nickel plus vanadium (Ni + V) content reduced from 206 to 196 and 200 ppm, while at 425 ^{o}C it was 181 and 187 ppm for Co-Mo and Ni-Mo catalysts, respectively. This indicates that Ni + V contents were further reduced by 7.24 and 6.31% for both catalysts as the temperature increased from 400 to 425 ^{o}C. It is therefore clear that the rate of desulphurisation and demetallisation reaction increased with temperature (Shah, et al., 2011; Ancheyta, et al., 2002). Under the conditions used in this study, the two catalysts showed different performance on sulphur and metal removal with Co-Mo being better for demetallisation and Ni-Mo better for the desulphurisation reaction (see Table 4.7).

4.3.7 Effect of Temperature on Produced Gas Composition

Table 4.8 provides quantitative composition of the produced gas during the experiments. The reported values are average of duplicate experimental runs. The presence of hydrogen in the gas indicates its *in situ* production during CAPRI. Its concentration increased from 2.57 to 2.70 vol.% with Co-Mo and 1.6 to 3.9% with Ni-Mo catalysts as the temperature increased from 400 to 425 ^{o}C. It is known that hydrogen is majorly produced by thermal cracking and dehydrogenation reactions either by hydrogen-abstraction from

saturated hydrocarbon to form unsaturated compounds or the cleavage of carbon-hydrogen bond.

Table 4.8 Average off-gas composition during CAPRI reaction at 400 and 425 °C; Reaction Media (N_2), Pressure 20 barg, Oil flow rate 1mL.min^{-1}, Gas flow rate 500mL.min^{-1}, Catalysts: Co-Mo, Ni-Mo and Glass beads.

	Co-Mo		**Ni-Mo**		**Glass bead**
Gas (vol.%)	**400°C**	**425°C**	**400°C**	**425°C**	**425°C**
Hydrogen	2.574	2.701	1.588	3.900	1.590
Methane	0.146	0.071	0.074	0.092	0.190
Ethane	0.279	0.277	0.150	0.405	0.120
Propane	0.124	0.131	0.104	0.182	0.610
Carbon dioxide	0.034	0.048	0.022	0.043	0.321
Propene	0.073	0.078	0.061	0.076	0.000
i-Butane	0.000	0.000	0.000	0.032	0.000
n-Butane	0.064	0.072	0.034	0.082	0.080
trans-2-Butane	0.038	0.033	0.014	0.037	0.040
1-Butene	0.033	0.048	0.020	0.032	0.000
Cis-2-Butene	0.036	0.000	0.000	0.000	0.070
i-Pentane	0.042	0.027	0.000	0.034	0.020
n-Pentane	0.000	0.047	0.000	0.055	0.020
Carbon monoxide	0.034	0.035	0.014	0.038	0.096
Hydrogen sulphide	0.0002	0.0004	0.00042	0.0042	0.0001

The dehydrogenation index (DHI), which is defined as the volume ratio of H_2 to the sum of C_1 and C_2 yields $\{H_2 / (C_1+C_2)\}$ in gas can be used to measure the degree of dehydrogenation reaction that leads to coke formation (Wang, et al., 2012; Zhang, et al.,

2013). In this regard, high DHI represents more H_2 in the gas phase with more carbon-rejection from the feedstock to balance H/C atomic ratio in all products (i.e., gas, light oil, and coke). Therefore, as the reaction temperature increases from 400 to 425 ^{o}C the DHI increased from 6.1 to 7.8 (Co-Mo) catalyst and 7.1 to 7.9 (Ni-Mo), respectively. This increase in DHI values favours dehydrogenation and coke formation which causes catalyst deactivation (Wang, et al., 2012; Section 4.3.2, Table 4.3).

In line with Table 4.3, the overall amount of gas also rises with temperature in the catalytic runs. The level of CO and CO_2 were roughly identical in the two catalytic runs, whereas in the experiment conducted with glass beads the percentage of CO and CO_2 were 2.5 and 6.6 times that produced in the use of Co-Mo/Ni-Mo catalyst at 425 ^{o}C. The high concentrations of olefins in the off-gas are considered as a sign of effectual cracking reactions. Clearly, thermal cracking over glass beads produces more of certain gas components such as methane, propane, n-butane, trans-2-butane and cis-2-butene and n-pentane compared with catalytic cracking, however, some other components such as propene, i-butane and 1-butene were not produced over glass beads that were present over the catalyst. For both catalysts when the reaction temperature increased from 400 to 425 ^{o}C, the yield of hydrogen, light olefins and paraffin gases increased. This is because temperature rise makes the cracking reactions propagate faster (Fesharaki, et al., 2013). These trends are in conformity with trends reported elsewhere, where upgrading has largely been attributed to simultaneous thermal and catalytic cracking effects (Krumm, et al., 2011; Hashemi, et al., 2013).

The production of hydrogen during the catalytic upgrading process is vital to support hydroconversion in-situ. Hydrogen, methyl and ethyl are the smallest radicals in the reaction medium. Their presence therefore would help cap radicals of macromolecules that readily

recombined to larger molecules and coke. They are rich in hydrogen, their abstraction from hydrocarbon molecules of the heavy oil leads to the formation carbon-rich material coke. In Figure 4.4 (a), (b), and (c) the plots of the amount of hydrogen, methane and ethane in the gas stream with time-on-stream are presented.

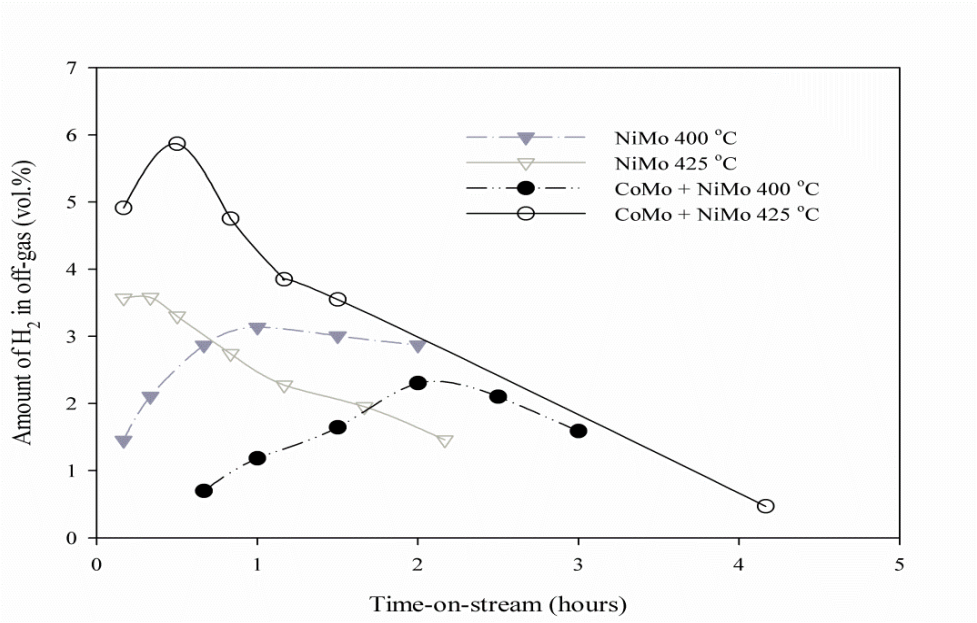

(a)

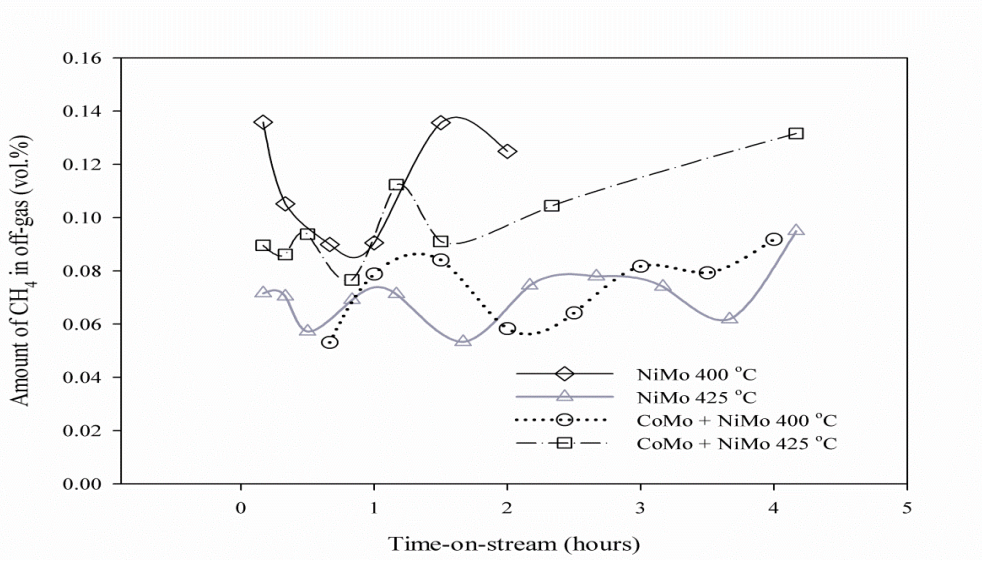

(b)

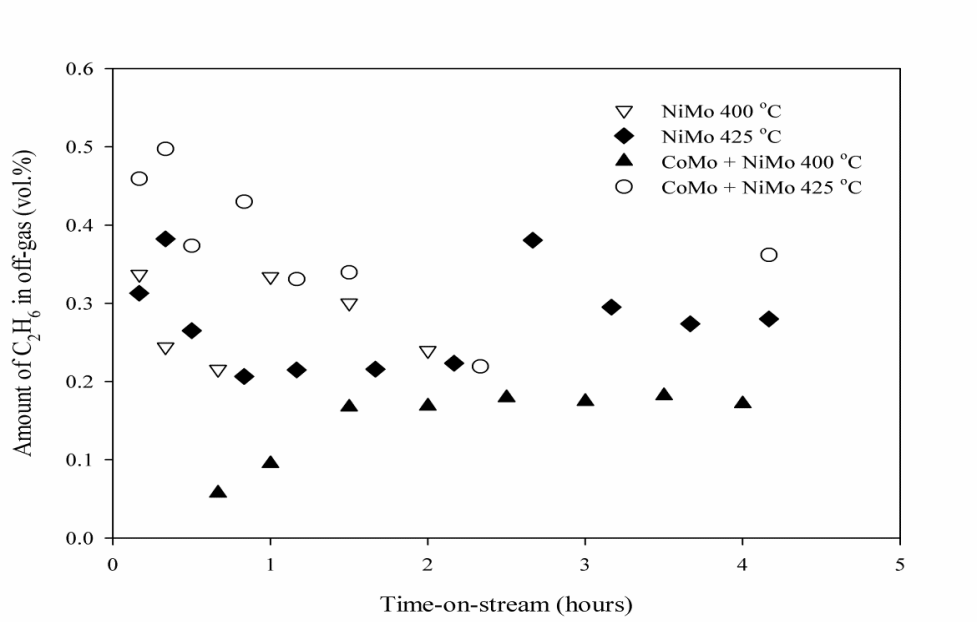

(c)

Figure 4.4 Amount of (a) hydrogen, (b) methane and (c) ethane in outlet gas stream as a function of time-on-stream at 400 and 425 °C; Reaction Media N_2, Pressure 20 barg, Oil flow rate 1 mL.min^{-1}, Gas flow rate 500 mL.min^{-1} and Catalysts: Ni-Mo/Al_2O_3 and Co-Mo + Ni-Mo.

From Figure 4.4, it can be seen that the amount of hydrogen, methane and ethane in the gas stream increased as the reaction temperature increases from 400 to 425 ^{o}C. The scattered data points can be attributed to pressure fluctuations due to coke and macromolecules deposition on the catalyst bed. The generation of hydrogen was high at the early hours compared to its use for hydrogenation; however its generation falls due to catalyst loss of activity to coke deposits (Ovalles, et al., 2003). The results have shown that the in-situ generated hydrogen as well as methane cannot sustain hydroconversion reactions effectively. Therefore, the need for an external source of hydrogen supply becomes necessary.

4.4 Effect of WHSV

In the Section above, the reported upgrading at 425 ^{o}C gave a better result in terms of increase in API gravity, viscosity reduction, conversion, and reduction of sulphur and metals content. In this section, the experiments were performed at constant reaction temperature 425^{o}C, pressure 20 barg, gas-to-oil ratio 500 mL.mL^{-1}, oil flow rate 1mLmin^{-1} and the effect of WHSV was investigated in the range of 9 to 21.8 h^{-1} by changing the weight of the catalyst used for six hours time-on-stream operation. The catalyst bed characteristics for the different WHSVs are presented in Table 4.9.

Table 4.9 Catalyst bed characteristics at oil flow 1 mL.min-1 and different WHSV.

Catalyst weight (g)	**Catalyst bed height (cm)**	**Oil residence time in the catalyst bed (min)**	**WHSV (h^{-1})**
2.5	5.2	1.84	21.8
4.0	8.1	2.86	13.6
6.0	11.6	4.10	9.1

4.4.1 Effect of WHSV on API gravity, viscosity, asphaltenes, and conversion

In Table 4.10 the average value of API gravity, asphaltenes content, absolute viscosity, and the conversion of 343 ^{o}C+ HCs for the produced oil after six hours time-on-stream operation as a function of WHSV is presented. It is clear that as WHSV decreases the produced oil API gravity increased from 16 to 18.4 ^{o}API and the viscosity reduced significantly from 0.1 to 0.72 Pa.s which is better than the original feed oil (13 ^{o}API and 0.5Pa.s). This occurs in view of the fact that the WHSV is inversely proportional to the residence time of the oil in the catalyst bed. Because the catalyst bed height decreased with increasing WHSV (see Table 4.9).

Table 4.10 Effect of WHSV on the API gravity, viscosity, Asphaltenes content, and conversion of 343 ^{o}C+ HCs at 425 ^{o}C reaction temperature, 20 barg pressure, nitrogen-to-oil ratio 500 mL.mL^{-1}, and oil flow rate 1 mL.min^{-1} (Mean values for 6 hours time-on-stream operations).

Catalyst	WHSV (h^{-1})	API gravity (^{o})	Viscosity (Pa.s)	Conversion 343^{o}C+ (%)	Asphaltenes (wt.%)
Co-Mo	21.8	15.7	0.0998	24.9	8.2
Co-Mo	13.6	16.8	0.0993	37.7	6.1
Co-Mo	9.1	18.4	0.0728	45.1	5.5
Ni-Mo	21.8	16.1	0.0976	22	7.7
Ni-Mo	13.6	17.5	0.0843	28.6	6.4
Ni-Mo	9.1	18.2	0.0731	36	6.75

The WHSV is inversely proportional to the contact time between the feed oil and the catalyst-bed, and is defined as weight per hour of feed oil divided by the weight of catalyst (Gao, et al., 2012). At higher WHSV the residence time is lower and hence the contact time of the oil with the catalyst bed is less. Conversely, as the contact time increased at low WHSV, cracking reactions would have increased giving rise to a higher yield of lighter hydrocarbon components. This can be seen in the next section on simulated distillation characteristics of the produced oil at the different WHSV. This finding however is in agreement with the results reported by Abuhesa and Hughes (2009); they found 7-9^{o} API points' increase in oil produced by catalytic *in situ* combustion of middle Clair crude oil of 19.8^{o} API when the amount of catalyst was increased from 1 to 5 g.

On the other hand, the produced oil viscosity was 0.0728 Pa.s (9.1 h^{-1}), and 0.098 Pa.s (21.8 h^{-1}) relative to the feed oil (0.49 Pa.s). This represents a DVR of 79 % (21 .8 h^{-1}) and 85% at 9.1 h^{-1}, respectively. This showed that the lower WHSV of 9.1 h^{-1} gave the highest percentage reduction in viscosity of the produced oil through catalytic upgrading process. However, high WHSV (i.e., short contact time) may have altered the extent of cracking

reactions leading to lower yield of light ends hydrocarbons in the oil produced (Wang, et al., 2009). Whilst, longer contact time gives the heavy oil adequate time to be cracked into lighter components.

Furthermore, the asphaltene content reduced from 11.14 wt.% (feed oil) to 8.2 and 7.7wt.% ($21.8h^{-1}$) and 5.5 and 6.7 wt.% ($9.1h^{-1}$) in the produced oil using Co-Mo and Ni-Mo catalysts, respectively. The catalytic conversion of asphaltenes into light hydrocarbons, gas, and coke increased as the WHSV decreased, due to increased contact time between the oil and catalyst as result of increased bed height. Hence, the extent of catalytic conversion in the CAPRI process can be correlated with the contact time between the catalyst active surface and the oil (Kim, et al., 1998). The effect of WHSV at the optimum reaction temperature 425 ^{o}C was noticeable for both Co-Mo and Ni-Mo catalysts types. From Table 4.10, the conversion of 343 ^{o}C+ HC fractions increases from 25 to 45 % (Co-Mo) and 22 to 36 % (Ni-Mo) catalyst when the WHSV decreased from 21.8 to 9.1 h^{-1} at constant 425 ^{o}C temperature. This represents a decrease by roughly 7 % for both catalysts. This demonstrates that the conversions of 343 ^{o}C+ fraction were limited at high WHSV due to limited acid sites of the catalyst responsible for cracking reactions. The opportunity of components in the feed oil to contact with acid sites increase as the WHSV decreases (i.e., amount of catalyst in the bed increase). Therefore, with sufficient acid sites (or catalysts) most components in the oil undergo sufficient cracking and conversion before they leave the catalytic bed (Li, et al., 2013).

4.4.2 Effect of WHSV on TBP distribution

The TBP distribution curve of the produced oil as a function of the WHSV is presented in Figure 4.5. It is clear that the yield of distillate of 40 vol.% in the TBP curves

corresponds to the shift to the left along the boiling temperature axis as the WHSV decreased. This indicates that the content of high carbon number hydrocarbons has been decreased while light hydrocarbons are increased in the produced oil (Junaid, et al., 2012).

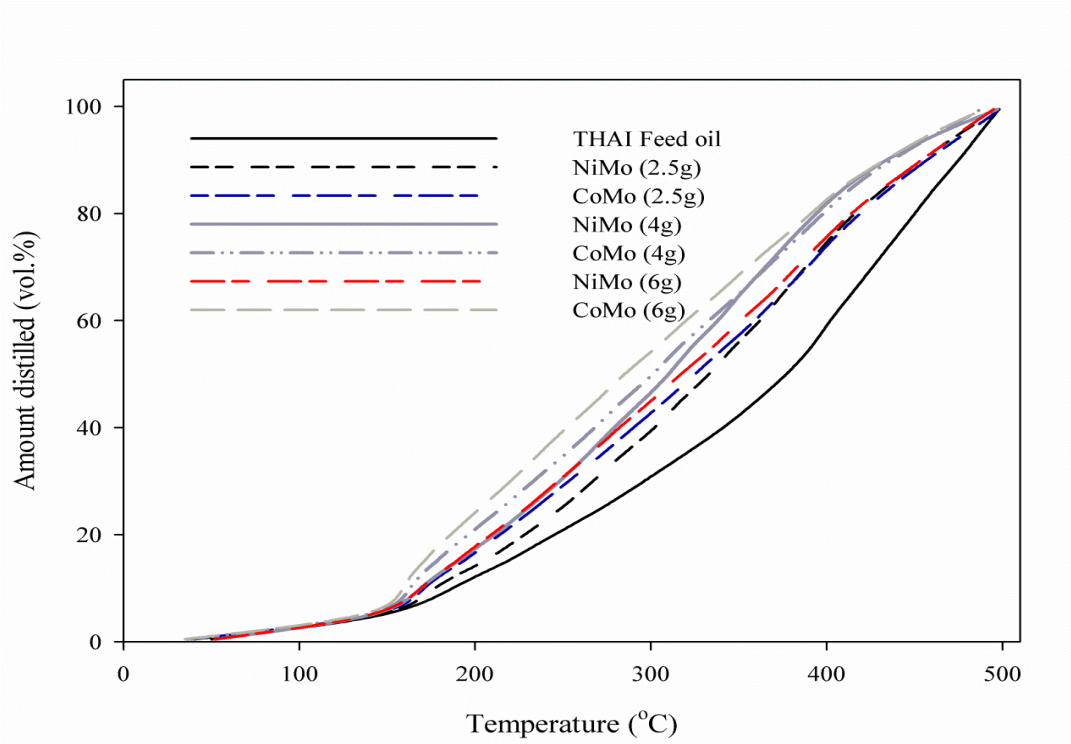

Figure 4.5TBP distribution curves of feedstock and produced oil as a function of WHSV at temperature 425 ^{o}C, pressure 20 barg, nitrogen-to-oil ratio 500 mL.mL^{-1} and Catalyst: Co-Mo and Ni-Mo.

The increase in conversion with decreasing WHSV was responsible for the shift of the TBP distribution curves of the upgraded oils to the left of the boiling temperature axis with reference to the feedstock curve. This means that high boiling (or high molecular weight) components in the feedstock have been converted into lighter ones. As expected, the increased API gravity and decreased viscosity of the produced oils confirmed the notion as WHSV decreased. Conclusively, the highest yield of the distillable fractions (i.e., fractions with

boiling temperature less than 343 ^{o}C) was accomplished at the highest reaction temperature of 425 ^{o}C and lowest WHSV of 9.1 hr^{-1}.

4.4.3 Effect of Catalyst Type

Alumina (Al_2O_3) supported molybdenum oxide catalysts promoted with nickel, cobalt, or tungsten are mostly used in the refinery for hydrodesulphurisation (HDS). In this study, Co-Mo/Al_2O_3 and Ni-Mo/Al_2O_3 was used to experimentally investigate the CAPRI conversion of heavy oil into light oil. Both catalysts have the same shape, and similar pellet length and diameter. However, Co-Mo catalyst has larger surface area and bigger pore diameter compared to that of the Ni-Mo catalyst (214.1 vs. 195.4 m^2g^{-1}; 63.7 vs. 33.7 nm). The performance of both catalysts was evaluated based on changes in API gravity, viscosity, asphaltenes content, metal and sulphur removal, and the conversion of boiling-fractions higher than 343 ^{o}C into low-boiling fractions.

In this study, the Co-Mo catalyst shows considerably higher conversion of 343 ^{o}C+ hydrocarbons into low-boiling fractions 25-45 % against 22-36 % for Ni-Mo catalyst depending on the WHSV. Though at the optimum temperature and WHSV there is no difference in the average API gravity and absolute viscosity of the produced oil (Co-Mo: 0.073 Pa.s, 18.4^{o} API and Ni-Mo: 0.073 Pa.s, 18.2^{o} API), compared to the original feed oil (0.5 Pa.s and 13^{o} API), nonetheless from Figure 4.5 the upgraded oil with Co-Mo/Al_2O_3 catalyst has a higher percentage of low-boiling fractions than the upgraded oil with Ni-Mo/Al_2O_3 catalyst. However, for the conversion of asphaltenes, Co-Mo catalyst reduced the asphaltene content of the feed oil from 11.14 to 5.5 wt.% compared to 6.75 wt.% (Ni-Mo) catalyst. This indicates that Co-Mo performed better than Ni-Mo, because of its large surface area and pore size provides easy access to the active site for macromolecules such as resins

and asphaltenes in the feed oil while the high acid strength enhanced the cracking activity for them to be converted into low molecular weight fractions compared to small pore and moderate acid sites Ni-Mo catalyst (Stanislaus, et al., 1996; Mouli et al., 2011; Boahene et al., 2011). In section 4.3.5, it is clear that while Ni-Mo performed better in desulphurisation reactions, however Co-Mo catalyst was better for demetallisation reactions.

4.5 Effect of Mono- Vs. Bi-metallic Catalysts

The metal sites of the catalyst promote hydrogen-dehydrogenation function and the acidic sites of the support perform cracking reactions. The performance of bimetallic Ni-Mo/Al_2O_3 was compared with mono-metallic Ni/Al_2O_3 counterpart.

4.5.1 Effect of Mono- and Bi-metallic Catalyst on API gravity and Viscosity

In Figure 4.6 (a) and (b), the API gravity and the viscosity of the produced oil using Ni-Mo/Al_2O_3 and Ni/Al_2O_3 as a function of time-on-stream is presented. It is clear that the bimetallic Ni-Mo catalyst performed better with a mean API gravity increase of 2.9 ± 1.5^{o}API compared to Ni based catalyst with 1.5 ± 1.2 ^{o}API, which indicate additional 1.4^o points API gravity increase using bimetallic Ni-Mo catalyst. At the same time, the DVR is 86.9 % for Ni-Mo/Al_2O_3 bimetallic against 78.8 % for Ni/Al_2O_3 monometallic catalyst below the viscosity of the feed oil (i.e., 1.091 Pa.s). As expected, the Ni-Mo bimetallic catalyst produced oil showed 1.4 ^{o}API further increments in API gravity and 8.1 % additional viscosity reduction to that obtained when Ni monometallic catalyst was used. Additionally, the asphaltene contents were respectively 6.8 wt.% (Ni-Mo/Al_2O_3) and 8.2 wt.% (Ni/Al_2O_3) catalysts against the feed oil (10.3 wt.%). Shah et al. (2011) pointed out that the rise in API and decrease in viscosity was due largely to hydroconversion in addition to cracking reactions by the acid sites.

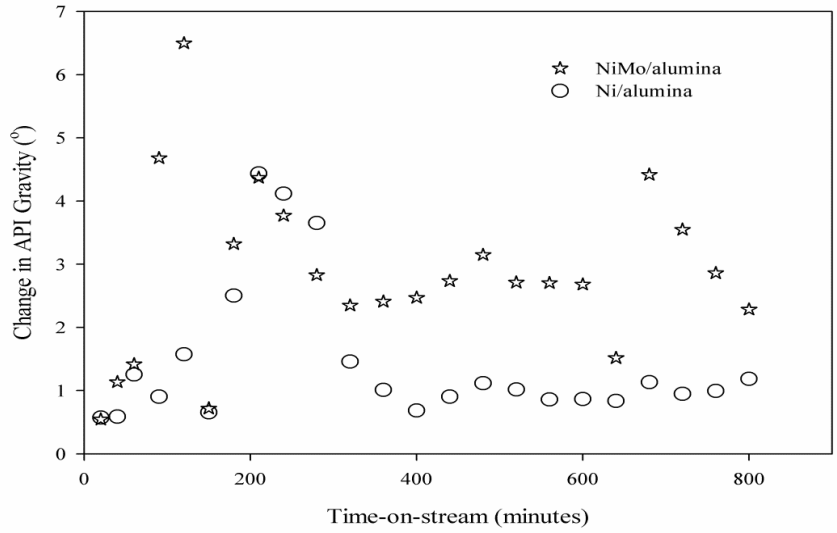

(a)

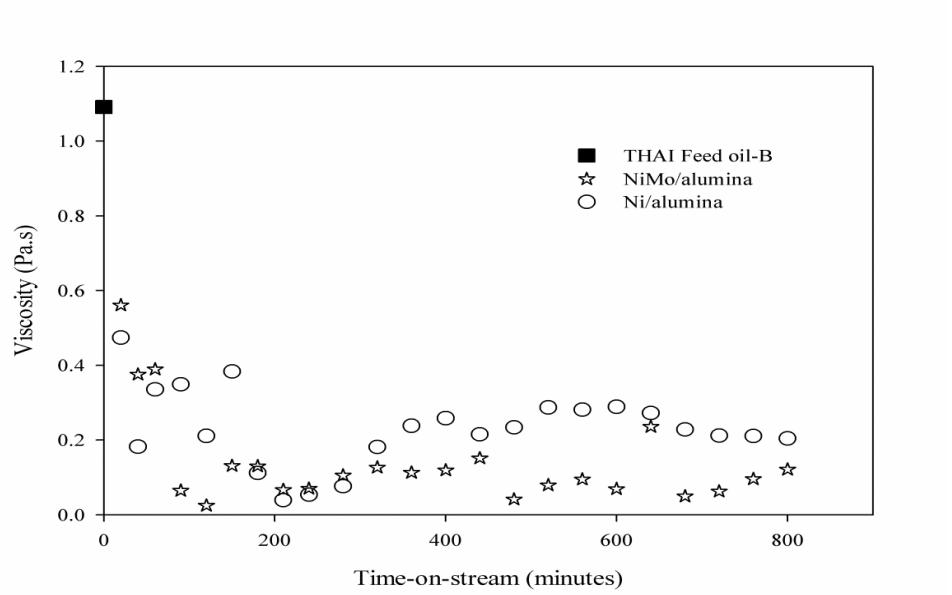

(b)

Figure 4.6 Effect of mono and bimetallic catalysts on produced oil (a) API gravity and (b) viscosity at temperature 425 ^{o}C, pressure 20 barg, nitrogen-to-oil ratio 500 mL.mL^{-1} and Catalysts: Ni-Mo/Al_2O_3 and Ni/Al_2O_3.

Therefore, bimetallic catalyst promotes hydrogen uptake by free radicals to facilitate hydrogenation reactions than their monometallic counterpart. It has also been reported that the presence of molybdenum in the catalyst gives it intrinsic activity for hydrodesulphurisation (HDS) reactions (Vishwakarma, et al., 2007). Shah et al. (2011) concluded that the rise in API and viscosity was due largely to hydroconversion in addition to HDS, HDM or HDA activity. To confirm this, the produced hydrogen gas for the use of Ni-Mo/alumina and Ni/alumina catalysts was measured. It was found that the mean produced hydrogen gas for Ni-Mo/alumina is 1.88 ± 0.37 compared to 1.21 ± 0.78 vol.% for Ni/alumina.

This superiority of bimetallic Ni-Mo/Al_2O_3 catalyst over monometallic Ni/Al_2O_3 is the result of the synergistic effect of the Mo metal which enhanced the catalyst activity (Jeon, et al., 2011). This synergistic effect is sustained as far as the two metals in the bimetallic catalyst remain chemically bound without decomposing to individual metals. In addition, Panariti et al. (200a, b) found that Mo metal is more active and activate faster than Ni metal, which explained the high performance of Ni-Mo over Ni based catalyst.

4.6 Commercial Vs. Prepared Zeolite-based Catalyst

The compositions of the commercial HDT catalysts previously used are Co, Ni, and Mo supported on alumina. The cracking activity, stability, and selectivity can be manipulated by modifying the support (Biswas, et al., 2011). In this Section, the results of the test carried out with prepared Ni/Zeolite-Alumina compared with that of commercial Ni-Mo/Al_2O_3 and Ni/Al_2O_3 all cylindrically shaped are presented and discussed. Properties of the prepared Ni/Zeolite-Alumina catalyst are presented in Appendix A.

4.6.1 Effect on API Gravity and Viscosity

The produced oil API gravity and viscosity as a function of time-on-stream using the prepared Ni/Zeolite-Alumina, commercial Ni-Mo/Al_2O_3 and Ni/Al_2O_3 at the same conditions of temperature, pressure, and N_2/oil flow ratio is presented in Figures 4.7 (a) and (b), respectively. The results showed that in all cases the produced oil API gravity in Figure 4.9a is at least roughly 1^o above that of the feed oil (14 ^{o}API). Clearly, the API gravity of the produced oil samples with commercial Ni-Mo/Al_2O_3 was higher than those of prepared Ni/Zeolite-Alumina and Ni/Al_2O_3 catalysts. Consequently, the API gravity of the produced oil samples with prepared Ni/Zeolite-Alumina was significantly higher than that of commercial Ni/Al_2O_3.

When prepared Ni/Zeolite-Alumina was used a maximum API gravity of 5.7^o was achieved before dropping to 1.3^o in 200 minutes and thereafter settles at an average of 2.4 ± 1.2^o API. However, the average upon the use of commercial Ni-Mo/Al_2O_3 and Ni/Al_2O_3 were 3.2 ± 1.2 and 1.4 ± 1.1^o API, respectively. The rapid decrease in API gravity can be attributed to the loss of catalytic activity due to early coke deposition on the catalyst. Also, the basic nitrogen compounds present in the feed oil could have also contributed to acid sites deactivation via neutralisation of the alumina support and the zeolite during cracking reactions (Bej, et al., 2001).

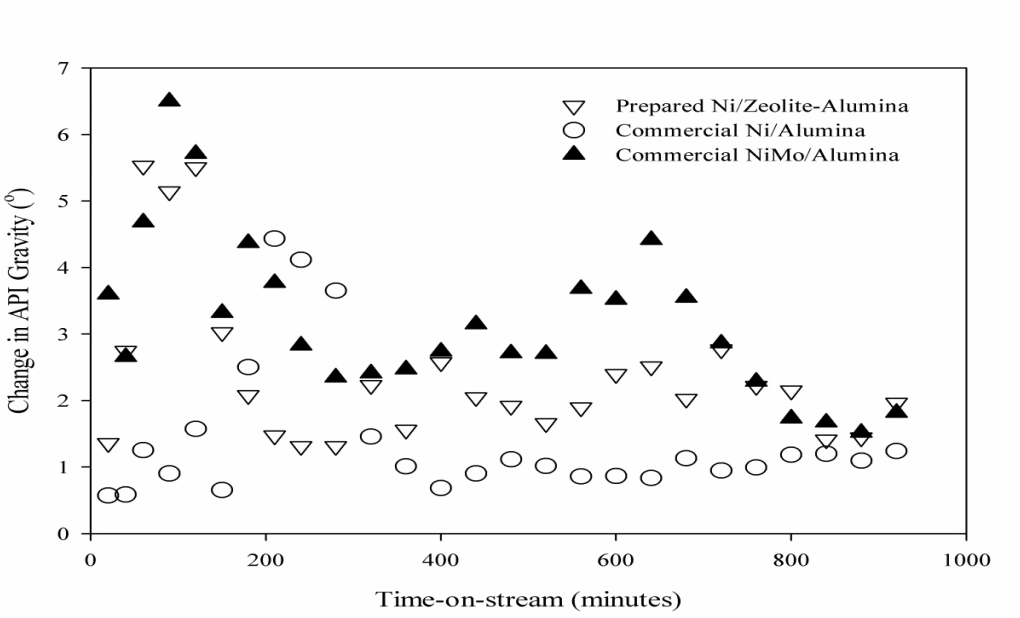

(a)

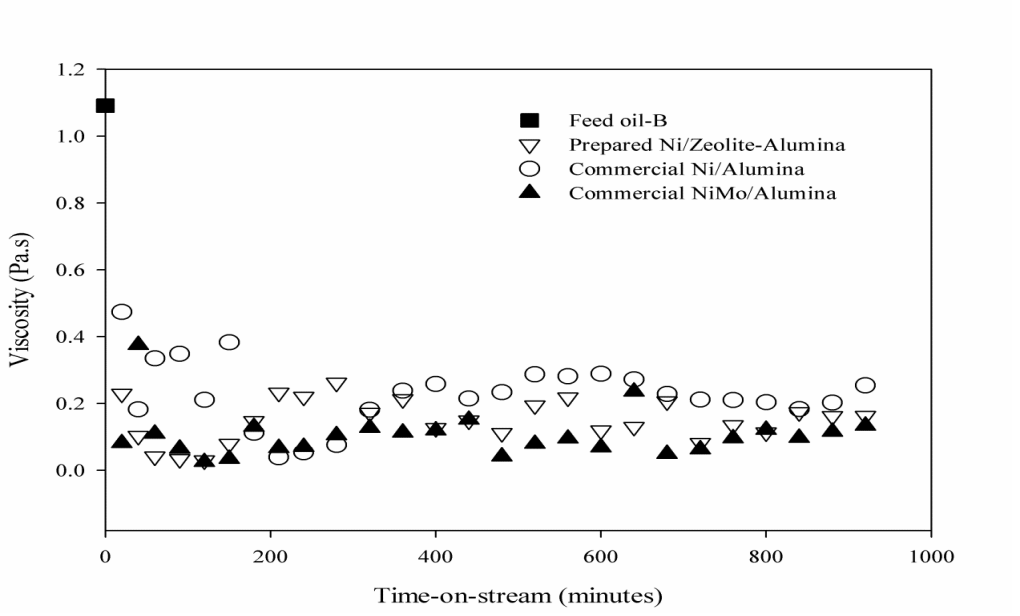

(b)

Figure 4.7 (a) API gravity and (b) viscosity of Produced oils as a function of time-on-stream using prepared Ni/zeolite-alumina, commercial Ni-Mo/Al_2O_3 and Ni/Al_2O_3 catalysts, reaction temperature 425 ^oC, pressure 20 barg, and N2/oil ratio 500 $mL.mL^{-1}$.

From Figure 4.7b, the viscosities of the produced oil samples with commercial HDT Ni-Mo/Al_2O_3 catalyst are lower than that obtained with the prepared Ni/Zeolite-Alumina catalyst. The viscosity of the produced oil samples with the prepared Ni/Zeolite-Alumina catalyst increases from 0.03 to 0.15 Pa.s at 200 minutes and thereafter it settles at an average of 0.148 ± 0.06 Pa.s with time-on-stream. This represents 86.5 % reduction of 1.091 Pa.s (feedstock) after catalytic upgrading with Ni/Zeolite-Alumina. On the other hand, commercial Ni-Mo/Al_2O_3 and Ni/Al_2O_3 respectively gave 90.2 and 78.8 % viscosity reduction. The superiority of commercial Ni-Mo/Al_2O_3 over prepared Ni/Zeolite-Alumina catalyst is because of its larger pores, bimetallic, in addition to the active phase Ni – Mo – S that possesses high hydrocracking activities (Vishwakarma, et al., 2007). Eventually, the nitrogen adsorption-desorption isotherm revealed that the prepared Ni/Zeolite-Alumina catalyst had smaller pore sizes compared to the commercial catalysts, which limits the diffusion of macromolecules and their cracking activity. Instead, the macromolecules adsorbs on the zeolite-based catalyst surface, thereby limiting effective cracking of large and complex molecules (Stoyanov, et al., 2008). However, the cracking performance of the prepared zeolite-based catalyst over commercial Ni/Al_2O_3 catalyst can be attributed to the molecular sieve structure of the zeolite and their crystalline aluminosilicates nature which enhanced their cracking functions, because the Si-O-Al framework within the zeolite pore channels optimise the acid strength and distribution within the catalyst (Zhicheng, et al., 2012).

4.7 Effect of Feedstock

The extent of catalytic upgrading could differ depending on the feedstock properties and the location of the oil. Two heavy oil feedstocks were investigated; Feed-A (13 ^{o}API and

0.49 Pa.s) and Feed-B (14 ^{o}API and 1.091 Pa.s). However, detailed properties of both feedstocks have been reported in Table 3.1 of Chapter 3.

4.7.1 Effect of Feedstock on API Gravity and Viscosity

In Figure 4.8 (a) and (b), the upgrading trend of the produced oil in terms of change in API gravity points for both feed oils is presented using Co-Mo and Ni-Mo catalysts are presented. The average API gravity rise for the produced oil with Co-Mo is 3 ± 0.9 ^{o}API (Feed-A) and 2.3 ± 1.2 ^{o}API (Feed-B). Whilst with the use of Ni-Mo catalyst an average API gravity points increase of Feed-A and Feed-B are 3.8 ± 1.6 and 2.7 ± 1.3 ^{o}API, respectively. The lower API gravity points for the produced oil observed in Feed-B is due to its higher viscosity compared to Feed-A. Generally, the in situ catalytic process achieved a similar further increase of approximately 2 to 7 ^{o}API points for both feedstock and catalysts.

This is consistent with previous results on CAPRI reported by Xia and Greaves (2001) and Xia et al. (2002). They found a maximum of 6.4 ^{o}API point gain to THAI upgraded oil. However, with Ni-Mo catalyst, it requires almost 100 minutes to achieve a similar of catalytic upgrading obtained in Feed-A as in the run of Feed-B. This may be due to difference in feedstock properties and their influence on flow.

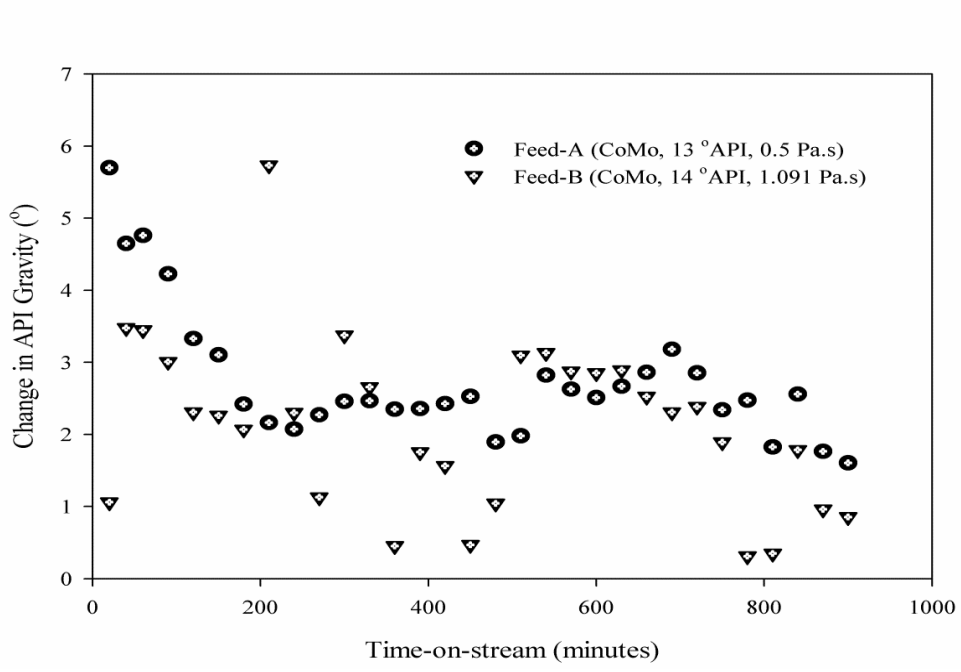

(a)

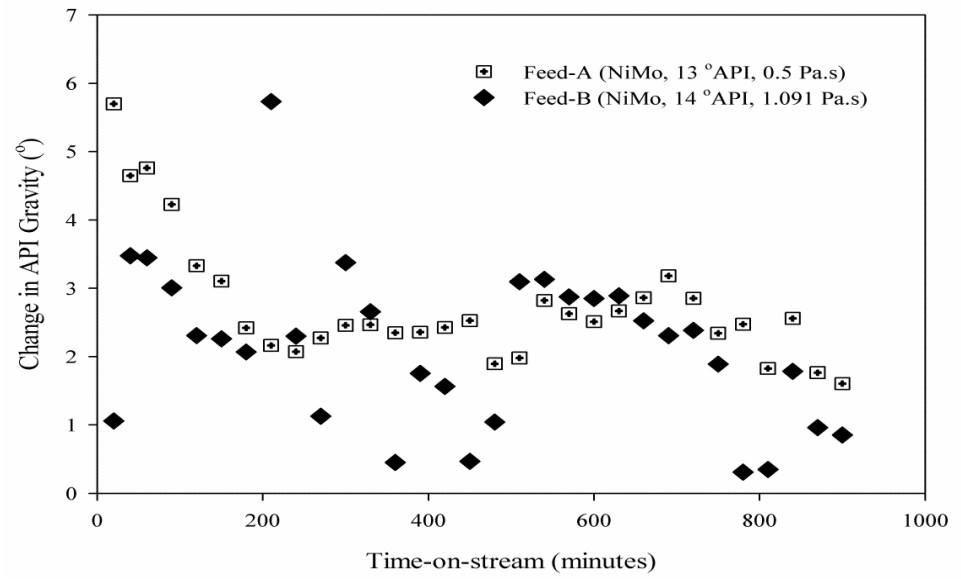

(b)

Figure 4.8 Effect of feedstock on produced oil API gravity at temperature 425 °C, pressure 20 barg, nitrogen-to-oil ratio 500 mL.mL^{-1} and Catalysts: (a) Co-Mo/Al_2O_3 and (b) Ni-Mo/Al_2O_3 (the legend indicate the feed oils start API gravity and viscosity values).

It is noteworthy that flow rate control for the highly viscous feed-B proved challenging because of the presence of sediments in the oil and its tendency to block and/or obstruct flow in the lines and the catalyst bed. This contributed to the possible source of the scatter of data points observed in the API gravity as well as viscosity with repeatability for duplicate runs within ± 3.8 % for API and ± 4.7 % for viscosity, respectively. Therefore, the volume of oil collected in a given time was used to estimate the flow rate. The average flow rate was 1 ± 0.3 $mL.min^{-1}$. For this reason, whenever there is a slight change in flow, this could have led to changes in residence time which influences the contact time between the oil and the catalyst, resulting in the observed scatter in the API gravity and viscosity, respectively. Similar flow fluctuations are likely in the down-hole CAPRI process because the mobile oil zone (MOZ) passes through the oil sand at varying permeability and flow rate.

The measurement of produced upgraded oil samples viscosity in comparison to that of the feedstock is necessary for predicting the easiness of oil flow during the recovery process. The viscosity of the produced oils from both feedstock with Co-Mo and Ni-Mo catalysts are presented in Figure 4.9 (a) and (b). There is significant reduction of viscosity in both experimental runs with both catalysts compared to the original feed oils. Figures 4.8 and 4.9 are reversed trend as a decrease in API gravity conforms to an increase in viscosity of the produced oil samples with time-on-stream.

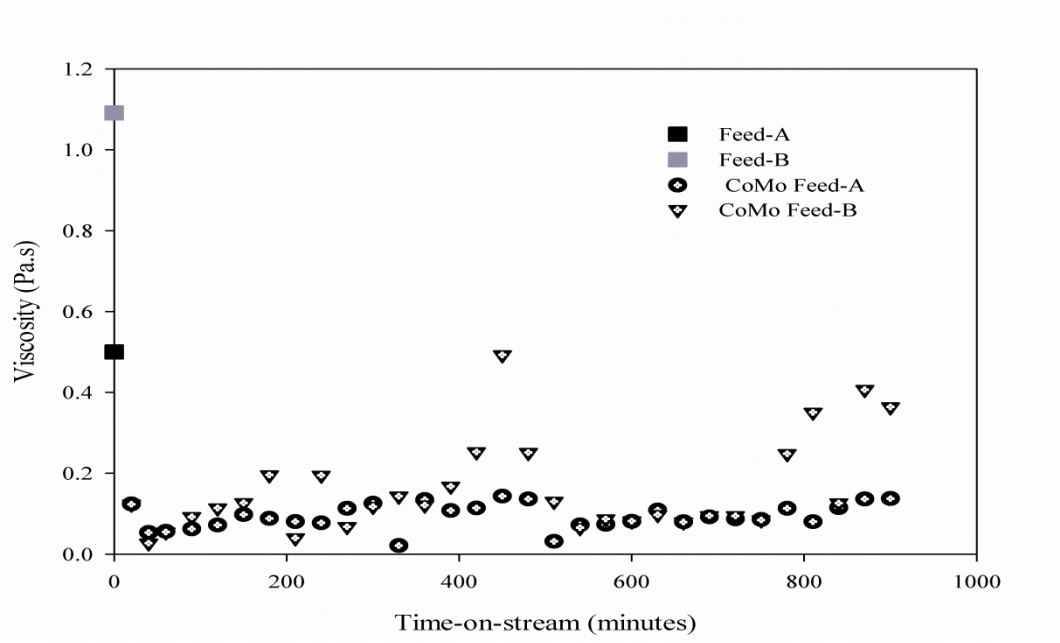

(a)

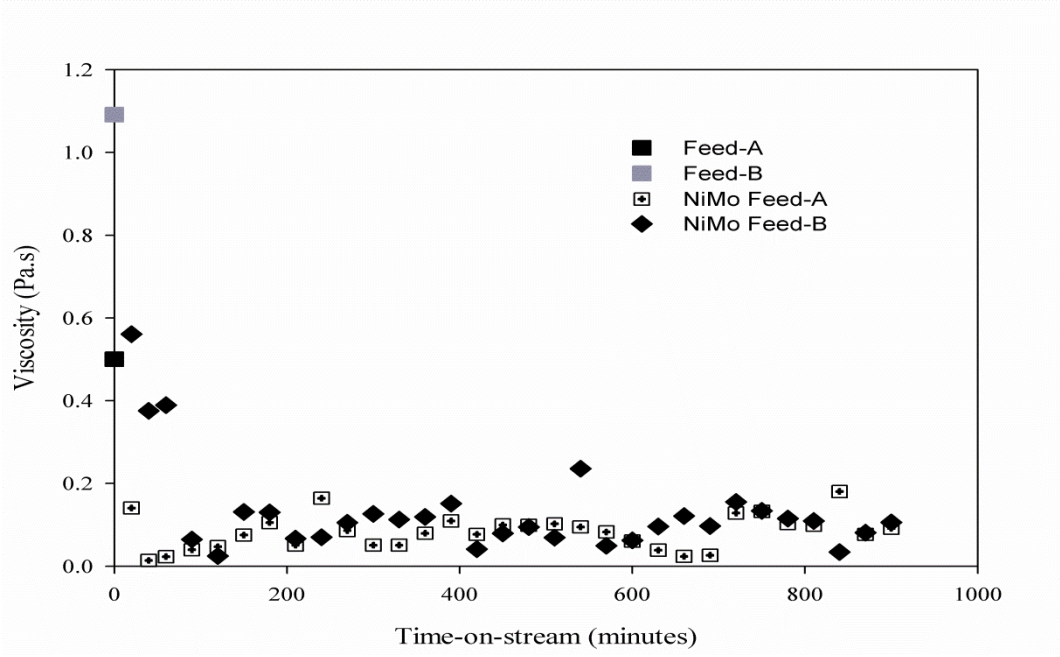

(b)

Figure 4.9 Effect of feedstock on produced oil API gravity at temperature 425 ^{o}C, pressure 20 barg, nitrogen-to-oil ratio 500 mL.mL^{-1} and Catalysts: (a) Co-Mo/Al_2O_3 and (b) Ni-Mo/Al_2O_3.

At the end of the experimental runs, the average viscosity of the produced oils with Co-Mo and Ni-Mo catalysts were 0.092 and 0.082 Pa.s (feed-A) and 0.151 and 0.133 Pa.s (feed-B) compared to the original 0.49 and 1.091 Pa.s for feed-A and B, respectively. This indicates that the viscosity reductions with Co-Mo and Ni-Mo catalysts were 81.2 and 83.3 % (feed-A) and 86.2 and 87.8 % (feed-B), respectively. This shows roughly the same DVR and API gravity rise is achievable despite the difference in feedstock properties. Similarly, Xia and Greaves, (2001) reported 70-80% reduction in viscosity using CAPRI. They found that after CAPRI, the amounts of resins and asphaltenes decreased, while the amounts of saturates and aromatics increased in the produced oil. Notably, the asphaltenes content with Co-Mo and Ni-Mo catalysts reduced from 11.14 wt.% (feed-A) to 6 and 6.7 wt.% and for feed-B from 10.3 wt.% to 5.11 and 4.4 wt.%, respectively. Therefore, conversion of asphaltenes was roughly 39-47 % (feed-A) and 52-58 % (feed-B), depending on the catalysts.

4.7.2 Effect of Feedstock on TBP Distribution

The TBP distribution curves for this sample were obtained using the integrated PTV injector and Agilent 6850N gas chromatography according to the ASTM-2887-08. Figure 4.10 provides the results of the cumulative volume percent yield of feed and produced oils at selected simulated distillation temperatures for Co-Mo/alumina and Ni-Mo/alumina catalysts. It can be observed that the upgraded oils from the experiments performed with Co-Mo and Ni-Mo catalysts caused a significant shift towards lighter distillate fractions with low-boiling temperatures in comparison to the feedstock.

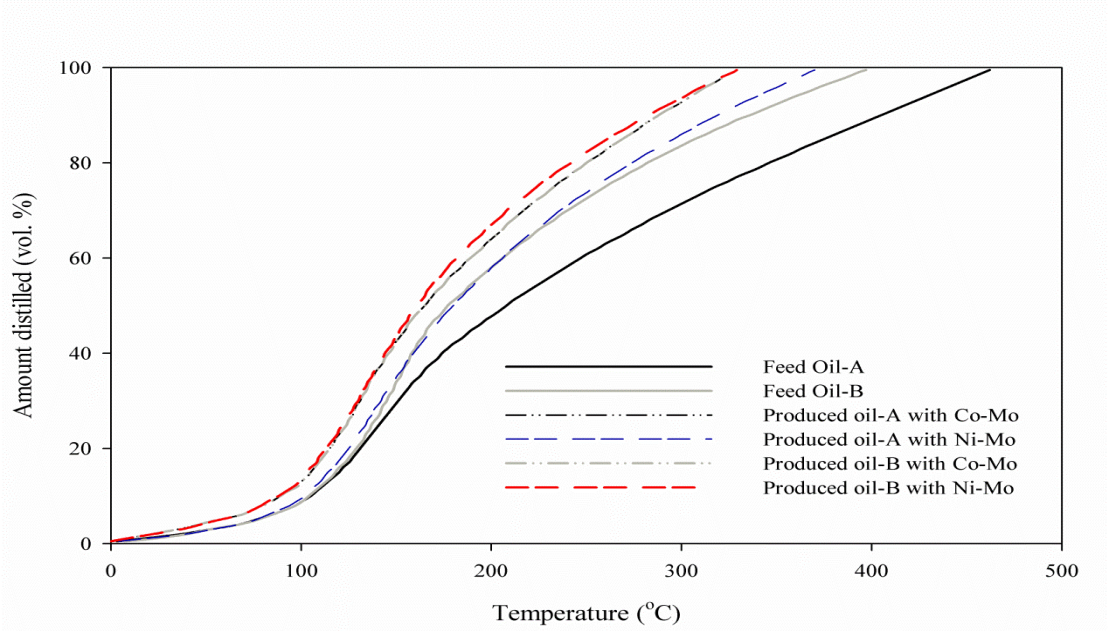

Figure 4.10 TBP distribution curves for the feed and produced upgraded oils at 425 °C; Catalysts: Co-Mo/Al_2O_3 and Ni-Mo/Al_2O_3, Reaction Media (N_2), Pressure 20 barg, Oil flow rate 1 mL.min^{-1}, Gas flow rate 500 mL.min^{-1}.

For instance, a dramatic 4 °C shift in the boiling temperature was noticed at 10 vol.% yield compared to feed oil-A. This rises to 10, 29, 60, and 101 °C as the cumulative amount distilled increased from 30 to 90 vol.% yield for Co-Mo catalyst at upgrading temperature of 425 °C and feed oil-A. A similar trend can be observed for the use of Ni-Mo catalyst with feed oil-A as well. The shift towards lower distillable temperatures is an indication that the produced oils contain lower molecular weight components compared to the original feedstock. However, for feed oil-B approximately 14 °C shift towards low-boiling temperature was observed up to 50 vol.% cumulative yield followed by 23 and 46 °C rise in the shift as the yield increased from 70 to 90 vol.% with the use of Co-Mo. The level of upgrading in the presence of Co-Mo/Al_2O_3 and Ni-Mo/Al_2O_3 catalysts for both feedstocks is approximately similar irrespective of the difference in feedstock properties. The level of impurities reduction after upgrading is presented in Appendix B.

4.8 Conclusions

The in-situ catalytic upgrading process (CAPRI) starts with in situ combustion to supply thermal energy to the reservoir by heating the heavy oil/bitumen and the rock to high temperature (400-550 ^{o}C). These conditions induce thermal cracking as well as drive catalytic conversion of the oil as it flows across the catalyst bed incorporated on the horizontal production well, thus reducing its viscosity and generating lighter hydrocarbon fractions. This entire process was demonstrated in a laboratory scale in a fixed-bed reactor. The effect of temperature, WHSV, feedstock, mono- and bi-metallic catalyst and catalyst type was investigated. It was found that temperatures of 425 ^{o}C and WHSV 9.1 h^{-1} gave the optimum upgrading level in API gravity, viscosity reduction and yield of light distillates.

Chapter 5

Effect of Reaction Gas Media on Upgrading

5.1 Introduction

Hydrogen-addition offers an alternative route to upgrade heavy oils, resulting in less coke formation and higher liquid yield compared to the carbon-rejection route (Liu, et al., 2003). Hydrogen and methane are sources of the smallest radicals (i.e., active hydrogen and methyl) found in the reaction media that can quench free radical addition reactions. If free radical reactions are not terminated they would otherwise lead to the formation of larger molecules which confer characteristics of high viscosity, low API gravity, and low conversion of (BP > 343 ^{o}C) in the produced oil and subsequently high coke. Apart from the use of hydrogen itself, other sources of hydrogen such as light hydrocarbons or hydrogen donor solvents could be considered (Alemán-Vázquez, et al., 2012). In fact, high H/C ratio of methane makes it a potential alternative to expensive hydrogen gas as a source of hydrogen atom in the reaction medium.

In Chapter 2 and Sections 2.6.6 and 2.9.1 the THAI and its catalytic CAPRI are presented. In the Mobile Oil Zone (MOZ) the combustion reactions generate gases as illustrated by the following four equations (Xia and Greaves, 2001; Xia, et al., 2002; Wenlong, et al., 2011; Greaves, et al., 2012):

heavy oil → light oil + gas + coke + absorbed heat (5.1)

coke + O_2 → H_2O + CO_2/CO + heat (5.2)

heavy oil + O_2 → H_2O + CO_2/CO + heat (5.3)

$$\text{light oil} + O_2 \rightarrow H_2O + CO_2/CO + \text{heat} \qquad (5.4)$$

These reactions aid the thermal upgrading of the heavy oil; light oil is first generated as shown in eq. 5.1 and the other reactions generate heat to drive the reaction. In the CAPRI 'add-on' further upgrading occurs by catalytic conversion into light oil.

In this Chapter 5, the effect of reactant gases upon the extent of upgrading and coke formation are investigated and reported in Section 5.2. In Section 5.3 hydrogen-addition route to upgrading was reported. Ex situ oxidative-regeneration of spent catalyst and hydrocracking of anthracene as model compound of typical poly-aromatics are reported in Sections 5.4 and 5.5, respectively.

5.2 Effect of Reaction Gas Environment

Upgrading results are presented below for experiments carried out under hydrogen, methane, nitrogen, and a blended THAI gas (see Chapter 3 and Section 3.3) representing the typical gases generated during the field THAI process, which were studied over a Co-Mo/γ-Al_2O_3 catalyst. The experiments were conducted at a reaction temperature of 425 ^oC, pressure 10bar, oil flow rate 1 $mL.min^{-1}$, and gas-to-oil ratio 50 $mL.mL^{-1}$ for 6 hours time-on-stream operation using feed oil-B.

5.2.1 Effect of Hydrogen and Methane on Mass Balance

In Table 5.1, the mass balance of gas, liquid (i.e., light oil) and coke yields from catalytic upgrading of heavy oil under nitrogen, hydrogen and methane reaction gas at the same conditions is presented. The reported values are an average of duplicate experimental runs. The chemistry of upgrading is presented in Section 4.2 of Chapter 4.

Table 5.1 Mass balances; Catalyst Co-Mo/Al_2O_3, Reaction Media: N_2, H_2, and CH_4, Reaction Temperature 425 ^oC, Pressure 10 barg, Oil flow rate 1 $mL.min^{-1}$, Gas flow rate 50 $mL.min^{-1}$.

Products	**N_2 (wt.%)**	**H_2 (wt.%)**	**CH_4 (wt.%)**
Liquid	92.6	94.64	93.28
Gas	4.49	3.88	4.35
Coke	2.91	1.48	2.37

Clearly, the coke yield when the reaction was carried under hydrogen atmosphere was 1.43 wt.% lower than of nitrogen. Also, under methane environment the coke yield was 0.54wt.% below 2.91 wt.% (nitrogen). Most of the upgrading reaction with nitrogen atmosphere proceeds via carbon-rejection with less indirect hydroconversion reactions because of limited *in situ* hydrogen generated by hydrocarbons. On the other hand, yield of liquid product increased by 2.04 wt.% (hydrogen) and 0.68 wt.% (methane) above 92.6 wt.% obtained under nitrogen atmosphere. As Graue (2001) observed that the liquid yield from hydrogen-addition to heavy oil upgrading processes can increase up to 20-25 volume percent greater than the yield from carbon-rejection counterparts. The hydrogenation and methylation of fragments improved liquid yield.

5.2.2 Effect Reaction Media upon API Gravity, Viscosity and Distillable yield

The reported data points on the graphs are average values taken from duplicate experimental runs with maximum standard deviation of ± 0.41^{o}API. The API gravity, viscosity and the true TBP distribution curves for the feed and the produced oil samples as a function of time-on-stream are respectively shown in Figures 5.1 (a), (b) and (c) for hydrogen, methane, THAI gas, and nitrogen reaction gas. The feed oil had an API gravity of 14^{o}. Upon processing in hydrogen, the initial change in API gravity for the first sample taken from the reactor at 25 minutes was quite low, before increasing up to a maximum of 8^{o} points after 50 minutes, thereafter decreasing and settling at an average of 4.4 ± 1.3^{o} increase in API points. Similarly for reaction in methane the increase in API gravity was initially 5^{o} thereafter settling at an average of 3.33 ± 1^{o} API, whilst for THAI gas the initial upgrading was 6.9^{o} settling at an average increase of 2.93 ± 1.5^{o} API. For nitrogen the maximum upgrading of 5^{o} occurred thereafter settling at an average increase of 2.72 ± 1^{o} API. A possible reason for the low API gravity change of the first sample taken from the reactor could be instability of oil flow at start up due to the difficulties of regulating the flow manually using a metering valve. The price of crude oil increases exponentially with its API gravity, in other words the higher the API gravity the higher the price (Ancheyta and Rana, 2007). Hence, every degree rise in API gravity of the produced oil will enhance the value of the oil in the market.

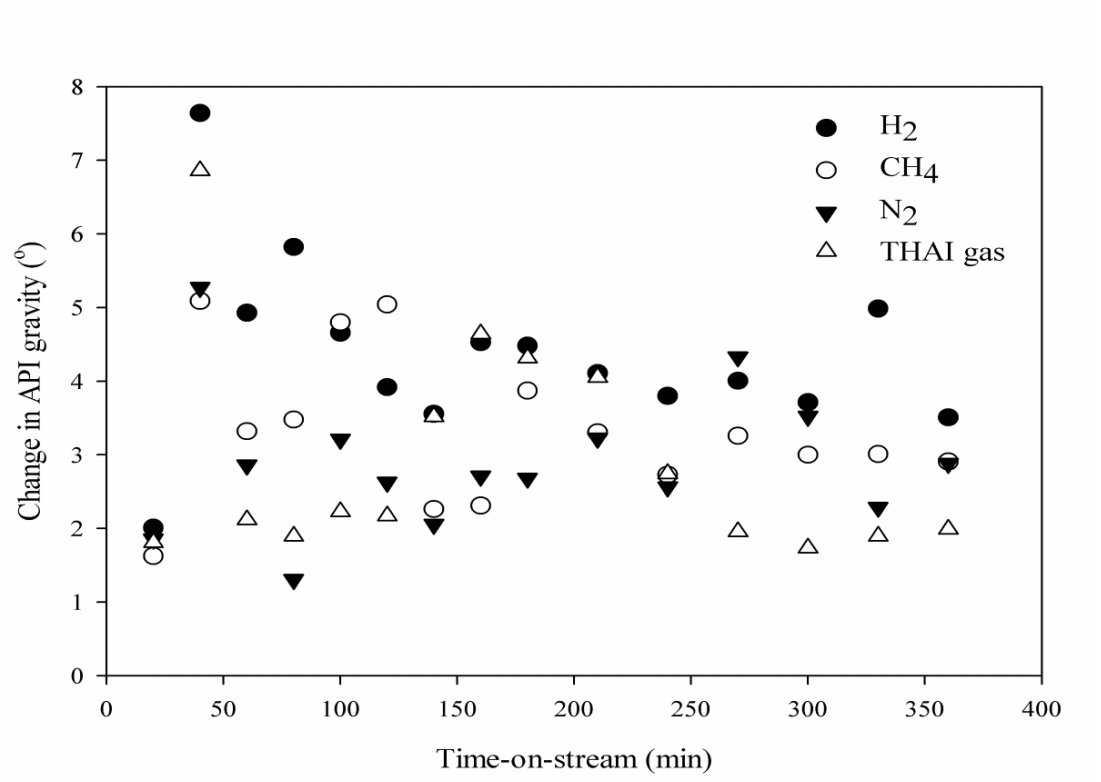
Change in API gravity (°)
Time-on-stream (min)
H2
CH4
N2
THAI gas

(a)

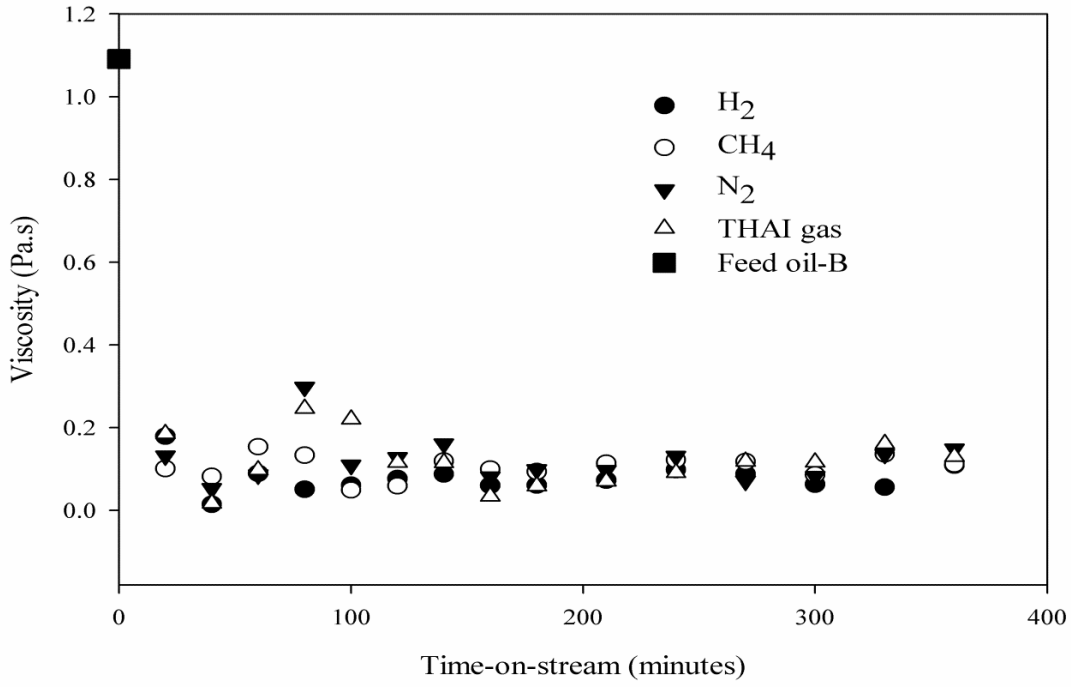
Viscosity (Pa.s)
Time-on-stream (minutes)
H2
CH4
N2
THAI gas
Feed oil-B

(b)

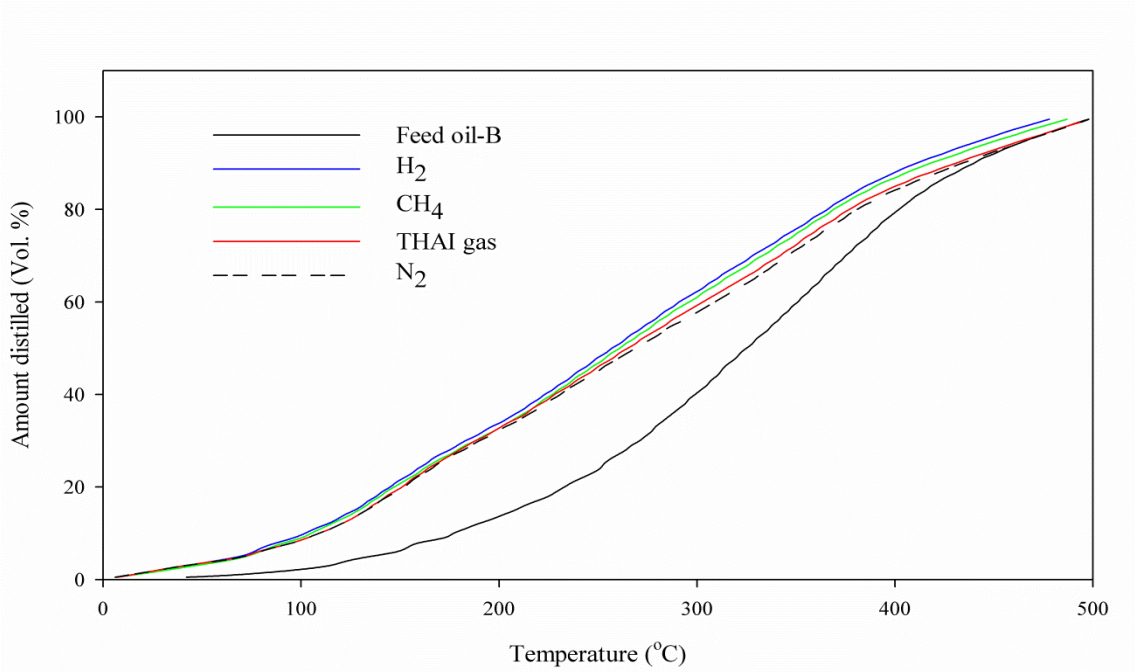

(c)

Figure 5. 1 Effect of hydrogen, methane, THAI gas and nitrogen reaction media upon (a) API gravity, (b) viscosity of produced oil, and (c) the true boiling point distribution curves for the feed oil and the produced oils at reaction temperature 425 ^{o}C, pressure 10barg, and gas-to-oil ratio 50 mL.mL^{-1} using Co-Mo/Al_2O_3 catalyst and feed oil-B.

Viscosity is an important physical property of the crude oil and as a guideline should be lower than 0.2 Pa.s at 20 ^{o}C to achieve pumping in order to aid pipeline transport (Ancheyta, et al., 2005; Hart, 2013). In Figure 5.1b, the absolute viscosity reduced from the feed value of 1.091 Pa.s to 0.078 Pa.s (92.8 % reduction) in hydrogen, 0.105 Pa.s (90.4 % reduction) in methane and 0.1181 Pa.s (89.2 % reduction) in THAI gas blend. An upgrading experiment carried out under nitrogen as an inert/control experiment led to oil with lowest change in API gravity of 2.71^{o} and smallest viscosity reduction of 0.121 Pa.s (88.9 % reduction).

A comparison of performance under different gases, the major change in API gravity of 1.68° and viscosity reduction of 3.9% occurred under hydrogen above the values obtained

when nitrogen was used. This suggested the involvement of hydrogen in further upgrading reactions. The produced oil under methane also showed additional improvement, with a further increase of 0.44^{o} API and 1.5 % viscosity reduction compared with nitrogen. From the above results it appears that there was no significant difference in API gravity and viscosity of produced oil upon the use of THAI gas, with API gravity increase of 0.21^{o} and viscosity reduction 0.3%, from produced oil upon the use of nitrogen. The slight improvement in API gravity and viscosity under THAI gas above that of nitrogen can be attributed to the activity of 4% methane in the THAI gas (see Section 5.1), which could have been a source of hydrogen to assist in upgrading reactions.

In Figure 5.1c, the true boiling point (TBP) distribution curves for the feed oil and the produced upgraded oil samples carried out under hydrogen, methane, THAI gas, and nitrogen reaction media are presented. It is clear that the yield of low-boiling fractions increased above that of the feed oil for all the experimental runs as shown by the shift of the distillation curves to the left of the feed oil curve. However, the distillables increased further upon the addition of hydrogen and a slight increase was also noticed with methane compared to the use of THAI gas and nitrogen in relation to the feed oil. The improvement upon hydrogen addition is in line with the reports of Hart et al. (2013) and Longstaff, et al. (1994).

The conversions of 343^{o}C+ HC fractions under hydrogen, methane, THAI gas, and nitrogen atmospheres were 41%, 38.1%, 32.6% and 29.5%, respectively. These values follow the trends observed in Figure 5.1c, and also reflect similar results observed for the API gravity and viscosity, thus confirming the participation of hydrogen and methane in the upgrading reactions. The increased low-boiling fractions of the produced oil with hydrogen and methane are thought to be mainly due to the moderated retrogressive polymerisation reactions of macromolecular radical addition reaction which led to high-boiling fractions observed with

inert nitrogen. The hydrogen-donor reaction mechanisms are thought to be responsible for the increased yield of light and middle hydrocarbon distillates (Aleman-vazquez, et al., 2012). Ancheyta et al. (2005) reported that the viscosity of the oil depends on the amount of the > 350 ^{o}C heavy fractions and/or the yield of < 350 ^{o}C distillates fractions. The increased lighter fractions in the upgraded samples thin the unconverted heavy fractions, which resulted in lower viscosity (see Figure 5.1b).

As observed in Figures 5.1a-c, the CAPRI upgrading reactions conducted under hydrogen atmosphere produced oil with improved API gravity, viscosity and conversion of 343^{o}C+ fraction than the values obtained under methane, followed by THAI gas and nitrogen. Hence, the order of reactivity of these gases during reaction may be summarised as H_2 > CH_4 > THAI gas > N_2, which is consistent with the reports of Ovalles et al. (1998 & 2003). The capping of free radical under hydrogen atmosphere, as shown in equations (5.5-5.6), could have contributed to these improvements. Also, the free-radical pathway that occurs in methane during upgrading (equations 5.7-5.9) is thought to be a mechanism by which the API gravity and viscosity of the oil are improved (Ovalles, et al., 1998).

active chains + active H_2 → low molecular weight compound (5.5)

active chain + active chain → high molecular weight compound (5.6)

$$R - R' \rightarrow R^{\bullet} + R'^{\bullet} \quad (5.7)$$

$$R^{\bullet} + CH_4 \rightarrow RH + CH_3^{\bullet} \quad (5.8)$$

$$CH_3^{\bullet} + R - R' \rightarrow R'CH_3 \text{ (or } RCH_3) + R^{\bullet} \text{ (or } R'^{\bullet}) \quad (5.9)$$

where R and R' are naphthenic or aromatic hydrocarbons

Upon methane activation hydrogen and methyl radicals are produced. The radicals react with hydrocarbon molecules to give either hydrogenated or methylated species (RH or RCH_3) with free radicals ($R^{\bullet}$) in a continuous chain process, as illustrated in equations 5.7-5.9 (Ovalles, et al., 1998). Ovalles et al. (1998) found that methane decomposes to form CH_x (where x =1, 2, or 3) and H_{4-x} species on the surface of MoS_2 catalyst, with lot of methyl (CH_3) species all attached to the catalyst surface at a temperature of 420^{o}C and pressure 0.3 MPa. The adsorbed CH_x on the catalyst can be incorporated into the hydrocarbon molecules to form methylated products, and subsequently the H_{4-x} species are available to hydrogenate cracked fragments, moderate coke precursors and remove sulphur in the form of H_2S (Ovalles, et al., 2003).

The fundamental cleavage that results in substantial upgrading is the temperature driven splitting of C – C and C-heteroatom bonds (Hart, et al., 2014). This can lead to remarkable viscosity decrease, notable increase in distillable fractions, and increase API gravity. In the reported work of Hart et al. (2013) and the results presented in Chapter 4 in which nitrogen gas media was investigated at 350, 400 and 425 ^{o}C, the average changes in API gravities were respectively 2, 2.8, and 3.7^{o} API, viscosity reductions were 42, 65.3 and 81% and conversions of boiling fractions >343 °C were 16.5, 28.6 and 36.5 %. In this Chapter 5, improvements in the API gravity, viscosity, and the distillable yield upon upgrading with methane, THAI gas and nitrogen only vary within a relatively narrow range but slightly higher differences are observed for reactions performed with hydrogen (Figures 5.1a-c). This confirms that the primary upgrading reactions depend mostly on the reaction temperature, whereas the reaction media play a role in the chemistry of upgrading reactions.

5.2.3 Effect on Produced Gas Composition

The composition of the produced gas during CAPRI reaction experiments under hydrogen, methane, THAI gas, and nitrogen atmospheres are presented in Table 5.2. It is clear that the produced gas consists of paraffin and olefin hydrocarbons. Olefins are known coke precursors because they can transform into larger molecular weight compounds if there is insufficient active hydrogen available to quench their addition reaction. In Table 5.2, the total paraffin content of the gas under hydrogen and nitrogen are 9.23 and 6.67 vol.%, respectively. Whilst, the olefin contents for the produced gases upon upgrading under the following feed gases were: hydrogen (0.81 vol.%), methane (0.86 vol.%), THAI gas (1.1 vol.%), and nitrogen (1.24 vol.%). Notably, the amount of olefins in the gas upon the use of THAI gas was 0.14 vol.% less than that of nitrogen used in the inert control run.

It was deduced that the amounts of ethene, propene, trans-2-butene, and cis-2-butene decreased upon the use of hydrogen and methane as reaction media compared to the use of THAI and nitrogen gases. This confirmed the participation of hydrogen and methane in the reaction, meaning that the addition of hydrogen promotes hydrogenation of olefins to paraffins, which can be confirmed by a corresponding increase in the amount of paraffins in the produced gas. Under a hydrogen environment, the generated methyl radicals during upgrading reactions may have been terminated by hydrogen which gave rise to the increased amount of methane gas in the produced gas stream compared to nitrogen atmosphere.

Table 5.2 Produced gas composition for different reaction gas media; temperature 425^{o}C, pressure 10barg, oil flow rate 1 mL.min^{-1}, gas flow rate 50 mL.min^{-1}.

Gas Composition	Hydrogen (Vol.%)	Methane (Vol.%)	THAI gas (Vol.%)	Nitrogen (Vol.%)
Methane	5.93	Used	10.5	2.3
Ethane	0.37	0.49	0.35	0.47
Ethene	0.19	0.21	0.31	0.29
Propane	1.21	2.37	1.63	2.06
Propene	0.37	0.39	0.41	0.58
n-butane	0.52	1.02	0.79	0.82
i-butane	0.54	0.38	0.21	0.34
1-butene	0.13	0.13	0.18	0.18
Trans-2-butene	0.1	0.09	0.14	0.14
Cis-2-butene	0.03	0.04	0.06	0.05
i-pentane	0.29	0.36	0.34	0.37
n-pentaane	0.37	0.45	0.49	0.37
Hydrogen	Used	14.76	4.41	6.22
Hydrogen sulphide	0.001	0.00073	0.00063	0.00036
Carbon dioxide	0.11	0.1	6.36	0.68
Carbon monoxide	0.12	0.15	1.45	0.15
Total paraffin	9.23	5.07	3.81	6.67
Total olefins	0.81	0.86	1.1	1.24

*Note the methane component of the outlet gas stream was not included in the calculation of total paraffin under THAI gas due to its initial presence in the gas.

Furthermore, Table 5.2 shows that the produced hydrogen sulphide under hydrogen atmosphere is respectively 1.4 and 2.8 times the values obtained under methane and nitrogen gas reaction media. This provides evidence that hydrodesulphurisation (HDS) reactions occurred to a greater extent under hydrogen reaction media compared to methane, THAI gas,

and nitrogen. Additionally, the produced H_2S under methane and THAI gas atmosphere were 2 and 1.75 times that produced when nitrogen gas was used. This indicates that the generated active hydrogen from catalytic decomposition of methane can be partly consumed by HDS, resulting in additional H_2S in the released gas. It should be noted that the higher concentrations of CO_2, CO and CH_4 in the gas under THAI gas atmosphere compared to the other reaction media are because of their presence in the feed (see Chapter 3 and Section 3.3).

5.2.4 Effect on Asphaltenes, Metal and Sulphur Content

The asphaltene, sulphur and metal contents of the feed and produced oil samples under the different reaction media are presented in Table 5.3. The asphaltene content decreased remarkably after CAPRI upgrading in the different reaction media relative to the feed oil. This suggests that the conversion of the heaviest fraction (asphaltene) to lighter fractions such as maltene, gases, and coke occurred. However, the use of hydrogen and methane produced higher conversions of asphaltene of 43.4 and 51.6 %, respectively, compared to 13 % (nitrogen). This is concluded to be because the generated active hydrogen in hydrogen and methane media neutralised the cross-linking of macromolecular intermediate radicals that are generated during cracking of the heavy oil (Liu, et al., 2013).

Conversely, the asphaltene content of the produced oil upon the use of methane is lower than that of hydrogen. This can be attributed to the larger amount of dissolved hydrogen under an atmosphere of pure hydrogen at 10 bar compared with the low partial pressure of generated hydrogen from methane. The increased hydrogen dissolved in the oil with the hydrogen feed was assumed to promote condensation reactions between radicals of asphaltene macromolecules (Liu, et al., 2013).

Table 5.3 Asphaltene, metals, and sulphur content before and after CAPRI reaction using Co-Mo/γ-Al_2O_3 catalyst under hydrogen, methane, THAI gas, and nitrogen atmospheres at reaction temperature of 425 ^oC, pressure 10barg, oil flow rate 1 $mL.min^{-1}$, and gas flow rate 50$mL.min^{-1}$.

Impurities	**Feed oil-B**	**CoMo + N_2**	**CoMo + CH_4**	**CoMo + THAI gas**	**CoMo + H_2**
Asphaltene (wt.%)	10.3	9.2	5.3	8.4	6.1
Aluminium (ppm)	2	2	2	2	2
Boron (ppm)	3	2	2	2	2
Iron (ppm)	5	2	< 1	< 1	< 1
Sulphur (wt.%)	3.52	3.4	3.09	3.03	2.77
Silicon (ppm)	1	< 1	< 1	< 1	< 1
Nickel (ppm)	41	34	30	37	36
Vanadium (ppm)	108	90	79	82	89
Ni + V (ppm)	149	124	109	119	125

* Sulphur and metals content was performed by Intertek Laboratories, Sunbury Technology Centre, UK, using ICP-OES (Inductively Coupled Plasma Optical Emission Spectrometry).

One of the objectives of upgrading is to remove impurities such as metals and sulphur to a level that will minimise their impact on downstream processing catalysts, equipment and also improve the yield of low-boiling fractions. The results show that in all cases the sulphur and metals content of the produced oil in different reaction media were less than those of the feed oil, which indicates that the Co-Mo/Al_2O_3 HDT catalyst was active for desulphurization and demetalization reactions. It was therefore deduced that the breaking of C-heteroatom bonds in addition to C-C bond cleavage contributed to the increased API gravity, decreased viscosity, and improved yield of distillates noticed in the previous sections. However, when hydrogen gas was used as reaction gas medium, sulphur removal was 21.4%, which is

significantly higher than the values obtained using methane (12.2%), THAI gas (13.9), and nitrogen (3.4 %), correspondingly. Some of the sulphur content is removed in gaseous form as H_2S, which was confirmed by the high concentration of H_2S detected in the produced gas when hydrogen feed was used. Also, sulphur is deposited on the catalyst as metallic sulphide during reaction (Hart, et al., 2014). This is because HDS reaction was promoted in the presence of hydrogen, which was not experienced to the same extent in the methane, THAI gas and inert nitrogen atmosphere. The reaction pathways through which sulphur can be removed from the different structures in the heavy oil during CAPRI process is illustrated in Figure 5.2.

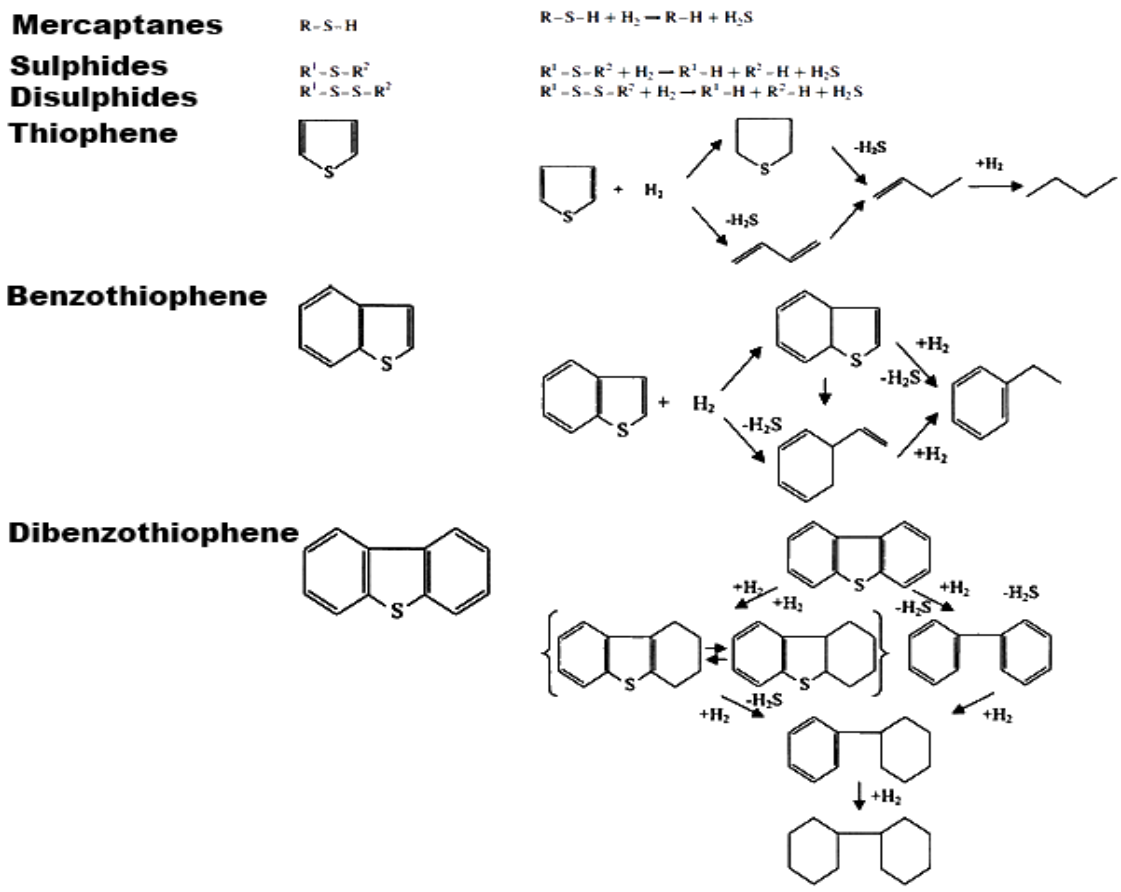

Figure 5.2 Typical organosulphur compounds (where; R^1 and R^2 are alkyl hydrocarbon) found in heavy oil and their reaction pathway during upgrading reactions (Babich and Moulijn, 2003).

The thiophenes can either undergo hydrogenolysis and/or hydrogenation to non-aromatic sulphide prior to been subjected to cracking and desulphurisation to give H_2S obvious in the off-gas presented in Table 5.2 (Gray and Ayasse, 1995).

It can be seen from Table 5.3 that the cracking of asphaltenes resulted in a decrease in sulphur and metal content in the produced oil. This suggests that sulphur and metals such as nickel and vanadium in porphyrin-like form, were associated with asphaltene molecules (Ancheyta, et al., 2002). The percentage reductions of nickel plus vanadium (Ni + V) content under the different environments were: 16.8 % (nitrogen), 26.9 % (methane), 20.1 % (THAI gas), and 16.2 % (hydrogen) relative to the value of 149 ppm (feed oil). This observed behaviour can be attributed to the conversion of asphaltenes into smaller molecules in the different environments as shown in Table 5.3. Under the same conditions other trace elements such as boron, iron, and silicon were reduced after upgrading. These metals are transformed into metal sulphides upon deposition on the catalyst (Ancheyta, et al., 2002). This suggests that catalyst high activity should be harmonized with high metal tolerance.

5.2.5 Effect on Elemental Composition

The elemental composition of the feedstock and produced oil from the different reaction gas media was determined using micro-elemental analyser EA 1110 CHNS and presented in Table 5.4.

Table 5.4 Elemental composition of feed and produced oil from upgrading under nitrogen, hydrogen, methane, and THAI gas reaction gas media using Co-Mo/Al_2O_3 catalyst at temperature 425 ^oC, pressure 10 barg, and gas-to-oil ratio 50 $mL.mL^{-1}$.

Sample	Nitrogen (%)	Carbon (%)	Hydrogen (%)	H/C	Carbon-rejection (%)
Feedstock	0.57	88.82	10.17	0.114	N/A
Feed oil + N_2	0.48	85.80	10.55	0.123	3.01 ± 0.4
Feed oil + CH_4	0.44	87.53	10.96	0.125	1.28 ± 0.2
Feed oil + THAI gas	0.47	87.66	10.72	0.122	1.15 ± 0.2
Feed oil + H_2	0.28	87.75	11.01	0.126	1.06 ± 0.1

It can be seen that the H/C atomic ratio increased from the feed value of 0.114 to 0.126 (hydrogen), 0.125 (methane) and 0.122 (THAI gas). However, an experiment carried under nitrogen atmosphere as control gave the highest carbon-rejection of 3.01 % while the hydrogen environment gave the lowest 1.06 %. This is evident that the upgrading reaction in nitrogen atmosphere is majorly carbon-rejection with limited hydrogen-transfer reaction from the hydrocarbons. On the other hand, the nitrogen content of the feedstock decreased from 0.57% to 0.28% (hydrogen) compared to 0.48% (nitrogen). This represents 51% removal of nitrogen upon the use of hydrogen. This is because of increased hydrodenitrogenation (HDN) reaction occurring in the presence of hydrogen.

The effect of reaction gas environment on the spent catalyst coke content after reaction in each of the gas environment is presented in Appendix C. However, the spent catalyst coke content decreased in this order H_2 < CH_4 < THAI gas < N_2 (see Appendix C and Table C.1).

5.3 Hydrogen-Addition Route to Upgrading

The amount of hydrogen available for catalytic upgrading reactions is directly proportional to its partial pressure at constant temperature according to Henry's law. In other words, operating at high pressures will enhance solubility, mass transfer and inhibits coke formation (Elizalde, et al., 2010; Aleman-Vazquez, et al., 2012). The effect of hydrogen-addition and hydrogen pressure were investigated at the following operating conditions: reaction temperature 425 ^{o}C, pressure 20 barg, oil flow rate 1 mL.min^{-1}, and gas-to-oil ratio 200 mL.mL^{-1} using feed oil-A. The effect of injected hydrogen compared to nitrogen in the catalytic upgrading process on the produced oil API gravity as a function of time-on-stream using Co-Mo/Al_2O_3 and Ni-Mo/Al_2O_3 are presented in Figure 5.3 (a) and (b), respectively.

It is clear from Figure 5.3a that under nitrogen gas reaction media the API gravity decreased sharply from 7 to ~2.5 ^{o}API at 200 minutes, however under hydrogen atmosphere the API gravities of the produced oil samples were sustained at approximately 5^{o} above the feedstock value (13^{o}API) with time-on-stream for most of the samples. Also, when Ni-Mo catalyst was used at the same conditions as Co-Mo the API gravity decrease from 6.8^{o} to 3.1^{o} at 210 minutes, thereafter it settles at 2.58 ± 1.45^{o} API under nitrogen. However, under hydrogen atmosphere, the API gravity decrease from 7^{o} and settles at 4.3 ± 1.3^{o} API (see Figure 5.3b). The fluctuations in the data are largely due to hydrogen gas flow control issues. This shows that the injected hydrogen could have inhibited the extent of catalyst deactivation experienced in nitrogen reaction media (Hart, et al., 2013a,b).

The effect of hydrogen-addition compared to nitrogen on the produced oil viscosity as a function of time-on-stream using Co-Mo/Al_2O_3 and Ni-Mo/Al_2O_3 are presented in Figure 5.4 (a) and (b), respectively. It can be seen that the upgraded oil samples under hydrogen

atmosphere for both Co-Mo and Ni-Mo catalysts have lower viscosities compared to those obtained with nitrogen.

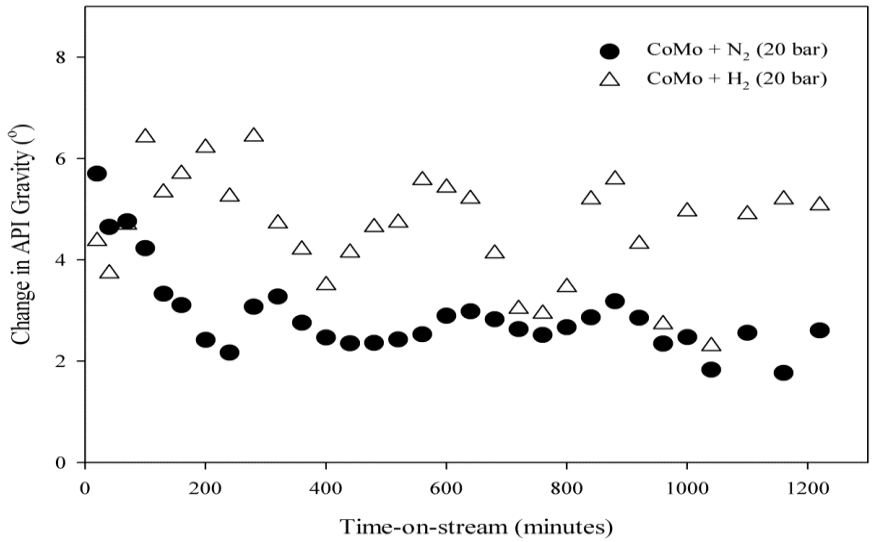

(a)

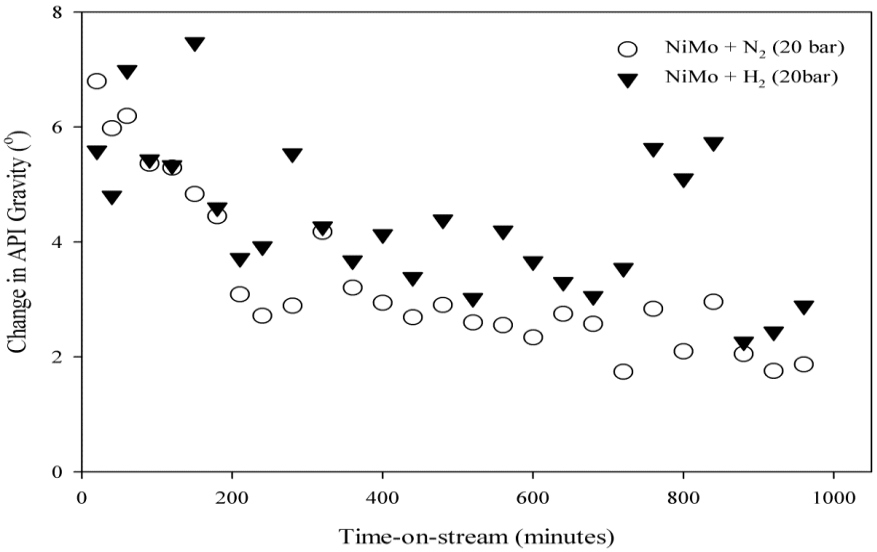

(b)

Figure 5.3 Effect of hydrogen-addition on API gravity of produced oil; reaction temperature 425 °C, Reaction Media H_2 or N_2, Pressure 20 barg, Oil flow rate 1mL.min^{-1}, Gas flow rate 200 mL.min-1; Catalysts: (a) Co-Mo/Al2O3, and (b) Ni-Mo/Al_2O_3 as a function of time-on-stream using feed oil-A.

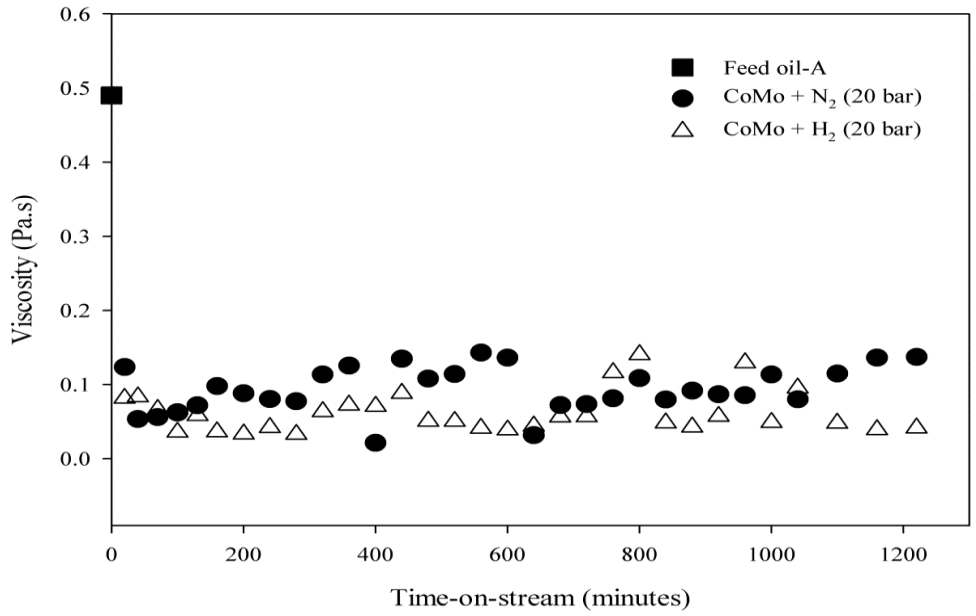

(a)

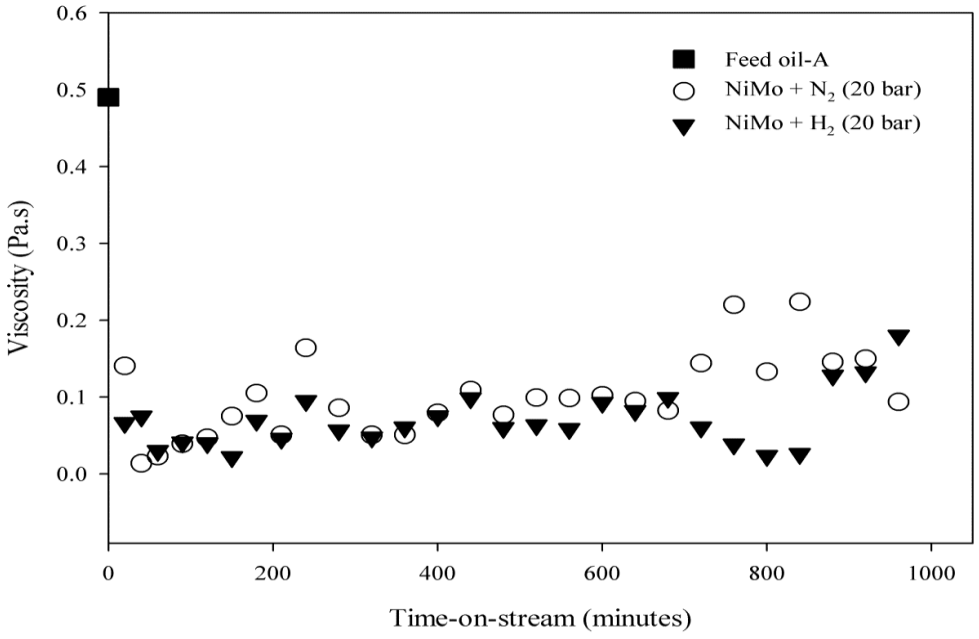

(b)

Figure 5.4 Effect of hydrogen-addition on viscosity of produced oil; reaction temperature 425 °C, Reaction Media H_2 or N_2, Pressure 20 barg, Oil flow rate 1mL.min^{-1}, Gas flow rate 200 mL.min^{-1}; Catalysts: (a) Co-Mo/Al_2O_3, and (b) Ni-Mo/Al_2O_3 as a function of time-on-stream using feed oil-A.

Co-Mo/Al_2O_3 and Ni-Mo/Al_2O_3 are bifunctional catalysts (i.e., metal and acidic), which are favourable for hydrocracking and hydrogenation (Ivanova, et al., 2011). The metal sites promote hydrogen-addition and the acidic sites of the supports and promote cracking reactions through carbocationic mechanism (Lee, et al., 2010; Ivanova, et al., 2011). From Figure 5.4a the absolute viscosity of the produced oils upon the use of Co-Mo/alumina catalyst is 0.06 Pa.s (hydrogen) and 0.09 Pa.s (nitrogen), respectively compared to the 0.49 Pa.s (feed oil-A). This represents a 6.3% further reduction in the absolute viscosity on top of the 80.9% reduction for nitrogen. Upon the use of Ni-Mo/alumina catalyst (see Figure 5.4b) the absolute viscosity of the upgraded oil samples are 0.100 Pa.s (nitrogen) and 0.079 Pa.s (hydrogen). This shows 4.2 % further decrease in viscosity when the reaction was carried out under hydrogen. This consistent with the results presented on API gravity in Figure 5.3 and also with the studies of Liu and Fan (2002) and Galarrage and Pereira-Almao (2010). As Wang, et al. (2010) noted that the higher breaking of C-heteroatom bonds in the presence of hydrogen contributed to the further viscosity reduction and increased yield of lighter hydrocarbon fraction in addition to isomerisation, ring opening, dealkylation, and hydrogenation reactions as illustrated below:

Cracking of side chains

The cracking and isomerisation reactions occur on the acidic sites of the alumina support. The cracking of side chains of aromatic rings in the resins and asphaltenes are shown below:

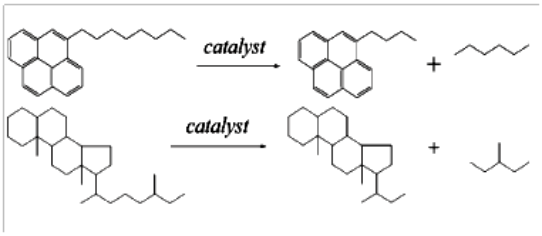

Hydrogenation reactions

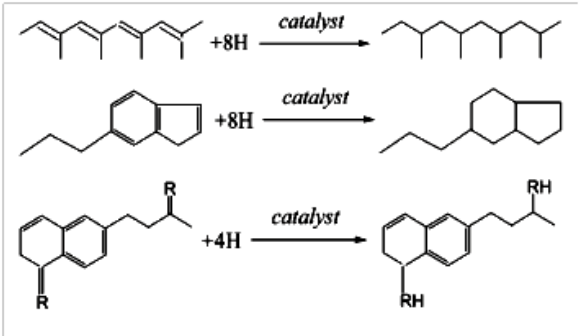

The hydrogenation function is provided by the Co, Ni, and Mo metals. This reaction occurs on the unsaturated hydrocarbons (i.e., olefins and aromatic) and the heteroatom-containing compounds (Wang, et al., 2010).

Ring opening reaction

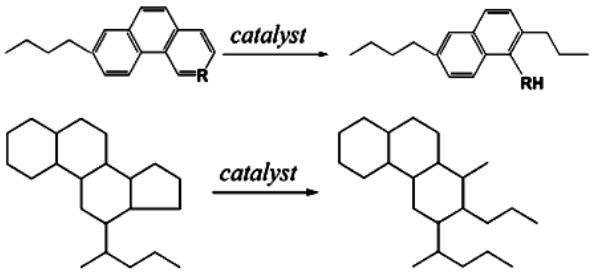

Where; R represents alkyl hydrocarbon. This type of reaction occurs to the cycloalkanes in the saturated hydrocarbons and the heterocyclic aromatic groups (Wang, et al., 2010).

Isomerisation reaction

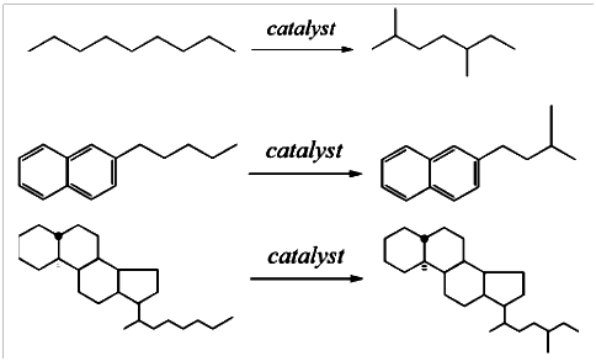

This kind of reaction occurs commonly on straight chain paraffins, the side chains of aromatic compounds, and cyclopraffins in the heavy oil (Wang, et al., 2010). The presence of iso-paraffins and iso-olefins, H_2S, and C_1-C_5 gases in the produced gas analysed using the RGA clearly confirmed these reactions (see section 5.2.3). Although, hydrocarbons take part in hydrogen-transfer reactions, their impact on hydroconversion is limited, as external hydrogen source is required.

The comparison between TBP distribution curves for hydrogen and nitrogen atmospheres with Co-Mo or Ni-Mo catalysts is presented in Figure 5.5. As can be seen, the amount distillate fractions increased upon catalytic upgrading under hydrogen compared to the use of nitrogen. It was found that with hydrogen a further 10-12°C shift towards low-boiling temperature distillates can be observed compared to nitrogen in order to obtain a cumulative distillate of 75 vol.%.

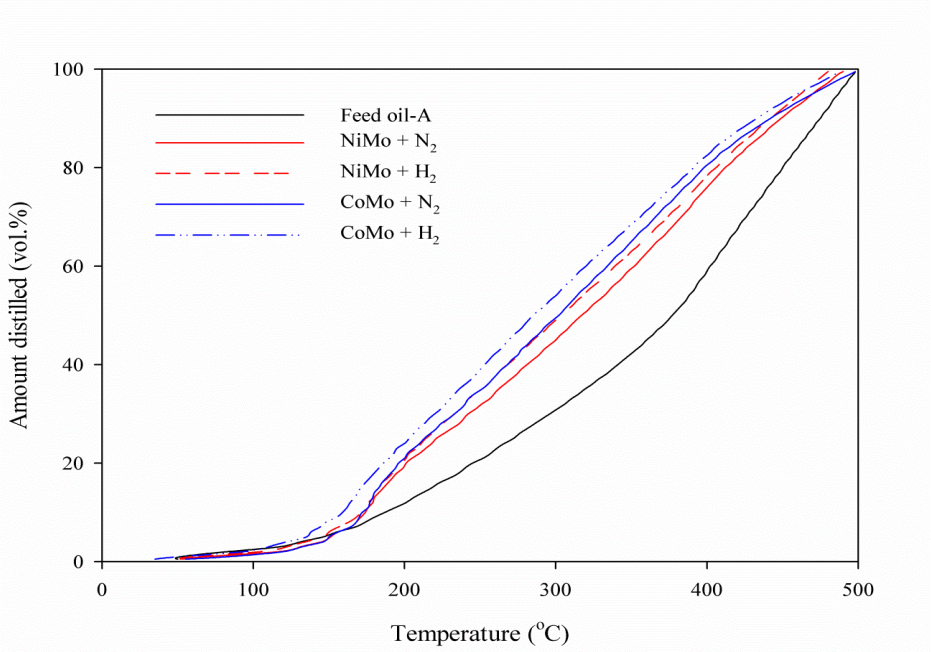

Figure 5.5 Effect of hydrogen-addition on TBP distribution of produced oil; Reaction Temperature 425 °C, Reaction Media; H_2 or N_2, Pressure 20 barg, Oil flow rate 1mL.min^{-1}, Gas flow rate 200 mL.min^{-1}; Catalysts: Co-Mo and Ni-Mo.

The conversion of residue fractions (> 343^{o}C) to light fractions (BP < 343^{o}C) are as follows: under nitrogen (28.6 and 37.4 %) and hydrogen (34.5 and 44.1 %) for Ni-Mo and Co-Mo catalysts, respectively. The involvement of hydrogen in the chemistry of the reaction is evident of 6-7 % conversion increase noticed. In distillates distribution, the resins and asphaltenes components concentrate majorly in the residue fractions while saturates concentrate in the low-boiling distillates (Zhao, et al., 2007). Therefore, the major differences between the TBP distribution curves presented in Figure 5.5 for the upgraded oils under nitrogen and hydrogen environments is related to the difference saturates and macromolecules components.

5.3.1 Effect of Hydrogen Pressure on API Gravity and Viscosity

In Figure 5.6, the effect of hydrogen pressure on the API gravity of the produced oil samples as a function of time-on-stream is presented. It can be seen that the API gravity increases slightly as the pressure increases with an average of 0.3^{o} API for every 10 bar rise in hydrogen pressure. This is because increased hydrogen pressure increases the availability of hydrogen for hydroconversion reactions (Sambi, et al., 1982; Elizalde, et al., 2010).

Also, the effect of hydrogen pressure on the viscosity of the produced oil samples is presented in Figure 5.7. In the same way, the viscosity of produced oil is slightly lowered as the hydrogen pressure increases from 20 to 40 bar with mean DVR increase of 1% for every 10 bar rise in pressure.

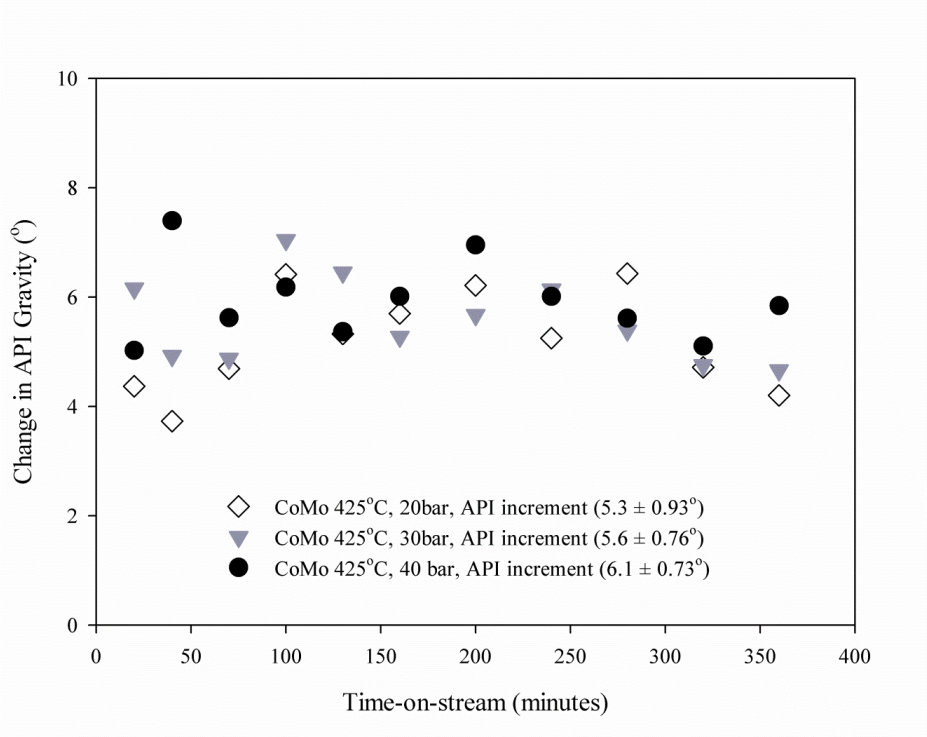

Figure 5.6 Effect of hydrogen pressure on API gravity of produced oil as a function of time-on-stream at temperature 425 ^{o}C, gas-to-oil ratio 200 mL.mL^{-1}, Catalyst: Co-Mo/Al_2O_3.

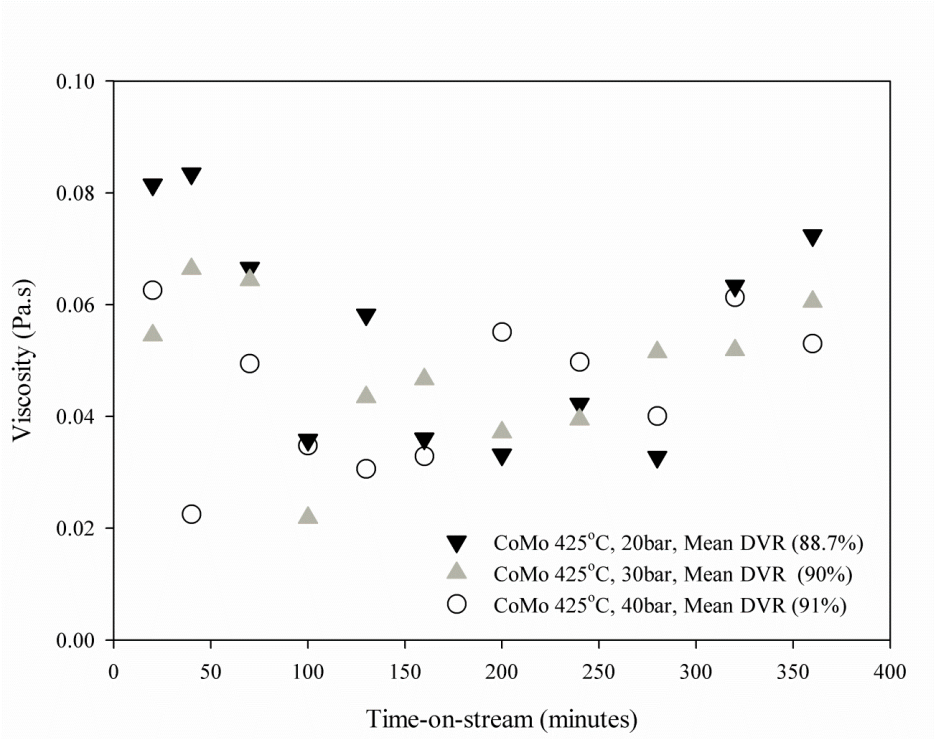

Figure 5.7 Effect of hydrogen pressure on viscosity of produced oil as a function of time-on-stream at temperature 425 ^{o}C, gas-to-oil ratio 200 mL.mL^{-1}, Catalyst: Co-Mo/Al_2O_3.

This shows that hydrogen pressure does not exert as much effect on API gravity increase and viscosity reduction as reaction temperature and WHSV reported in Chapter 4. Though catalytic upgrading reaction proceeds by large molecules breaking down into smaller ones, the cracked intermediates can reassemble into larger molecules when there are inadequate active hydrogen and methyl radicals in the reaction environment to moderate their addition reactions. The formation of large molecular weight compounds under nitrogen atmosphere leads to low API gravity and increase viscosity of the produced oil samples with time-on-stream (see section 5.2.2).

The measured difference between inlet and outlet hydrogen concentration in the produced gas showed a decrease by 13.3, 17.33 and 19.83 vol.% below 99.99 vol.% pure hydrogen fed into the CAPRI reactor as pressure increased from 20 to 40 bar. Though equations of state for the calculation of hydrogen consumption have been proposed by Maipur et al. (2010), in this work the outlet gas flow was not measured, so overall loss of hydrogen in moles was not calculated. However, this drop in hydrogen concentration shows that the solubility and involvement of hydrogen drastically improved as the pressure increased (Cai, et al., 2001; Maipur, et al., 2009; Rezaei, et al., 2010). This provides evidence that during the reactions hydrogen involved in hydrogenation of free radicals and aromatics, saturation of olefins, removal heteroatom, and hydrocracking (Longstaff, et al., 1994).

5.3.2 Effect of Hydrogen Pressure on TBP Distribution

The TBP distribution data of six selected samples obtained at hydrogen pressure of 20, 30, and 40 barg, with that obtained under nitrogen (20 barg) are presented in Figure 5.8. The

experiment was performed in duplicate with deviation of ± 1.8 %. It is clear that increase in hydrogen pressure slightly shifted the distillation curve to the left, with 30 bar producing the highest shift to the left.

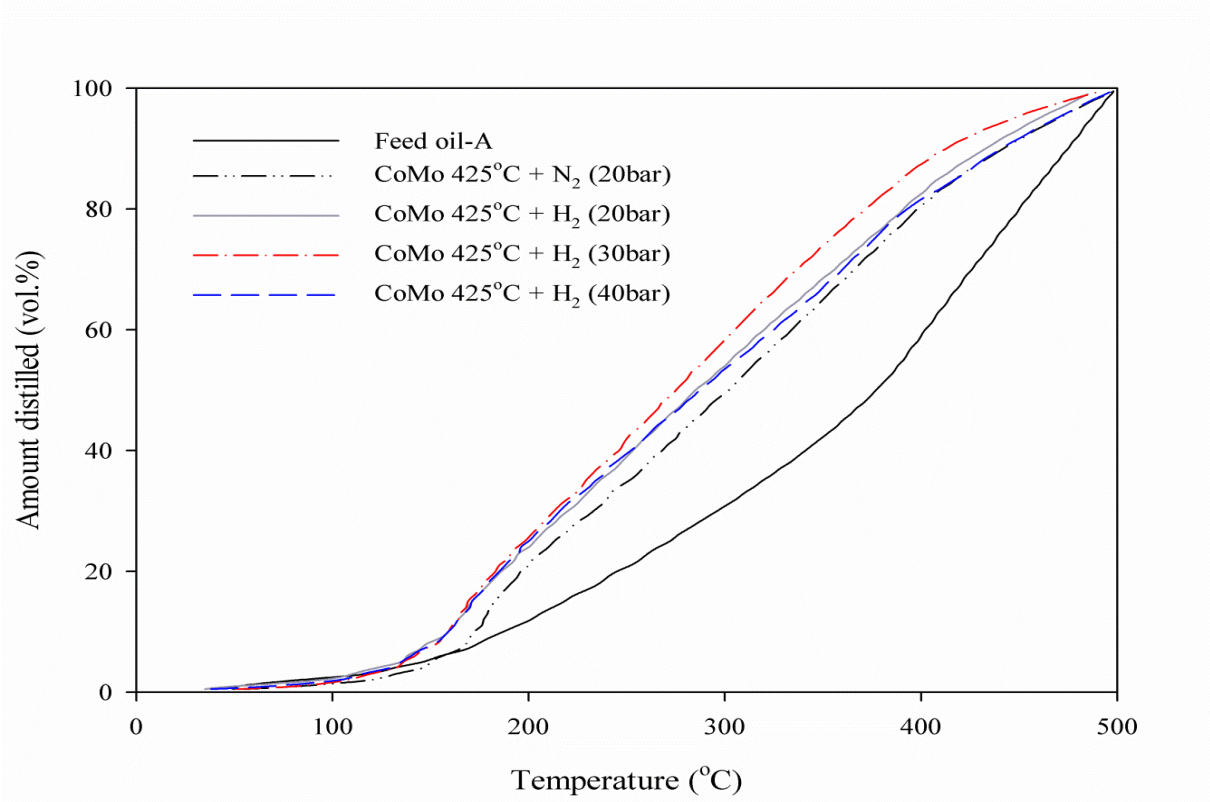

Figure 5.8 Effect of hydrogen pressure on TBP distribution at temperature 425 °C, gas-to-oil ratio 200 mL.mL^{-1}, Catalyst: Co-Mo/Al_2O_3.

It was noted that 65 vol.% cumulative amount distilled was obtained at boiling temperature of 414 °C for the feed oil, and after catalytic upgrading under nitrogen atmosphere it shifted to 350 °C, that is a shift to the left by 64 °C at 20 bar. However, under hydrogen at 20 bar it shifted to 338 °C, which is 12 °C to the left of the TBP curve under nitrogen. The increase in hydrogen pressure from 30 to 40 bar resulted in a shift to the left of TBP curve under nitrogen by 6 and 30 °C, respectively. It is therefore clear that hydrogen addition to catalytic upgrading process increased the yield of low-boiling fractions. As noted

by Jarullah and co-workers (2011), that the yield of middle distillate fractions increased after the hydrotreatment of the whole crude oil in a trickle-bed reactor.

The calculation of residue fractions (>343 ^{o}C) conversion showed that at 20 bar the conversion was 37.4 % (nitrogen) and 44.1 % (hydrogen), and with the increased in hydrogen pressure leading to increased conversion of 52.5 % (30 bar) and 41.2 % (40 bar). This represents 6.7-15.1 % above that of nitrogen which further affirms the fact that hydrogen was involved in the upgrading reactions, activated by the Ni, Co and Mo metals to produce active hydrogen that terminates active hydrocarbon chains generated during the cracking reactions. This is consistent with early result presented in section 5.2.2 (Figure 5.1c).

5.3.3 Effect of Hydrogen Pressure on Asphaltene Content

Table 5.5 shows the asphaltenes content of the produced oil under the different hydrogen pressure. As the hydrogen pressure increased, the asphaltenes content of the produced oil decreases to 8.63 wt.% (20 bar), 7.5 wt.% (30 bar) and 5.68 wt.% (40 bar) relative to 11.14 wt.% (feed oil-A). Thus, the maltene components which comprises of saturates, aromatics, and resins increases from 2.51 to 5.46 wt.% in the produced oil above 88.86 wt.% (feedstock). A similar trend with increasing hydrogen pressure was observed and reported by Liu et al. (2013).

Table 5.5 Asphaltene content of produced oil as a function of hydrogen pressure at temperature 425 ^{o}C; gas-to-oil ratio 200 mL.mL^{-1}; Catalyst: $CoMo/Al_2O_3$.

Hydrogen pressure (barg)	**Asphaltene Content (wt.%)**
20	8.63
30	7.5
40	5.68

The trends described above may have occurred because the conversion of asphaltenes in the presence of hydrogen enhanced the hydrogenation of cracked fragments which could have reduced their recombination to larger molecular weight species and subsequent precipitation during the catalytic upgrading process. This reaction is favoured at high hydrogen pressure and temperature, and involves hydrogen transfer from gas phase to the hydrocarbon radicals and asphaltenes fragments in the liquid phase (Fathi and Pereira-Almao, 2013; Liu, et al., 2013). This transfer of active hydrogen reduces hydrogen abstraction from the deposited macromolecules such as asphaltenes on the catalyst. The asphaltenes content decreased significantly therefore at 40 bar hydrogen pressure, because more active hydrogen radicals were available to neutralise the condensation of aromatic radicals that are generated during the cracking reactions. Whilst at 20 bar hydrogen pressure, the macromolecule of asphaltenes radicals were less constrained, which led to increased content of asphaltenes. Moreover, asphaltenes are major contributors to high crude oil viscosity and low API gravity, therefore the decreasing content of asphaltenes in the upgraded oil samples could have contributed to increase fluidity (i.e., low viscosity) and high API gravity increments observed in Figures 5.6 & 5.7.

5.4 Fresh vs. Regenerated Catalyst

Catalyst deactivation by coke is potentially reversible by burning-off the carbonaceous deposits in air at high temperature. It is well known that upgrading reactions occur on the catalyst surface (Hart, et al., 2013), which needs to be recovered to restore catalyst activity. Ex-situ oxidative-regeneration of the spent Co-Mo/Al_2O_3 catalyst recovered after upgrading under nitrogen atmosphere was carried out, and its performance compared with the fresh counterpart.

5.4.1 Characterisation of Fresh and Regenerated Catalyst

The nitrogen adsorption-desorption isotherms of the fresh Co-Mo catalyst, spent Co-Mo after reaction under nitrogen atmosphere and oxidative-regenerated spent Co-Mo catalyst from the nitrogen medium experiment are presented in Figure 5.9. It is clear that the catalyst textural properties such as pore volume, specific surface area, and pore-size distribution changed after oxidative-regeneration in air environment at 600^{o}C relative to the fresh and spent Co-Mo catalysts. This is mainly because of coke and metal deposits, which were not fully removed by the burning process.

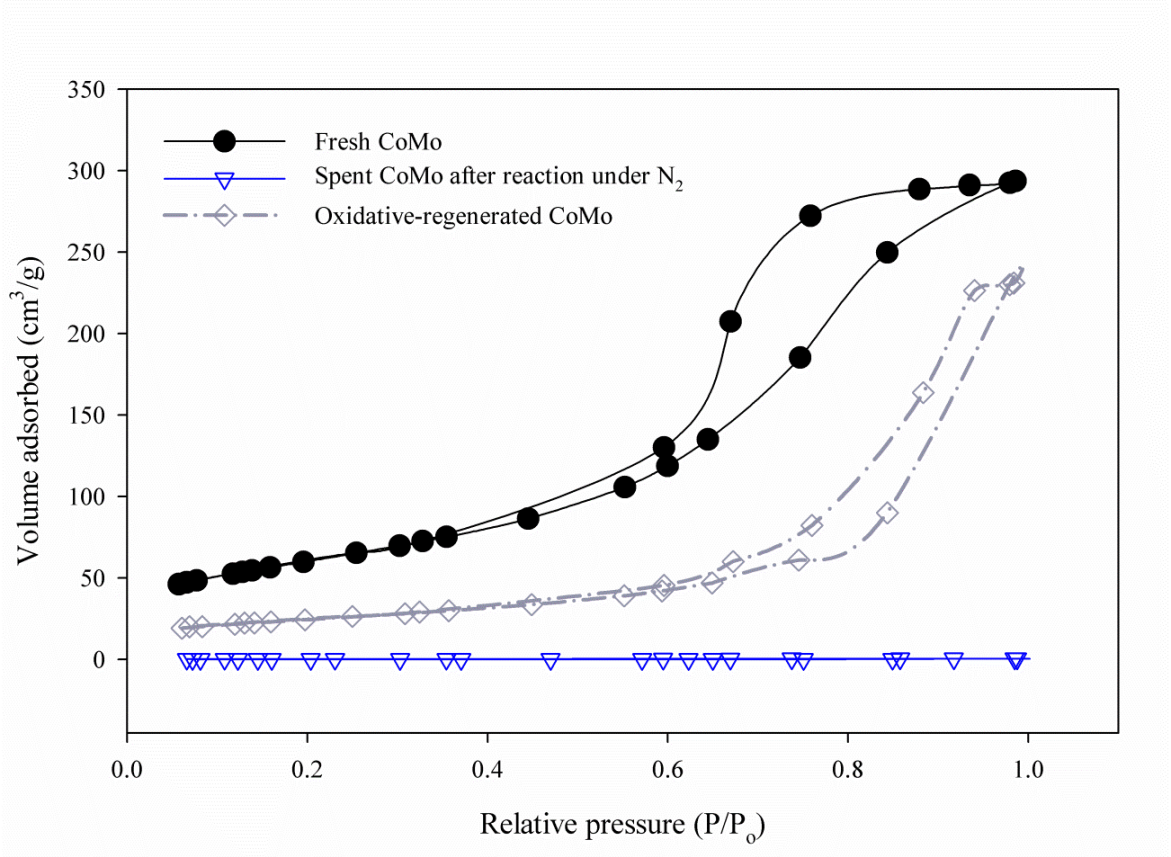

Figure 5.9 Nitrogen adsorption-desorption isotherm of fresh Co-Mo catalyst, spent Co-Mo after reaction under nitrogen, and oxidative-regenerated spent Co-Mo catalyst at 600 ^{o}C.

Additionally, the catalyst pore sizes became narrower with some of the micropores blocked as can be seen in the shift of the hysteresis loop towards higher relative pressure and lower adsorbed volume. From these data the specific surface area of the spent catalyst was $0.36 m^2.g^{-1}$ while the oxidative-regenerated Co-Mo was calculated to be $103.9 m^2 g^{-1}$, which is lower than the value of $214.4 m^2 g^{-1}$ for the fresh catalyst sample. This indicates that only 48.5% of the specific surface area was recovered after oxidative-regeneration at 600 ^oC.

The fresh and oxidative-regenerated Co-Mo/alumina catalyst at 600^oC were also characterised with Scanning Electron Microscope (SEM). Figure 5.10 shows the SEM images of the same catalyst microstructure before reaction (i.e., fresh) and oxidative-regenerated after upgrading reactions (i.e., Figure 5.13B).

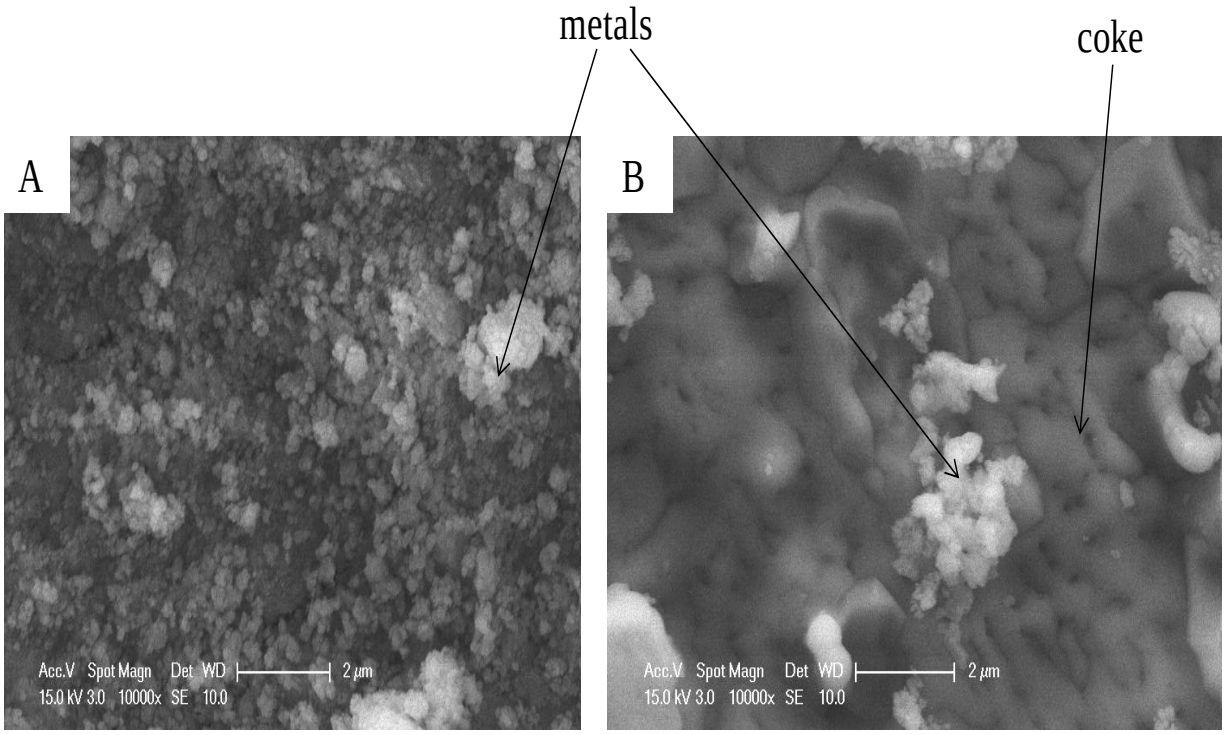

Figure 5.10 SEM photomicrograph of Co-Mo/Al_2O_3 catalyst; (A) fresh and (B) oxidative-regenerated spent catalyst after upgrading reaction under nitrogen atmosphere.

The surface morphologies of the oxidative-regenerated Co-Mo/alumina revealed a visible coating of coke and metals blocking the pores observed in the fresh catalyst. This is consistent with Figure 2.9. Because of the metals and unburned coke within regenerated catalyst, 51.5 % specific surface area of regenerated catalyst was loss. Consequently, it shows that oxidative-regeneration can not completely burn-off the deposited coke onto the surfaces within the catalyst pores. The performance of oxidative-regenerated spent Co-Mo/Al_2O_3 against its fresh counterpart is presented in Appendix D.

5.5 Hydrocracking of Poly-aromatic Model Compounds

Generally, Ni-Mo, Co-Mo, etc. supported on alumina and/or silica promote hydrogen-transfer reactions while the acidic support promotes cracking, ring-opening, and de-alkylation reactions (Korre and Klein, 1995). The large bond dissociation energy of aromatic rings is lessen by converting C=C bonds (i.e., 146-151 Kcal/mol.) to C-C bonds (i.e., 83-85 Kcal/mol.), thereby enhancing the cracking of poly-aromatic hydrocarbons into lighter hydrocarbons (Sun, et al., 2004).

The chemistry of heavy oil is complex since it contains several compounds such as paraffins, naphthenes, mono-aromatics, diaromatics, and poly-aromatics, respectively. Poly-aromatic hydrocarbons (PAHs) account for a large portion of the structures contained in the heavy oil, therefore hydrocracking (HDC) of a model compound representative will provide a comprehensive understanding of their conversion during the catalyst upgrading process. In this regard, a tricyclic aromatic fused ring structure anthracene ($C_{14}H_{10}$) was investigated as a model compound representing the PAHs family. The HDC of the anthracene was investigated using the same CAPRI experimental set up, Co-Mo/Al_2O_3 catalyst at temperatures 350 and

400 ^{o}C, hydrogen pressure 20 barg, and flow rate 200 mL.min^{-1}. The liquid product was analysed using Thermo Electron Corporation Trace GC Ultra DSQ II. The results are discussed in Appendix E and elucidate the roles of hydrogen in the catalytic upgrading of highly aromatic heavy oil into light oil which include aromatic hydrogenation, olefin saturation, and active chain termination.

5.6 Conclusions

The deposition of coke on the catalyst surface during the upgrading reactions in CAPRI is a major contributor to catalyst deactivation. It was found that the hydrogen and hydrogen-donor reactive media play a role in inhibiting coke formation and growth, while also improving the quality and stability of produced upgraded oil. Addition of hydrogen or a hydrogen-donor to the feed promotes hydrocracking and hydrogenation reactions, whereas in a nitrogen atmosphere most of upgrading occurred via carbon-rejection with associated heavy coke deposition upon the catalyst. Hence, reaction under nitrogen leads to characteristically low API gravity, high viscosity, and low distillates in the produced oil compared with gases containing hydrogen and hydrogen-donor. Additionally, it was found that hydrogen and hydrogen-donor atmospheres promote olefin saturation, enhance the paraffin yield, and improve distillable hydrocarbon fractions. The spent catalyst regenerated *ex situ* by oxidising the deposited asphaltenes and coke lost 52.5 % of the surface area compared with the fresh catalyst. However its upgrading performance in terms of change in API gravity, viscosity reduction and the yield of distillable was similar to that of the fresh catalyst.

Chapter 6

Effect of Guard Bed on CAPRI Upgrading

6.1 Introduction

In Chapter 4 it was found that better upgrading at reaction temperature (425 ^{o}C) and WHSV (9.1 h^{-1}) occurs at the expense of high coke formation, leading to rapid catalyst deactivation. Larger molecular weight compounds such as resins and asphaltenes are major contributors to coke formation. Therefore, a guard bed on top of the catalyst bed could selectively adsorb these macromolecules. Hence, the catalyst lifetime could potentially extend as premature catalyst deactivation due to coking would have reduced. It is known that foulants such as metals, sulphur, and sediments that cause catalysts deactivation and shorten catalyst lifespan during the upgrading process are associated with these macromolecules in the heavy oil.

Activated Carbon (AC) has shown an affinity for macro-hydrocarbon molecules, adsorptive selectivity for asphaltenes, resins and coke precursors (Fukuyama, et al., 2004; Ming et al., 2007). Besides, the use of AC as catalyst support for heavy oil upgrading has also been reported in the literature (Fukuyama, et al., 2004; Ming et al., 2007; Terai, et al., 2000; Solar, et al., 1991). This is because of its large surface area, macro- and mesoporous characteristics and affinity for large molecular weight species. An AC with a surface area of 819.92 $m^2.g^{-1}$ and pore diameter 412 nm was selected for use as the guard bed on top of the Co-Mo/Al_2O_3 and Ni-Mo/Al_2O_3 catalysts. The results of AC and pelleted alumina as guard-beds are reported in this Chapter. Meanwhile, the nitrogen sorption isotherm, the porosimetry, and the properties of the AC and the alumina support are presented in Appendix A.

6.2 Effect of Guard-Bed

6.2.1 Effect of Guard Bed on API Gravity

The API gravity is a measure of the heaviness or lightness of crude oils. The higher the API gravity of the crude oil the lighter and the higher the market value. In Figures 6.1 (a) and (b), the API gravity of the upgraded oil samples over AC only, Co-Mo/Al_2O_3 only and Co-Mo/Al_2O_3 catalyst with AC or Alumina guard bed as a function of time-on-stream are presented.

In the experimental run with AC guard bed on top of Co-Mo/Al_2O_3 catalyst, a substantial level of upgrading was evident by the further increase in the API gravity of the produced oil in the range of 3 to 9^{o}API points above 13^{o}API of the feed oil can be observed. Whilst, in the experiment carried out with Co-Mo/Al_2O_3 catalyst only the oil produced was upgraded by ~2 to 5^o API, as compared with the feed oil. Furthermore, 7^o was the maximum obtained API gravity using Co-Mo/Al_2O_3 catalyst only, while 9^o API is achievable when AC guard-bed was added on top of the same catalyst. This shows an additional 2^o API gravity increment. Without the guard bed, the API gravity for the catalyst significantly fell shortly after the reaction started and reached its lowest value of about 2° at around 200 minutes into the experiment and retained a plateau of lower API upgrading until the end of the experiment. However, the addition of AC guard bed to the catalytic upgrading bed sustained the activity of the catalyst with the API gravity of the produced oil above 2^o (observed upon the use of Co-Mo/Al_2O_3 only) for almost 840 minutes before a noticeable decrease of API gravity was observed in the produced oil (see Figure 6.1a). This effectively adds an additional 10 hours of catalytic activity compared to the use of Co-Mo/Al_2O_3 catalyst only.

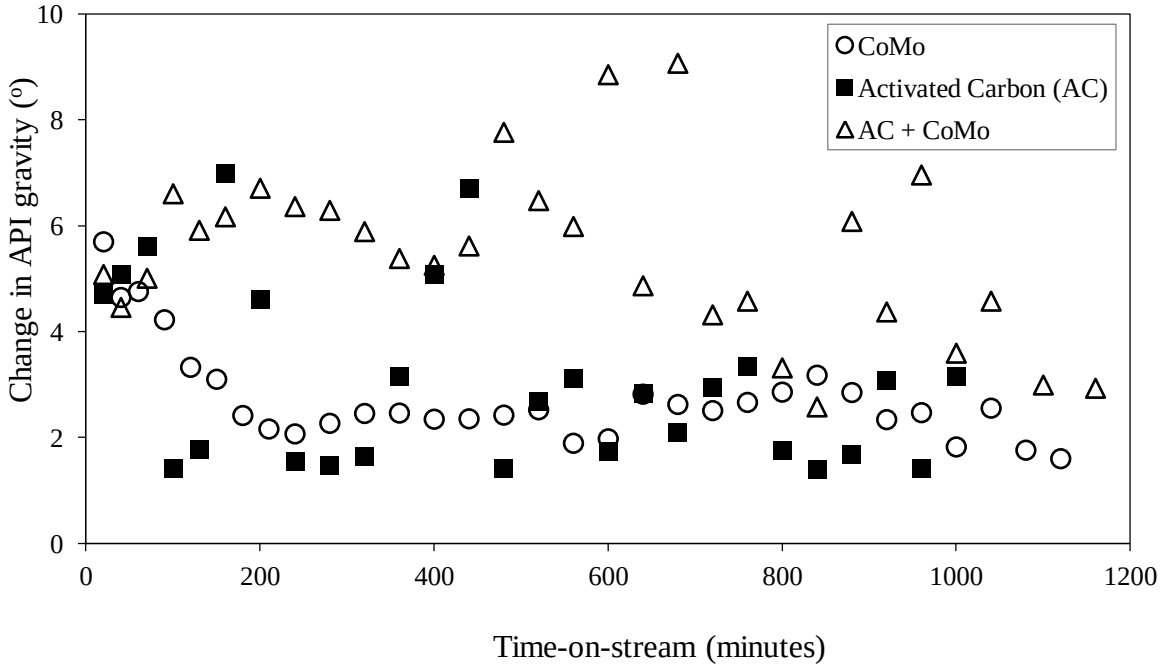

(a)

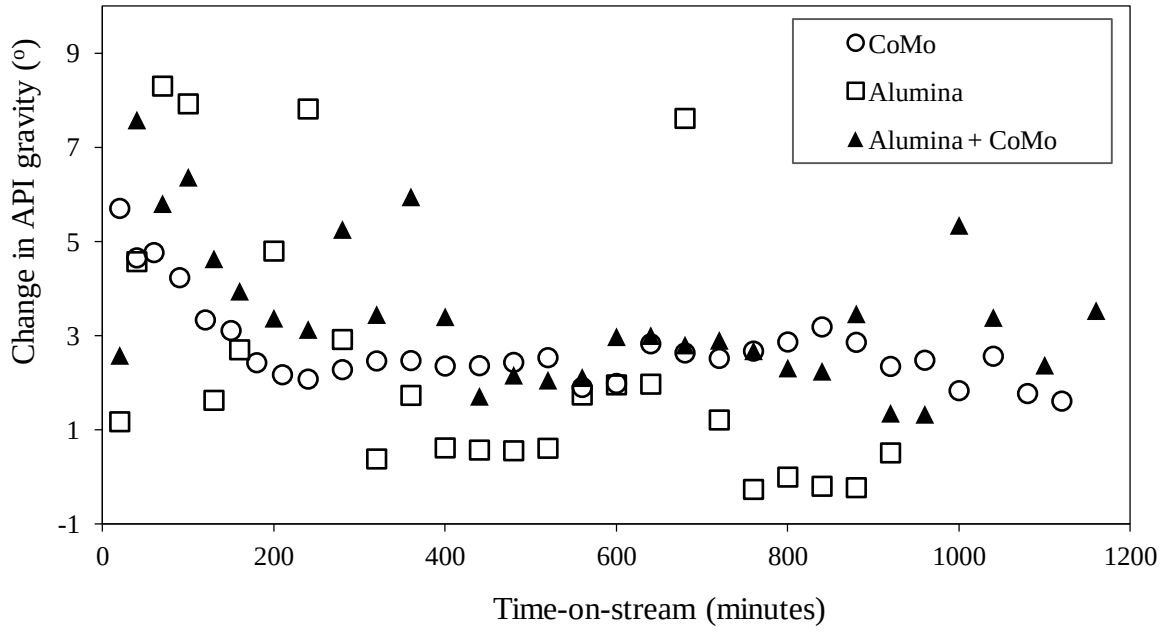

(b)

Figure 6.1 API gravity of produced oil as function of time-on-stream for Co-Mo/Al_2O_3 only, AC only, alumina only, and Co-Mo/Al_2O_3 with (a) activated carbon (AC) and (b) Alumina; Temperature 425 °C, Reaction Media N2, Pressure 20 barg, Oil flow rate 1 mL.min^{-1}, Gas flow rate 500 mL.min^{-1}.

This confirmed the loss of catalytic activity in a short time without the use of a guard bed. Moreover, the use of AC only produced oil with an average API gravity of 3.1 ± 1.7° compared to 3 ± 0.92° and 5.6 ± 1.6° observed for Co-Mo/Al_2O_3 only and AC on top of Co-Mo/Al_2O_3 catalyst. The upgrading noticed upon the use of AC only can be attributed to adsorptive properties and thermal cracking occurring on its surface since the material is neutral, unlike alumina that is acidic.

In contrast with the use of an AC guard bed, the use of pelleted alumina guard bed on top of Co-Mo/Al_2O_3 catalyst follows a similar trend as that of the Co-Mo/Al_2O_3 catalyst only (see Figure 6.1b). The API gravity of the produced oil starts from 7.6° for the alumina plus Co-Mo/Al_2O_3 catalyst and rapidly fell to 3° in 200 minutes, before settling to an average value of 3.44 ± 1.54° with time-on-stream until the experiment was stopped. This represents an average change in API of approximately 0.6° above 2.8 ± 0.93° for Co-Mo/Al_2O_3 catalyst only. Interestingly, the use of alumina without catalytic metals (i.e., Co, Ni, or Mo) produced oil which increased to maximum of 8° and drastically fell to 1° after 200 minutes. After 400 minutes time-on-stream the API gravities of most of the produced oils approach that of the feed oil, with some measured values 0.03 – 0.24° less than 13° API for the feed oil. The decreased API gravity compared to that of the feed oil can be attributed to increased macromolecular weight species such as asphaltenes in the oil produced (Javadli and Klerk, 2012; Hart, et al., 2012). The strong acid sites of the alumina were responsible for cracking reaction which improved the API gravity of the oil produced at the early hours of operation. However, this resulted in a drastic change in composition towards the lighter end hydrocarbons within the reaction environment. This shift in composition could have caused asphaltenes aggregation, polymerisation and condensation to form large molecular weight compounds, thus leading to the decrease in API gravity and subsequent increase in the

viscosity of the oil produced with time-on-stream (Guangshou, et al., 2009). To confirm this, the asphaltenes content of the produced oil after 400 minutes was measured. It was found to be 0.4 to 0.8 wt.% higher than 11.14 wt.% (feed oil), which confirms asphaltenes precipitation and aggregation.

From the results presented in Figures 6.1 (a) and (b), it is clear that AC gave better performance than alumina. Notably, produced oil samples have an average API gravities of 5.6 ± 1.6^{o} for AC on top of Co-Mo/Al_2O_3 catalyst compared to 3.44 ± 1.54^{o} achieved upon the use of alumina. This is because of the difference in material properties, in particular it was noted that AC was neutral and alumina acidic.

6.2.2 Effect of Guard Bed on Viscosity

Lowering heavy oil viscosity significantly decreases the energy requirements for pumping. The viscosity of the produced oil samples versus time-on-stream for the Co-Mo/Al_2O_3 catalyst only, AC only, alumina only, and AC/alumina guard bed with Co-Mo/Al_2O_3 catalyst are shown in Figures 6.2 (a) and (b), respectively. It is clear that the viscosity of the produced oils in all cases was significantly lower than 0.5 Pa.s (feed oil). The standard deviation for duplicate runs is within ± 0.06.

It has been shown in previous chapters that the viscosity reduction can be attributed to the increase in the lighter hydrocarbon components in the produced oil as a result of the conversion of heavy molecular weight (i.e., boiling point < 343 ^{o}C) into lower fractions. It is clear therefore that Co-Mo/Al_2O_3 catalyst with AC guard-bed on top produced oil with lower viscosity than with Co-Mo/Al_2O_3 catalyst and AC only (see Figure 6.2a).

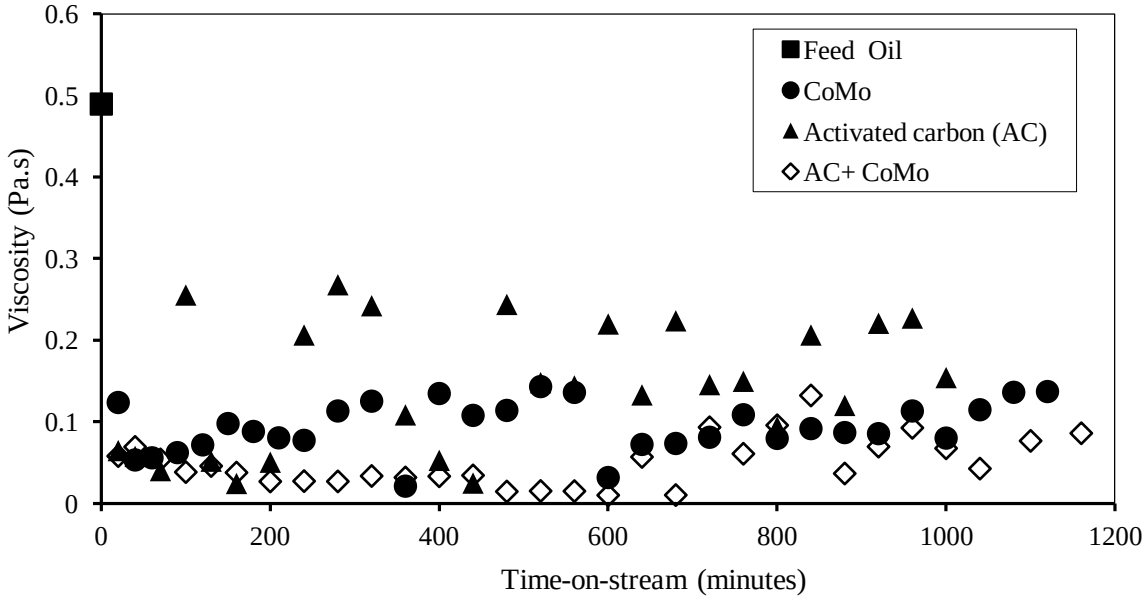

(a)

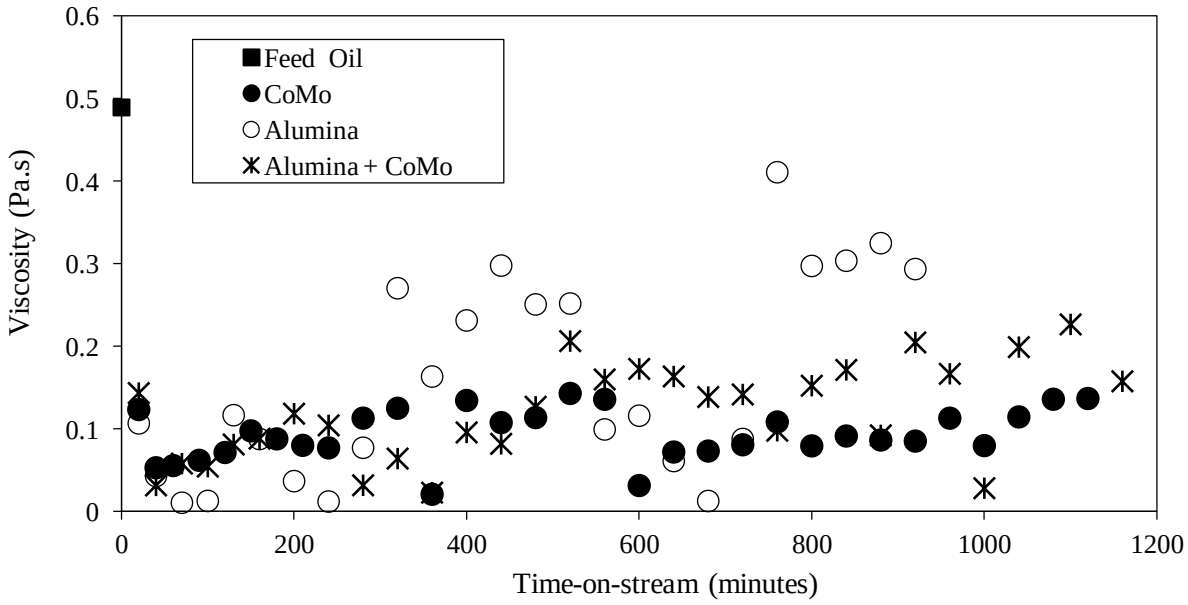

(b)

Figure 6.2 Viscosity of produced oil samples as a function of time-on-stream for Co-Mo/Al_2O_3 only, AC only, alumina only, and Co-Mo/Al_2O_3 with (a) AC and (b) alumina; Temperature 425 °C, Reaction Media N_2, Pressure 20 barg, Oil flow rate 1mL.min^{-1}, Gas flow rate 500 mL.min^{-1}.

This result is consistent with that reported in Figure 6.1a for API gravity of the produced oil samples for the same system. The average viscosity of the produced oil in 20 hours is approximately 0.052 Pa.s with AC only, 0.094 Pa.s with Co-Mo/Al_2O_3 only, and 0.048 Pa.s with AC plus Co-Mo/Al_2O_3, respectively compared to 0.49 Pa.s (feed oil). This represents a viscosity reduction of 81% (Co-Mo/Al_2O_3 only), whereas with AC on top of Co-Mo/Al_2O_3 viscosity reduction was 89.5% in the same time of operation. Hence, an additional 8.5% decrease in the produced oil viscosity occurred upon the use of AC guard-bed plus Co-Mo/Al_2O_3 catalyst.

The larger viscosity reduction is evident from Figure 6.2 (or API gravity increase from Figure 6.1) upon the addition of the guard bed compared with only Co-Mo/Al_2O_3 catalyst. The improved upgrading with guard bed is thought to occur largely because macro-molecules and coke precursors in the feed oil could have been adsorbed onto the AC due to its affinity for asphaltenes and resins (Ming, et al., 2007). As a result relatively less complex molecules proceed from the AC guard bed on to the Co-Mo/Al_2O_3 catalyst bed where they are cracked. This statement is further supported by the fact that neither the AC guard-bed nor the Co-Mo/Al_2O_3 catalyst achieved the higher upgrading on its own. The guard-bed acted as a sieve and allowed the diffusion of less complex molecules through into the catalytic pellet active sites of the main catalyst bed. In this scenario, the catalyst therefore exhibits better metal retention capacity and asphaltenes cracking than when used without the guard bed. This therefore prevents premature plugging of the catalyst pore network and allows effective use of surface area and metals (Rana, et al., 2007; Hart, et al., 2012).

The effect of using alumina support as an alternative material for the guard bed is presented in Figure 6.2 (b) at the same conditions. The result shows that the viscosity of the produced oil samples was sustained below 0.1 Pa.s up to 400 minutes (alumina plus Co-

Mo/Al_2O_3), while that of the Co-Mo/Al_2O_3 and alumina only lasted for 360 and 320 minutes, respectively. This represents a gain in 40 minutes at the early hours of operation. The cracking activity of the alumina guard bed was dominant because of its number and strength of acid sites (Leyva, et al., 2007). However, at the end of 20 hours time-on-stream, the average degree of viscosity reduction for the alumina guard bed with Co-Mo/Al_2O_3 catalyst, alumina only and Co-Mo/Al_2O_3 catalyst only are 73.9, 67.5, and 80.8%, respectively. This showed that in terms of viscosity reduction for the same time-on-stream operation the Co-Mo/Al_2O_3 improved the flow properties of the produced oil by approximately 7% compared to the integrated alumina guard bed system. Higher levels of average upgrading were not observed because of the premature deactivation caused by the plugging of the 8.2 nm pore mouths of the alumina as a result of deposition of the by-product coke. Secondly, the precipitation of asphaltenes and regrouping of free radicals to form larger molecular weight species lead to the decreased API gravity and increased viscosity of the produced oils observed beyond 400 minutes (see Figures 6.1b and 6.2b). Therefore, a neutral material like AC performed better as guard bed than acidic material such as alumina based on the above results. This is because acid sites are prone to fast deactivation within a short time due to carbon and metal deposition (Leyva, et al., 2007).

6.2.3 Effect of Guard Bed on TBP Distribution

The TBP distribution curves obtained from SIMDIS of selected samples from Co-Mo/Al_2O_3 only, alumina only, AC only, and AC or alumina on top of Co-Mo/Al_2O_3 with that of the feed oil for comparison are presented in Figure 6.3. It is obvious that the TBP curves of the produced oil samples in all cases shifted to the left of the feedstock TBP distribution

curve. This shows increased low-boiling fractions in the produced oils. For instance the yield of cumulative amount of 60 vol.% from the feedstock SIMDIS occurs at a temperature of 402^{o}C, but after upgrading was performed with Co-Mo/Al_2O_3, AC, and alumina each as standalone the boiling temperature shifted to the left to values of 339, 379, and 358 ^{o}C, respectively for the same 60 vol.% yield. The temperature shifts observed therefore are 23 ^{o}C (AC only), 44 ^{o}C (alumina only) and 63 ^{o}C (Co-Mo/Al_2O_3 only) to the left indicating increased low-boiling fractions in the produced oil. However, when AC and alumina was used on top of Co-Mo/Al_2O_3 catalyst as guard bed the temperature shifted from 339^{o}C (Co-Mo/Al_2O_3 only) to 334 ^{o}C (AC plus Co-Mo/Al_2O_3) and 336 ^{o}C (alumina plus Co-Mo/Al_2O_3). This represents respectively 3 and 5 ^{o}C temperature shift towards the low-boiling fractions.

It can be observed that the guard bed combination with the Co-Mo/Al_2O_3 catalyst does not differ significantly in the boiling point ranges from the experiment where only Co-Mo/Al_2O_3 catalyst was used. In fact they are almost identical (see Figure 6.3). The sieve like character of the AC guard-bed can further be evident from the fact that AC bed is neutral and therefore does not perform cracking functions as does the alumina, instead the upgrading observed is only due to adsorbed macro-molecules and thermal cracking reactions. The SIMDIS curves provide conclusive proof to this statement where both the Co-Mo/Al_2O_3 and AC with Co-Mo/Al_2O_3 TBP distribution were almost identical, suggesting no chemical role of the guard bed.

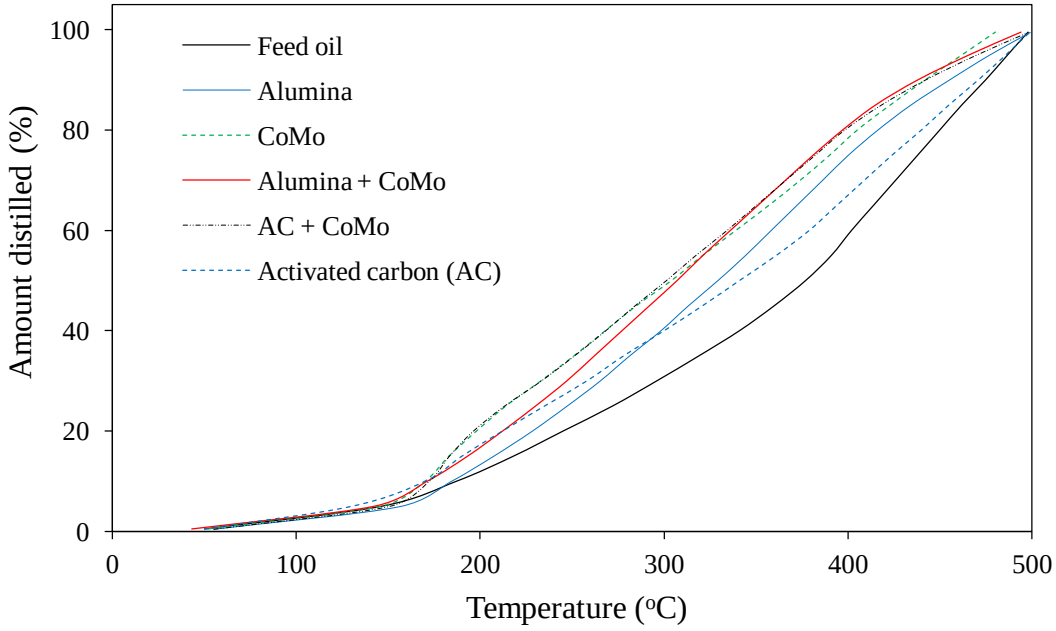

Figure 6.3 TBP distribution curves of feed and produced oils for guard bed integrated with catalyst, Co-Mo/Al_2O_3 catalyst only, Alumina only; AC only, AC + Co-Mo/Al_2O_3, and alumina + Co-Mo/Al_2O_3 catalysts; Temperature 425 °C, Reaction Media (N_2), Pressure 20 barg, Oil flow rate 1mL.min^{-1}, Gas flow rate 500mL.min^{-1}.

6.2.4 Effect of AC Guard Bed on Asphaltenes, Sulphur and Metals Contents

The results presented in previous sections showed that the AC performed better than alumina as a guard bed material. The asphaltene, sulphur and metals content of the produced oil from the use of Co-Mo/Al_2O_3 and AC on top of the Co-Mo/Al_2O_3 catalysts are presented in Table 6.1. It can be seen that the sulphur content of the feed oil reduced from 3.8 to 3.55 wt.% with Co-Mo/Al_2O_3 only and 3.25 wt.% with AC on top of the Co-Mo/Al_2O_3 catalyst. It was also observed that the nickel plus vanadium (Ni + V) metals content decreased from 206 to 186 ppm (Co-Mo/Al_2O_3 only) and 60 ppm (AC on top of Co-Mo/Al_2O_3 catalyst). This indicates reduction of (Ni + V) content by 10 % (Co-Mo/Al_2O_3) and 70.9 % (AC + Co-Mo/Al_2O_3), respectively. Additionally, other elements such as molybdenum, boron, iron, zinc, and phosphorus reduced significantly with the use of AC guard bed on top of Co-Mo catalyst

compared to the use of Co-Mo catalyst only. Notably, the level of Ni + V upon AC guard-bed with Co-Mo/Al_2O_3 catalyst was significantly higher than the level of sulphur removed.

Table 6.1 Asphaltene, sulphur, and metals content before and after reaction with and without activated carbon guard using Co-Mo/Al_2O_3 at 425 ^oC, 20 barg, 500 $mLmL^{-1}$ and feed oil-A.

Impurities	**Feedstock**	**Co-Mo/Al_2O_3**	**AC + Co-Mo/Al_2O_3**
Asphaltene (wt.%)	11.14	5.99	3.95
Aluminium (ppm)	6	7	< 1
Boron (ppm)	9	0.8	< 1
Cobalt (ppm)	< 1	0	< 1
Iron (ppm)	36	10	1
Molybdenum (ppm)	6	3	1
Sodium (ppm)	< 7	3	2
Nickel (ppm)	56	50	18
Vanadium (ppm)	150	136	42
Ni + V (ppm)	206	186	60
Phosphorus (ppm)	0.3	0.1	< 1.5
Sulphur (wt.%)	3.8	3.55	3.25
Silicon (ppm)	0.4	1	< 1
Zinc (ppm)	2	0.3	1

* Sulphur and metals content was performed by Intertek Laboratories Sunbury Technology Centre, UK, using ICP-OES (Inductively Coupled Plasma Optical Emission Spectrometry)

The deasphalting and/or cracking of asphaltenes into smaller molecules will reduce the sulphur as well as the metal content of the produced oil. Moreover, Ancheyta, et al. (2002) and Ancheyta (2011) found that higher asphaltene content in crude oil correlate with higher metals content; however pointed out that sulphur and nitrogen are very much present in light hydrocarbons. For this reason sulphur removal was low even though AC was used on-top of Co-Mo/Al_2O_3 catalyst. Ferreira et al. (2012) studied the reactivity of vacuum residue towards

HDS and HDM and it was found that HDS and HDM are not only controlled by process conditions and catalyst properties, but also the concentration and size of the heavy molecules such as asphaltenes and resins. Therefore, the low removal of sulphur and metals (i.e., Ni + V) when only Co-Mo/alumina catalyst was used is thought to be due to high concentration of asphaltenes in the heavy oil. However, the integration of AC guard-bed could also act as a hydrogen transfer agent in hydrocarbon cracking in addition to selective adsorption of macromolecules leading to high sulphur and metals removal (Dockner, 1988).

Consequently, the asphaltenes (nC_7) content decreased from 5.99 wt.% (Co-Mo/Al_2O_3) to 3.95 wt.% upon the use of AC on-top of the Co-Mo/Al_2O_3 catalyst because some of the high molecular weight species such as asphaltenes, resins and other heavy molecules were adsorbed onto the AC. This implies that lighter and less complex molecular weight species are processed onto the catalyst bed, which is easier to crack in order to remove the contaminants associated with the molecule (Hart, et al., 2013). This is confirmed as the produced oil from AC plus Co-Mo/Al_2O_3 catalyst contain less asphaltene and heavy metals components as also observed in the additional 2^o increment in API gravity and 8.5% further reduction of viscosity.

6.2.5 The Role of AC and Alumina Guard Bed

It is well known that the acid sites of the Co-Mo/Al_2O_3 promote cracking reactions. To elucidate the role of the AC or alumina in the heavy oil upgrading, TGA profile (i.e., weight loss as a function of temperature plot) and derivative weight loss curve for the recovered AC and alumina used as guard-bed superimposed with asphaltenes separated using n-C_7 is shown in Figure 6.4 (a) and (b). Clearly, the asphaltenes burn-off range 420-600 ^oC (see Figure 6.4a). From Figure 6.4 (a), the deposits of larger molecular weight compounds (e.g., resins and

asphaltenes) onto the AC bed was determined as 31 wt. %, which burns-off in the same temperature range of 440-600 ^{o}C. This shows that some of the macro-molecules have been adsorbed by AC prior to catalytic upgrading.

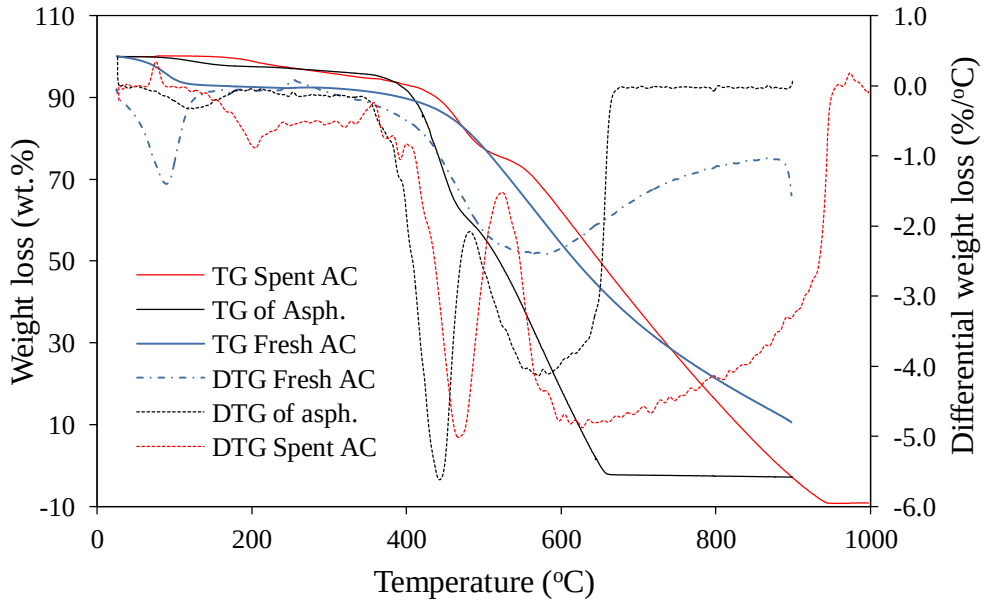

(a)

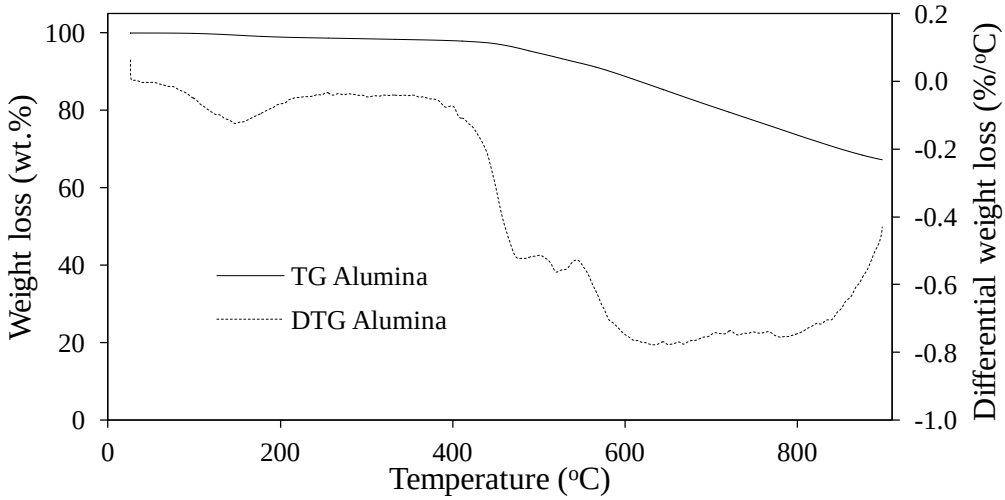

(b)

Figure 6.4 TGA and DTG of (a) fresh and spent AC and separated asphaltenes (Asph.); (b) alumina, used as guard bed placed on top of the Co-Mo/Al_2O_3 catalyst; Temperature 425 °C, Reaction Media (N_2), Pressure 20 barg, Oil flow rate 1 mL.min^{-1}, Gas flow rate 500 mL.min^{-1}.

Referring again to Figure 6.4 (b), the peaks between 476-600^{o}C represent burn-off of asphaltenes and sediments deposited on the alumina bed, which accounts for 9.8 wt.%, while the burn-off between 600-800 ^{o}C represents coke, which accounts for 17.6 wt.% loss of weight. The presence of coke on the alumina however indicates its propensity for cracking activity due to the acid sites, which was not the case in the use of neutral AC. Therefore, the macroporous and mesoporous characteristics of the AC were thought to have played critical roles in the adsorption by allowing the passage of small molecules and hydrocarbon free radicals generated by thermal cracking of adsorbed asphaltenes to reach the catalyst bed, thereby limiting polycondensation reaction (Viet, et al., 2012; 2013).

6.3 Effect of Hydrogen-addition and AC Guard Bed

In Chapter 5 it was shown that hydrogen-addition improved API gravity, viscosity and the conversion level. In this section, the combined effect of hydrogen-addition and AC guard-bed was investigated using cylindrical Ni-Mo/Al_2O_3 at temperature 425 ^{o}C, pressure 20 barg, H_2/oil ratio 200 mL.mL^{-1} and feed oil-B.

6.3.1 Effect on API gravity and Viscosity

The API gravity and the viscosity of the produced upgraded oil as a function time-on-stream for the three scenarios are shown in Figures 6.5 (a) and (b), respectively. From Figure 6.5 (a), the API gravity of the produced oil for all of the three runs increased by ~1 to 6^{o} API depending on the use of AC guard-bed, nitrogen or hydrogen, as compared to the original feed oil 14^{o}. The API gravity of the produced oil with cylindrical Ni-Mo/Al_2O_3 only started from roughly 3^{o} rise and falls to 1^{o} in 200 minutes, thereafter settles at an average of 1.7 ± 0.74^{o} API under nitrogen as the reaction media. Under the same nitrogen atmosphere, with AC on top of

the cylindrical Ni-Mo/Al_2O_3 catalyst the API gravity was raised to 5^o before settling at an average of 3.15 ± 1.22^o. This indicates 1.45^o further increase in API gravity.

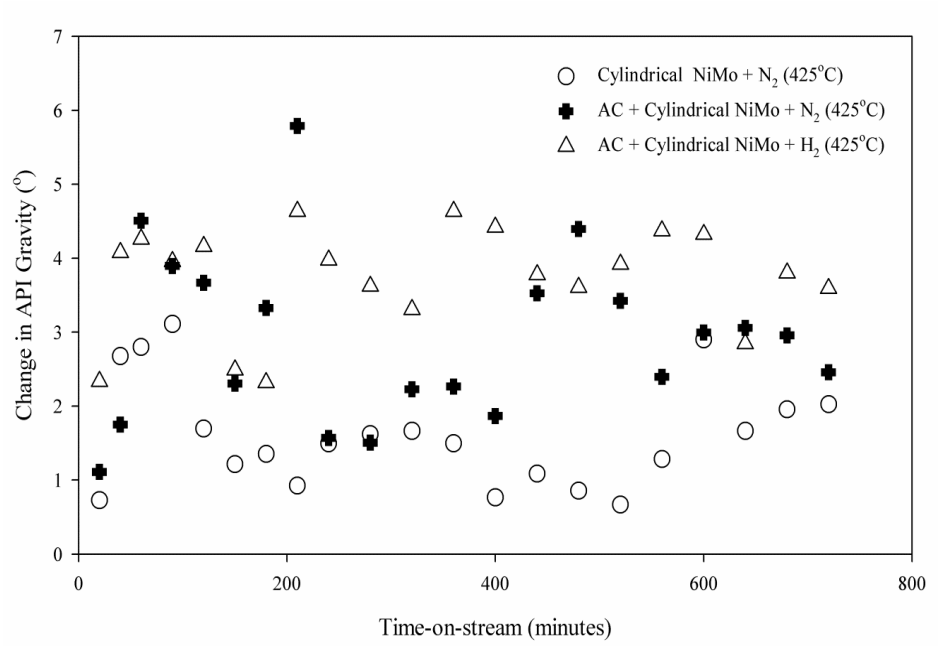

(a)

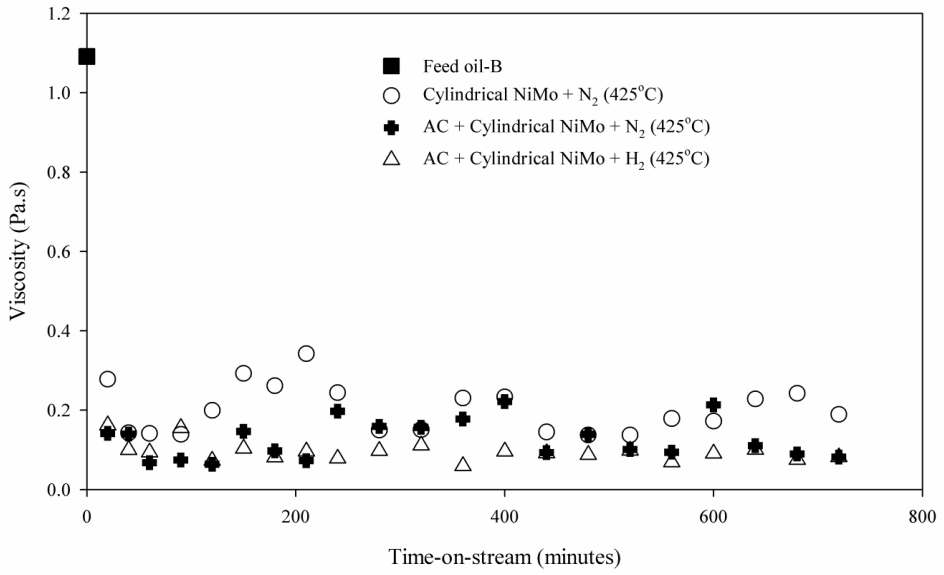

(b)

Figure 6.5 (a) Change in API gravity and (b) viscosity of produced oil using Ni-Mo/Al_2O_3 only, AC guard bed on top of the Ni-Mo/Al_2O_3 catalyst; Temperature 425 °C, Reaction Media H_2 or N_2, Pressure 20 barg, Oil flow rate 1mL.min^{-1}, Gas flow rate 200 mL.mL^{-1}.

The combined effect of hydrogen atmosphere with AC on top of the Ni-Mo/Al_2O_3 catalyst can be observed in Figure 6.6 (a), from which it can be seen that the increment in API gravity was more stable than the other investigated conditions, with most data points at 4^o with an average 3.93 ± 0.82^o for 12 hours time-on-stream. This is approximately 1^o above that obtained when nitrogen was used as reaction media with AC plus Ni-Mo/Al_2O_3 catalyst.

From Figure 6.5 (b) the average DVR after 12 hours time-on-stream operation are 81.5 % (Ni-Mo/Al_2O_3 only under N_2 media), 88.5 % (AC guard bed with Ni-Mo/Al_2O_3 under N_2 media), and 91.3 % (AC guard bed with Ni-Mo/Al_2O_3 under H_2 media) less than 1.091 Pa.s (feed oil-B). Therefore, it could be concluded that hydrogen-addition further reduced the viscosity by 2.8 % compared with that obtained with AC on top of Ni-Mo/Al_2O_3 catalyst under N_2 media. This is in line with previous results on the effect of hydrogen on upgrading (Chapter 5 and Section 5.3) and also with the 1^o API gravity rise presented in Figure 6.5a.

In the reaction environment cracking occurs as the carbon-carbon bond generate radicals that take part in abstraction of hydrogen, radical intermediate rearrangement, radical termination, or another β-scission propagation step to form other active hydrocarbon chains with products covering a range of lower molecular weight than the starting molecule. However, if the radical reacts with another radical via an addition-reaction then an adduct radical of larger molecular size will be formed (Habib, et al., 2013). This adduct radical intermediate may undergo cracking, abstract-hydrogen, or radical termination to a bigger molecule. The ability of the generated radicals to undergo addition-reaction to form adducts with larger molecular weight than the starting hydrocarbon has been reported by Gray and McCaffrey (2002). Under an inert environment such as nitrogen these reactions are favoured (Savage, et al., 1988). This type of reaction however decreases the yield of low-boiling components with the produced oil characterised by low-API gravity and high viscosity. In the

light of this, the higher API gravity and lower viscosity under hydrogen atmosphere suggests the suppression of addition-reactions between free radicals and olefins formed from hydrogen-abstraction or β-carbon cleavage (Habib, et al., 2013). Hydrogenation of cracked olefins and radicals would have decreased their concentration, lower the extent of addition-reactions, as well as inhibit macromolecules formation (Hashemi, et al., 2013; Speight, 2011). Consequently, adduct formation leads eventually to coke formation. In addition, Viet et al. (2012) found that AC act as a hydrogen transfer mediator in the catalytic hydrocracking of heavy oil which leads to high conversion high-boiling components into low-boiling fractions. Convincingly, the synergistic effect of the AC guard-bed and hydrogen-addition to catalytic cracking improved the physical and flow properties of the produced oil relative to the feed oil.

6.3.2 Effect on TBP Distribution

Heavy crude oil yields little of fuel distillates in the range of 10-30% with BP below 343^{o}C. In this respect, upgrading converts most of the high-boiling fractions with BP greater than 343^{o}C into valuable fuel fractions. The SIMDIS was performed using the integrated PTV injector and Agilent 6850N gas chromatography according to the ASTM-2887-08. The TBP distribution curves showing the effect of hydrogen-addition with AC guard bed on top of Ni-Mo/Al_2O_3 catalyst are presented in Figure 6.6.

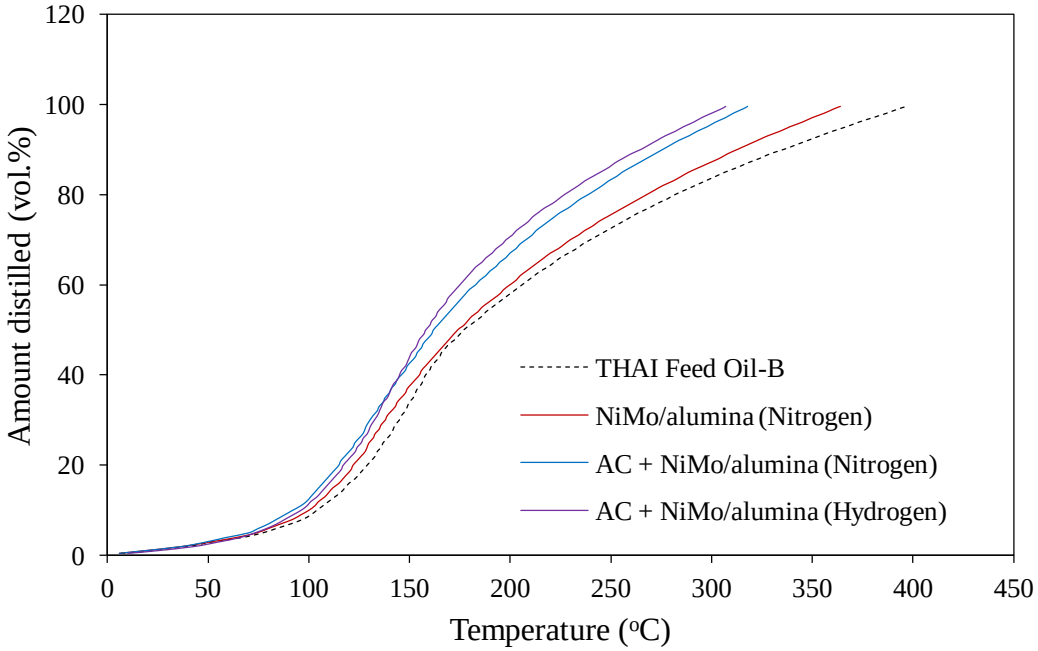

Figure 6.6 TBP distribution curves of feed and produced oil using Ni-Mo/Al_2O_3 only, AC used as guard bed placed on top of the Ni-Mo/Al_2O_3 catalyst; Temperature 425 °C, Reaction Media H_2 or N_2, Pressure 20 barg, Oil flow rate 1mL.min^{-1}, Gas flow rate 200 mL.mL^{-1}.

The accumulative amount distilled at the boiling temperature of 200^{o}C was 58% (feed oil-B). However, at the same boiling temperature the produced oil amount distilled is 60 % (Ni-Mo/Al_2O_3 only under N_2 media), 67 % (AC on top of Ni-Mo/Al_2O_3 under N_2 media) and 71.4 % (AC with Ni-Mo/Al_2O_3 catalyst under H_2 media). This represents 2, 9, and 13.4% upward shift of the cumulative amount distilled at the same boiling temperature of 200 ^{o}C, due to increased low-boiling fractions in the oil produced.

6.3.3 Effect on Produced Gas Composition

The off-gas composition during catalytic upgrading process can be classified into H_2, permanent gases (e.g., CO, CO_2, H_2S, etc), paraffins (C_1-C_5), isoparaffins (i-C_4), and olefins (C_1-C_4). In Table 6.2, the produced gas composition using AC with Ni-Mo/Al_2O_3 catalysts

under hydrogen and nitrogen reaction gas is presented. It is clear that the use of hydrogen increased the yield of light saturated hydrocarbon gases such as methane, ethane, propane, butane, and pentane while their corresponding olefins were decreased as a result of hydrogenation reaction in the presence of bi-functional Ni-Mo/Al_2O_3 catalyst. Consequently, the use of hydrogen increased the paraffinic gas content from 13.16% (use of nitrogen gas) to 25.85% and subsequently reduced the olefinic content from 0.25% (use of nitrogen gas) to 0.06%.

Table 6.2 Produced gas composition during catalytic upgrading process under nitrogen and hydrogen atmospheres using AC with Ni-Mo/Al_2O_3 catalyst at temperature 425 ^oC, pressure 20 barg, gas/oil ratio 200 $mL.mL^{-1}$.

Gas	**AC + Ni-Mo/Al_2O_3 (N_2) (vol.%)**	**AC + Ni-Mo/Al_2O_3 (H_2) (vol.%)**
Methane	12.1	24.6
Hydrogen	5.15	(61.23)
Ethane	0.54	0.63
Carbon dioxide	2.54	4.13
Ethene	0.04	0.00
Propane	0.12	0.13
Propene	0.14	0.05
i-Butane	0.16	0.21
n-Butane	0.05	0.06
1-Butene	0.05	0.01
Cis-2-butene	0.00	0.00
Trans-2-butene	0.02	0.00
n-Pentane	0.12	0.014
i-Pentane	0.08	0.11
Carbon monoxide	0.65	0.52
Hydrogen sulphide	0.00041	0.0006

It is known that the olefins are the most reactive class of hydrocarbons in the presence of catalyst and readily undergo polymerisation as well as condensation reactions to give aromatic species which are known coke precursors (Speight, 2011). Therefore, hydrogen-addition has helped to saturate some of the olefins and aromatics to produce more paraffins, thereby yielding more low-molecular weight components that improved API gravity, viscosity, and the yield of fuel distillates.

It is noteworthy that the amount of produced H_2S in the gas increased from 0.00041 % (N_2 reaction gas) to 0.0006 % (H_2 reaction gas), that is 31.7% increase under hydrogen atmosphere. This is indicative of increased HDS reaction as a result of excess hydrogen in the reaction environment. Subsequently, the gas generated via cracking reactions during the in-situ catalytic upgrading process can act as a solution gas drive to push the oil from the pore matrix into the producer well (Alpak, et al., 2013).

6.3.4 Effect on Asphaltenes content

The asphaltene component contributes greatly to high density/low-API-gravity and high viscosity of the heavy oil. The produced oil asphaltenes content was measured using n-C_7 solvent separation and presented in Table 6.3. After upgrading over Ni-Mo/Al_2O_3 catalyst only the produced oil asphaltenes content reduced from 10.3 wt% (feed oil) to 8.3 wt%, but the addition of AC on top of Ni-Mo/Al_2O_3 catalyst caused further reduction of 2 wt.% (nitrogen atmosphere) and subsequently 6.3 wt.% (hydrogen atmosphere).

Table 6.3 Asphaltene content of oil produced with cylindrical Ni-Mo/Al_2O_3 catalyst only and with AC guard bed under nitrogen or hydrogen addition at 425 ^oC, 20 barg, and gas-to-oil ratio 200 $mL.mL^{-1}$.

System	Reaction media	Aspaltene content (wt.%)	Conversion (343 ^oC+) (%)
Feed oil-B	NA	10.3 ± 0.6	NA
Ni-Mo/Al_2O_3	N_2	8.3 ± 0.4	12.3
AC + Ni-Mo/Al_2O_3	N_2	6.1 ± 0.4	43.8
AC + Ni-Mo/Al_2O_3	H_2	2.0 ± 0.8	77.7

This 4 wt.% further decrease in asphaltenes content under hydrogen can be attributed to the synergistic effect of AC guard-bed and hydrogen. While the AC guard-bed filters out the macromolecules before catalytic cracking, the hydrogen saturate the generated cracked fragments, thus suppressing their recombination to large molecular weight compounds.

6.4 Conclusions

It has been demonstrated that the use of a neutral material such as activated carbon as guard bed could selectively filters out some macromolecules such as asphaltenes and resins that are responsible for catalyst pores plugging and coke formation. Also, impurities such as asphaltenes and metals (e.g., Ni, V, etc.) in the feedstock were extensively decreased in the produced oil. Additionally, the produced oil API gravity and viscosity are further improved by ~1-3^o and 6.8 %, respectively above that obtained with a standalone refinery catalyst. However, the TBP distribution curves shows that the chemistry of the upgrading reactions was not altered by the AC guard-bed. Secondly, the synergistic effect of AC guard-bed and hydrogen however further reduced the produced oil asphaltenes content compared to that produced under nitrogen atmosphere.

Chapter 7

Coke and Metals Deposition Analysis

7.1 Introduction

Coke formation is a complicated process involving chemical reactions, changes in composition of the liquid medium, and thermodynamic behaviour (Speight, 1998). During the catalytic upgrading, the formation of light liquid hydrocarbons causes instability in the solubility parameter of the highly aromatic and polar species to separate from the oil phase as an insoluble phase and deposits on the catalyst (Zhang and Shaw, 2006; Speight, 1998; Gray et al., 2000). Once these highly aromatic compounds are deposited on the catalyst, reactions that promote coke can occur, such as (Speight, 1998 &2011):

- Cracking of side chains from aromatic hydrocarbons.
- Dehydrogenation (i.e., the removal of hydrogen from the parent molecule) of naphthenes to form aromatics.
- Condensation of aliphatic structures to form aromatics.
- Polymerisation and condensation of olefins.
- Condensation of aromatics to form higher fused-ring aromatics.
- Dimerisation or oligomerisation reactions.

The results in previous Chapters show that the API gravity of the produced oil decreases, viscosity increases and yield of low-boiling distillates lowers with time-on-stream during the heavy oil upgrading, which is thought to be mainly due to the deposition of carbon and metals. In this Chapter, the effect of operating conditions, feedstock, hydrogen, and activated

carbon guard-bed on the catalyst coke content is explored. Also, the catalyst deactivation rate and coke content with time-on-stream were modelled using semi-empirical models and the impurities deposited on the catalyst after upgrading reaction identified using SEM-EDX.

7.2 Effect of Reaction Temperature on Spent Catalyst Coke Content

Coke is one of the by-products of the upgrading reactions, which becomes adsorbed on the acid sites of the catalysts. It consists of high-molecular weight poly-aromatic species, hydrogen-deficient, non-volatile components and usually the main cause of catalyst deactivation by fouling and poisoning active sites and or plugging catalyst pores (Wang and Manos, 2007; Chen and Manos, 2004). In order to determine the start of coke burn-off, the asphaltenes content of heavy oil was precipitated with n-heptane and thermogravimetric analysis (TGA) performed. The TGA and DTG (differential thermogravimetric) of the asphaltenes are presented in Figure 7.1. It is clear that the asphaltenes are completely burned-off at a temperature of about 610 ^{o}C. This observation is in line with the findings of Douda et al. (2004), Trejo et al. (2010) and Barman et al. (1997). They found that asphaltenes from Maya heavy crude oil begin to volatilise and decompose at 410 ^{o}C and these processes end at 620 ^{o}C, which is consistent with the signal range observed in the DTG curve shown in Figure 7.1.

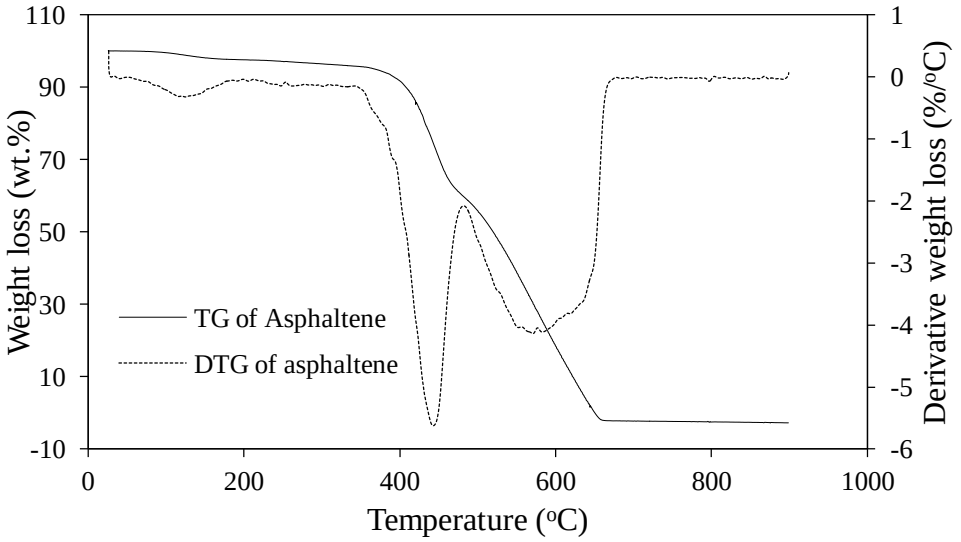

Figure 7.1 TGA thermogram and DTG of asphaltenes precipitated with n-heptane.

Figure 7.2 (a) and (b) provides the TGA thermograms or weight loss curves as a function of ramp temperature for the spent Co-Mo/Al_2O_3 and Ni-Mo/Al_2O_3 recovered catalysts after the upgrading experiments. The ramp temperature increase enables the interpretation of the different chemical changes occurring during the burn-off when compared to the asphaltenes TGA and DTG curves. The isothermal temperature of 1000 ^oC towards the end ensures that all carbon species are completely burnt off during the heating period. However, above 620 ^oC (see Figure 7.1), the deposits on the spent catalysts are defined as coke, because of the higher energy requirement to burn-off coke than asphaltenes. Nonetheless, Murugan et al. (2009 and 2011) observed that the non-isothermal weight loss during the combustion of the deposits on the spent catalyst especially coke in air atmosphere is a complex phenomenon, with numerous reactions proceeding at the same time, from which products include carbon oxide (CO_x), carbon monoxide and water, as expressed in the following equation 7.1:

$$\text{Coke} + O_2 \xrightarrow{\text{Heating rate } (20^oC/\text{min})} CO_x + CO + H_2O. \qquad (7.1)$$

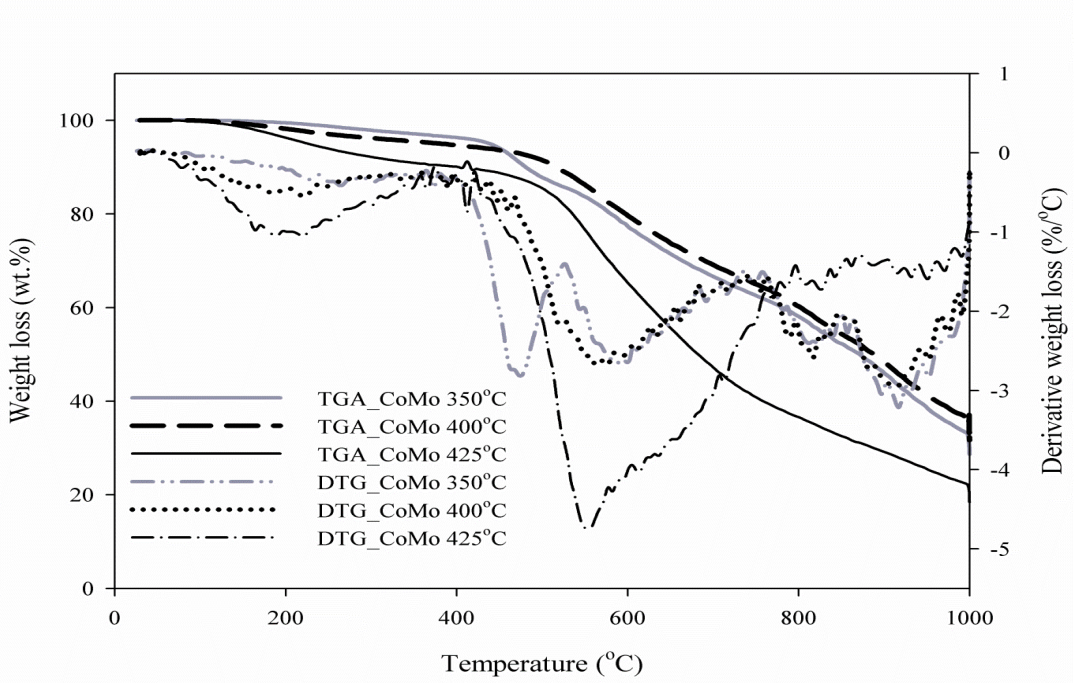

(a)

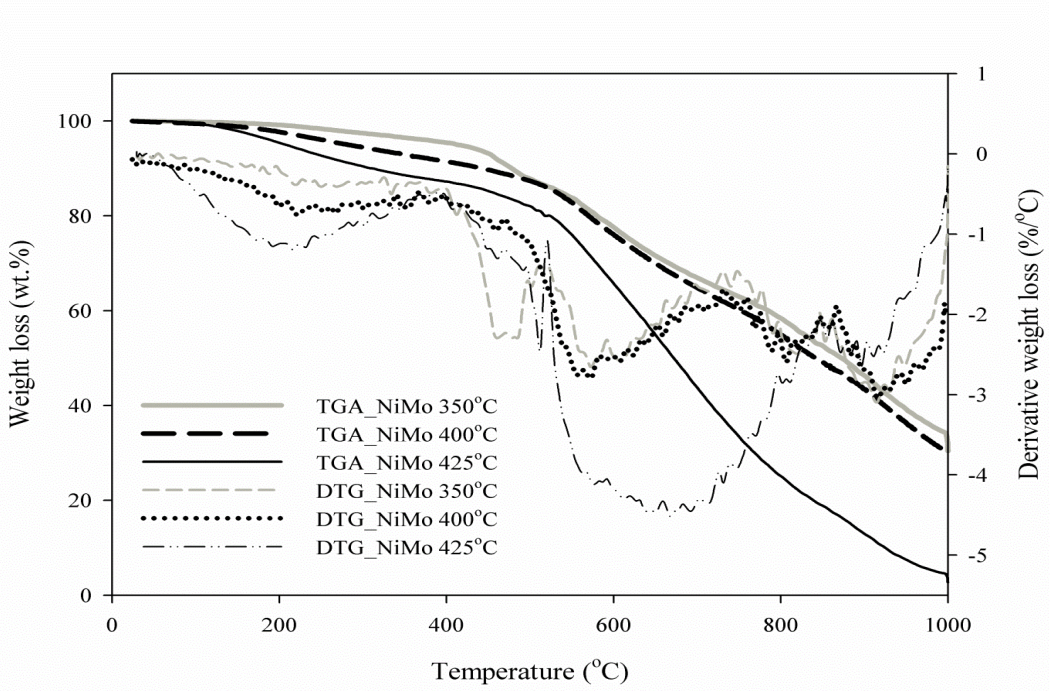

(b)

Figure 7.2 TGA and DTG of spent Co-Mo/Al_2O_3 (a) and Ni-Mo/Al_2O_3 (b) catalysts under reaction temperatures of 350, 400, and 425 °C; Catalyst Co-Mo/Al_2O_3, Reaction Media N_2, Pressure 20 barg, Oil flow rate 1mL.min-1, Gas flow rate 500mL.mL^{-1}.

Subsequently, to interpret the different stages during the heating period, the derivative of the weight loss curve (DTG) was obtained as presented in Figure 7.2. Figure 7.2 shows that the weight loss process of the spent catalyst can be divided into several steps; the region from 25 to 210 ^{o}C represents loss due to de-volatilisation of light oil, 210-620 ^{o}C represents burn-off of macromolecules such as asphaltenes, resins, and sediments, and beyond 620 ^{o}C is coke. Beside catalyst fouling and clogging, coke build up on the catalyst bed is one of the main routes for deactivation and shortening of lifespan (Ali, et al., 2006). However, coke on the catalysts has been described as evidence of catalytic cracking (Krumm, et al., 2011). The coke content of the spent Co-Mo/alumina catalyst increased in the order 48.4, 53.5 and 57.3 wt.% at 350, 400 and 425 ^{o}C. Whilst the coke content of spent Ni-Mo/alumina catalyst increased in the order 37.2, 46.5, and 48.9 wt.%, respectively for 25 hours time-on-stream operation. Notably the coke content of spent Co-Mo was higher than that of Ni-Mo catalyst due to its stronger acid sites. A stronger acid site improves catalyst activity, but promotes high coke formation and deactivation (Leyva, et al., 2007; Marafi and Stanilaus, 2001). Also, it can be seen in Figure 7.2 that the coke formed at 350 ^{o}C started to burn-off at a lower temperature compared to coke deposited on the spent catalysts at 400 ^{o}C and 425 ^{o}C. This observation is in line with the report of Murugan et al. (2009) that coke formed at higher temperature has higher molecular weight species with condensed structures of poly-aromatics, whereas those formed at lower reaction temperature have less condensed structure (Ren, et al., 2007).

Consequently, Sanford (1994) has pointed out that during the earlier stages of coking and hydrocracking reactions in residue conversion, C-C bonds are broken. At higher temperatures of 425 °C and above the coking reactions become more predominant, which accelerate catalyst deactivation and change in selectivity toward undesirable products i.e. coke and gaseous species occurs (Yan, 1980; Furimsky and Massoth, 1999; Zhao, et al., 2001;

Meng, et al., 2007). This is evident from the effect of reaction temperature on mass balance where 4.34 % of products formed were gases at 425 °C compared to 1.96 % at 350 °C and coke was 1.86 at 425 °C compared to only 0.64 % at 350 °C. This can be explained by the fact that at higher temperatures bond scission of the side chains of compounds present in crudes such as alkylaromatics increases and results in the formation of more coke, gases and lower liquid products (Marafi, et al., 2008). This resulted in higher upgraded oil in terms of increased API gravity and lowered viscosity as evident and also the TBP curve shift towards low-boiling fractions as reaction temperature increased. However, deactivation caused by coke is reversible and generally removed via oxidative regeneration.

7.3 Effect of WHSV on Spent Catalyst Coke content

The coke content of the spent Co-Mo/Al_2O_3 catalyst as a function of WHSV at 425 ^oC, pressure 20 barg, nitrogen-to-oil flow ratio 500 $mL.mL^{-1}$, and 6 hours time-on-stream is presented in Figure 7.3. It can be seen that coke deposition on the catalyst decreased as the WHSV increases. A similar trend of the effect of WHSV on coke yield was reported by Li et al. (2012 & 2013) for fluid catalytic cracking of heavy gas oil. This is because the conversion of heavy hydrocarbon increases as the contact time between the oil and catalyst increase. Notwithstanding, catalytic upgrading reactions are endothermic cracking reactions favoured by high temperature and long contact time.

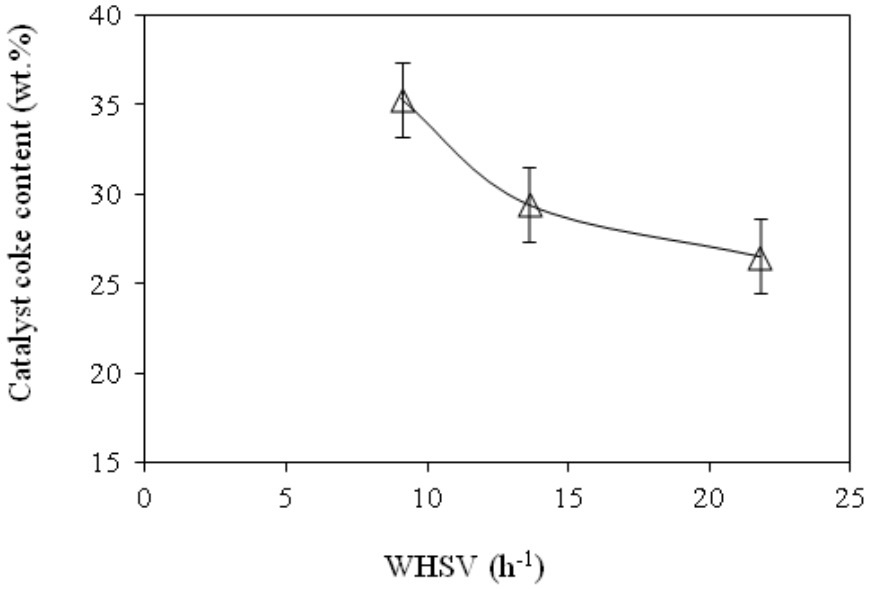

Figure 7.3 Spent Co-Mo/Al_2O_3 catalyst coke content as a function WHSV at temperature 425^oC, Reaction Media (N_2), Pressure 20 barg, Oil flow rate 1 mL.min^{-1}, Gas flow rate 500mL.mL^{-1}.

In the light of this, improved upgraded oil obtained at high reaction temperature of 425 ^oC and lower WHSV will result in more undesired side reactions leading to high coke and gas yields. The result of higher API gravity and lower viscosity in produced oil is therefore accompanied by high coke deposition on the catalyst and gas production, in order to elementally balance the carbon and hydrogen distribution in the upgraded oil, coke, and gas (Gao, et al., 2012).

7.4 Effect of Hydrogen-addition on Spent Catalyst Coke content

It is well known that coke deposition on the catalyst decreases its activity and lifespan due to active sites coverage. Figure 7.4 presents the amount of coke deposited on the Co-Mo/Al_2O_3 catalyst after 25 hours time-on-stream operation under hydrogen or nitrogen atmosphere. From the TGA curves the coke content was 52.4 wt.% (nitrogen atmosphere) and

35 wt.% (hydrogen atmosphere). This represents 17 wt.% spent coke content reduction under a hydrogen environment.

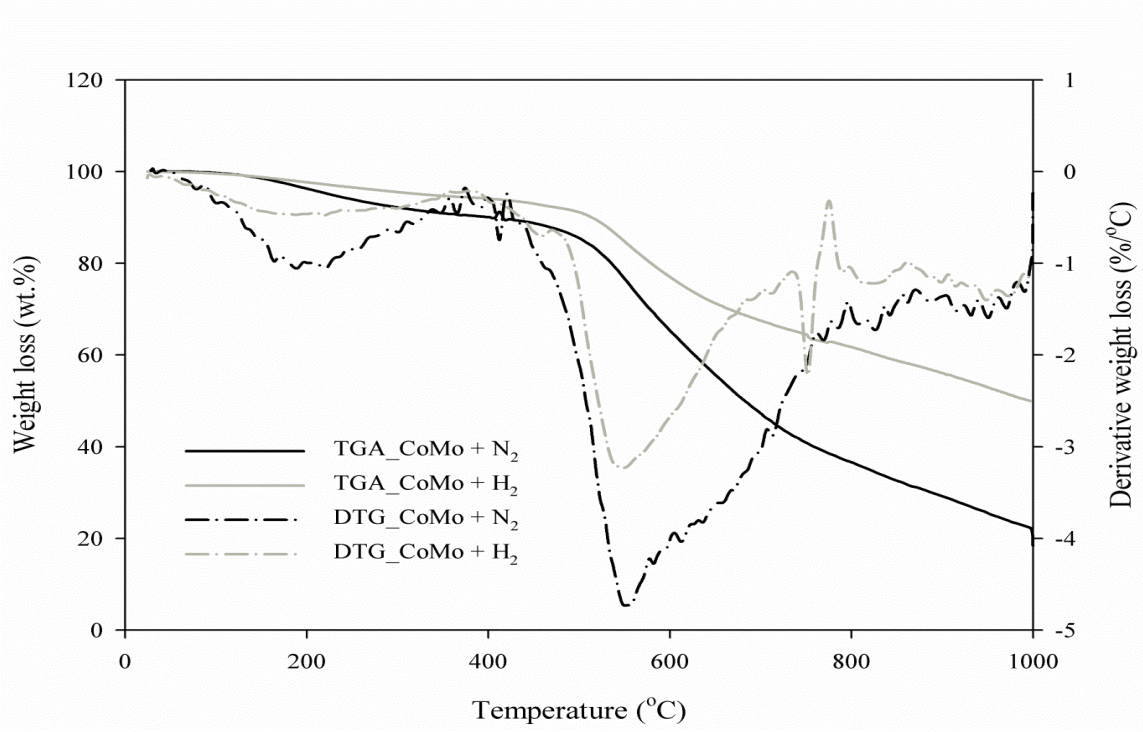

Figure 7.4 TGA and DTG of spent catalyst Co-Mo/Al_2O_3 obtained after reaction from CAPRI reactor with and without hydrogen-addition; Temperature 425 °C, Reaction Media H_2 and N_2, Pressure 20 barg, Oil flow rate 1mL.min^{-1}, Gas flow rate 200mL.mL^{-1}.

Coke precursors such as poly-aromatics, olefins, radicals of resins and asphaltenes macromolecules become adsorbed on the catalyst active sites and slowly form protocoke (i.e., large sediments commonly called soft coke) via polymerisation and condensation reactions and subsequently through dehydrogenation reactions to coke, as illustrated in equation 7.2 (Liu, et al., 2003):

$$\text{Coke precursors} \xrightarrow{\substack{\text{polymerisation} \\ \text{and condensation} \\ \text{reactions}}} \left[\begin{array}{c}\text{protocoke} \\ (\text{i.e., large polyaromatic} \\ \text{species})\end{array}\right] \xrightarrow{\substack{\text{dehydrogenation} \\ \text{reactions}}} \text{coke} \qquad (7.2)$$

A significant effect of hydrogen in this study was its ability to suppress the formation of coke compared to nitrogen as the reaction gas environment, and as is commonly practised in the refining industry, where the phenomenon is known to increase the yield of distillates and its quality (Aysar, et al., 2011; Meyer and Attanasi, 2004; Mapiour, et al., 2009). It is noteworthy that with nitrogen atmosphere the produced oil API gravity is 18^{o} and viscosity reduction 80.9 %. Hydrogen-addition further increased the API gravity and decreased viscosity up by 3^{o} and 6.3 %, respectively. The presence of hydrogen therefore promote hydrogenation reactions and decreased coke formation, as previously reported by (Galarraga and Pereira-Almao, 2010; Al-Saleh, et al., 2003).

7.4.1 Effect of Hydrogen Pressure on Spent Catalyst Coke Content

In this section, the effect of hydrogen pressure on coke content of the spent Co-Mo/Al_2O_3 catalyst is presented for reactions carried out under hydrogen pressure ranging from 20 to 40 barg at constant reaction temperature of 425 ^{o}C, hydrogen flow rate of 200mL.min^{-1}, and WHSV of 9.1 h^{-1}. The coke content of the recovered spent catalyst from the CAPRI reactor for hydrogen pressures 20 to 40 barg is presented in Table 7.1.

Table 7.1 Spent Co-Mo/Al_2O_3 catalyst coke content at temperature 425 ^{o}C, hydrogen-to-oil flow ratio 200 mL.mL^{-1}, and hydrogen pressure from 20-40 barg.

Hydrogen pressure (barg)	**Coke content (wt. %)**
20	27.2
30	24.8
40	21.6
Standard deviation	± 1.02

It can be seen that the coke content of the spent catalyst decreased as the hydrogen pressure increased from 20 to 40 bar, indicating that higher hydrogen pressure can effectively suppress coke formation. From Table 7.1 every 10 bar rise in hydrogen pressure produced approximately 2 wt.% decrease in coke. Zhang and Shaw (2006) and Matsumura et al. (2005) observed a similar trend in coke content of the catalyst as hydrogen pressure increased. This can be attributed to the increase hydrogen solubility with pressure rise. At a higher hydrogen pressure more hydrogen is soluble in the reaction medium, therefore increasing its availability on the catalyst surface for hydrogenation and hydrocracking reactions (Al-Mutairi and Marafi, 2012; Cai, et al., 2001; Mapiour et al., 2010). Consequently, it has been reported that high hydrogen pressure thermodynamically favours hydrogenation reactions (Al-Mutairi and Marafi, 2012). Since less coke is formed in hydrogen-addition, loss of the catalyst surface area, pore volume and active sites comparatively lower compared to the use of nitrogen.

7.4.2 Empirical Model of Catalyst Coke Content

The catalytic coke is the by-product of cracked hydrocarbons on the acid sites of the catalyst. Therefore, it is necessary to understand coke deposition and its deactivation effect. Voorhies (1945) reported that catalyst coke content is a function of time-on-stream in a fixed-bed reactor at given condition, as defined by equation (7.3):

$$C_c = A.t^n \qquad (7.3)$$

where; A and n are constant depending on catalyst, feedstock, and reaction temperature, C_c is coke on catalyst and t is time-on-stream.

Figure 7.5 depicts the correlation between experimental data and the Voorhies model for catalyst coke content as a function of time-on-stream during upgrading reaction using Co-Mo/Al_2O_3 at 425 ^oC reaction temperature, under nitrogen and hydrogen reaction media. Each data point on the chart represents an experimental run in duplicate on a fresh batch of catalyst for both nitrogen and hydrogen reaction media.

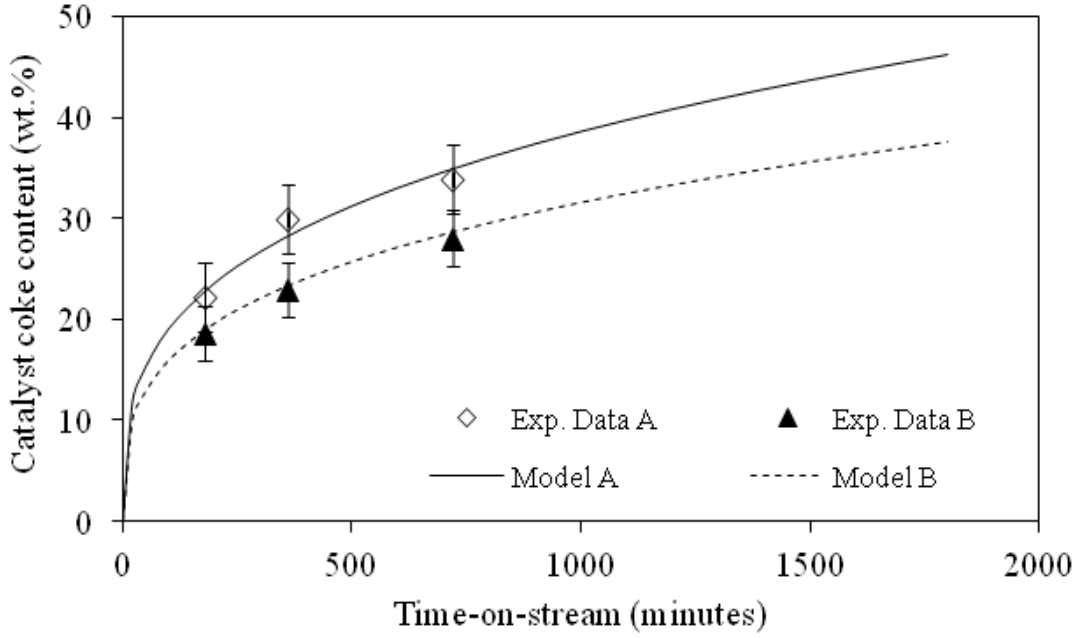

Figure 7.5 Co-Mo/Al_2O_3 catalyst coke content as a function of time-on-stream during upgrading reaction in N_2 or H_2 reaction media at temperature 425 ^oC, pressure 20 barg, oil flow rate 1 mL.min^{-1}, gas flow rate 200 mL.mL^{-1} and feed oil-B; (A) in N_2 model (i.e., $C_c = 4.661t^{0.306}$) and (B) in H_2 Model ($C_c = 4.097t^{0.296}$).

It is clear that the initial coke formation is rapid followed by progressive build-up with time-on-stream. A similar trend in coke formation with time was reported by Maity et al. (2012). The high coke formation observed at the early hours of the upgrading reactions can be explained by high catalytic activity and acidity which result in high cracking rate, as reflected in the early upgraded oil samples which showed high API gravity and low viscosity. However, this rapid coke formation caused deactivation which lowers the cracking activity, as

well as decreases the rate of coke formation with time (Garcia-Dopico, et al., 2006; Sun, et al., 2010). Unlike nitrogen atmosphere, the generated active hydrogen under hydrogen atmosphere hampers the progressive addition-reaction that leads to coke (Bagheri, et al., 2012). It can be clearly seen in Figure 7.5 that the key to reducing the impact of coke formation on catalytic activity depends on the reduction in amount of initial coke formed.

7.4.3 Catalyst Deactivation Rate

Catalyst deactivation is a combined effect of coke, metal and hetero-atoms (e.g., S, N, etc.) deposits during upgrading reactions. The rate of catalyst deactivation has been defined by Chen and Hsu (1997), Hollander, et al. (1998) and Maity et al. (2012) using equation (7.4):

$$X_t = X_o \exp(-b.t^n) \qquad (7.4)$$

where; X_t is the conversion of heavy fraction (> 343 ^oC) at time t, X_o is the initial conversion, and b is the deactivation rate constant (s^{-1}), n = 1 (Chen and Hsu, 1997).

In Figure 7.6, the plot of $-\ln(X_t/X_o)$ against time-on-stream for Co-Mo/alumina catalyst at 350, 400, and 425 ^oC under nitrogen media is presented. The correlation coefficient between the data and equation (7.4) is 0.98.

A higher value of b (i.e., deactivation rate constant) implies faster deactivation of the catalyst. As the reaction temperature increased from 350 to 425 ^oC, the value of b increases as thus 0.077, 0.082 and 0.085 s^{-1}. It can be seen from the above values that the deactivation rate at 425 ^oC reaction temperatures is slightly faster than that of 350 and 400 ^oC. Conspicuously, in a fixed-bed system, the instantaneous conversion decreases with time-on-stream as the catalyst becomes fouled and poisoned with coke and metal deposits (Voorhies, 1945; Chen

and Hsu, 1997; Maity, et al., 2012). This progressive decrease of the catalysts activity is called deactivation rate, which resulted in decreased API gravity and increased viscosity of upgraded oils samples with time-on-stream.

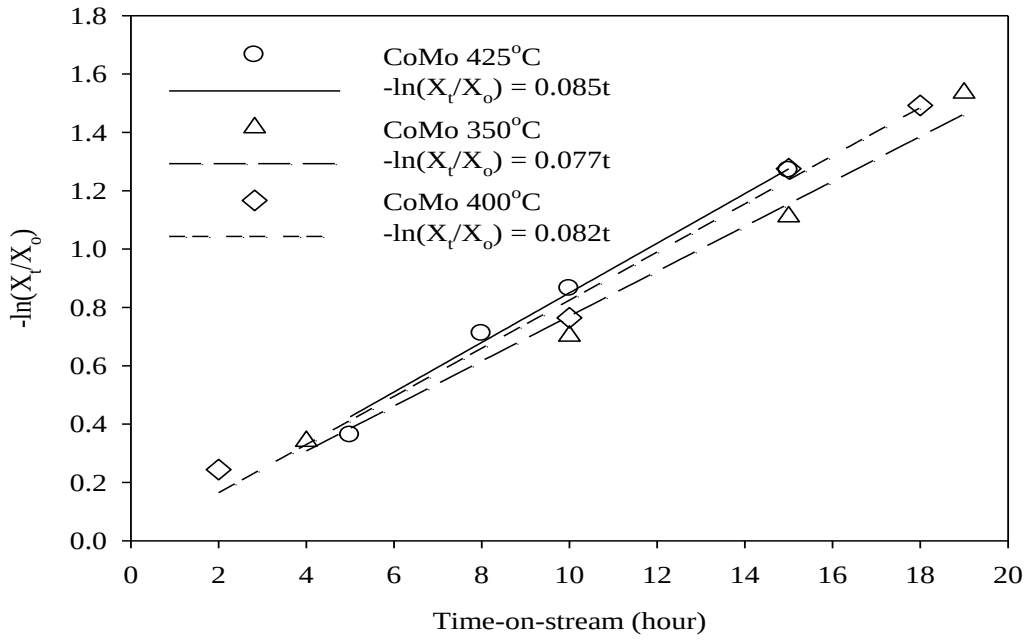

Figure 7.6 Conversion vs. time-on-stream as a function of activity Co-Mo/Al_2O_3 catalyst at temperatures 350, 400, and 425 ^oC, constant pressure 20 barg and N_2/oil ratio 500 $mL.mL^{-1}$.

7.4.4 Nitrogen Adsorption-Desorption of Fresh and Spent Catalyst

The nitrogen sorption isotherms of the fresh and spent catalysts were analysed using BET theory. The analysed spent catalysts were collected from the centre of the fixed-bed reactor. The adsorption-desorption isotherm of the fresh and spent Co-Mo/Al_2O_3 and Ni-Mo/Al_2O_3 catalysts are compared for the nitrogen and hydrogen atmospheres after the upgrading experiment, as shown in Figures 7.7a, b and c.

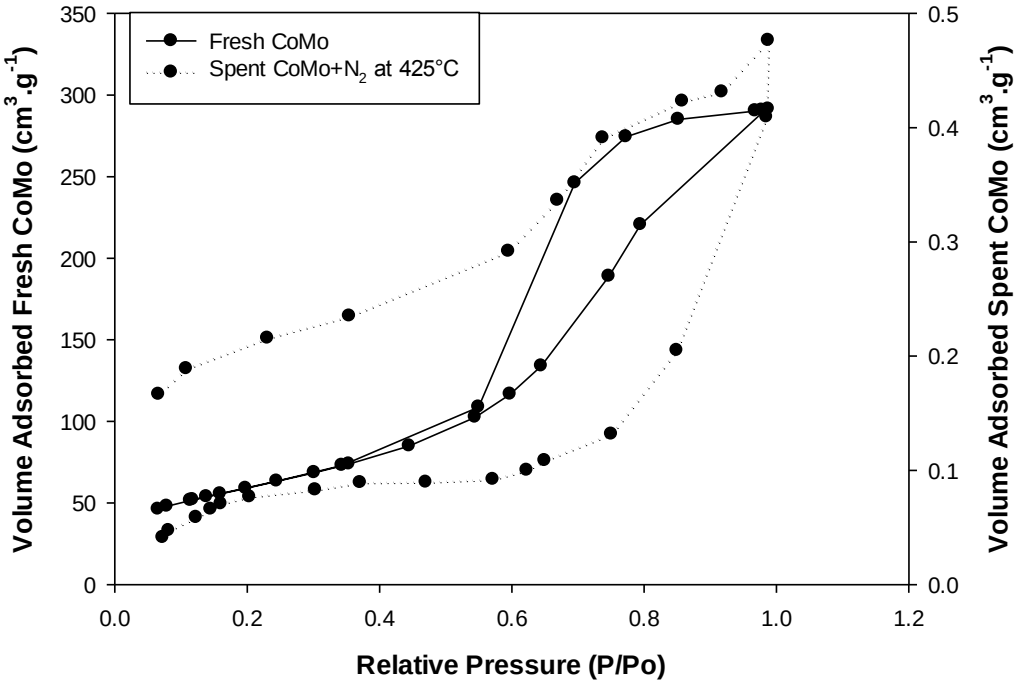
Fresh CoMo
Spent CoMo+N2 at 425°C
Volume Adsorbed Fresh CoMo (cm3.g-1)
Volume Adsorbed Spent CoMo (cm3.g-1)
Relative Pressure (P/Po)
0
50
100
150
200
250
300
350
0.0
0.1
0.2
0.3
0.4
0.5
0.0
0.2
0.4
0.6
0.8
1.0
1.2

(a)

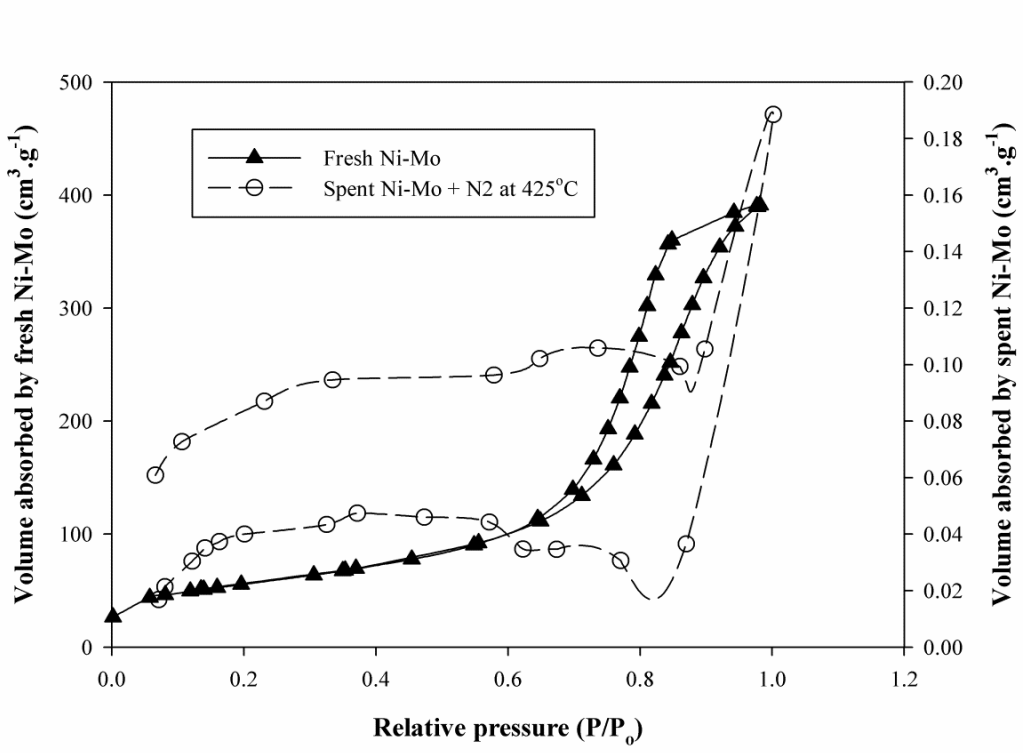
Fresh Ni-Mo
Spent Ni-Mo + N2 at 425°C
Volume absorbed by fresh Ni-Mo (cm3.g-1)
Volume absorbed by spent Ni-Mo (cm3.g-1)
Relative pressure (P/Po)
0
100
200
300
400
500
0.00
0.02
0.04
0.06
0.08
0.10
0.12
0.14
0.16
0.18
0.20
0.0
0.2
0.4
0.6
0.8
1.0
1.2

(b)

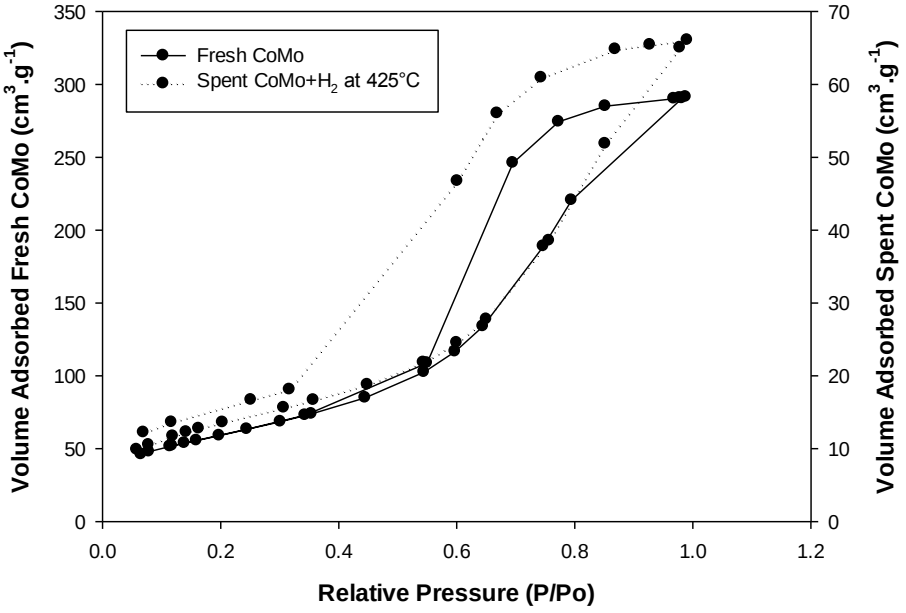

(c)

Figure 7.7 Fresh and spent (at 425 °C reaction temperature) Co-Mo and Ni-Mo catalysts adsorption-desorption isotherm (a) fresh and spent Co-Mo under nitrogen atmosphere, (b) fresh and spent Ni-Mo under nitrogen atmosphere, and (c) fresh and spent Co-Mo under hydrogen environment; Temperature 425 ^{o}C, Reaction Media H_2 or N_2, Pressure 20 barg, Oil flow rate 1mL.min^{-1}, Gas flow rate 200mL.mL^{-1}.

The adsorption-desorption curve reveals a large hysteresis loop in the isotherm indicative of the type IV which is associated with meso-pores for the fresh Co-Mo and Ni-Mo catalysts. The adsorption-desorption curve reveals a large hysteresis loop in the isotherm of the spent catalyst, which confirms deposits in the pores and blockage of active sites (Rana, et al., 2008). The loss of surface area due to coke and metal deposits is approximately 99.9% under nitrogen environment. Similar loss in surface area was reported in the literature by Ancheyta et al. (2002). It is known that during the upgrading reaction hydrocarbon molecules diffuse into the catalyst first before they are cracked into smaller molecules. While small hydrocarbon components diffuses faster, the diffusion of macromolecules such as resins and

asphaltenes was slow inside the catalyst pore channels which contributed to early coking and pore blockage.

As can be seen from Figure 7.7a-b, the spent Co-Mo/Al_2O_3 and Ni-Mo/Al_2O_3 catalysts have a significantly lower volume of adsorbed-desorbed nitrogen at the same relative pressure compared to their fresh counterparts. This loss in porosity and pore volume may have resulted from the highly aromatic and coke-forming molecules such as resins and asphaltenes residing within the small pores of the catalysts, due to limited diffusion of reactants and products (Dupain, et al., 2006; Absi-Halabi, et al., 1995). The significant decrease in specific surface area and pore volume of the spent catalyst also indicates that deposits (e.g., coke, metals, etc.) may have altered the pore structure, textural properties, and subsequent catalytic activity. Absi-Halabi et al. (1991) found that the initial coke deposition was most significant in the smaller pores of the catalyst pellet while asphaltenes and coke deposition block catalyst pore throat, thereby reducing the bed porosity and increasing pressure drop. Also, Dupain et al. (2006) identified external coke deposits on the outer surface of the catalyst as a major contributor to inaccessibility of pores.

On the other hand, when the upgrading reaction was performed under hydrogen gas media the loss of surface area by the spent Co-Mo/Al_2O_3 catalyst was 78.6% compared to 99.8% under nitrogen atmosphere at the same operating conditions. Also, the pore volume was higher compared to spent catalyst after upgrading in nitrogen. This indicates lesser deactivation due to the blockage of catalytic site by coke deposition in the presence of hydrogen (see Figure 7.7c). This is because hydrogen helps to suppress the polymerisation reaction of the coke precursors formed large molecules and coke during the CAPRI process.

To confirm the pore blockage due to coke and metal deposits, mercury porosimetry of the fresh and spent Co-Mo after upgrading at 425 ^{o}C, 20 barg, and 200 mL.mL^{-1}under

nitrogen and hydrogen reaction media was performed and the results presented in Figure 7.8. It is clear that the pore size distribution of the fresh Co-Mo/Al_2O_3 was much broader while the entire pores of the spent Co-Mo/Al_2O_3 catalyst were completely blocked by coke and metals deposits after upgrading under nitrogen atmosphere. Additionally, anarrow pore size distribution was observed in spent Co-Mo catalyst recovered from the reactor after upgrading under hydrogen environment. This result is consistent with that of the adsorption-desorption isotherm using nitrogen adsorption presented in Figure 7.7c. This can be attributed to hydrogenation reactions occurring under hydrogen leading to lower coke deposit (Millan, et al., 2008).

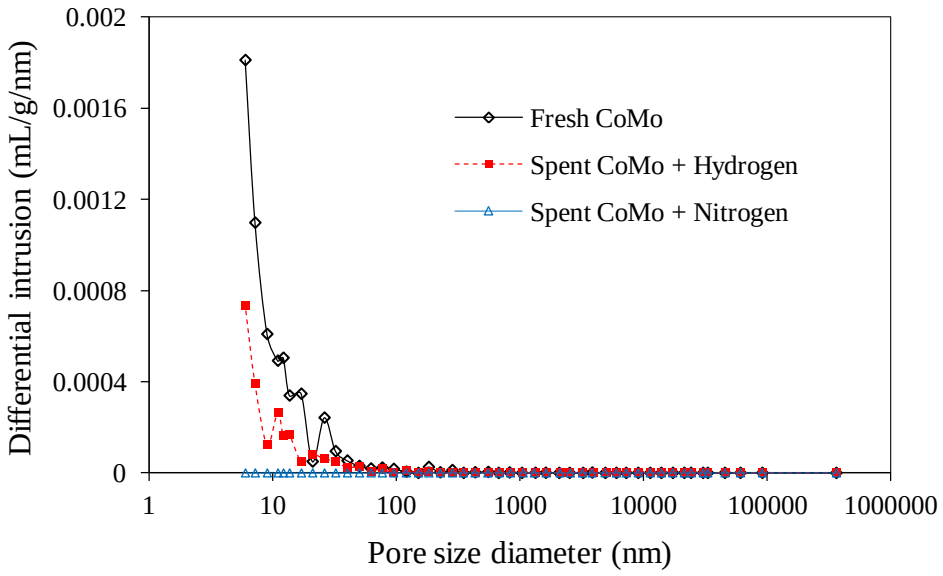

Figure 7.8 Co-Mo/Al_2O_3 catalyst pore size distribution before and after upgrading reaction at 425 ^oC, 20 barg, and 200 $mL.mL^{-1}$ in the presence of nitrogen or hydrogen atmosphere.

The above results show that most of the upgrading occurs at the early hours of the CAPRI process; thereafter the pore channels of catalyst are plugged and only the low molecular weight fractions could enter the pore and then be cracked, while the poly-aromatics are adsorbed on the external surface of catalyst and through dehydrogenation reactions formed coke (Zhang, et al., 2013). This eventually prevents the optimum utilisation of the

internal surface of the catalyst. The consequences of this on the catalyst performance are reduced accessibility, activity, and lifetime.

7.4.5 Carbonaceous Deposits on Catalyst

The coke and metals deposited during the CAPRI process block the pore space, reduce oil flow rate and increase pressure drop across the bed. Additionally, it lowers the efficiency and performance of the catalyst. The cross section of coked Ni-Mo/Al_2O_3 catalyst bed in the reactor after upgrading reactions is presented in Figure 7.9. As can be seen the catalyst particles with the deposited asphaltenes, coke and contaminants tend to form agglomerates within the bed leading to bed clogging. The extent of clogging of the inter-particle voids and subsequent rise in pressure drop in reactor greatly impacts on the process economy.

Figure 7.9 Photograph of coked Ni-Mo/Al_2O_3 catalyst of the CAPRI reactor cross-section after upgrading at temperature 425 ^{o}C, nitrogen-to-oil ratio 500 mL.mL^{-1}, and pressure 20 barg (Reactor tube internal diameter 10 mm).

It is clear that the inter-particle void of the bed is almost completely filled with macromolecules of asphaltenes, sediments, and coke. These are rejected by-products of the

catalytic upgrading reactions. This photograph correlates with the nitrogen-sorption isotherm and mercury porosimetry results of the spent Ni-Mo/Al_2O_3 catalyst which showed the catalyst pore blockage which occurred after the upgrading reaction. Millan et al. (2008) studied catalytic activity of pre-coated Ni-Mo/Al_2O_3 catalyst with carbonaceous material and found that despite large coke deposition and a significant drop in surface area and pore volume, the catalyst continued to display some activity. This could be because of thermal cracking reactions occurring, which are not catalyst activity dependent (Shah, et al., 2011). Secondly, the deposited metals, coke, and sediments themselves can act as catalyst through exchange of hydrogen, methyl, ethyl, radicals or groups with the molecules in the oil phase. This explains the reason for the sustained catalytic activity despite coke and metal deposition.

7.4.6 Surface Morphology and Composition

SEM-EDX was used to study the fresh and spent catalyst surface morphology as well as to determine their elemental composition. The SEM photomicrographs of the fresh and the spent catalyst after upgrading reactions in different environments are shown in Figure 7.10.
SEM provides detailed surface morphology with magnification up to x10000, allowing submicron-scale features such as metal and coke deposits, characterisation of defects and particulates to be seen when compared with the fresh catalyst. It is clear that the deposition of carbonaceous materials and metals occurs in the pores and on the surface of the catalysts, which have contributed to loss of activity and reduced product quality with time-on-stream. Under nitrogen and hydrogen atmosphere the coke form was amorphous while the metal clusters are distributed around the catalyst surface and pores. However, under a steam environment it was observed that the coke forms relatively small graphite-like planes and agglomerates with some smaller globular coke growth.

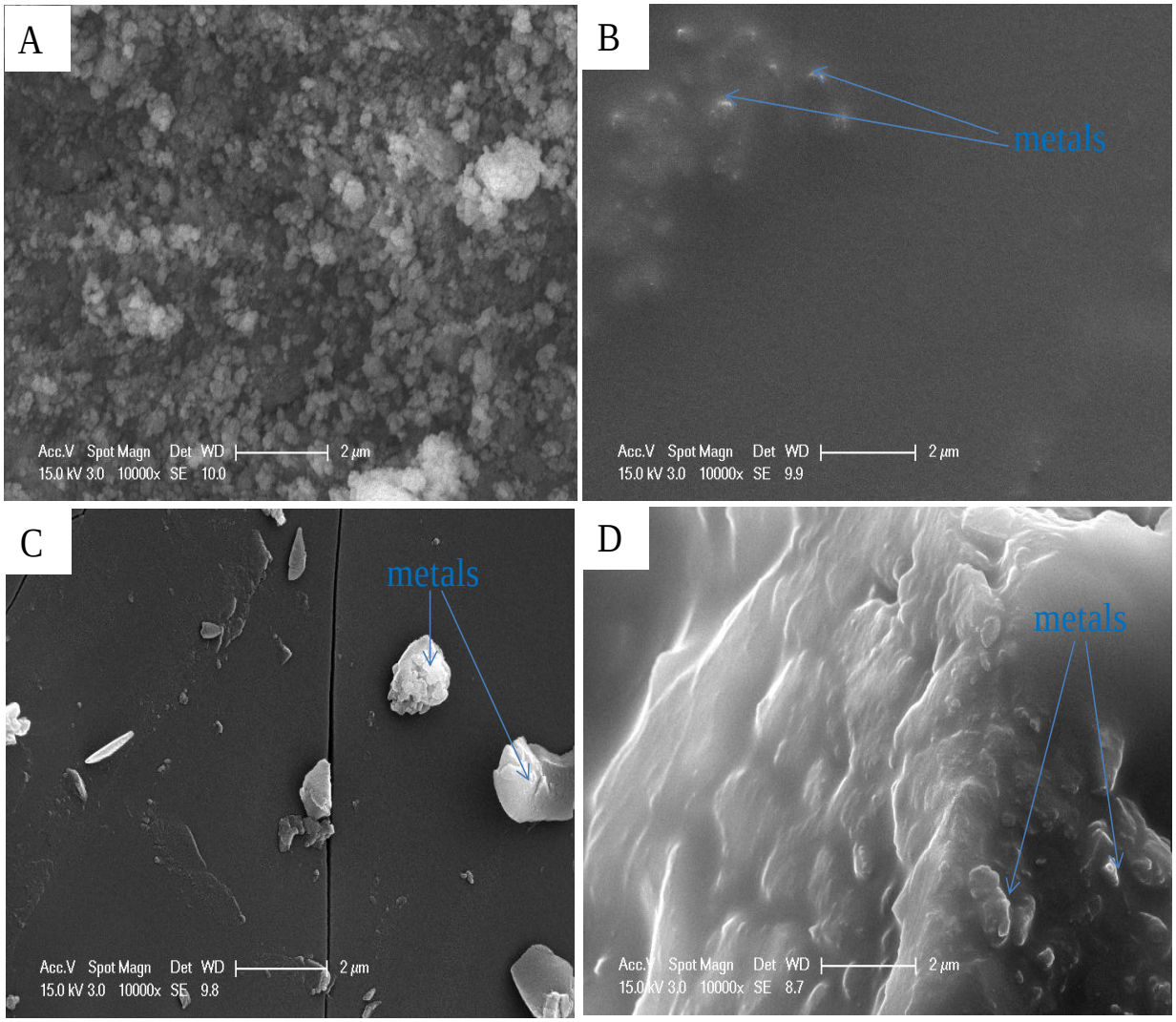

Figure 7.10 SEM photomicrographs of fresh Co-Mo/Al_2O_3 (A) and spent catalysts after upgrading under different reaction media (B) Spent Co-Mo in N_2 425 ^oC, (C) Spent Co-Mo in H_2 425 ^oC, and (D) Spent Co-Mo in steam 425 ^oC.

The elemental composition of the fresh and spent catalysts was determined using Energy Dispersive X-ray analyser (EDX). The EDX mapped a small micro-area of the fresh Co-Mo/alumina and Ni-Mo/alumina catalysts and their spent counterpart surface are presented in Figure 7.11 (a) and (b). The analysis results revealed the deposition of carbon (i.e., coke), sulphur, as well as metals onto the surface of the catalyst. The deposited

impurities also contributed towards the loss of catalytic activity revealed in the decreased API gravity and conversion of 343^{o}C+ HCs with time-on-stream.

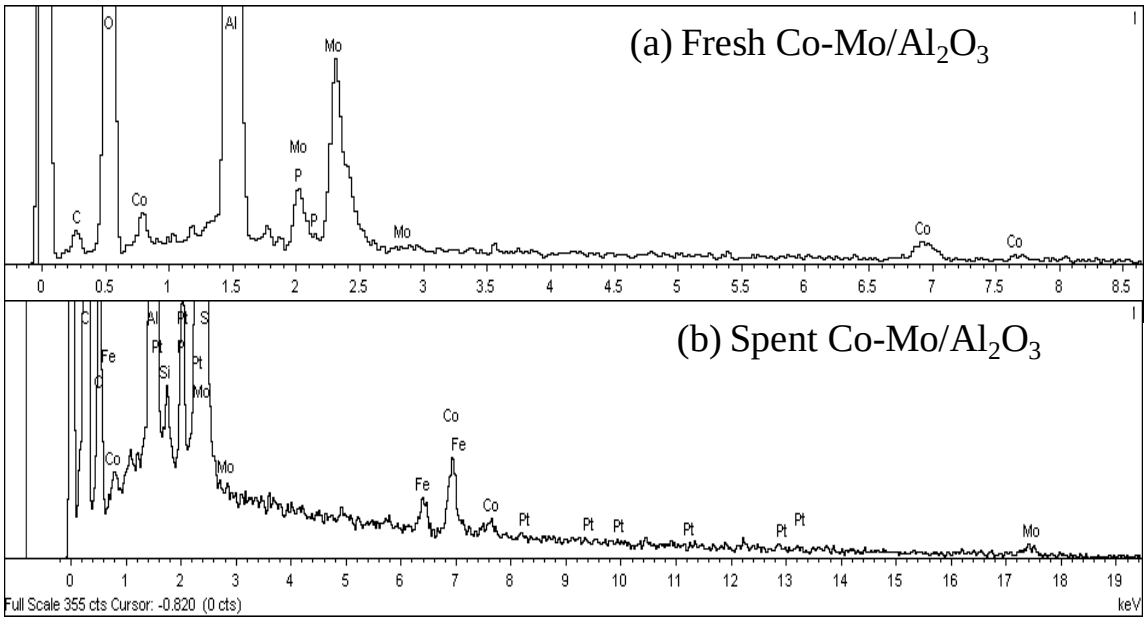

(a)

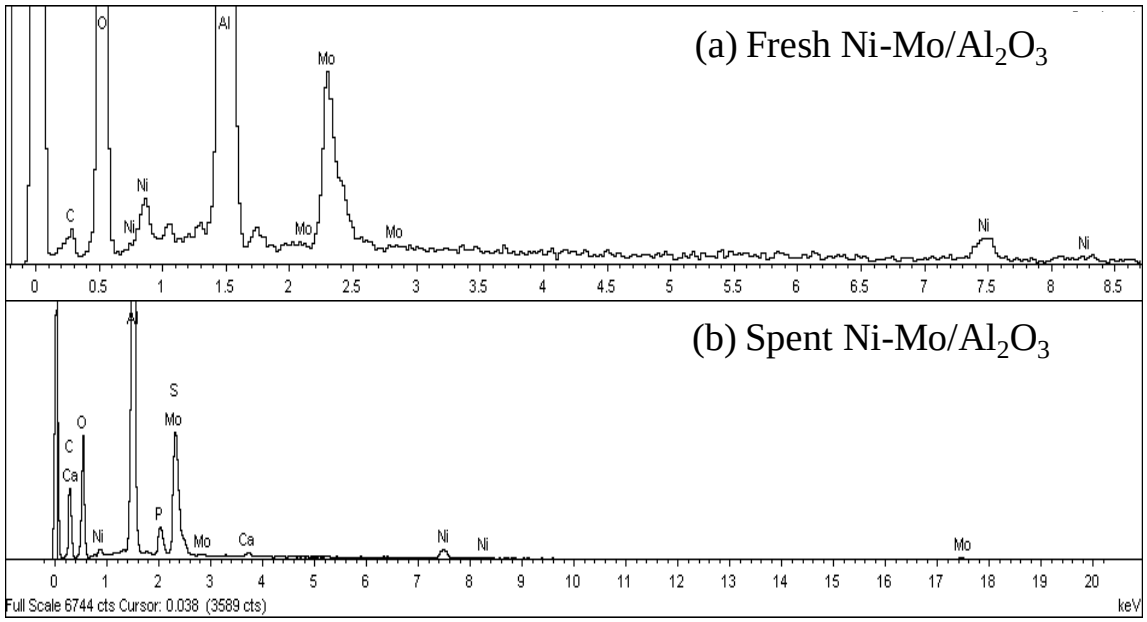

(b)

Figure 7.11 EDX of (a) fresh and spent Co-Mo/Al_2O_3 after upgrading in H_2 atmosphere at 425 ^{o}C, 20 barg, and 200 mL.mL^{-1}; (b) fresh and spent Ni-Mo/Al_2O_3 catalyst after upgrading in N_2 atmosphere at 425 ^{o}C, 20bar, and 500 mL.mL^{-1}.

It is worthy to note that the active metals (i.e., Ni, Mo, and Co) of the catalyst are converted from oxides to sulphide form during the catalytic upgrading reactions, due to the sulphur content of the heavy oil. The metals are therefore deposited on the catalyst as metallic sulphides e.g M_xS_y, where; M is V, Ni, Fe, etc. (Rezaei, et al., 2012; Leyva, et al., 2007). In the light of this, the conversion of high-boiling species into low-boiling fractions led to boiling point shift to the left of the feed oil TBP curve due to the following reactions:

- cracking of C-C bonds in the heavy oil
- cracking of C-S and C-N (i.e., C-hetero-atoms bonds) and
- metals removal

Gray (1994) has also pointed out that the reduction of the heteroatoms content of the produced oil could contribute to its low-boiling range more than the original heavy oil. Conclusively, catalyst deactivation was caused by coke and metal deposition, resulting in pore constriction and blockage. However, the SEM morphology revealed that the effect of coke deposition on deactivation was more than that of metal deposits. Furthermore, it was found by Wilson (1975) that the metals deposited on the catalyst contribute massively to coke formation, hydrogen subtraction, and excessive yield of gases in the outlet-gas stream at the expense of light oil.

7.5 Effect of Feedstock on Catalyst Coke Content

In section 7.2 and 7.3 the effect of reaction temperature and WHSV on catalyst coke content were presented. In this section, effect of feedstock on catalyst coking is presented. Figure 7.12 shows the effect of feedstock on spent catalyst coke content for Co-Mo and Ni-

Mo catalysts after upgrading reaction. It is clear that the coke content of the spent catalyst after 18 hours time-on-stream operation is different for feed-A and B.

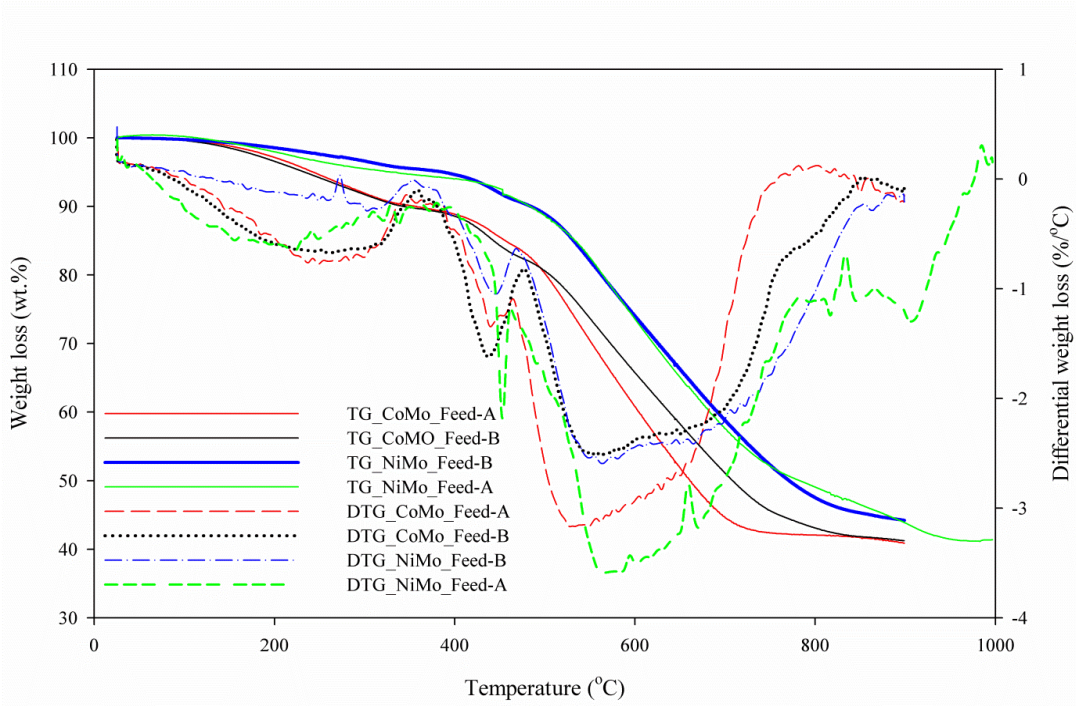

Figure 7.12 TGA and DTG of spent catalyst obtained from the CAPRI reactor after upgrading reaction using feed oil-A & B with Co-Mo/Al_2O_3 and Ni-Mo/Al_2O_3; Temperature 425 °C, Reaction Media (N_2), Pressure 20 barg, Oil flow rate 1mL.min^{-1}, Gas flow rate 500 mL.mL^{-1}.

The coke contents of the spent Ni-Mo/alumina catalyst after reaction with the two oils were 48.2 wt.% (feed oil-A) and 39.6 wt. % (feed oil-B). Whilst, for spent Co-Mo/alumina it was 49.84 wt.% (feed-A) and 41.07 wt.% (feed oil-B), respectively. This represents a difference of approximately 9 wt.% between feed oil-A and B for the use of each catalyst. Gray et al. (1999) found that the catalyst coke content increase is directly proportional to the asphaltenes content of the heavy oil. Therefore, the difference in the spent catalyst coke content could be attributed to the higher asphaltenes content of feed oil-A (11.14 wt.%) compared to 10.3 wt.% for feed-B, knowing that asphaltenes are major contributors to coke.

7.6 Effect of AC Guard-bed on Catalyst Coke Content

The TGA and DTG of spent Co-Mo/Al_2O_3 catalyst recovered after upgrading with AC on top of Co-Mo/Al_2O_3 catalyst and that without guard-bed are presented in Figure 7.13. It is clear that the coke content of the experiment with guard-bed placed ahead of the Co-Mo/Al_2O_3 catalyst was 39.6 wt. % compared to the run where only Co-Mo/Al_2O_3 was used which is 57.4 wt. %. This represents 17.8 wt.% coke content decrease for 25 hours time-on-stream operation.

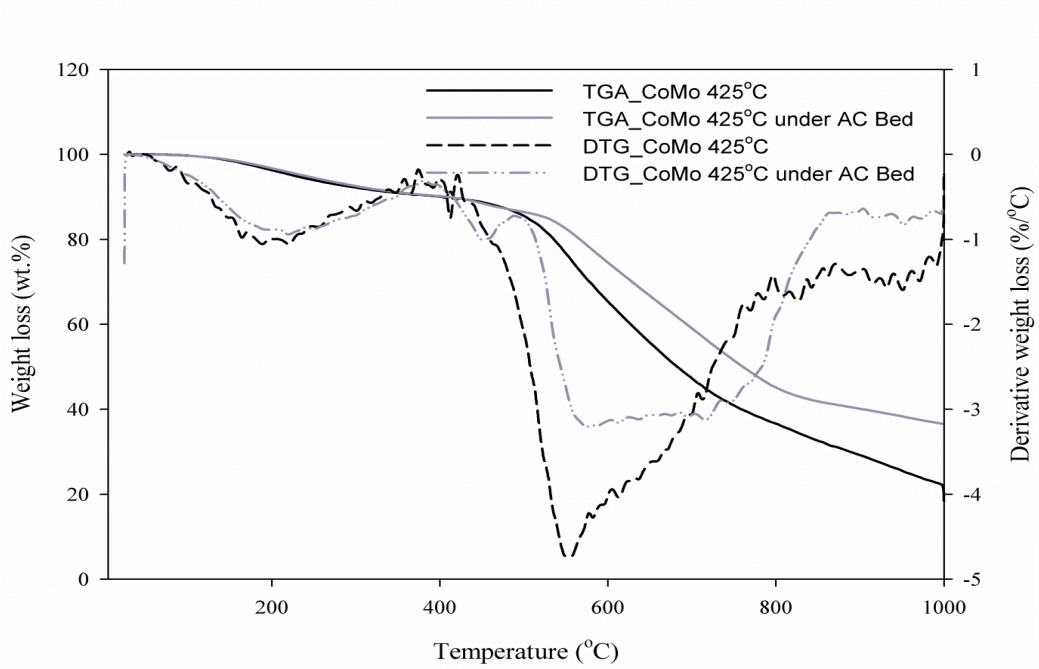

Figure 7.13 TGA and DTG of spent Co-Mo/Al_2O_3 catalyst obtained from a guard-bed reactor and without guard bed; Temperature 425 °C, Reaction Media (N_2), Pressure 20 barg, Oil flow rate 1 mL.min^{-1}, Gas flow rate 500 mL.mL^{-1}.

This confirmed the previous impact of AC guard-bed to further improved the API gravity, viscosity, asphaltenes, and metals contents of the produced oil compared to using Co-Mo/alumina catalyst only. This is because the AC guard-bed selectively adsorbed some of the large molecules that are polar and hydrogen-deficient such as resins, asphaltenes and

heteroatom containing compounds upstream the catalyst bed (Hart, et al., 2013). The affinity of AC for these heavier molecules has been reported by Ming et al. (2007) and Fukuyama et al. (2004). The act therefore lowered early catalyst deactivation due to the initial formation of coke resulting from asphaltenes and resins adsorption onto the catalyst, according to the chemistry of coke formation illustrated in Figure 7.14.

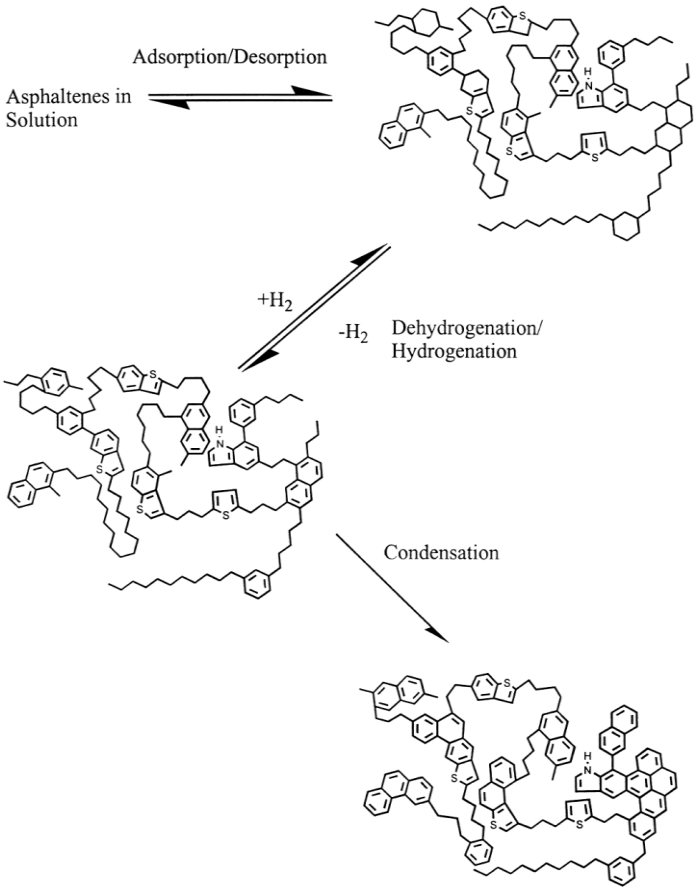

Figure 7.14 Chemistry of coke formation on catalyst surface during upgrading reaction (Gray, et al. 2000).

Therefore, as the feed oil passes through the AC guard-bed on top of the Co-Mo/alumina catalyst, its coking tendency lowers before catalyst cracking, however less condensed aromatics are readily adsorbed strongly on the catalyst surface. The coke formation process however set in with the transfer of hydrogen from the deposited macro-molecules to

stabilise lower hydrocarbon radicals in the light oil phase, resulting in the formation carbon-rich material (i.e., coke).

7.7 Conclusions

The results of the coke and spent catalyst analysis show that the lay-down of coke on the catalyst during upgrading reaction is temperature-dependent and higher temperature subjected the catalyst to severe deactivation effect. It starts with macromolecular weight species adsorption onto the catalyst, proceeds with loss of hydrogen and eventually forms coke with various degrees of hardness. The covered active sites consequently choke-off access to the catalyst interiors and acid sites. Also, metals deposition contributed to the blockage of the pores and catalyst deactivation. Catalyst deactivation is the gradual loss its activity to convert heavy fraction (> 343 ^{o}C) into lighter fractions (< 343 ^{o}C) with time-on-stream. However, hydrogen-addition and activated carbon guard-bed on top of the catalyst bed significantly decreased coke formation.

Chapter 8

Effect of Steam on Catalytic Upgrading and Coke Formation

8.1 Introduction

During heavy oil extraction using THAI-CAPRI, the combustion zone can reach temperatures of 450-700 ^{o}C which can heat up the water in the oil layer to generate steam, resulting in steam flooding and/or hot water flooding (Jinzhong, et al., 2012; Xia, et al., 2002; Wenlong, et al., 2011). The addition of steam to the generated gases during THAI process may impact on the upgrading reactions occurring in CAPRI, and thus it is important to understand the effect of the steam environment upon upgrading and coke formation.

In Chapter 5 and 6, the use of an activated carbon guard-bed on top of the catalyst and hydrogen-addition was reported as a remedy for reducing coke formation and sustaining catalyst lifetime. Hydrogen-addition from an external source can however prove challenging to introduce into the oil reservoir unless sufficient hydrogen can be generated *in situ*. In this Chapter, the effect of steam on the extent of CAPRI upgrading and its contributions to reducing coke formation are reported. *In situ* hydrogen can be generated from steam via the water-gas-shift reaction and this source of hydrogen could promote hydrocracking and hydroconversion reactions (Hart, et al., 2014b). The in-situ generated hydrogen could potentially improve the economics of the process compared to surface processing and externally injecting hydrogen into the well. In addition to reducing the viscosity of the heavy oil, it has been reported that there are chemical reactions between steam and heavy oil which changes the composition of the heavy oil towards the light ends. Hyne et al. (1982) describe this chemical interaction between steam and heavy oil as aquathermolysis. The experimental

results presented in this chapter therefore provide further insight into the extent of aquathermolysis occurring in THAI-CAPRI.

The reaction was carried out at a previously optimized temperature of 425^{o}C and the other conditions are presented in Table 8.1. Steam was generated by feeding water into trace heated lines having a set temperature of 280^{o}C and thereafter mixed with the feed oil prior to entering the CAPRI reactor where the desired reaction temperature of 425^{o}C was achieved. Therefore, the steam-to-oil ratio (SOR) stated in Table 8.1 represents millilitre cold water equivalent (CWE) of water per millilitre of feed oil (CWE/oil) into the CAPRI reactor.

Table 8.1 Operating conditions in the experiments.

Paramete	**value**
Oil flow rate (mL.min^{-1})	1 ± 0.3
Catalyst (g)	6
Pressure (barg)	20
Reaction temperature (^{o}C)	425
Weight hourly space velocity, WHSV (h^{-1})	9.1
Gas-to-oil ratio, GOR (mL.mL^{-1})	500
Steam-to-oil ratio, SOR (mL.mL^{-1})	0.02 – 0.1

8.2 Effect of Steam on Mass Balance

The yields of gas, liquid and coke after 15 hours time-on-stream catalytic upgrading reactions with and without steam are presented in Table 8.2. It is however clear that the yield of liquid product when the reaction was carried out under nitrogen only was 93.4% and upon steam-addition 94.8%.

The liquid yield of the experiment represents a 1.4 wt. % increase, while the coke yield decreased by 0.88 wt. % when the reaction was carried out in a steam atmosphere compared to 2.11 wt. % coke observed under nitrogen environment alone. Following the

decrease in the yields of coke and gas under steam atmosphere, the increase in liquid product was expected. Accordingly, Gao et al. (2010) reported a similar trend that the addition of steam to catalytic upgrading of heavy oil reduces coke formation and increases the yield of light oil. Consequently, as the carbon-carbon bond scissions occurred to give low-boiling hydrocarbons, the hydrogen gas generated by the steam inhibits the secondary reactions that lead to coke formation as well as hydrogenates the cracked products, once formed, thereby increasing the yield of liquid product (Zachariah, et al., 2013). Notably, the amount of produced gas under steam atmosphere was reduced by 0.52 wt. % compared to that obtained under nitrogen gas only, as shown in Table 8.2.

Table 8.2 Product yields from CAPRI process without and with steam at reaction temperature of 425^{o}C, pressure 20 barg; N_2-to-oil ratio 500 mL.mL^{-1}; steam-to-oil ratio 0.05 mL.mL^{-1}

Reaction system	**Liquid yield (wt.%)**	**Coke yield (wt. %)**	**Gas yield (wt. %)**
Feed oil + N_2	93.4	2.11	4.49
Feed oil + N_2 + Steam	94.8	1.23	3.97
Standard deviation	± 0.43	± 0.6	± 0.14

8.3 Effect of Steam-to-Oil Ratio

In this section, the results of the experimental runs conducted in triplicate, including API gravity and viscosity measurements, TBP distribution curve of feedstock and liquid products, produced gas composition, and coke content of spent catalyst are presented and discussed.

8.3.1 Effect of Steam on API Gravity and Viscosity of Produced Oil

The simultaneous reactions of thermolysis, the action of high-temperature steam, and cracking are known to occur in catalytic aquathermolysis environment. These reactions help

to pyrolyse large hydrocarbon molecules into smaller ones while the catalytic actions improve the cracking of the heavy oil. In Figure 8.1, the API gravity of the produced oil samples under steam and steam-free environment as a function of time-on-stream is presented. Each data point in the figure represents an average of triplicate of experimental run. The maximum observed standard deviations between the experimental runs for API gravity and viscosity are: steam-free (0.9^o and 0.046 Pa.s), SOR 0.02 (1.02^o and 0.065 Pa.s), SOR 0.05 (0.93^o and 0.057 Pa.s) and SOR 0.1 (0.88^o and 0.038 Pa.s), respectively. Clearly, the API gravity of the produced oil samples was higher than the feed oil. There is a noticeable difference in API gravity of the produced oil with and without steam addition.

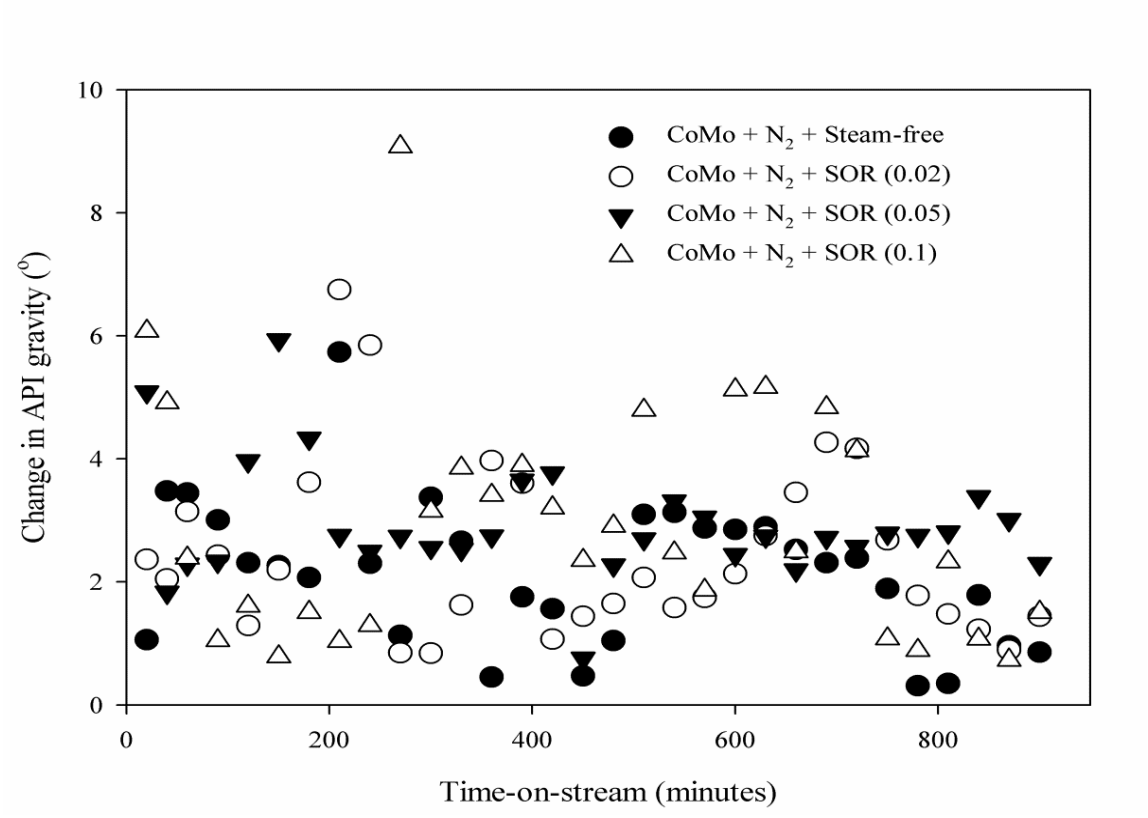

Figure 8.1 Change in API gravity of Produced oils as a function of time-on-stream using Co-Mo/γ-Al_2O_3 catalyst, reaction temperature 425 ^oC, pressure 20 barg, N_2-to-oil ratio 500 $mL.mL^{-1}$; steam-to-oil (SOR) ratios 0.02, 0.05, and 0.1 $mL.mL^{-1}$.

In a steam-free environment, the API gravity increases by a maximum change of roughly 6^o during the early part of the experiment and thereafter settles at an average increase of 2.14 ± 1.2^o API for 15 hours time-on-stream, above an initial value of 14^o API for the feed oil. Compared with a maximum increase of 6° using nitrogen, when steam was introduced the API gravity increased to 9^o API. Thereafter, the average value settled into the following ranges: 2.5 ± 1.44^o, 2.93 ± 0.98^o, and 2.91 ± 1.92^o API for steam/oil ratios (SORs) 0.02, 0.05 and 0.1, respectively. This represents approximately 0.4 to 1^o further increment in API gravity upon steam addition above the value obtained in a steam-free atmosphere.

The feedstock has high viscosity (1.091 Pa.s at 20 ^{o}C) and low API gravity (14^o). This shows that the feed oil has poor fluidity that can cause difficulty in pipeline transportation and refine-ability. In this regard, to meet refinery and pipeline transportation specifications, it is necessary therefore to increase the API gravity by 5-9^o and decrease the viscosity to 0.25 Pa.s at 20 ^{o}C (Hashemi, et al., 2014). Figure 8.2 shows the viscosity of produced oil samples in the absence of steam and at different SORs as a function of time-on-stream operation. Clearly, the viscosity of the produced oil in each of the experimental runs is lower than that of the partially upgraded THAI feed oil (1.091 Pa.s). It is noteworthy that under a steam-free atmosphere the average viscosity of the produced oil reduces from 1.091 to 0.158 Pa.s, representing a decrease by 85.5 %. However, upon steam-addition, the average viscosity of the produced oil is reduced by 87.8, 92.1 and 89.2 % respectively as the SOR increases from 0.02 to 0.1.

These data represent a further decrease in viscosity by 2.3 to 6.6% above the value of 85.5 % viscosity reduction obtained under steam-free atmosphere. This shows that the impact of steam environment on viscosity reduction was comparatively higher than its effect on API gravity increase. Li et al. (2013) reported 86.1 to 94.7 % viscosity reduction after catalytic upgrading in a steam atmosphere using Cu^{2+} and Fe^{3+} as catalytic ions for six different heavy

oils obtained from China with original viscosities from 22 to 180 Pa.s at 50 ^{o}C. A similar trend of observation was also reported by Fan et al. (2004). It also suggests that steam addition to the process is able to affect further upgrading than catalytic carbon-rejection which is thought to occur with under nitrogen.

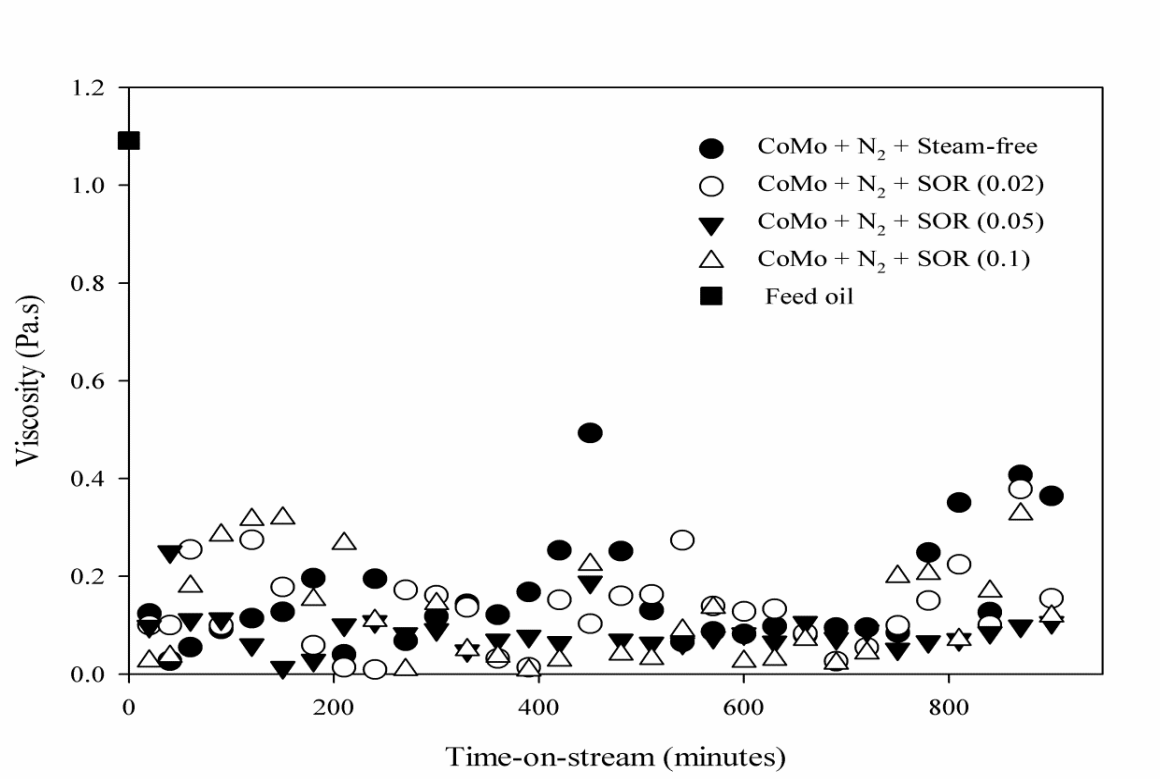

Figure 8.2 Viscosity of Produced oils as a function of time-on-stream using Co-Mo/γ-Al_2O_3 catalyst, reaction temperature 425 ^{o}C, pressure 20 barg, N_2-to-oil ratio 500 mL.mL^{-1}; steam-to-oil (SOR) ratios 0.02, 0.05, and 0.1 mL.mL^{-1}.

Consequently, Chuan, et al. (2010) and Wang, et al. (2012) found that during catalytic upgrading of heavy oil under steam atmosphere, the steam not only acts as a solvent, reactant, and hydrogen donor, but also aids the production of acid sites by interacting with catalytic metals and contributes to many reactions such as catalytic cracking, hydrogenation, ring opening, and desulphurisation involving the splitting of C-S, C-N, C-O, C-C, C=S, and C=O bonds. These reactions affect viscosity reduction (see Figure 8.2), increase API gravity (see

Figure 8.1), remove heteroatoms, and improve the produced oil quality. Additionally, *in situ* donation of hydrogen via water-gas shift reaction will help reduce the chances of recombination of free radicals or active chains formed by the cleavage of C-C, C-S, C-N, and C-O bonds to form large molecules by terminating the active chains (Maity, et al., 2010).

Fan et al. (2001b) attributed these compositional changes and viscosity reduction of the produced oil to the synergistic effects of catalyst and steam. It is clear that this synergistic effect of the catalyst and steam improved the cracking behaviour and the yield of light oil (see Table 8.2) as reflected in the API gravity and viscosity reduction. This can be illustrated by the reactions in Equations 8.1-3 below:

$$\text{Heavy oil} + H_2O \xrightarrow{\text{Catalytic aquathermolysis}} \text{light hydrocarbon} + \text{gases}\ (C_1 - C_5, CO, H_2, \text{etc.}) + \text{active chains} \quad (8.1)$$

$$\text{active chains} + \text{active } H_2 \rightarrow \text{low molecular weight compound} \quad (8.2)$$

$$\text{active chain} + \text{active chain} \rightarrow \text{high molecular weight compound} \quad (8.3)$$

Furthermore, Li et al. (2013) pointed out that the acid sites of the catalyst cracks the C-heteroatom bonds of the macromolecules of the heavy oil, in which the C-S, C-N, and C-O bonds are weakened and the injected steam interaction with these bonds to facilitate cleavage. During crude oil production, oil flow is inversely proportional to its viscosity through the porous reservoir matrix, as very light oil has enough mobility that aids production by natural reservoir pressure or water flooding. From the results above, it is therefore interesting to note that the 87 to 92 % viscosity reduction in the steam assisted catalytic upgrading process is

capable of producing oil with the required fluidity for pipeline transport with little or no diluent addition.

8.3.2 Effect of steam on TBP Distribution

SIMDIS provides the TBP distribution of hydrocarbon fractions in the samples. The estimated standard deviation falls within ± 4.6% for triplicate run. Figure 8.3 shows the TBP distribution curves for the feed and produced oil samples with Co-Mo/Al_2O_3 catalyst when the reaction was carried out under a nitrogen atmosphere only and in combination with steam at the different SOR. The feed oil TBP curve is presented for the purpose of comparison.

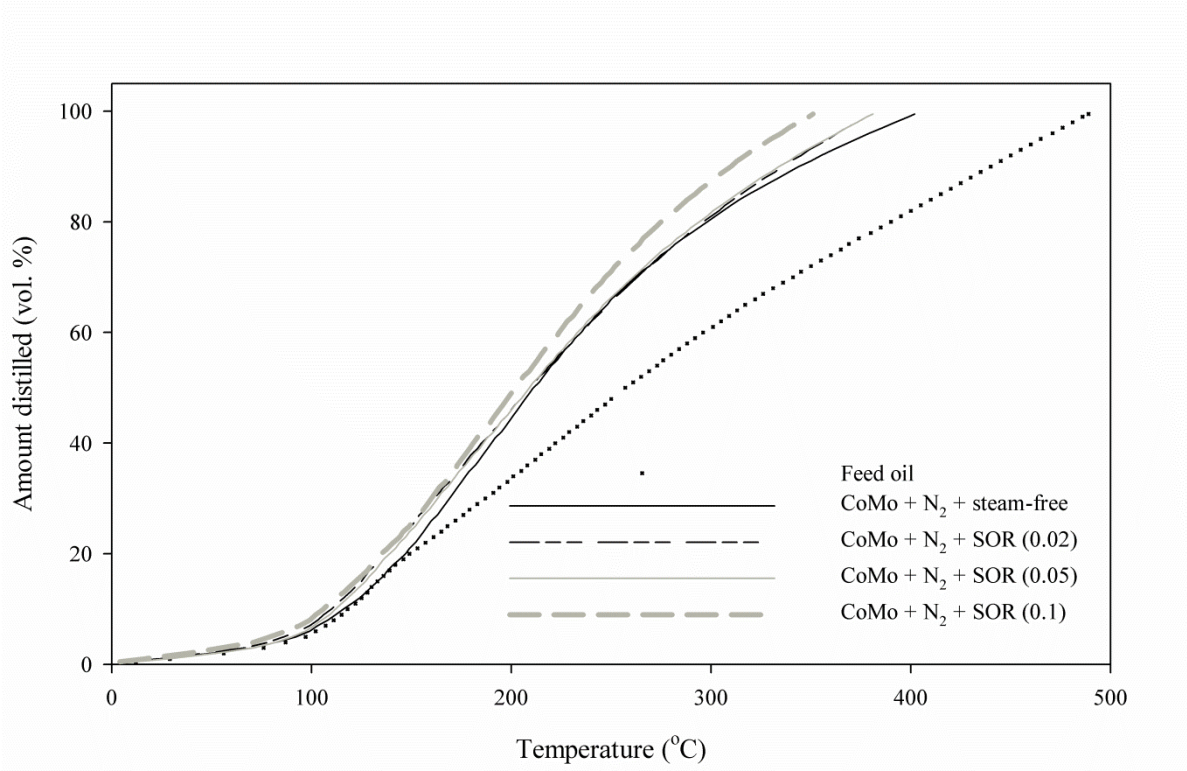

Figure 8.3 TBP distribution curves for feed and produced oils using Co-Mo/γ-Al_2O_3 at reaction temperature 425 °C; pressure 20 barg; N_2-to-oil ratio 500 mL.mL^{-1}; SORs: 0.02, 0.05, and 0.1 mL.mL^{-1}.

The effect of steam environment on the conversion of heavy fractions and the production of lighter fractions is illustrated by the shift in TBP curves of the produced oil samples to the left, indicating that the samples contain lower boiling components than the feed oil. Thus, the cumulative amount distilled at a boiling temperature of 343 ^{o}C increases from 70.5 % in the feed oil to 89.8 % in nitrogen atmosphere alone. However, when steam was added this value rose to 97.2, 92 and 91.6% for SORs 0.1, 0.05, and 0.02, respectively. Compared to the feed oil, catalytic upgrading improved the distillate yield by up to 20 % which is thought to occur mainly through carbon-rejection with limited indirect hydrogenation via hydrogen-transfer reactions in a steam-free atmosphere. It can be concluded from the results that a higher steam injection rate improves the yield of low-boiling fractions. The additional 1 to 7 % increase in distillates yield as a result of steam environment can be attributed to the hydrogenation of cracked fragments by the hydrogen generated from water-gas-shift reaction of steam and carbon monoxide within the upgrading media. This therefore indicates an increase in the percentage of middle fractions (200-343 ^{o}C) in the produced oil due to the hydrogen donor ability of steam. A similar increase in the amount of middle distillates was found when pure hydrogen was added to the reaction media during catalytic upgrading process (Hart, et al., 2013 & 2014a).

From the TBP curves shown in Figure 8.3, it can be inferred that some of the heavy molecular weight hydrocarbons in the partially upgraded THAI feedstock have been converted to hydrocarbons of the middle distillate fractions (200-343 ^{o}C) while the middle fractions are converted to light hydrocarbons (IBP-200 ^{o}C), gases (C_1-C_5) and coke. In Table 8.3 the conversion of 343 ^{o}C+ HCs as a function of SOR is presented. It is clear that the conversion increased as the SOR increased from 0.02 to 0.1.

Table 8.3 Conversion of 343 ^{o}C+ HCs to lower boiling fractions at reaction temperature 425^{o}C, pressure 20barg; N_2-to-oil ratio 500 mL.mL^{-1}, and varying SOR using Co-Mo/Al_2O_3 catalyst.

SOR (mL.mL^{-1})	**Conversion (%)**
No steam	65.4
0.02	71.5
0.05	72.9
0.1	90.5

It can be seen in Figure 8.3 that there is greater impact on conversion above 343 ^{o}C. For instance, the production of the distillate fractions in the range of temperature (200-380 ^{o}C) is higher compared to distillates in the lower temperature range (100-200 ^{o}C). The further shift of the TBP curve for SOR of 0.1 to the left (between temperatures 200-380 ^{o}C), relative to that without steam addition, means that there is a higher proportion of lighter components upon SOR (0.1) and is accompanied by a reduction in the viscosity from 1.091to 0.121 Pa.s. The simulated distillation results provide an explanation of why most of the macromolecules in the feed oil are converted to middle distillates, rather than lighter fractions. Similar trends were also reported for HDS catalysts on hydrocracking of atmospheric residue (Lababidi and AlHumaidan, 2011; Marroquin-Sanchez, et al., 2001). Also, Wang et al. (2012) reported a similar improvement in the amount of distillate yield from produced oil after catalytic upgrading of heavy oil in a steam environment using tungsten oxide on zirconia (W/Zr) catalyst.

8.3.3 Effect of Steam on Asphaltenes, Sulphur, and Metals Content

Heavy oil and bitumen are rich in asphaltenes, containing roughly 10-30 wt.% of this component, which give rise to the characteristics high viscosity as well as contaminants such as heavy metals, sulphur and nitrogen (Galarraga, et al., 2012). In Table 8.4, the asphaltenes,

metals and sulphur content of the feed and selected samples for steam-free and with different SOR are presented. Interestingly, the asphaltenes content of the upgraded samples decreased from 5.1 wt.% in a steam-free environment to 4.9 and 2.4 wt.% as the SOR increased from 0.05 to 0.1. Hyne et al. (1982) and Fan et al. (2001a) investigated aquathermolysis and catalytic aquathermal cracking of heavy oils and found that after reaction, the saturates and aromatics increased, while the resins and asphaltenes decreased. Saturates fractions are the lightest and consist mainly of paraffinic and naphthenic molecules. Therefore, the compositional shift of the upgraded samples towards the low-boiling temperature after catalytic upgrading reactions as shown in the TBP curves in Figure 8.3 is an indication of increased saturate content. As a consequence, the decreased amount of asphaltenes content correlated with viscosity reduction and improved distillable yields. Similar observation was reported in the literature (Maity, et al., 2010; Hongfu, et al., 2002).

Table 8.4 Asphaltenes, sulphur, and metals content before and after CAPRI reaction with and without steam addition at reaction temperature 425 ^{o}C, pressure 20 barg, N_2-to-oil ratio 500mLmL^{-1}, and different SORs.

Impurities	**Feedstock**	**No steam**	**SOR (0.02)**	**SOR (0.05)**	**SOR (0.1)**
Asphaltene (wt. %)	10.3	5.1	5.1	4.9	2.4
Aluminium (ppm)	2	2	< 1	1	< 1
Boron (ppm)	3	2	1	1	< 1
Iron (ppm)	5	< 1	1	< 1	< 1
Nickel (ppm)	41	34	30	23	12
Vanadium (ppm)	108	90	78	62	32
Ni + V (ppm)	149	124	108	85	44
Sulphur (wt. %)	3.52	3.4	3.08	2.95	2.62
Silicon (ppm)	1	< 1	< 1	< 1	< 1

* Sulphur and metals content was performed by Intertek Laboratories Sunbury Technology Centre, UK, using ICP-OES (Inductively Coupled Plasma Optical Emission Spectrometry).

As the active oxygen and hydrogen generated from steam over the catalyst reacts with the heavy oil fractions to produce lighter fractions and carbon dioxide, the hydrogen terminates free radical addition reactions and increases the saturates and aromatic content of the produced oil (Fumoto, et al., 2011; Sato, et al., 2013).

From Table 8.4, the sulphur content of the produced oils decreased from 3.52 wt.% for the feedstock to 3.4 wt. % (steam-free), and 3.08, 2.62 and 2.95 wt.% as the SOR increased from 0.02 to 0.1 $mL.mL^{-1}$. This indicates sulphur removal of 3.4% (steam-free), 12.2 % (SOR 0.02), 16.2% (SOR 0.05), and 25.6 % (SOR 0.1), thus the trend increased as the SOR increases. The significant reduction of sulphur content upon steam addition provides evidence that a greater degree of C-S bond cleavage occurred under steam atmosphere. This is because steam addition promoted hydrodesulphurisation (HDS) reactions which were evident from the high concentration of hydrogen sulphide in the produced gas analysis. Moreover, it has been widely reported in the literature that the mechanism of viscosity reduction during catalytic upgrading of heavy oil in the presence of steam is based on the theory of C-S bond breaking (Li, et al., 2013; Fan, et al., 2001a; Clark and Hyne, 1990; Liu and Fan, 2002). They pointed out that the C-S bond is one of the weakest bonds amongst heavy oil molecules; hence the additional increase in the viscosity reduction of the samples relative to the feed oil and that obtained in steam-free atmosphere can be attributed to increased HDS reactions in the presence of steam (Table 8.4). This confirmed the potential of steam to donate hydrogen through water-gas-shift reaction, where steam participated as reactant and solvent (Li, et al., 2013). As SOR increases more active hydrogen became available, which increased the extent of HDS reaction causing additional 8.8 to 22.2% sulphur reduction above 3.4% (steam-free). Also, 2.3 to 6.6 % increase in viscosity reduction was noticed above the value of 85.5 % (steam-free) due to the cleavage of more C-S bonds.

Concurrent with the trends in sulphur removal, the nickel and vanadium (Ni + V) content of the samples was reduced from 149 ppm (feedstock) to 124 ppm (steam-free), and with steam environment 108, 85 and 44 ppm as SOR increased from 0.02 to 0.05 and 0.1, respectively. Therefore, demetallization increased from 16.8 % (steam-free) to 43-70.5 % as the SOR increased from 0.05 to 0.1. This indicates 26-54 % further reduction of (Ni + V) content upon steam-addition. The reduction in sulphur and metals content of the oil produced is consistent with the conversion of asphaltene molecules. It is possible that this significant reduction in the metal content of the produced oil contributed to the 1^{o} increase in API gravity upon steam-addition above obtained under steam-free atmosphere, since the presence of metals influences the heavy oil density. Additionally, the donated hydrogen via WGSR therefore promoted hydrodemetallization (HDM) reactions, which is not experienced to the same extent in steam-free environment. Moreover, the concentrations of other impurities such as aluminum, boron, and iron were also reduced.

8.4 Spent Catalyst Coke Content

In chapter 7, it was found that coke formation in the catalytic upgrading process can be suppressed by adding hydrogen (Hart, et al., 2013 & 2014a). In this Chapter, steam environment was investigated as a potential source of hydrogen via WGS reaction. TG and DTG analysis of the fresh and spent Co-Mo/Al_2O_3 catalyst recovered from the CAPRI reactor after upgrading reactions with and without steam injection is presented in Figure 8.4. The spent catalyst contains unconverted oil, cracked oil products and intermediates, and coke. The latter starts to burn-off at about 530 ^{o}C during TGA analysis (Hart, et al., 2013). In Table 8.5, the coke content of the recovered spent catalyst is presented. The recovered catalyst from the CAPRI reactor after an upgrading experiment was carried out in a steam atmosphere showed lower coke content compared to the experiment in nitrogen atmosphere only.

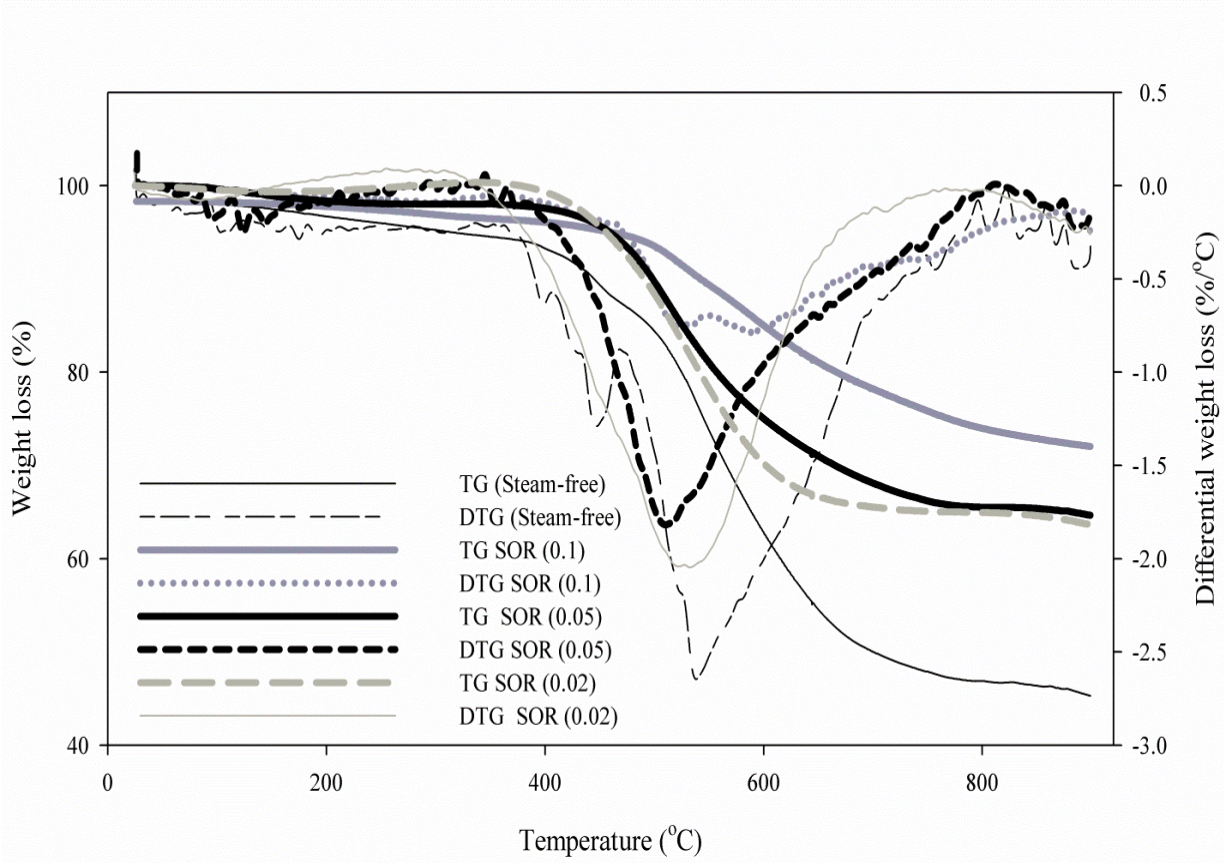

Figure 8.4 TG and DTG of fresh and spent Co-Mo/Al_2O_3 catalyst recovered from CAPRI reactor after reaction with and without steam addition at reaction temperature 425 °C, pressure 20 barg, and N_2-to-oil ratio 500 mL.mL^{-1}.

Table 8.5 Spent Co-Mo catalyst coke content after CAPRI upgrading with and without steam addition at reaction temperature 425 °C, pressure 20 barg, and N_2-to-oil ratio 500 mLmL^{-1}.

SOR (mL.mL^{-1})	**Spent catalyst coke content (wt. %)**
No steam	27.53 ± 1.43
0.02	21.81 ± 0.94
0.05	18.07 ± 0.86
0.1	16.23 ± 1.09

The feed oil cracked over the Co-Mo/Al_2O_3 catalyst at 425^oC yields light hydrocarbon fractions, gas, and coke. However, in a steam atmosphere the coke content of the spent catalyst decreased from 27.53 wt. % (steam-free) to 21.81, 18.07 and 16.23 wt. % as the SOR increased from 0.02 to 0.05 and 0.1, respectively. In this respect, the coke content was reduced by 5.72-11.3 wt.% as SOR increased. Consequently, the DTG curves indicate that the coke formed in the presence of steam started to burn-off at a lower temperature of approximately 521 ^oC compared with the coke formed in a steam-free atmosphere which starts to burn-off about 539 ^oC. These results also provide evidence that steam was involved in the catalytic upgrading reactions, as hydrogen donor solvent. The 18 ^oC difference in burn-off temperature is thought to arise from structural differences in the coke molecules. The impact of steam-addition on reduction of catalyst coke is significantly higher compared to that of API gravity increase and viscosity reduction.

Nevertheless, Maity et al. (2010) pointed out that the addition of a small amount of water depressed coke formation, with the coke content of catalyst decreasing with additional water and levelled off after 10 wt.% of water. This is thought to be because the high SOR increased the generation of active *in situ* hydrogen for hydrogenation reactions. Similarly, Fumoto, et al. (2009) found that at lower steam flow rate, there is inadequate generation of these active species, causing coke build-up on the catalyst. Since the reaction medium has insufficient hydrogen-transfer capability at low SOR, free radical propagation could not be adequately moderated. This is supported by the decrease in the methane and hydrogen concentration in the off-gas as the SOR decreased from 0.1 to 0.02 (Zachariah, et al., 2013).

The decreased coke deposition due to steam addition can be attributed to the reaction between steam and coke, generating carbon monoxide and hydrogen (Kapadia, et al., 2011). This hydrogen produced can further react with coke as a precursor to form methane; details of

the reactions are presented in Equations 8.4 and 8.5. In addition, Fumoto et al. (2009) reported that active oxygen and hydrogen are produced from steam over the catalyst (see equation 8.6 and 8.7). The reaction between the coke and active oxygen can also help to suppress coke build-up (Fumoto, et al., 2011). Some of the produced hydrogen is utilized to stabilize unsaturated and unstable hydrocarbons products such as olefins and coke precursors.

$Coke_{(s)} + H_2O_{(g)} \rightarrow CO_{(g)} + H_{2(g)}$ Kapadia, et al. (2011) (8.4)

$Coke_{(s)} + 2H_{2(g)} \rightarrow CH_{4(g)}$ Kapadia, et al. (2011) (8.5)

$2H_2O_{(g)} \leftrightarrow 2H_2 + O_2$ (8.6)

$Coke_{(s)} + O_2 \rightarrow CO_{2(g)}$ (8.7)

In the work of Fumoto and co-workers (2009) it was shown that the reaction of oxygen generated from steam with the heavy oil over the catalyst produced an appreciable amount of light oil and carbon dioxide with a lower amount of coke. Also, Sato et al. (2013) pointed out that the presence of a hydrogen donor (through WGS reaction) in the oil-rich phase is effective for suppression of coke formation during the catalytic upgrading process.

8.5 Effect of Steam on Produced Gas Composition

The produced gas composition during the experiments determined using RGA analyser and the results are presented in Table 8.6. The gases are products of the upgrading reactions resulting from the splitting of large molecules into smaller ones. The gas composition provides further insight into the reaction mechanism. The presence of hydrogen in the gas indicates the potential of the process to generate hydrogen in the reservoir.

Table 8.6 Produced gas composition during catalytic upgrading reaction in nitrogen atmosphere only and in combination with steam using Co-Mo/γ-Al_2O_3 catalyst at temperature 425 ^oC; pressure 20 barg; N_2/oil ratio 500 $mL.mL^{-1}$ and different SORs.

Gas	No steam (vol. %)	SOR (0.1) (vol. %)	SOR (0.05) (vol. %)	SOR (0.02) (vol.%)
Methane	2.33	1.15	1.27	1.46
Hydrogen	2.4	1.37	1.1	1.41
Ethane	0.82	0.06	0.033	0.03
Carbon dioxide	0.03	0.07	0.064	0.054
Ethene	0.03	0.07	0.08	0.073
Propane	0.23	0.21	0.15	0.113
Propene	0.14	0.10	0.07	0.068
i-Butane	0.12	0.14	0.03	0.062
n-Butane	0.06	0.14	0.03	0.073
1-Butene	0.051	0.035	0.034	0.044
Cis-2-butene	0.00	0.037	0.029	0.038
Trans-2-butene	0.02	0.033	0.00	0.023
n-Pentane	0.19	0.11	0.064	0.11
i-Pentane	0.17	0.07	0.034	0.064
Carbon monoxide	0.02	0.016	0.018	0.019
Hydrogen sulphide	0.00042	0.00052	0.00044	0.00043

Notably, 2.4 vol.% of hydrogen was detected in the outlet gas stream in a steam-free environment against 1.1-1.4 vol.% in steam atmosphere depending on the SOR. This decrease in hydrogen volume is deduced to be because some of the generated hydrogen is consumed in hydrogenation, HDS, HDM reactions, and the inhibition of hydrogen abstraction from macro-hydrocarbon molecules, leading to coke formation, even though additional hydrogen may be generated in the presence of steam. The evolved hydrogen originates from two reaction routes: firstly through hydrogen subtraction from the excited saturated hydrocarbon to form an unsaturated hydrocarbon molecule as illustrated by Equation 8.8:

$$2RH_{\text{saturated}} \rightarrow 2R_{\text{unsaturated}} + H_2 \quad (8.8)$$

$$RH \rightarrow R^{\bullet} + H^{\bullet} \quad (8.9)$$

$$RH + H^{\bullet} \rightarrow R^{\bullet} + H_2 \quad (8.10)$$

where, R is a hydrocarbon molecule

Furthermore, C–H bond cleavage produces hydrocarbon radicals and active hydrogen. The active hydrogen on collision with another molecule abstracts hydrogen to form a hydrogen molecule, as illustrated by Equations 8.9 and 8.10 (Alfi, et al., 2013). In this way the macromolecule structure continues to grow further while the free radical sites at the formed coke surface are revived by continuous hydrogen abstraction (Reyniers, et al., 1994; Wang, et al., 2007). The free radicals formed, unsaturated molecules, and aromatics, are common coke precursors. They promote coke formation by terminating reactions with coke macro-radicals. Alternatively, the active hydrogen can react with other hydrocarbon radicals to form a stable molecule via hydrogen-transfer reactions. Reactions 8.8 to 8.10 could have been inhibited by injection of steam as hydrogen donor giving rise to less hydrogen in the produced gas.

Consequently, the total olefin content of the produced gas is as follows: 0.241 vol.% (steam-free), 0.31 vol.% (SOR, 0.1), 0.242 vol. % (SOR, 0.05) and 0.246 vol.% (SOR, 0.02). Under the same conditions, the paraffinic contents are, respectively, 3.92 vol.% (steam-free), 1.804 vol.% (SOR, 0.1), 1.661 vol.% (SOR, 0.05) and 1.912 vol.% (SOR, 0.02). It is clear, therefore, that the presence of steam limits olefin saturation (Gao, et al., 2010). Furthermore, when steam was introduced to the catalytic upgrading process, less gases such as light hydrocarbons (i.e., C_1-C_5), carbon monoxide, and hydrogen were produced, because in the presence of steam the catalyst accelerates aquathermolysis of the oil, in addition to

hydrogenation. However an increase in carbon dioxide production was observed, from 0.03 vol.% (steam-free) to 0.054, 0.064 and 0.07 vol.%, as the SOR was increased from 0.02 to 0.05 and 0.1, respectively. This is because the water-gas-shift reaction occurs within the upgrading media. The lower gas production in the presence of steam is consistent with result of the mass balance presented in Table 8.2 and with the result reported by Fan et al. (2001).

The two reaction routes for sulphur removal are: direct removal of the sulphur atom from the straight chain molecule and hydrogenation of aromatic rings, followed by removal of the sulphur atom (Marroquin-Sanchez, et al., 2001). Upon injection of steam, the amounts of hydrogen sulphide in the produced gas increased from 0.00042 % (steam-free) to 0.00052% for SOR of 0.1, indicating that additional C-S bonds in the sulphur-containing compounds of the feed oil have been ruptured and converted to H_2S. The removal of the sulphur as hydrogen sulphide demonstrated that HDS reaction occurred during the catalytic upgrading process and the injection of steam increased the extent. The amount of methane and hydrogen in the gas decreased with the increasing amount of added steam. The results were consistent with those reported in the literature (Maity, et al., 2010; Hongfu, et al., 2002). The decrease in the amount of methane with increase in steam addition can be attributed to the following reactions (see Equation 8.11) postulated by Hongfu, et al. (2002):

$$CH_4 + H_2O \xrightarrow{\text{catalyst}} 3H_2 + CO \qquad (8.11)$$

The observed decrease in the amount of hydrogen was attributed to *in situ* HDS, hydrogenation of the free radicals and olefins produced during the process (Hongfu, et al., 2002).

8.6 Water-Gas-Shift Reaction

The produced carbon dioxide and carbon monoxide in the gas as a function of time-on-stream, for nitrogen only and nitrogen with steam environment are presented in Figure 8.5. It is clear that steam environment increased the amount of carbon dioxide gas produced while carbon monoxide decreased. The high amount of carbon dioxide produced can be attributed largely to the water-gas-shift (WGS) reaction ($CO + H_2O$ (g) = CO_2+ H_2, ΔH= -41.1 kJ.mol^{-1}) that occurs in the presence of steam, catalyst and CO generated from aquathermolysis of heavy oil (Fan, et al., 2001a; Li et al., 2013; Smith, et al., 2010).

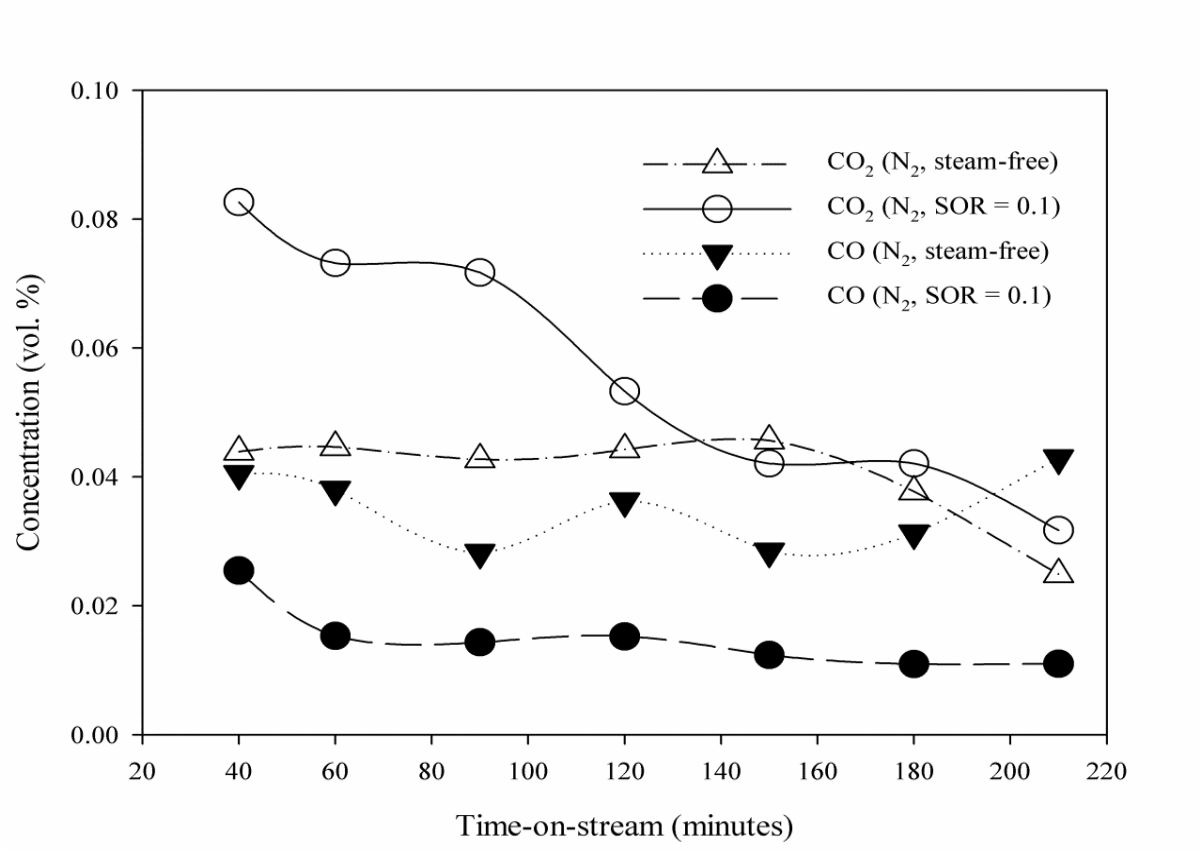

Figure 8.5 CO_2 and CO production during catalytic upgrading in the presence and absence of steam at temperature of 425 ^{o}C, pressure 20 barg, SOR 0.1 mL.mL^{-1}, and N_2-to-oil ratio 500mL.mL^{-1}.

It is also noteworthy the increased amount of carbon dioxide and the decreased amount of carbon monoxide in the gas in the presence of steam provides evidence that the WGS reaction occurred to a greater extent with the addition of steam. It can also be seen from Figure 8.5 that the carbon dioxide produced via WGS reaction decreased with time-on-stream, because of loss of catalytic activity resulting from catalyst surface, pores, and voids been fouled by coke produced during cracking reactions of hydrocarbons.

Therefore, during the upgrading reaction, water acts as a hydrogen donor, providing hydrogen for hydrogenation, HDM and HDS. Carbon dioxide and C_2-C_5 light hydrocarbons could have also helped to decrease the produced oil viscosity via miscible and/or immiscible displacement and improve recovery of heavy oils in reality. Carbon dioxide generated in-situ via water-gas shift reaction could be potentially sequestered in the reservoir so that emissions to the atmosphere are reduced (Kapadia, et al., 2011).

8.7 Conclusions

The extent of aquathermolysis occurring in THAI-CAPRI process was investigated at reaction temperature of 425 ^{o}C, gas/oil ratio 500 mL.mL^{-1}, pressure 20 bar, and water/oil ratio 0.02, 0.05 and 0.1 mL.mL^{-1}. It was found that viscosity reduction of the produced oil further increased by 2-7 % under steam atmosphere compared to 85.5 % viscosity reduction under steam-free atmosphere. Also, the API gravity of the produced oil increased by at least 1^{o} above obtained under steam-free environment. Depending on the steam/oil ratio used, the sulphur and metals (Ni + V) content removal increased by 8.1-22.2 % and 26-54 % respectively, compared to 3.4 % and 16.8 % under steam-free atmosphere.

Chapter 9

Comparative Study of Fixed-bed and Dispersed Catalysts

9.1 Introduction

In Chapters 4 to 8, the conventional CAPRI reactor, requiring the packing of the horizontal well with pelleted HDS catalysts prior to starting up, was reported. It was found that catalyst deactivation remains an issue during production. Coke deposition is a major drawback of fixed-bed catalyst. In other words, the activity of the catalyst rapidly decreases with time-on-stream, eventually plugging the pores and voids of the fixed-bed (Froment, 1991; Cerqueira, et al., 1997). This adversely impact on the process economy. In this Chapter 9, a substitute approach to dealing with this challenge using a once-through nano-particulate catalyst is reported.

In reality, the application of dispersed particles could potentially avoid the hurdles of pre-packing the horizontal well with catalyst pellets prior to starting up, but requires the transport of the nano-particles into the mobile oil zone during the THAI process. The delivery of nano-catalyst to the oil-bearing formations at reservoir condition still imposes a great challenge, which is alleviated as nanocatalyst can readily be injected for *in situ* upgrading in the oil reservoir pore matrix with an injected fluid as slurry (Weissman and Kessler, 1996; Hassanzadeh and Abedi, 2010). Consequently, dispersed nanoparticulate catalysts increase contact as well as effective reactor volume for upgrading reactions.

In this Chapter, dispersed nanocatalyst for in situ catalytic upgrading was tested in a batch reactor at the same residence time (10 minutes), catalyst-to-oil ratio (CTO) 0.02-0.1, temperature (425 ^{o}C), pressure (20 bar), and gas media (N_2 and H_2) used in the fixed-bed

experiments. A test run without adding catalyst was performed to evaluate the effect of thermal cracking only. In Section 9.4, the result of testing biomanufactured catalyst and its chemical counterpart (Co-Mo/γAl_2O_3) was reported.

9.2 Fixed-Bed vs. Dispersed Catalyst

The results of experiments performed in fixed-bed and the dispersed microcatalyst tested in a batch reactor at the same residence time (10 minutes) and CTO (0.1 g/g) are presented in this Section. A stirring speed of 133 rpm was used, as it approximately gives the same Reynolds number of 0.2 experienced in the fixed-bed reactor (see Appendix F), thereby ensuring dynamic similitude. Also, the nitrogen sorption isotherm of the pellets and crushed Co-Mo/Al_2O_3 is presented in Appendix F.

9.2.1 Produced oil API Gravity, Viscosity, Conversion and Products yield

The comparison of the extent of upgrading achieved with fixed-bed and dispersed micro-particulates of Co-Mo/γ-Al_2O_3 catalyst in a batch process are presented in Table 9.1, based on equivalent residence time and CTO. For duplicate runs, the average API increment was 8.7 ± 0.7^o and 5.6 ± 1.8^o for dispersed micro-catalyst and fixed-bed system respectively. The API gravity achieved using micro-particulates of Co-Mo/γ-Al_2O_3 catalyst was 3^o points above that obtained with fixed-bed catalyst. Ovalles et al. (1998) observed API gravity increase of 7^o and 55 % conversion of heavy fractions using dispersed molybdenum catalyst at 410^{o}C reaction temperature. Additionally, the price of crude oil is directly related to its API gravity, in other words the higher the API gravity the higher the price (Ancheyta and Rana, 2007).

Table 9.1 Comparison of upgrading level with fixed-bed Co-Mo pellets and dispersed micro-Co-Mo at temperature 425 ^{o}C, pressure 20 bar, CTO 0.1, Stirring speed 133 rpm, and thermal cracking only (in batch). Feed oil (14 ^{o}API and 1.091 Pa.s).

Experimental Run	API Increment (^{o})	Viscosity (Pa.s)	Conversion (343^{o}C+) (%)	Coke (wt.%)	Gas (wt.%)	Liquid (wt.%)
Thermal (No catalyst)	6.6	0.008	33.1	12.95	8.15	78.9
Dispersed micro-catalyst	8.7	0.007	59.7	7.1	8.05	84.85
Fixed-bed catalyst	5.63	0.028	46.4	1.86	3.34	93.8

Similarly, the 1.091 Pa.s (feed oil) was reduced to 0.0284 Pa.s (fixed-bed) and 0.007 Pa.s (dispersed). This represents 97.4 and 99.4 % viscosity reduction, which is 2% increase in DVR upon use of dispersed micro-catalyst of Co-Mo/γ-Al_2O_3. Wei et al. (2007) reported 98.9 % viscosity reduction of Liaohe extra-heavy oil using nano-nickel catalyst. This magnitude of viscosity reduction could increase the fluidity of the oil through the porous reservoir, thereby increasing production rate and ensure pipeline transport.

Thermal cracking without a catalyst showed the lowest conversion of heavy fractions (BP > 343 ^{o}C) of 33.1 %, whereas the conversion was improved with catalyst 46.4 % (fixed-bed) and 59.7 % (dispersed). The superiority of dispersed micro-catalyst over fixed-bed pellets is because they offer better contact as probability of preferential channelling encountered in fixed-bed is decreased. Additionally, they promote faster cracking reactions because of their reduced particle size and large surface-area-to-volume ratio, high heat and mass transfer, and effective contact and wetting of the macro-dispersed catalyst compare to the fixed-bed catalyst (Angeles, et al., 2013; Le Perchec, et al., 1993). According to Le Perchec et al. (1993), nano-catalyst exhibited higher reaction rate than their fixed-bed counterpart, because the generated hydrogen *in situ* activated by the finely divided particles

for hydroconversion reactions helped to stabilise the free radicals produced during the cracking of heavy oil.

The API gravity of the produced oil was compared for catalytic and thermal cracking run as well. As can be seen in Table 9.1, the oil produced in non-catalytic run was upgraded by 6.6 ± 0.65 ^{o}API, above the original feed oil of 14 ^{o}API. Whilst the catalytic run with dispersed micro-particulates of Co-Mo/Al_2O_3 produced oil was upgraded by 8.7 ± 0.7 ^{o}API. This represents 2 ^{o}API above thermal cracking alone. Abuhesa and Hughes (2009) reported similar findings on catalytic and noncatalytic *in situ* combustion. However, the effect of dispersed micro-catalyst on viscosity of produced oil seems to be roughly the same with that obtained with thermal at 425 ^{o}C. This is because temperature is the driving force for viscosity reduction.

The yields of gas, light oil, and concentrated carbon material; coke was calculated using equations 3.10 and 3.11 (Castañeda, et al., 2012). The material balance presented in Table 9.1 shows that the amount of coke produced at 425 °C was 12.95 wt.% (thermal cracking only) compared to 7.1 wt.% (dispersed micro-particulate Co-Mo/Al_2O_3), and the corresponding liquid yields were 78.9 and 84.85 wt.% respectively. Observation of reactor internals revealed that the coke formation starts at the bottom near the wall and then proceeds towards the centre of the reactor with accumulation at dead volume areas (see Figure 9.1). Coke formation is the consequence of precipitation and accumulation of unconverted asphaltenes cores resulting from the decrease of solvent power (i.e., ability to dissolve another substance) due to composition changes caused by cracking reactions, temperature and hydrogen-abstraction (Sawarkar, et al., 2007; Rogel, et al., 2013).

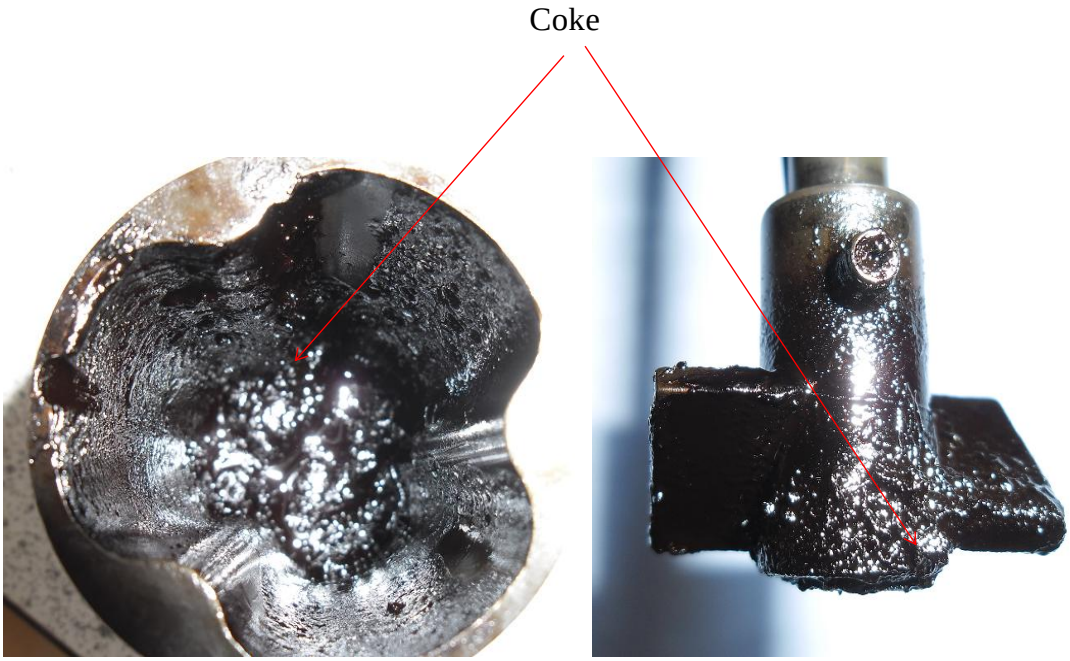

Figure 9.1 Photograph of reactor internal and impeller after reaction at 425 ^{o}C (vessel 100 mL and impeller diameter 10 mm).

In the case of micro-particulate catalyst, the strong affinity between them and asphaltenes serves as a starting point for their cracking, thereby suppressing the polymerisation and condensation reaction to form coke (Zhang, et al., 2007). Nonetheless, aggregation of micro-catalyst and the carbonaceous deposits inside the batch reactor was observed. It can be seen therefore that thermal cracking produced high coke and lower liquid yields compared to catalytic upgrading process. High yield of coke affirms that thermal upgrading is majorly accomplished by carbon-rejection.

9.2.2 Produced oil TBP Distribution

Heavy crude oil produces less fuel distillates with more of residue fraction when distilled. The demand for low-boiling distillates is ever growing (Jarullah, et al., 2011). The SIMDIS of the feedstock and upgraded oils was divided into the following distillates; gasoline (IBP to 200 ^{o}C), middle distillates (200 – 343 ^{o}C), and residual fraction (BP >

343°C). In Figure 9.2, the yields of the distillate fractions are presented for the feedstock and produced oil with dispersed micro-particles and fixed-bed Co-Mo/Al_2O_3 catalyst, respectively.

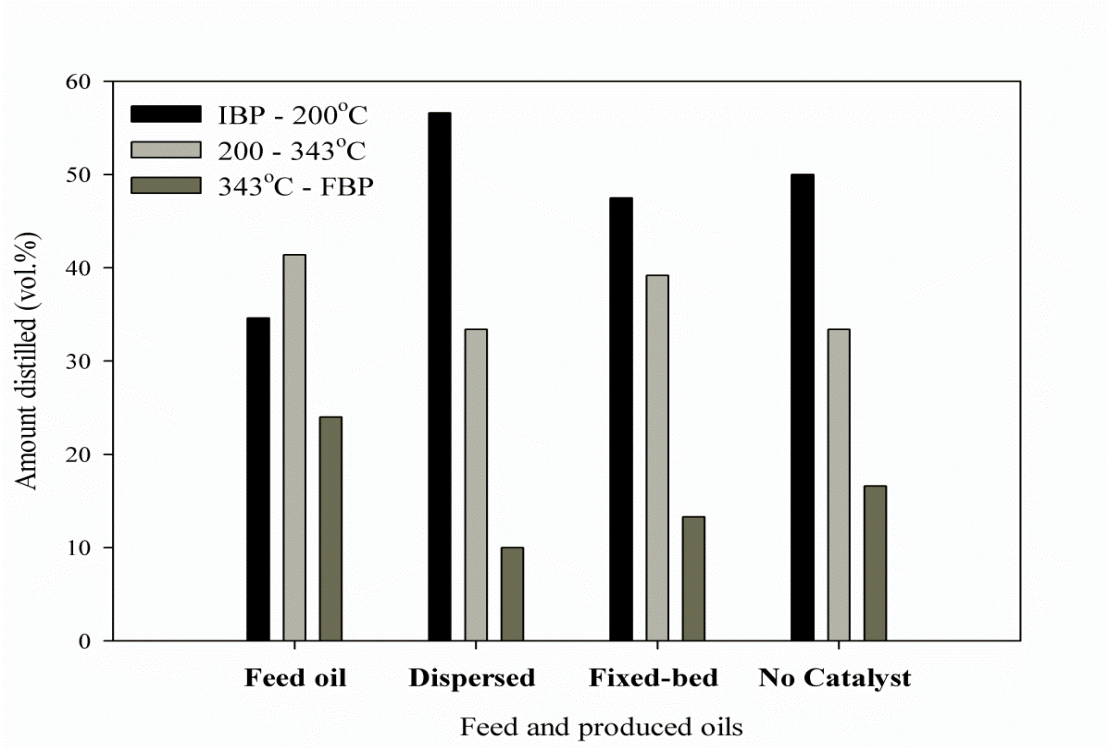

Figure 9.2 Amount distilled as a function of boiling-point fractions for feedstock and produced oil from thermal cracking (batch), fixed-bed and dispersed micro-particulates of Co-Mo/Al_2O_3 catalyst at temperature 425 °C, pressure 20 bar, nitrogen gas media, CTO ratio 0.1, stirring speed 133 rpm, and residence time 10 minutes.

It is clear that while the residual fraction decreased from 24 vol.% in the feedstock to 13.3 and 10 vol.%, the gasoline fractions increased from 34.6 vol.% (feedstock) to 45.5 and 56.6 vol.%, respectively for the produced oils from fixed-bed and dispersed Co-Mo/Al_2O_3 catalysts. However, with fixed-bed more middle distillates (200 – 343 °C) were produced compared to dispersed micro-particulates of Co-Mo/Al_2O_3 in batch. The heavy molecules are transported to the active sites of the micro-particulates earlier, unlike in the fixed-bed where diffusional limitation leading to pore plugging was experienced. The reduced particle sizes

improved contact, reaction rate, hydroconversion, and subsequently yield of light distillates increased (Panariti, et al., 2000a; Noguera, et al., 2012). As can be seen in Figure 9.2, that thermal cracking produced the highest residue fraction of 16.6 vol.% (343 ^{o}C – FBP) compared to dispersed particulate and fixed-bed Co-Mo/Al_2O_3. The improved gasoline fractions as well as decreased residual fractions in the produced oils after catalytic upgrading process positively contributed to the increased API gravity and reduced viscosity as shown in Table 9.1, compared to the original feed oil.

9.2.3 Micro Elemental Analysis

The results of the micro elemental analysis of the samples obtained from thermal, fixed-bed and dispersed micro-particulates of Co-Mo/Al_2O_3 upgrade compared to that of the feedstock are shown in Table 9.2. It can be seen that the H/C atomic ratio increased after thermal and catalytic upgrading. However, thermally upgraded oil sample showed the highest carbon-rejection of 5.16 % and the lowest atomic hydrogen of 10.06 %. Notably, the amount of carbon-rejected upon thermal upgrading is approximately 3 times that of catalytic upgrading. This confirmed the mass balance presented in Table 9.1 and also evident that thermal cracking is majorly carbon-rejection. As a consequence, the incorporation of catalyst improved the H/C ratio and suppressed carbon-rejection (see Table 9.1 and 9.2).

It has been reported by Klerk et al. (2014) that an increase in H/C ratio indicates a decrease in naphthenic and aromatic content relative to the original feed oil. The poly-form of these could have adversely impact on the H/C, API gravity and viscosity because of their high density and carbon content. Correspondingly, the nitrogen content decreased as thus 0.07, 0.13 and 0.12% upon thermal, fixed-bed, and dispersed micro-particulates upgrading below 0.57% (feedstock). It follows that the denitrogenation reaction was not experienced in the

same extent under thermal cracking as it was in catalytic upgrading; nevertheless the reaction was performed under nitrogen atmosphere.

Table 9.2 Micro elemental analysis of samples obtained from thermal, fixed-bed, and dispersed micro-particulates of $CoMo/Al_2O_3$ upgrading at temperature of 425 ^oC, pressure of 20 bar, stirring speed 133 rpm, CTO 0.1, and residence of 10 minutes under nitrogen atmosphere.

Samples	C (%)	H (%)	N (%)	H/C (%)	Carbon rejection (%)
Feedstock	88.82	10.17	0.57	0.114	
Produced oil (Thermal)	83.66	10.06	0.50	0.120	5.16 ± 0.8
Produced oil (Fixed-bed)	87.01	11.49	0.44	0.132	1.81± 0.4
Produced oil (micro-particulates Co-Mo/Al_2O_3)	86.85	10.75	0.45	0.124	1.97 ± 0.1

9.2.4 Produced Gas Composition

The produced gas forms one of the major products of the upgrading process with the yield up to 5.6 wt.% depending on the reaction temperature. The gas composition was determined using RGA and the results are presented in Table 9.3.

The amounts of methane and ethane produced with thermal upgrading were higher than those of catalytic upgrading process. This observation is in agreement with the results of methane and ethane in off-gas during thermal upgrading of blend of vacuum residues in a batch reactor by Sawarkar and co-workers (2007). This is because thermal cracking proceeds through free radical mechanism with methyl and ethyl being the smallest hydrocarbon radicals generated by arbitrary splits of the hydrocarbon chains while catalytic cracking of the

hydrocarbon chains in the oil proceeds in a systematic fashion of carbonium ion intermediates and beta-scission. Thus, releasing large amount of methane and ethane promoted carbon-rejection to balance the elemental hydrogen and carbon between the upgraded oil, produced gas, and coke deposit (see Table 9.1 and 9.2 for thermal upgrading alone).

Table 9.3 Produced gas composition for supported and dispersed Co-Mo/Al_2O_3 catalyst at temperature 425 ^oC, pressure 20 bar, nitrogen gas media, catalysts-to-oil ratio 0.1, stirring speed 133 rpm, and residence time 10 minutes.

Gas	Dispersed micro-CoMo (vol.%)	Fixed-bed CoMo (vol.%)	Thermal cracking (vol.%)
Methane	5.25	2.33	7.68
Hydrogen	1.66	2.4	1.47
Ethane	0.36	0.82	0.92
Carbon Dioxide	0.23	0.03	0.063
Ethene	0.1	0.03	0.13
Propane	1.48	0.23	0.94
Propene	0.3	0.14	0.25
i-Butane	0.19	0.12	0.07
n-Butane	0.45	0.06	0.16
1-Butene	0.094	0.051	0.21
cis-2-Butene	0.04	0	0
trans-2-Butene	0.06	0.02	0.05
n-Pentane	0.14	0.19	0.4
i-Pentane	0.12	0.17	0.38
Nitrogen			
Carbon Monoxide	0.01	0.02	0.063
Hydrogen sulphide	0.002	0.00042	0.00025

The light hydrocarbon gases C_1-C_5 produced with dispersed catalyst were higher than that of fixed-bed, except for ethane, n-pentane, and i-pentane. Overall, the experiment carried out with dispersed micro-catalyst produced twice the gas produced from fixed-bed. This affirmed the increase rate of reaction with fine particulate catalyst. Hashemi et al. (2013) found that in addition to light oil been produced, the emitted gases under in situ upgrading

could contribute towards viscosity reduction via miscible displacement and subsequently enhance oil recovery. It is worth mentioning that the produced H_2S upon the use of dispersed micro-particulate Co-Mo/Al_2O_3 was 4.8 and 8 times more than that produced by fixed-bed process and thermal upgrading.

9.3 Effect of Agitation and Catalyst-to-Oil Ratio

For a comprehensive understanding of mass transfer between gas-oil-solid phases, experimental runs were carried out by varying the agitation speed and catalyst loading (i.e., CTO). The amount of dispersed micro-Co-Mo/Al_2O_3 catalyst range 0.4-2 g and stirring speed 133-500 rpm at constant reaction temperature of 425 ^oC, pressure 20 bar, and time 10 minutes.

9.3.1 Effect on API Gravity, Viscosity and Products Yield

In Table 9.4, the effect of agitation and CTO on API gravity, viscosity and mass balance using micro-Co-Mo/γ-Al_2O_3 catalyst are presented. The API gravity of the produced oil increases from 9^o to 12.9^o as the stirring speed increase from 133 to 500 rpm. This represents further increase of 3.9^o at 500 rpm. The upgrading of heavy oil with dispersed micro-particulate catalyst involves mass transfer of molecules between gas-oil-catalyst phases coupled with cracking reactions occurring simultaneously. As a consequence, low stirring speed of 133 rpm causes mass transfer limitation. On the other hand, high agitation rate can cause a shift from mass transfer limited to kinetic control regime because of the increased contact allowing adequate utilisation of high surface-area-to-volume ratio of the micro-particulate catalyst.

Table 9.4 Effect of agitation and CTO using dispersed micro-particulates of Co-Mo/Al_2O_3 catalyst at 425 ^oC, 20 bar, 10 minutes reaction time and nitrogen-reaction medium. Feed oil (14^o API and 1.091 Pa.s).

Stirring speed (rpm)	**CTO (g/g)**	**API increase (^{o})**	**Viscosity (Pa.s)**	**Conversion (343 ^oC+) (%)**	**Liquid (wt.%)**	**Gas (wt.)**	**Coke (wt.%)**
133	0.1	9	0.0071	60	84.85	8.05	7.1
500	0.1	12.9	0.0032	77.4	80.55	8.15	11.3
500	0.02	9.8	0.0039	55	80.8	7.05	12.15

The above results show that the catalyst activity is controlled by the degree of catalyst dispersion via agitation (Hashemi, et al., 2013). Furthermore, higher agitation maintains the fine particles in homogenised suspension in the oil-phase which improves catalyst performance. The same trend was observed in the produced oil viscosities 0.0071 Pa.s (133 rpm) and 0.0039 Pa.s (500 rpm). As expected well-dispersed catalyst showed higher activity. However while the yield of coke increase by 4.2 wt.%, the yield of liquid products decrease by 4.3 wt.% at 500 rpm compared to 7.1 wt.% (coke) and 84.85 wt.% (liquid) at 133 rpm. Micro-particulate catalyst increases the yield of low-boiling fractions by lowering the activation energies (Rezaei, et al., 2013).

From Table 9.4, it can be observed that high CTO increased API gravity, high conversion (BP > 343 ^oC), and lowered viscosity values were obtained compared to low CTO at the same agitation 500 rpm. As the CTO increased, the yield of coke and light oil decreased. A similar trend was reported by Shuyi et al. (2008). This is because at high CTO catalytic cracking dominate thermal cracking, thereby inhibiting the extent of carbon-rejection. Furthermore, comparing the level of upgrading at CTO (0.02) and agitation 500 rpm with that obtained at CTO (0.1) and agitation 133 rpm at the same temperature (425 ^oC)

and pressure (20 bar), it can be observed that the mass transfer between gas-oil-solid phases during upgrading reactions at 133 rpm was limited.

9.3.2 Effect on TBP Distribution

The yield of the (IBP-200 ^{o}C), (200-343 ^{o}C) and (343 ^{o}C-FBP) fractions from the produced oil as a function agitation and CTO are presented respectively in Figure 9.3 (a) and (b). It can be seen that some of the middle fractions (200-343 ^{o}C) and the heavy fractions (> 343 ^{o}C) in the feedstock have been converted to low-boiling fractions (IBP-200 ^{o}C) during the upgrading using micro-particulate Co-Mo/Al_2O_3. Subsequently, the conversion of high-boiling fractions (> 343 ^{o}C) at 500 rpm was 77.4 % and 60 % (133 rpm). This represents 17.4 % increase, as reflected in additional 4 % rise in low-boiling distillates and 4.4 % drop in heavy fractions compared to that obtained at 133 rpm (see Figure 9.3a).

From Figure 9.3b, it can be seen that the produced oil at CTO (0.1) has high low-boiling fractions (IBP – 200 ^{o}C) and low residue fraction (> 343 ^{o}C) than that of CTO (0.02) at 500 rpm. However, the middle distillates (200 – 343 ^{o}C) of the produced oil at CTO (0.02) was 4.53 vol.% higher than 33.8 vol.% for CTO (0.1). This shows that higher catalyst loading advanced the conversion of heavy fractions into low-boiling fractions. The results therefore show that the cracking reaction mechanism follows the pathways shown in Figure 9.4: the heavy feedstock molecules crack to form gas (C_1-C_5, H_2), gasoline fractions, middle distillates, coke, and unconverted heavy fraction. As the agitation and CTO increases, it resulted in subsequent conversion of middle and residue fractions into light fractions, gas, and coke. Puron et al. (2014) found that the yield of coke was majorly from the cracking of residue fraction. Therefore, the low viscosity and API gravity increase observed can be attributed to the thinning effect of the high yield of IBP-200 ^{o}C.

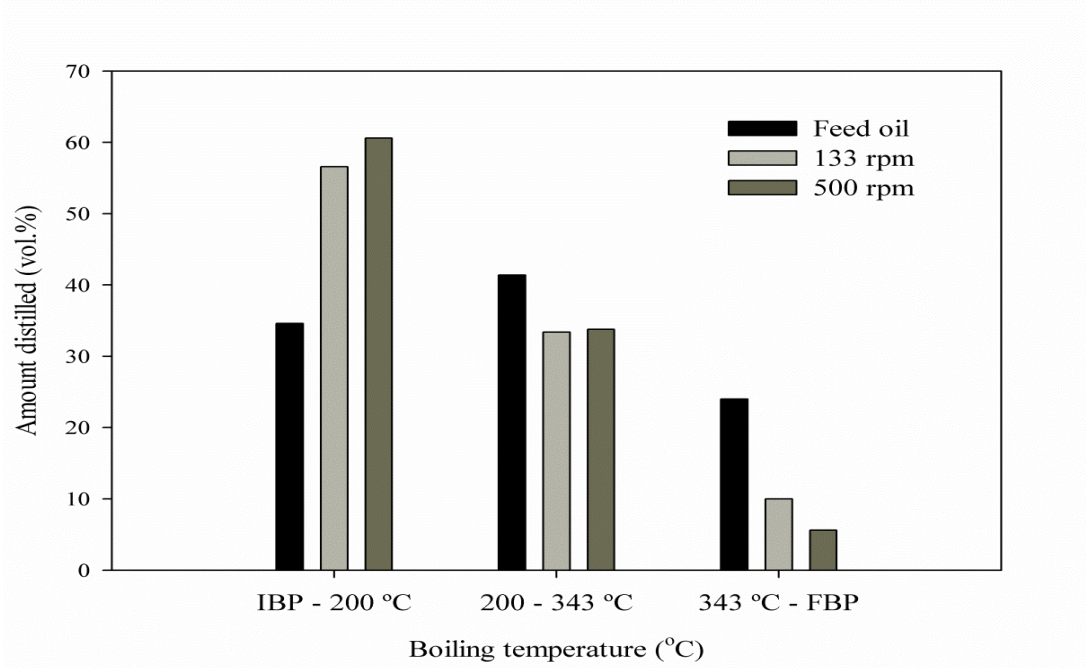

(a)

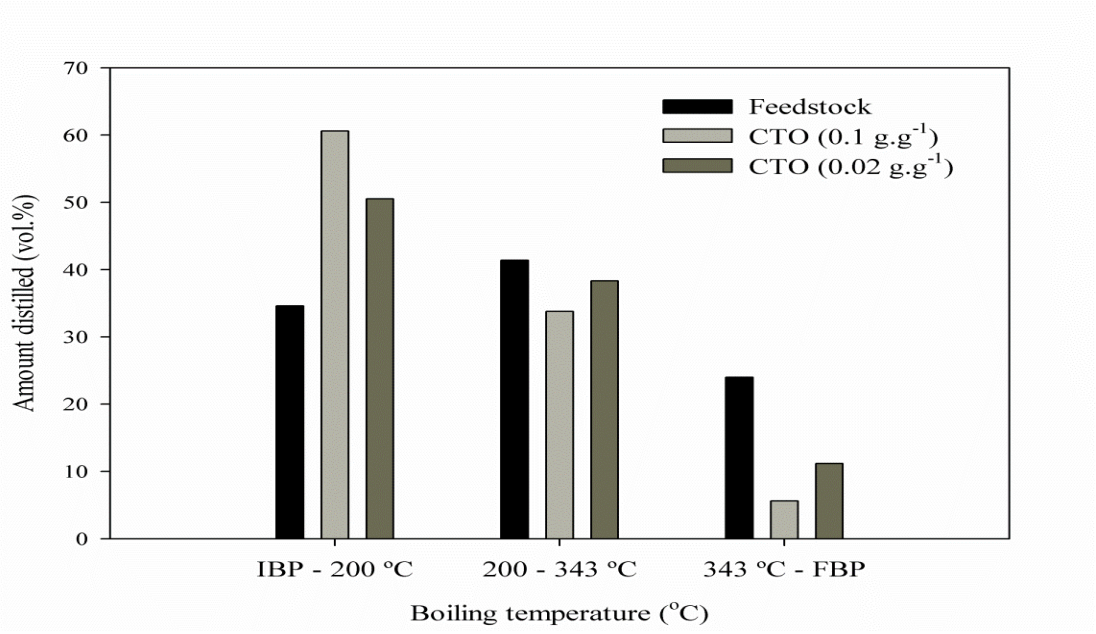

(b)

Figure 9.3 Produced oil amount distilled as function of (a) Agitation, and (b) CTO; using micro-particulates of Co-Mo/Al_2O_3 catalyst at temperature of 425 °C, pressure 20 bar, nitrogen gas media, catalysts-to-oil ratio 0.1, and residence time 10 minutes.

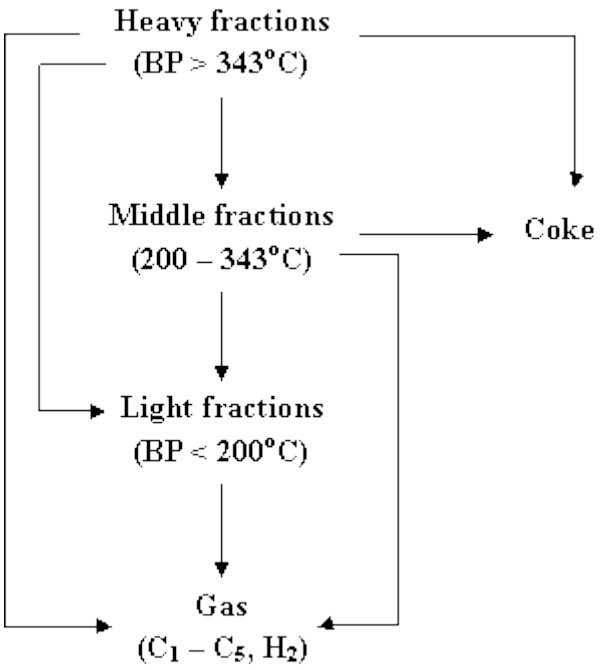

Figure 9.4 Reaction pathways during dispersed catalyst upgrading.

9.4 Microparticulates of Bio-Pd vs. Co-Mo/Al_2O_3 Catalysts

In this section, the level of heavy oil upgrade obtained by dispersed micro-particulates of Co-Mo/Al_2O_3 (2.5 µm) and microparticulates of bio-Pd (20%) were tested. The microparticulates of bio-Pd were prepared by reducing a solution of sodium tetrachloropalladate (II) (Na_2PdCl_4) on an anaerobic bacterium (*Desulfovibrio desulfuricans* NCIMB 8307 to make a 20% bio-Pd) with an average particle size of 13.8 µm. Therefore, upgrading by the biomanufactured catalyst was compared with its chemical counterpart.

9.4.1 Mass Balance, API Gravity, Viscosity and Conversion

In Table 9.5, the level of upgrading by thermal, microparticulates of Co-Mo/Al_2O_3, microparticulates of Al_2O_3, and microparticulates of bio-Pd (20%) at 425 ^oC temperature, 0.02

CTO, 20 bar pressure, 500 rpm agitation under nitrogen and hydrogen reaction gas are presented. The reported data are an average of duplicate experimental runs with standard deviation for API gravity and viscosity as follows: thermal (0.32 ^{o}API and 0.004 Pa.s), micro-CoMo/Al_2O_3 (0.26 ^{o}API and 0.002 Pa.s), micro-bioPd (0.3 ^{o}API and 0.001 Pa.s), and micro-Al_2O_3 (0.34 ^{o}API and 0.003 Pa.s), respectively. After upgrading, the produced oil API gravity increased while the viscosity decreased significantly compared to the feed oil (14 ^{o}API and 1.091 Pa.s). However, the incorporation of micro-particulates of Co-Mo/Al_2O_3 or bio-Pd catalysts further increased the API gravity by 2 to 3.5^{o} above that obtained in a blank experimental run (6.5 ^{o}API) for both nitrogen and hydrogen environment. A similar trend of observation can be seen for the viscosity. The overall viscosity reductions therefore range from 96 to 99.4 % below 1.091 Pa.s (feedstock).

Table 9.5 Produced oil upgrade using thermal, micro-CoMo/Al_2O_3, micro-Al_2O_3, and micro bioPd (20%) at 425 ^{o}C temperature, 0.02 CTO (except thermal upgrading), 20 bar pressure, and 500 rpm agitation under nitrogen or hydrogen reaction media. Feed oil (14 ^{o}API and 1.091 Pa.s).

Experiments	**API increment (^{o})**	**Viscosity (Pa.s)**	**Conversion (343^{o}C+) (%)**	**Liquid (wt.%)**	**Gas (wt.)**	**Coke (wt.%)**
Thermal + N_2	6.4	0.018	33.2	77.1	10.55	12.35
Thermal + H_2	6.5	0.013	46	78.9	11.3	9.8
Micro-CoMo + N_2	9.8	0.004	55	80.8	7.05	12.15
Micro-CoMo + H_2	10.1	0.006	67.7	83.15	7.95	8.9
Micro-Al_2O_3 + H_2	8.9	0.004	51.6	73.05	13.3	13.65
Micro bio-Pd (20%) + N_2	8	0.0097	37.1	87.13	6.94	5.93
Micro bio-Pd (20%) + H_2	8.2	0.009	63.7	88.4	7.73	3.87

Comparing the level of upgrading, it is clear that the produced oil with micro-particulates of Co-Mo/Al_2O_3 has roughly 2 ^{o}API gravity higher and 0.005 Pa.s viscosities lower than that produced with micro-bioPd (20%). This noticeable difference in API gravity and viscosity can be attributed to the acid sites of the alumina support of Co-Mo, which are thought to be responsible for the cracking reactions.

In contrast, the yield of coke in the experimental run with micro-particulates of Co-Mo/Al_2O_3 doubled that of micro-bioPd for both nitrogen and hydrogen environment. This is because in addition to thermal reactions the alumina support was actively involved in cracking reactions, which triggers the formation of radicals that polymerise into coke. Puron et al. (2014) pointed out that the formation of coke during catalytic upgrading process depends on catalyst type in addition to reaction temperature and mass transfer. Hence, the non-acidic support of micro-bioPd could have played an active role in suppressing coke formation. In fact this was confirmed from the experiment performed with micro-particulates of Al_2O_3, which showed an increase in coke yield by 4.8 wt.% above observed 8.9 wt.% (Co-Mo/Al_2O_3) under hydrogen atmosphere. Correspondingly, the 13.3 wt.% yield of gas upon the use micro-Al_2O_3 against 7.95 wt.% (Co-Mo/Al_2O_3) also supported the effect of acid sites in promoting the reaction routes that lead to coke and gas formation instead of maximising liquid product under hydrogen atmosphere.

Hydrogen-addition to the catalytic upgrading experiment using dispersed micro-particles promoted the conversion of residue fraction while maximising the yield of liquid product. Thermal upgrading appears to give high yield of coke, while the use of dispersed micro-CoMo/Al_2O_3 and micro-bioPd resulted in low yield of coke except micro-Al_2O_3. The fact that micro-Al_2O_3 did not have any hydrogenation function (with no added metals such as Co, Mo, etc.) led to catalytically controlled C-C bond cleavage reaction. Meaning the splitting

of C-C bonds was enhanced by their strong acid sites, therefore yielding large amounts of gas and coke (Leyva, et al., 2007; Klerk, et al., 2014). Despite the presence of hydrogen, hydroconversion was limited because of the absence of metals such as Ni, Co, Mo, etc.

9.4.2 TBP Distribution

The amount of distillate fractions upon SIMDIS of the produced oil from the use of thermal, micro-CoMo/Al_2O_3, micro-Al_2O_3, and micro-bioPd (20%) are presented in Figures 9.5(a), (b) and (c), respectively. It is worthy to note that the difference in the yields of low-boiling fractions between the feedstock and the samples after reaction confirmed that upgrading took place.

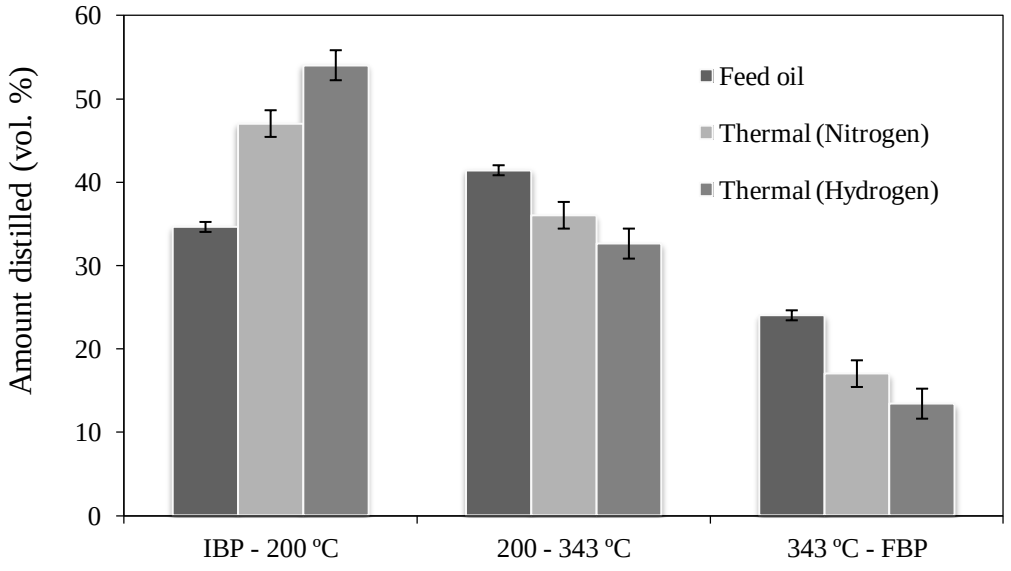

(a)

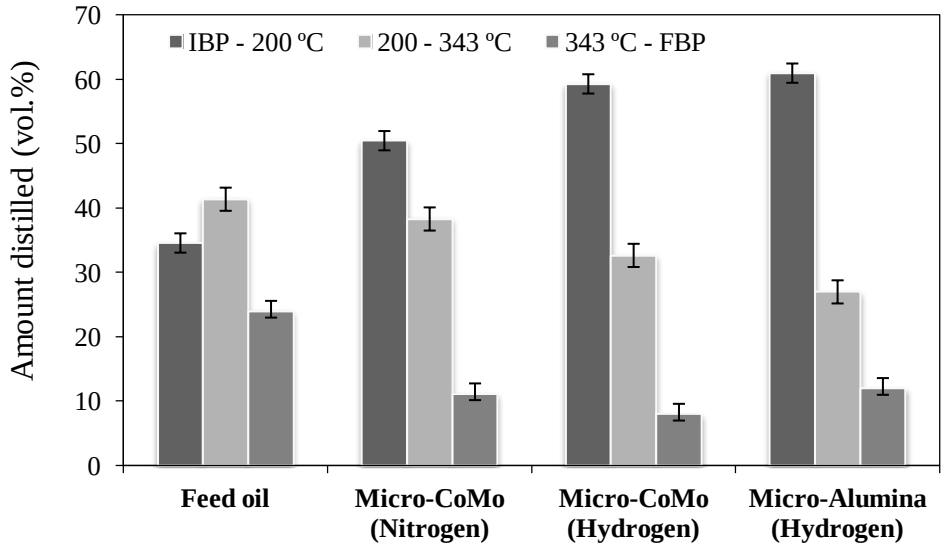

(b)

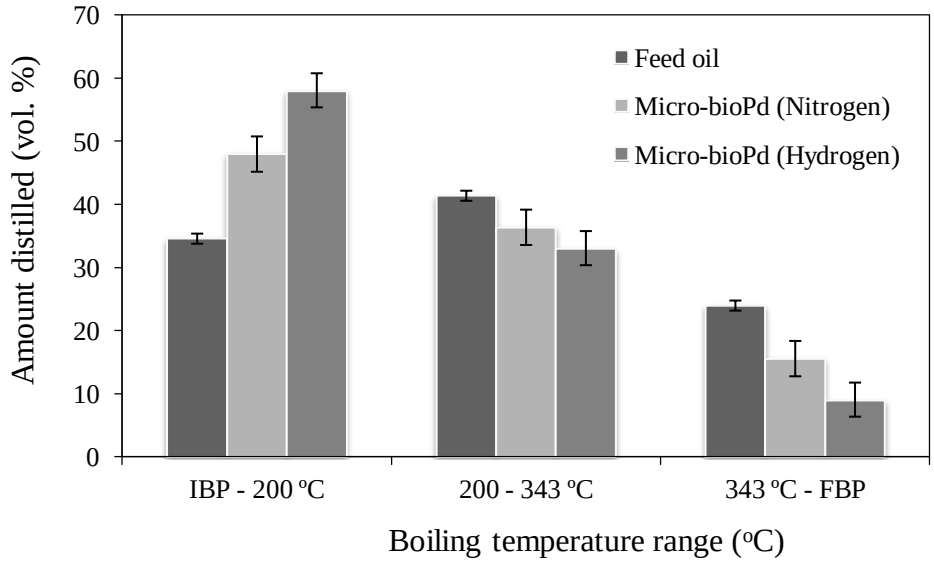

(c)

Figure 9.5 Amount distilled at different boiling temperature ranges upon simulated distillation of produced oil from the use of (a) thermal upgrading, (b) micro-particulates of Co-Mo/Al_2O_3 and Al_2O_3, and (c) micro-bioPd (20%) catalysts at temperature of 425 ^oC, pressure of 20 bar, CTO of 0.02, stirring speed 500 rpm, and residence time 10 minutes under N_2 and H_2 environments.

The common transport fuels are gasoline, diesel, and jet fuel of which their boiling range falls within 35-343 ^{o}C. Therefore, comparing hydrogen and nitrogen reaction environment, it is clear from Figures 9.5 (a)-(c) that hydrogen-addition route to upgrading increased the yield of (IBP – 200 ^{o}C) fraction by 7 % (thermal), 8.83% (micro-CoMo/Al_2O_3) and 10% (micro-bioPd), while the residue fraction (343 ^{o}C+) decreased by 3.6% (thermal), 3.17% (micro-CoMo/Al_2O_3), and 6.6% (micro-bioPd), respectively compared to upgrading under nitrogen atmosphere. Thermally upgraded oil gave the lowest and highest yields of low-boiling fractions and residue. Hydrogen-addition therefore increased the fuel distillates without a substantial decrease in liquid product yield (see Table 9.5). Hydrogen molecules are known to split into active H• over the catalyst surface, and the H• radicals are thought to be responsible for hydrogenation of coke precursors and lowering coke yield. Whereas reaction under nitrogen atmosphere the intermediate radicals readily reassemble to form residue fraction and coke.

Fine particulate catalyst possesses much more accessible active sites per unit mass, which enhances the extent of metal utilisation. The results presented here are line with those reported by Alkhaldi and Husein (2014). They found that heavy oil upgrading activity of fine particulate catalyst is metal dependent. However, most of the particulates tend to agglomerate and become incorporated with the produced coke, but yield of coke decreased under hydrogen because of hydrogenation reaction. Furthermore, under the same conditions the bioPd releases Pd metal to activate the hydrogen required to stabilise the free radicals produced by thermal cracking of heavy oil. The structure of the micro-bioPd promote hydrogen uptake for hydroconversion reactions.

9.4.3 Produced Gas

The composition of produced gas evolved using micro-particulates of Co-Mo/Al_2O_3, microparticulates of bioPd, and thermal upgrading under nitrogen environment are presented in Table 9.6. Upgrading by thermal cracking produced more nC_1 – C_5 light hydrogen in the gas compared to the catalytic counterpart. This explains the high carbon-rejection upon thermal upgrading. However, the use of micro-particulates of Co-Mo/Al_2O_3 produced more olefins than thermal cracking.

Table 9.6 Produced gas upon upgrading under nitrogen atmosphere using thermal, micro Co-Mo/Al_2O_3, and micro-bioPd at 425 ^oC, 20 bar, 500 rpm, 0.02 CTO, and 10 minutes reaction time.

Gas	Micro-CoMo (vol.%)	Micro-bioPd (vol.%)	Thermal (vol.%)
n(C_1-C_5)	7.68	6.34	10.1
i(C_4-C_5)	0.31	0.87	0.45
Olefin (C_2-C_4)	0.59	0.37	0.39
CO_2	0.23	0.41	0.1
CO	0.01	0.16	0.1
H_2S	0.002	0.001	0.0003
H_2	1.66	1.15	1.47

This indicates that catalytic upgrading reaction did occur. It is noteworthy that reaction carried out with microparticulates of bioPd produced less hydrogen compared to thermal and micro Co-Mo/Al_2O_3. This can be as a result of more interaction of Pd with hydrogen-transfer reactions.

9.5 Conclusions

The experimental results have demonstrated potential of in-situ catalytic upgrading process at laboratory-scale. It was found that the dispersed fine particulate catalyst has greater surface-area-to-volume ratio, therefore showed high activity and performance compared to fixed-pelleted catalyst. This study of dispersed particulates will provide better understanding and design of field-scale process. The upgrading effects were primarily due to heavy hydrocarbons cracking over the dispersed particulate catalysts in a heated zone, which delivers 7 to 10 ^{o}API gain in API gravity, 97.8 % viscosity reduction, as well as improved yield of fuel distillates. However, the challenge of recovery and reuse the nano-catalyst after reaction need to be addressed.

Chapter 10

Conclusions and Recommendations

10.1 Conclusions

In a time of surging global energy demand, petroleum industries and researchers are actively investigating means of extracting vast deposits of heavy oils and bitumen using diverse enhanced oil recovery (EOR) techniques. THAI-CAPRI technology involves subsurface catalytic upgrading process *in situ* aimed at simultaneously extracting heavy oils and converting them into light oil prior to reaching the surface. Upgrading produces a crude oil with similar characteristics to conventional light crude oil that can meet refinery feedstock qualities. This involves carbon-subtraction, hydrogen-addition as well as heteroatom removal.

The surface upgrading facilities presently in use demand huge capital investment to build and maintain the upgrader, and are energy-intensive leading to substantial amount of greenhouse gas emissions. Down-hole upgrading in situ using CAPRI offers the following advantages: 1) less energy-intensive as it utilises heat energy from an *in situ* combustion to drive the catalysis, 2) most of the impurities such as sulphur and heavy metals are left behind in the reservoir lowering environmental footprint, 3) reduce sand handling and 4) produce partially upgraded oil to the surface with significant fluidity that will reduce capital cost for lifting operation and transportation from underground to the refinery (Speight, 2013; Hashemi, et al., 2013).

The target was to upgrade the Whitesands partially upgraded heavy oil by THAI process of 13-14 ^{o}API gravity to an API gravity of 18-22 ^{o}API, considerably lower the viscosity to enhance fluidity for pipeline transportation. With the asphaltenes, sulphur and

metals content lowered remarkably. A laboratory micro-fixed catalyst bed was used to replicate the CAPRI section of the THAI process. The impact of operating parameters, feedstock, catalyst type, guard-bed on top the catalyst bed, hydrogen-addition, and steam-environment upon upgrading and coke formation was investigated. The major challenge of the fixed catalysts bed was the deactivation which decreases the activity and lifetime. The formation of coke and the deposit of metals were detrimental to the process efficiency and to the catalyst performance. In the light of this, alternative contacting method between the oil and catalyst was investigated using nanoparticulate catalyst.

Effect of Temperature, WHSV, and Feedstock

In reality, during the THAI process the lighter and more volatile hydrocarbon components move rapidly through the reservoir. The slower moving heavy molecular weight components such as resins and asphaltenes are subjected to cracking and coking reactions. Thermal upgrading by carbon-rejection occurs in the THAI process and subsequent catalytic cracking upgrading in CAPRI process incorporated to the horizontal producer well. The experimental results of the CAPRI process in this study have shown an increase in API gravity by ~3-9 ^{o}API points and 40-85 % reduction of viscosity on top the *in situ* thermally upgraded oil by THAI alone. This is dependent on the upgrading temperature, weight hourly space velocity (WHSV), and oil flow rate across the catalyst bed. Based on these results, the combination of THAI and CAPRI could deliver in situ upgrading that could produce oil that can be transported by pipeline without diluents, which lowers refining cost.

It was found that high reaction temperature (425 ^{o}C) favoured the C-C and C-heteroatom bond cleavages which led to improved yields of low-boiling distillates, removal sulphur and heavy metals, in addition to significant viscosity reduction compared to 350 and

400 ^{o}C. At the same time, it causes high dehydrogenation and condensation reactions, which resulted to high catalyst deactivation due to high coke formation. The results on the effect of WHSV clearly showed that low WHSV of 9.1 h^{-1} was necessary to accomplish a fairly good upgrading in terms of API gravity, viscosity reduction, and conversion of 343 ^{o}C+ fractions of the heavy oil into light oil. On the other side, deactivation by coke is minimised at high WHSV due to less acid sites, short residence and contact time between the oil and the catalyst bed. Deactivation is linked to activity and lifetime of the catalysts, as illustrated in Figure 10.1. The economy of the process strongly depends on the catalyst lifetime.

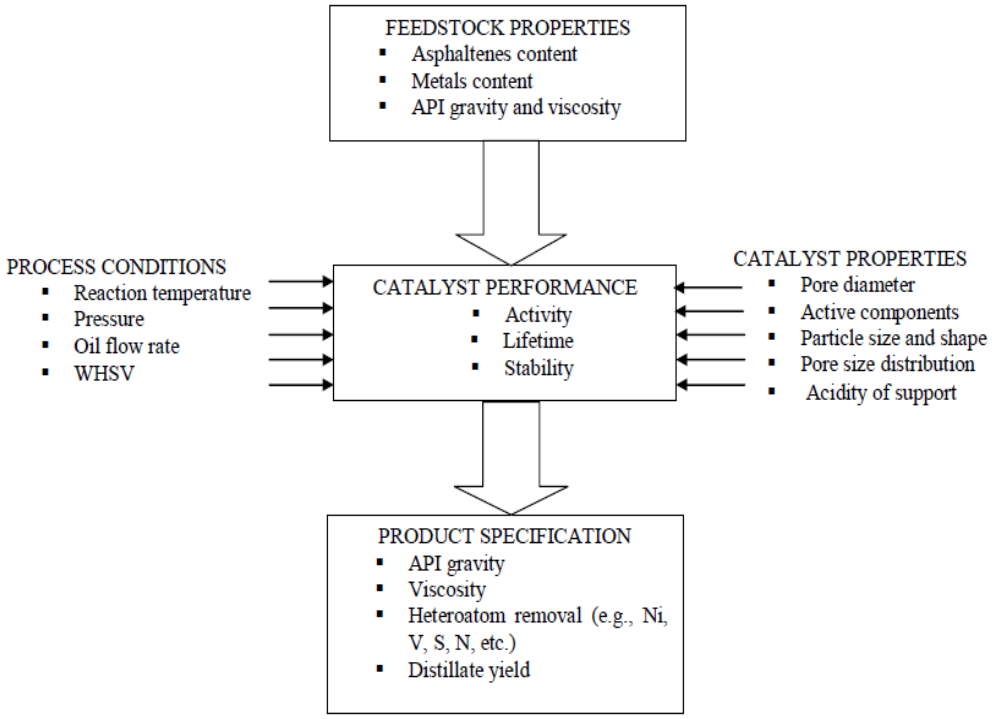

Figure 10.1 Factors affecting the performance of heavy oil upgrading catalysts.

The activity of the catalyst was found to decrease rapidly with time owing to aging of the catalyst caused by coke and metals deposition. This therefore suggests that the development of catalyst system which can tolerate deposition of coke, sediment, and metal,

under reservoir conditions will open up commercialisation of THAI-CAPRI process. The study has shown that the decrease in catalyst activity is the result of the deposited coke and metals which are associated with highly aromatic, hydrogen deficient, and metal-containing asphaltenic and resinic structure in the heavy oil released during the catalytic upgrading. In addition to catalyst deactivation, CAPRI process in fixed-bed catalyst involves typical challenges such as hot spot occurrence and pressure drop build-up. The performance of catalyst used in CAPRI is therefore dependent on numerous parameters: feedstock composition, contact time between oil and catalyst, catalyst properties, and operating conditions.

Effect of Hydrogen and Steam Environment

The ability to control deactivation in CAPRI will facilitate down-hole catalytic upgrading of heavy oil and its economy. With a view to controlling catalyst deactivation, hydrogen and steam addition were investigated. When hydrogen was added to the CAPRI process, it was also found that the API gravity of the produced oil increased further by point ~1 to 2 ^{o}API and viscosity reduced further by 6-8%, in addition to the 6^{o} API and 82% viscosity reduction obtained using Co-Mo/Al_2O_3 and/or Ni-Mo/Al_2O_3 under nitrogen atmosphere. After CAPRI upgrading under the different gas environments, the spent catalyst coke contents are as follows: 23.5 wt.% (nitrogen), 20.08 wt.% (THAI gas), 20.4 wt.% (methane) and 17.4 wt.% (hydrogen), respectively for 6 hours time-on-stream operation. It was observed that the spent catalyst coke content after upgrading was carried out under hydrogen atmosphere was significantly decreased compared to nitrogen and THAI gas environment. This is because hydrogen effectively moderates the addition reactions of macromolecules of asphaltenes and resins radicals that results in coke formation compared to

when the reaction was carried out under the other gas environments such as nitrogen and methane.

Consequently, because of the challenges of introducing hydrogen into the reservoir during the THAI-CAPRI recovery and upgrading process, an alternative in-situ technique of donating hydrogen via water-gas-shift reaction from steam was investigated. It was found that upon steam atmosphere an overall viscosity reduction of 88 to 92 % was observed as the steam/oil ratio increased from 0.02 to 0.1 compared to 85.5 % observed when the reaction was carried out under nitrogen environment alone. Correspondingly, demetallization and desulphurisation increase in the range of 43 to 70.5 % and 16 to 25.6 % as the steam/oil ratio increased from 0.02 to 0.1 compared to 16.8 % (demetallization) and 3.4 % (desulphurisation) observed under steam-free (nitrogen) atmosphere. Also, an additional 1 ^{o}API gravity above the 3 ^{o}API (steam-free atmosphere) was noticed upon steam-addition. This improvement of produced oil quality when steam was added can be attributed the role played by the donated hydrogen through water-gas-shift reaction. It was also found that after CAPRI upgrading in nitrogen and nitrogen plus steam environment, the spent catalyst coke content were thus 27.53 wt.% (nitrogen) and decreased to 17.02 – 11.2 wt.% as the steam/oil ratio was increased from 0.02 to 0.1. These results showed that steam and hydrogen environments were capable to improve the fluidity of the produced oil as well as decreased coke formation and removing sulphur and metals.

In order to understand the role of hydrogen on poly-aromatic compounds, anthracene was selected as model compound. It was found that hydrogenation, hydrocracking, and hydro-refining function of the bi-functional HDS catalyst (i.e., Co-Mo and Ni-Mo) in the presence of hydrogen was responsible for the improved API gravity, reduced viscosity and reduced coke formation. The effect of hydrogen pressure on coke content of the catalyst is more effective at

high pressure of 40 bar and 425 ^{o}C reaction temperature, because the hydrogen transfer to the gas-oil interface has been considered faster compared to the rate of hydrogen uptake due to upgrading reactions in the oil phase (Panariti, et al., 2000b). The produced gas analysed by RGA showed that the addition of hydrogen prevents olefin addition reactions by promoting direct olefin hydrogenation and partial hydrogenation of polynuclear aromatic hydrocarbons. The hydrogenation of olefins during the upgrading of heavy oil is vital as the polymerisation of olefins has the capacity to form large molecular weight compounds that can lead to the formation of coke. Nevertheless, hydrogen-addition to the CAPRI process suppressed these addition reactions.

Use of Guard Bed

The challenges of rapid fouling and coking leading to deactivation of the catalytic bed was remedied with the use of activated carbon (AC) guard bed on the top the catalyst bed to trap macromolecules and particulate which are known foulant and coke precursors in the feed oil. This was confirmed by 21 wt.% reduction of catalyst coke content after upgrading was carried out with Co-Mo/Al_2O_3 only and AC on top of Co-Mo/Al_2O_3 catalyst at the same conditions and 20 hours time-on-stream. In this way, it was possible to prolong the catalyst lifetime by additional 10 hours, improved API gravity by approximately 2^{o} and 4-6% further viscosity reduction. It therefore makes more effective use of the downstream catalytic bed. The Ni + V metal content of the feed heavy oil (206 ppm) decreased by 10 % (Co-Mo/Al_2O_3 only) and 70.9 % (AC on top of Co-Mo/Al_2O_3 catalyst). At the same time, the asphaltenes content of the produced oil was 5.99 wt.% when upgrading was carried out with Co-Mo/alumina catalyst only and 3.95 wt.% upon the use of AC on top of Co-Mo/Al_2O_3 catalyst against 11.14 wt.% for the feed oil.

The incorporation of a bed of AC on top of the catalytic bed gave better improvement in API gravity, viscosity reduction, and low coke content than the use of alumina support as guard bed. With this scheme, it was possible to remove some of the macromolecules from the feed oil at the first stage, reducing the asphaltenic and resinic content of the oil before proceeding to the catalytic cracking upgrading in the next stage; this reduced the coking propensity of the oil and improved upgraded oil flow properties compared to the upgrading performed without AC guard bed. The reduction in catalyst coke content for this scheme was due to the reduced possibility of asphaltenes precipitation in the catalytic bed. However, this scheme introduces additional challenge to packing the horizontal producer well.

Fixed-bed and Dispersed Micro-Catalyst

Based on the challenges associated with fixed-bed catalyst, alternative contacting technique using nanoparticulate catalyst was investigated. In this approach, once-through nano-particulate catalyst was used to surmount the catalyst deactivation caused by coke and metal deposition upon fixed-bed catalyst. The key factor to handling heavy oil is reducing the viscosity. After upgrading with fixed-bed and dispersed particulate catalyst, the produced oil API gravity and viscosity for fixed-bed (5.6 ^{o}API and 0.0284 Pa.s) and dispersed micro-catalyst (8.7 ^{o}API and 0.007 Pa.s) compare to the heavy feed oil (13 ^{o}API and 1.091 Pa.s). It was found that the API gravity and viscosity reduction further increased by 3 ^{o}API and 2% upon the use particulate catalyst. This is because of the improved contact and high surface-area to volume ratio resulting from particle size reduction.

In comparison to the thermal upgrading, all catalysts tested were effective for the conversion heavy fractions into low-boiling fractions as well as decreasing viscosity. However the effectiveness remarkably varied with the type of catalyst, the type of metals (Co,

Ni, Mo, Pd, etc.), the support material, and the textural properties of the catalyst. It was found that the extent of coke formation during CAPRI depends on the catalyst type and properties, the feedstock properties, and the operating condition. Additionally, the coke content of the catalyst increases with the increasing conversion of 343 ^{o}C+ HC fractions and decreasing viscosity of produced oil. Also, the yield of low-boiling fuel distillates increased and coke formation suppressed when upgrading was carried out under hydrogen compared to nitrogen atmosphere. The experimental results showed that the extent of heavy oil conversion to light oil via CAPRI is not only a function of reaction temperature but also dependent upon the heavy oil composition, residence time, catalyst properties, and reaction media.

Conclusively, *in situ* upgrading of heavy crude oil enhances oil production, benefits pipeline transportation through reduction of diluents, and most of the impurities such as sulphur and metals are left behind in the reservoir, lowering impact on downstream processes and the environment. There is a major benefit from reduction of surface upgrading facilities.

10.2 Recommendations

The use of fixed-bed catalyst display short service life due to carbon and heteroatoms deposits, poor operation stability because of gradual increase in pressure drop, and subsequently experienced periodic shut-down. In the light of the above challenges, slurry-phase catalytic upgrading process is proposed for further investigation. The concept adopts unsupported dispersed catalysts which include heterogeneous nano-catalysts and homogeneous (either water-soluble or oil-soluble) dispersed catalysts. The difference therefore is that catalytic upgrading reactions will take place at the porous media of the reservoir rather than across a fixed-catalyst bed incorporated to the horizontal producer well.

The gradual build up of pressure drop and subsequent shutdown due to asphaltenes and coke coverage of the catalyst pores and inter-particles void can be overcome using graded catalyst packing arranged as thus macro- and mesopores materials in layers is therefore recommended for future investigation. Also, a structured monolithic catalyst with macro-channels and meso-pores walls is potential candidate for future studies, as an alternative to overcoming the challenges of high pressure drop in fixed-bed and as a result of coke, asphaltenes, and heavy metal deposits.

Most of the experiments carried out in the fixed-bed CAPRI process were done in one-dimensional representation. Therefore, future studies should focus on 3-dimentional laboratory-scale of the CAPRI process. This will provide a comprehensive understanding of the field application compared to fixed-bed model. Additionally, the contribution of sulphur and heavy metals to catalyst deactivation requires further investigation as most of the deactivation evaluation here was done mainly on the bases of coke deposit.

In-situ regeneration of the spent HDT catalyst will improve process economics. Further studies should involved developing suitable catalyst for *in situ* upgrading process rather than using commercially manufacture HDS catalyst mainly for surface refining processes. Characteristics of the catalyst should include high metal retention capacity, moderate acidity, slow to deactivation by coke deposition, and ability to withstand the salinity of the reservoir fluids. As microporous catalysts limit diffusion and promote pore plugging and external deposition of coke and metals, the structural characteristics should include macro- and mesopores to facilitate the diffusion of macromolecules and minimise deposition within the pore channels. In addition to this, knowledge of the molecular size of the macromolecules in the heavy oil is therefore essential for the development of the catalyst.

Appendix A

Characterisation of Catalyst and Guard bed Material

A.1 Nitrogen adsorption-desorption isotherm of catalyst, activated carbon and alumina support

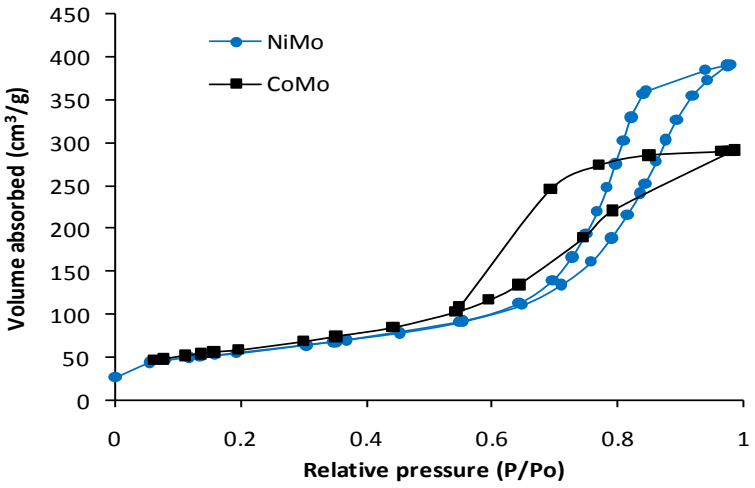

(a)

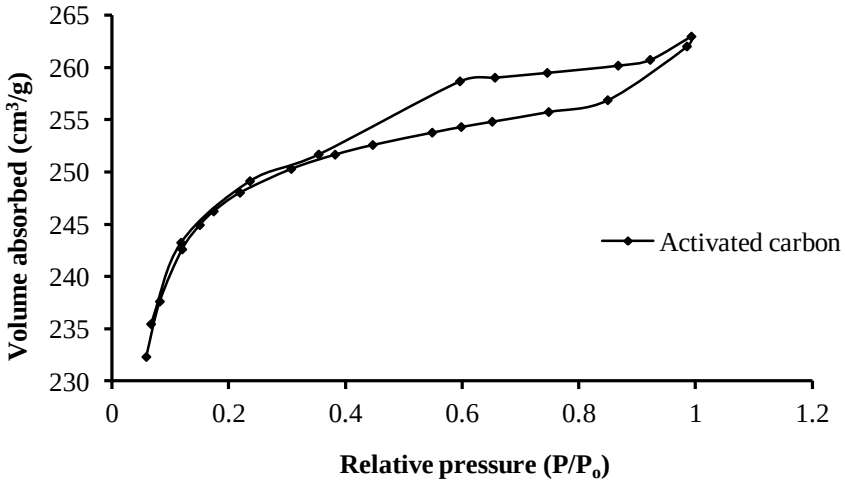

(b)

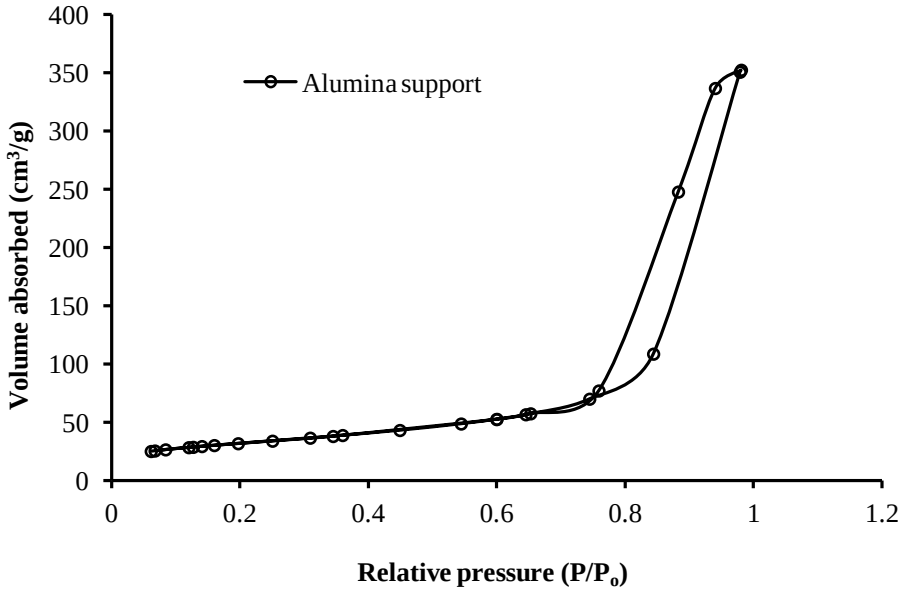

(c)

Figure A.1 Nitrogen adsorption-desorption isotherm: (a) Co-Mo/Al2O3 and Ni-Mo/Al2O3 catalyst, (b) Activated and (c) Alumina support.

It is clear from Figure A.2c that the alumina support has small pores and pore volume compared to the activated carbon (Figure A.2b) material as the hysteresis loop is small and falls in the region of high relative pressure.

A.1.2 Calculation of BET Surface Area

In Figure A.2, the BET plot of the nitrogen sorption data of fresh Co-Mo/Al_2O_3 using equation 3.12 is presented.

$$\frac{P}{V(P_o-P)} = \frac{1}{V_m C} + \frac{(C-1)P}{V_m C P_o} \qquad (3.12)$$

where p is the partial pressure of N_2, P_o is the saturation pressure at the experimental temperature, V volume adsorbed at P, V_m volume adsorbed at monolayer coverage, and C a constant.

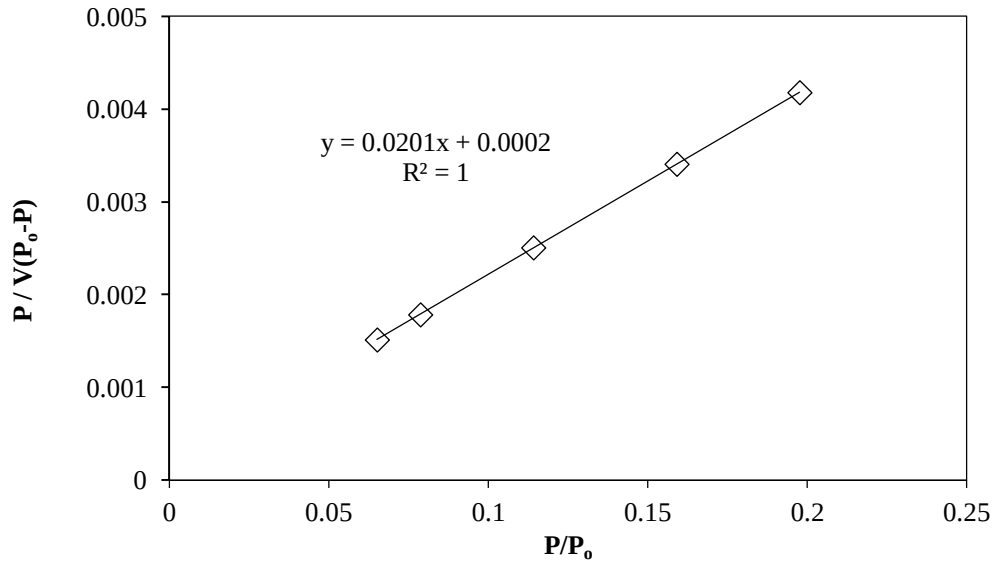

Figure A.2 BET plot of fresh Co-Mo/Al_2O_3.

From Figure A.2:

$1 / V_m C = 0.0002$

$(C – 1) / V_m C = 0.0201$

It follows that C = 101.5 and V_m = 49.26 $cm^3.g^{-1}$. The BET surface area is however calculated using equation (3.13):

$$S_{BET} = \frac{v_m n_a a_m}{m_v} \qquad (3.13)$$

where; V_m is 49.26 $cm^3.g^{-1}$, n_a is the Avogadro's number (6.022 x 10^{23} mol^{-1}), a_m is the cross-sectional area occupied by each adsorbate molecule at 77 K (0.162 nm^2) and m_v is the gram-molecule volume (22.414 mL). Therefore, SBET for fresh Co-Mo/Al_2O_3 is 214.1 $m^2.g^{-1}$.

A.2 Mercury porosimetry of catalyst, activated carbon and alumina support

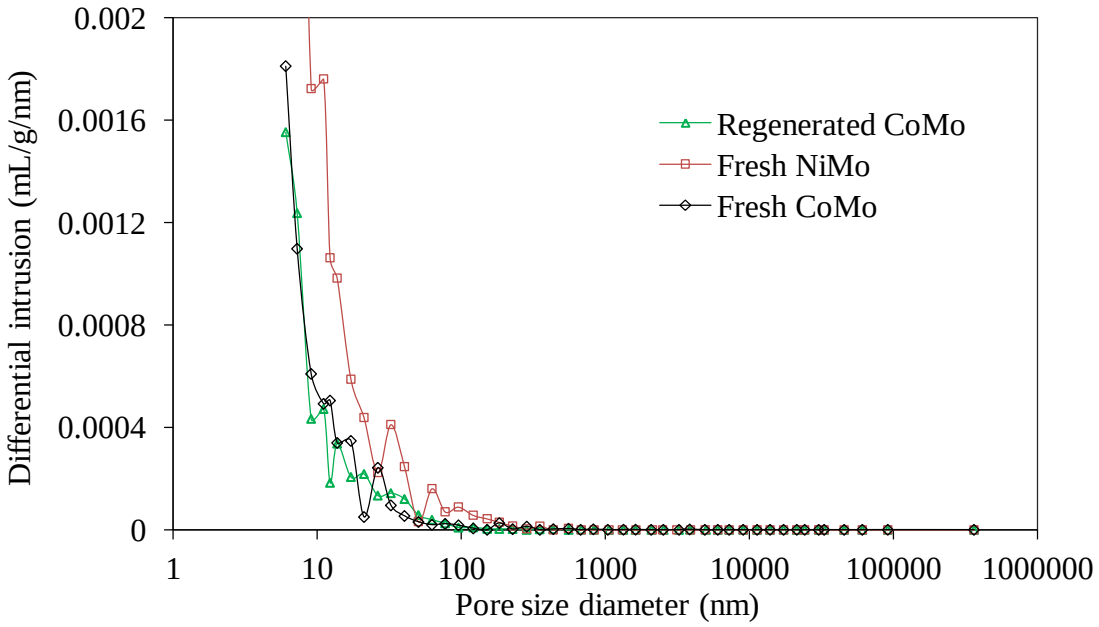

(a)

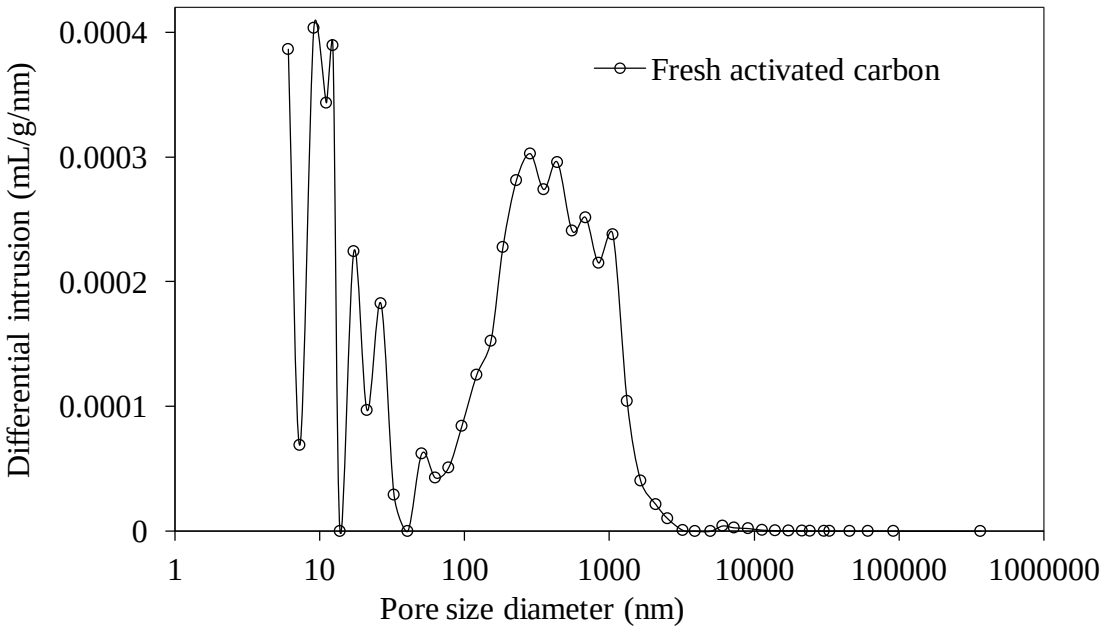

(b)

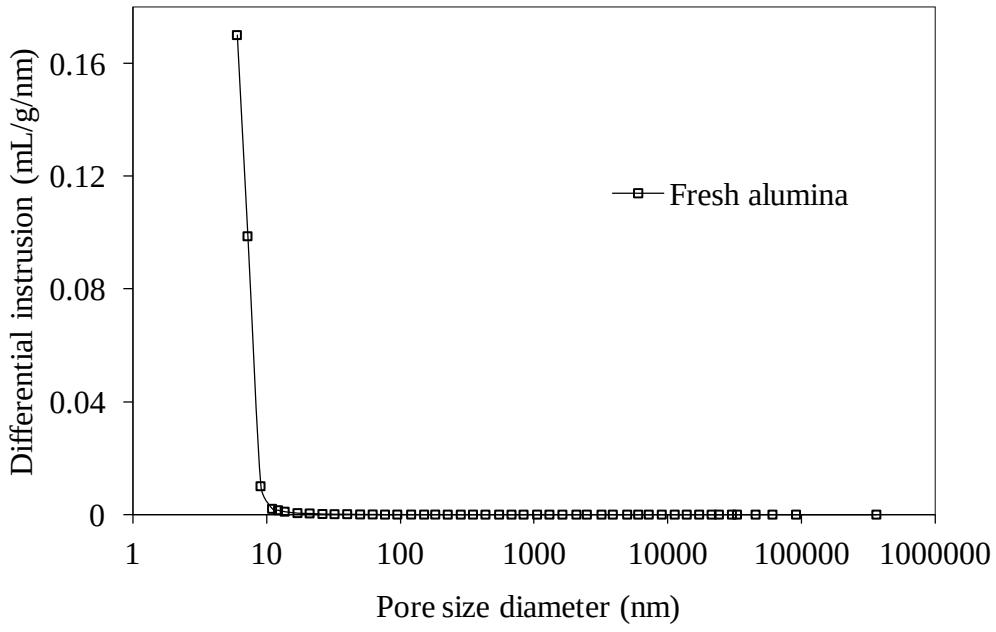

(c)

Figure A.3 Mercury porosimetry of (a) Fresh Co-Mo, Ni-Mo, and Regenerated Co-Mo catalysts, (b) activated carbon and (c) alumina support.

A.3 Properties of the Alumina and Activated Carbon Guard Bed Materials

The activated carbon (AC) used in this study was purchased from Sigma-Aldrich, United Kingdom. The trilobe alumina (Al_2O_3) purchased from Johnson Matthey PLC Catalyst & Chemical Division, England, was also used as a guard bed. The physical properties of both the AC and alumina are presented in Table A.1.

Table A.1 Properties of the activated carbon and alumina support used as guard bed.

Parameter	Activated carbon	Alumina support
Surface area ($m^2.g^{-1}$)	819.9	114.6
Micropore volume ($m^3.g^{-1}$)	0.3087	12.4
External surface area ($m^2.g^{-1}$)	168.9	102.2
Average pore diameter (nm)	411.6	8.2

A.4 Properties of prepared Ni/zeolite-alumina and Ni-Mo/Al_2O_3 catalysts

Prepared Ni/zeolite-alumina catalyst

Support composition (wt. %)

HY-zeolite	32.7
Al_2O_3 in support	36.2
SiO_2 in support	20.8

Catalyst composition (wt. %)

NiO	17

Catalyst physical properties

Shape	Cylindrical extrudate
Diameter (mm)	3
Length (mm)	4.3 ± 1.17
Specific surface area (m^2/g)	444.1 ± 5.85
Average pore diameter (Å)	62.3

Commercial Ni-Mo/Al_2O_3

Support composition (wt.%)

Al_2O_3 in support	38.3
SiO_2	7.9

Catalyst composition (wt. %)

NiO	9.8
MoO_3	40.8

Catalyst physical properties

Shape	Cylindrical extrudate
Diameter (mm)	1.6
Length (mm)	4.1 ± 1.88
Specific surface area (m^2/g)	239.7 ± 1.52
Average pore diameter (Å)	85.2

A.4.1 Nitrogen adsorption-desorption isotherm

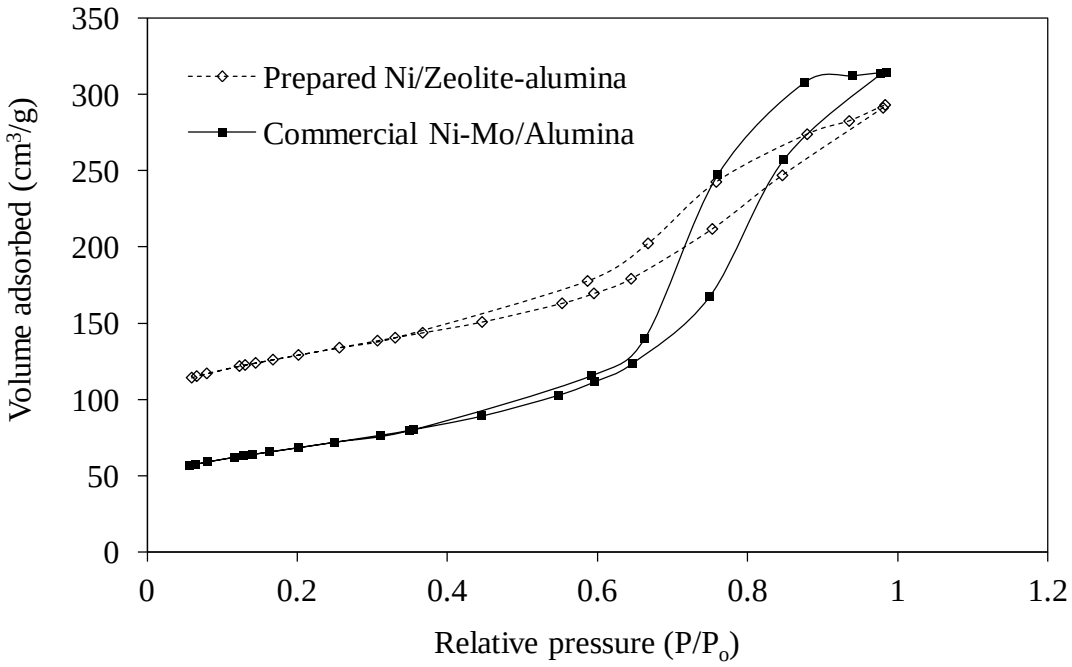

Figure A.4 N_2 adsorption-desorption isotherm for the commercial Ni-Mo/Al_2O_3 and prepared Ni/zeolite-based catalyst both cylindrically shaped.

Appendix B

Effect of Feedstock on Impurities Removal

B.1 Effect of Feedstock on Impurities Removal

One primary objective of catalytic upgrading is to remove impurities such as heteroatom and metal-containing compounds from the heavy oil. The cost of downstream processing however is influence by the content of sulphur and metals (Javadli and Klerk, 2012). The sulphur and metals content of the oils before and after catalytic upgrading process with Co-Mo/alumina catalyst at 425 ^{o}C is presented in Table B.1. It is clear that for feedstock-A and B, the sulphur and metals content of the produced oils after CAPRI process was remarkably reduced. It can be observed that after CAPRI with Co-Mo catalyst at 425^{o}C, the sulphur content was reduced from 3.8 to 3.55 wt.% for feedstock-A and from 3.52 to 3.4 wt.% for feedstock-B. This indicates 6.6 and 3.41 % desulphurisation reactions, respectively. This low level of desulphurisation is due to the refractory nature of the sulphur compounds as the oil becomes heavier (Javadli and Klerk, 2012). This is expected because feedstock-A contains has more sulphur content than feedstock-B. The sulphur in the organosulphur compound is commonly removed as hydrogen sulphide in the off-gas stream.

On the other hand, the Ni + V content was lowered from 206 to 181 ppm for feedstock-A and from 149 to 124 ppm for feedstock-B. The percentage removal therefore is 12.1 and 16.8 %, respectively for feed oil A and B after catalytic upgrading process. Ancheyta et al. (2002) pointed out that nickel and vanadium are mostly associated with the asphaltenes fractions in the oil. Therefore, high conversion of asphaltenes promotes the removal of nickel and vanadium metals. In the light of this, higher removal of Ni + V from feedstock-B can be

attributed to the 52.4 % conversion of asphaltenes against 46.8 % for feedstock-A. Also, the iron, zinc, and boron content reduced significantly after catalytic upgrading process.

Table B. 1 Sulphur and metals before and after catalytic upgrading process at temperature 425°C; Reaction Media N_2, Pressure 20 barg, Oil flow rate 1 $mL.min^{-1}$, Gas flow rate 500 $mL.min^{-1}$, Catalyst: Co-Mo/Al_2O_3.

Impurities	**Feed-A**	**After**	**Feed-B**	**After**
Aluminium (ppm)	6	7	2	2
Boron (ppm)	9	0.8	3	2
Calcium (ppm)	0.8	0	1	< 1
Cobalt (ppm)	< 1	0	< 1	< 1
Chromium (ppm)	0.4	0.3	< 1	< 1
Iron (ppm)	36	3	5	< 1
Molybdenum (ppm)	6	3	< 1	< 1
Sodium (ppm)	< 7	3	< 7	< 7
Nickel (ppm)	56	50	41	34
Vanadium (ppm)	150	131	108	90
Phosphorus (ppm)	0.3	0.1	< 1.5	< 1.5
Sulphur (wt.%)	3.8	3.55	3.52	3.4
Silicon (ppm)	0.4	1	1	< 1
Zinc (ppm)	2	0.3	< 1	< 1
Ni + V (ppm)	206	181	149	124

* Sulphur and metals content was performed by Intertek Laboratories Sunbury Technology Centre, UK, using ICP-OES (Inductively Coupled Plasma Optical Emission Spectrometry).

Appendix C

Effect of Reaction Gas Media on Spent Catalyst Coke Content

C.1 Effect of Reaction Gas Environment on Spent Catalyst Coke Content

Coke formation is an inevitable by-product during catalytic upgrading of heavy crude oil. Its deposition decreases catalyst activity, and can be determined as the weight percent of coke on the catalyst (Maity, et al., 2012; Hart, et al., 2013a). The term coke is used to describe a carbonaceous material of reasonably low hydrogen content (Hollander, et al., 1998). The spent Co-Mo/Al_2O_3 catalysts after reaction under hydrogen, methane, THAI gas, and nitrogen environments were analysed using TGA, the TG and DTG curves as presented in Figure C.1. The weight loss at the start of first peak around 200 ^oC is for the soft coke on the catalyst, whilst the weight loss from the start of the peak around 526 ^oC (see DTG curves) is sharp and prominent, and signified the start of hard coke burn-off.

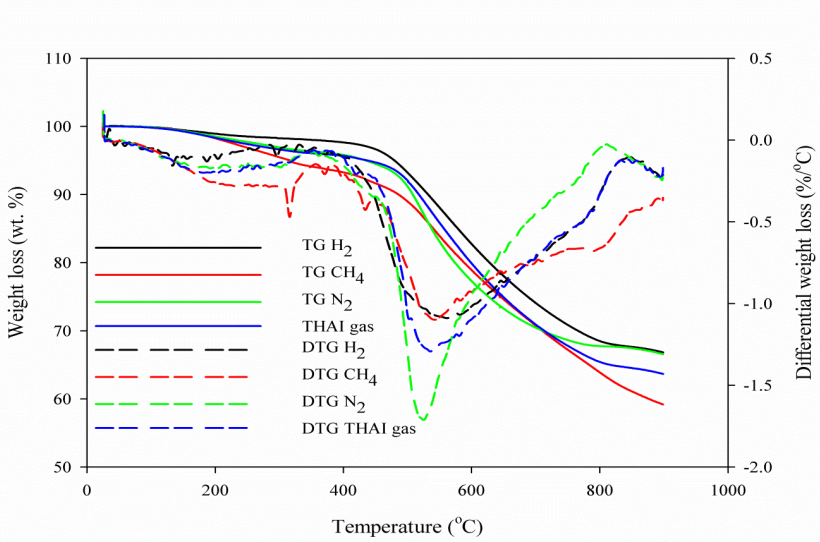

Figure C.1 TG and DTG of spent Co-Mo/γ-Al_2O_3 catalyst after 6 hours time-on-stream reaction under hydrogen, methane, THAI gas, and nitrogen atmospheres at reaction temperature of 425 ^oC, pressure 10 barg, and gas-to-oil ratio 50 $mL.mL^{-1}$.

The coke contents of the spent catalysts under the different reaction media are presented in Table C.1. It can be observed that the coke content of the spent catalyst after 6 hours time-on-stream operation under a hydrogen atmosphere was lower than those of methane, THAI gas, and nitrogen at the same reaction conditions.

Table C.1Coke content of spent Co-Mo/γ-Al_2O_3 catalyst under hydrogen, methane, THAI gas and nitrogen atmospheres at reaction temperature of 425 ^oC, pressure 10barg, and gas-to-oil ratio 50 $mL.mL^{-1}$, after 6 hours time-on-stream operation.

Reactants	**Coke content of the spent catalyst (wt.%)**
Heavy oil + Co-Mo + H_2	17.4 ± 0.82
Heavy oil + Co-Mo + CH_4	20.4 ± 1.32
Heavy oil + Co-Mo THAI gas	20.8 ± 0.97
Heavy oil + Co-Mo + N_2	23.5 ± 1.06

The spent catalyst coke contents are 6 % (hydrogen), 3.1 % (methane) and 2.7 % (THAI gas) respectively lower than that obtained after upgrading under nitrogen (23.5 wt.%). This implies that hydrogen and methane in the reacting media were involved in the upgrading reactions, hence most of the upgrading in nitrogen media can be attributed largely to carbon-rejection with a low degree of hydrogenation occurring (Hart, et al., 2013a,b; section 5.2.5).

During the CAPRI process, most of the C-C bond cleavages take place through a free radical mechanism described above, in which thermal cracking forms distillable fractions with lower molecular weight; the asphaltene molecules lose their paraffin side chains through de-alkylation reactions and in the process large aromatic radicals are produced (Liu, et al., 2013; Qi, et al., 2012; Zhao, et al., 2001). The subtraction of hydrogen rich components such as hydrogen, methane, and ethane by the gas phase radicals from the oil-phase and coke precursor molecules are therefore a potential contributor to the growth of coke lay-down on

the catalyst. The active hydrogen and methyl species in hydrogen, methane and THAI gas reaction environment are thought to suppress the addition reactions of coke precursors, and cause less coke formation because they subsequently inhibit the dehydrogenation reaction occurring after the condensation of poly-aromatics. In contrast, with nitrogen gas, these large radicals cross-link together, condense and finally form coke through hydrogen-subtraction. With hydrogen/methane, the produced large aromatic radicals are terminated by the released active hydrogen and methyl suppressing coke formation (Liu, et al., 2013; Qi, et al., 2012). Consequently the coke content of the spent catalyst under methane atmosphere is notably lower than that reacted under nitrogen (see Table C.1).

Deactivation of a catalyst can occur by poisoning, aging, fouling and sintering; however the major cause of deactivation in CAPRI is thought to be the formation of coke (Gray, et al., 1999). In the light of this, the nitrogen adsorption-desorption isotherms for the fresh and spent Co-Mo/Al_2O_3 catalyst recovered from the CAPRI reactor after 6 hours upgrading under hydrogen, methane, and nitrogen gas media were determined and are presented in Figure C.2. The percentage loss in specific surface area in the different reaction media are as follows: 57.2 % for hydrogen, 68 % for methane, and 96 % for nitrogen relative to the fresh catalyst with specific surface area 214.4 m^2g^{-1}.

The nitrogen adsorption-desorption of the spent catalyst recovered after upgrading reaction with THAI gas was not conducted because it contains a large amount of oil in both duplicate experimental runs which can create a vapour pressure and damage the Micromeretics Analytical Instrument ASAP® 2010 used. If dried externally the residual oil on the spent catalyst will add to surface area loss. However, Table C.1 shows that the coke content of the spent catalyst with methane and THAI gas were approximately 20 wt.%

compared to 23.5 wt.% with nitrogen. Therefore, the loss in specific surface area for THAI gas could be in the same range as that for methane gas.

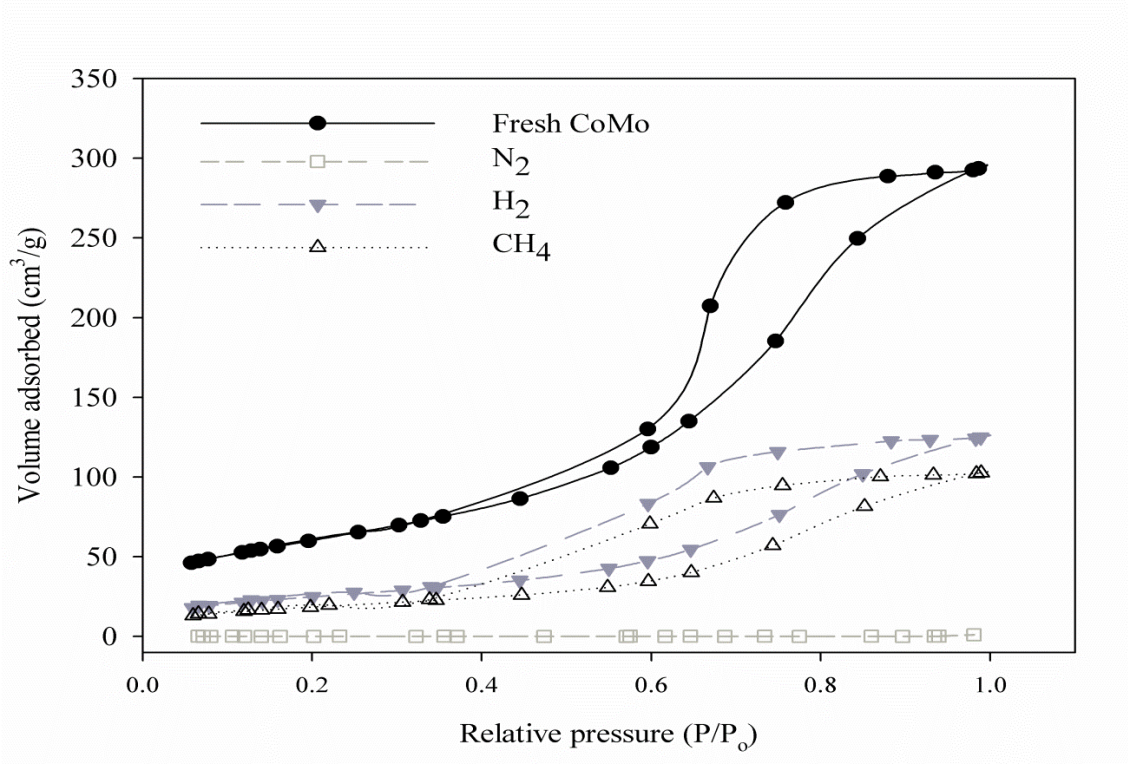

Figure C.2 Nitrogen adsorption-desorption isotherm of fresh and spent Co-Mo after 6 hours reaction in hydrogen, methane, and nitrogen media at reaction temperature of 425 ^{o}C, pressure 10 barg, and gas-to-oil 10 mL.mL^{-1}.

The reaction environment changes pathways of the upgrading reactions as well as interactions of molecules with the catalytic sites. For example under hydrogen environment sulphur and/or metal containing hydrocarbon first got adsorbed on the acid sites of the catalysts before cracking reactions proceed as illustrated in Figure C.3.

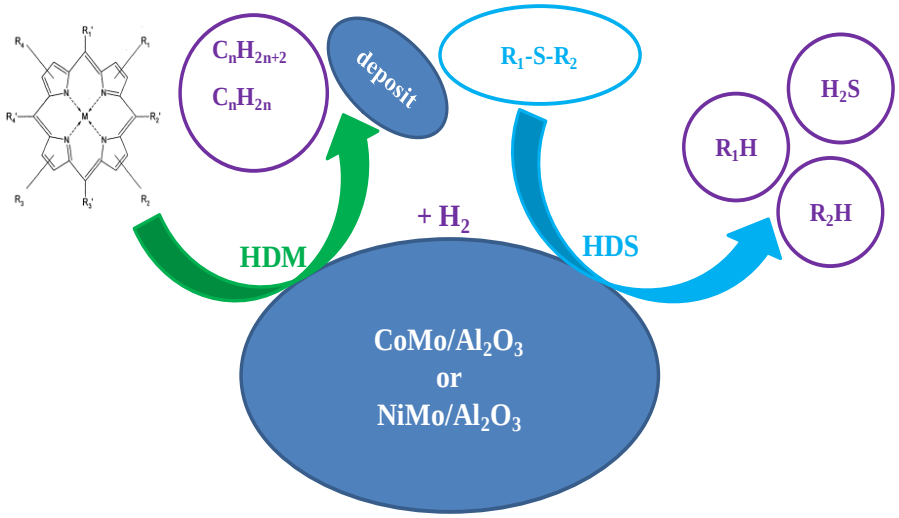

Figure C.3 HDM and HDS reactions under hydrogen atmosphere.

At the surface of the catalyst the cracked sulphur react with hydrogen and is removed as H_2S, while the generated active hydrocarbon chains (i.e., R_1 and R_2) are hydrogenated to stable molecules and released into the oil phase (see Figure C.3). This reaction is dependent on hydrogen availability and catalyst age. In hydrogen limited atmosphere therefore the hydrocarbon active chains re-unite to form larger molecules. In the light of this, the collective changes such as TBP distribution, sulphur and metals removal, and coke formation evident under hydrogen, methane, THAI gas, and nitrogen gas emerge from the interaction between the oil molecules, catalytic active sites and reaction gas media.

The surface areas are consistent with the coke contents of catalyst presented in Table C.1, showing that hydrogen and methane are effective reactants during catalytic upgrading to reduce coke deposition in the catalyst pores compared to nitrogen. The three stages of catalyst deactivation by coke are as follows: 1) rapid formation of initial coke with remarkable loss of catalytic activity; 2) gradual build-up of coke and metal deposits resulting in further loss of activity; and 3) pore blockage due to progressive deposition of coke and metals leading to loss

of activity (Gray, et al., 1999). Coke build up under nitrogen was higher than hydrogen, methane and THAI gas reaction media (Figure C.1), which is thought to be due to the inert nature of nitrogen which does not suppress poly-aromatics radical addition reactions. The losses in pore volume and surface area of the spent catalyst reacted under nitrogen atmosphere are an indication of pore mouth plugging (Hart, et al., 2013a; Ancheyta, et al., 2002; Puron, et al., 2013; Hart, et al, 2013b) caused by the deposition of asphaltenes and coke (Hart, et al., 2013). The small pores within the catalyst not only hinder access of macromolecules to the active sites but also are preferential sites for coke deposition, resulting in pore blockage and surface area loss (Puron, et al., 2013). Micro-structural properties of the catalyst support such as surface area and porosity, therefore determine to a certain degree the ability of the catalyst to adsorb asphaltenes and coke deposits.

Appendix D

Effect of Oxidative-Regeneration of Spent Catalyst on Upgrading

D.1 Fresh vs. Regenerated: API gravity and viscosity

The changes in API gravity and decrease in viscosity between the feed and produced oil samples for the fresh Co-Mo catalyst and the oxidative-regenerated spent Co-Mo catalyst from the nitrogen medium experiment are presented in Figures D.1 (a) and (b) respectively, as a function of time-on-stream. The maximum change in API gravity for fresh Co-Mo catalyst was 5.4 ^{o}API compared to 4.1 ^{o}API for regenerated Co-Mo. However, the average change in API gravity over the whole time-on-stream for both experimental runs settled at approximately 3.04 ± 1.01 ^{o}API. The regenerated catalyst showed a similar level of activity over the whole time period of investigation compared with the fresh catalyst despite its loss of surface area.

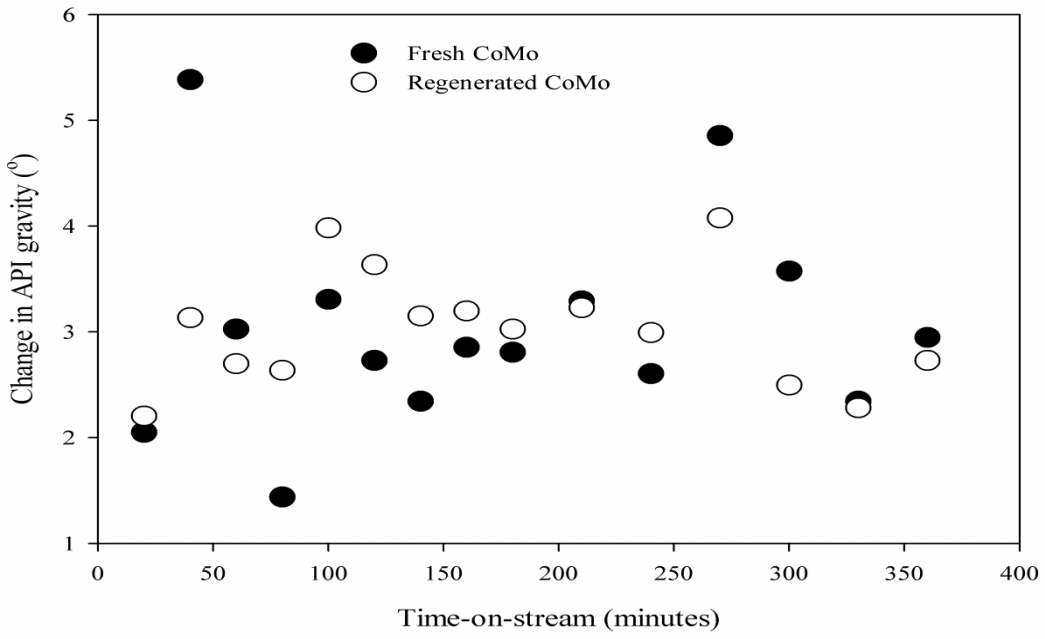

(a)

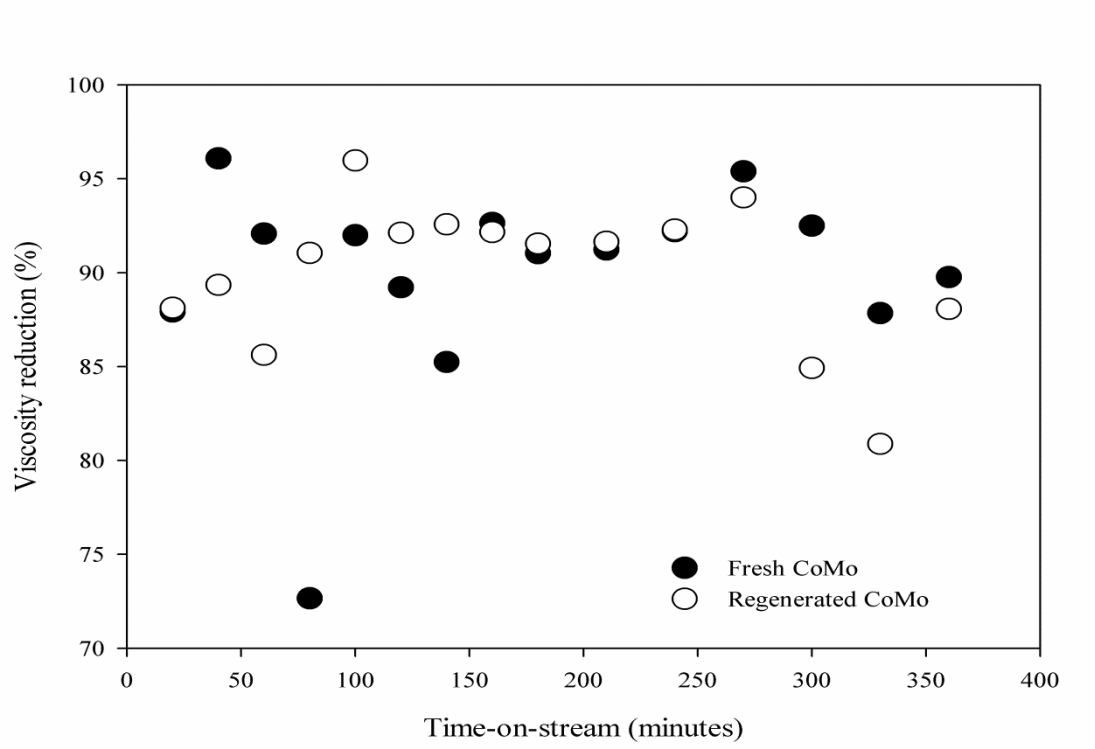

(b)

Figure D.1 Change in API gravity (a) and degree of viscosity reduction (b) for the produced oil using fresh Co-Mo catalyst and oxidative-regenerated spent Co-Mo catalyst from the nitrogen medium experiment at reaction temperature of 425 ^{o}C, pressure 10 barg, and nitrogen-to-oil ratio 50 mL.mL^{-1}.

In Figure D.1b, there is no significant difference in the trend of viscosity reduction as a function of time-on-stream between the use of fresh and rejuvenated Co-Mo catalyst. Notably, the average viscosity reduction in both runs was approximately 90 %. This trend is consistent with that of the API gravity.

D.2 Fresh vs. regenerated: TBP distribution

In Figure D.2, the simulated distillation curves for the feed and produced oil samples with fresh Co-Mo catalyst and oxidative-regenerated spent Co-Mo from experiment

performed under nitrogen reaction media are presented. It is clear from the curves that distillates in the produced oil from fresh Co-Mo were improved compared with regenerated Co-Mo. Conversion of 29.5 % of343 ^{o}C+ hydrocarbons from the feed oil into low boiling products occurred for the fresh Co-Mo and 25 % for the regenerated Co-Mo catalysts, showing a further decrease of 4.5 % after regeneration of the spent Co-Mo catalyst.

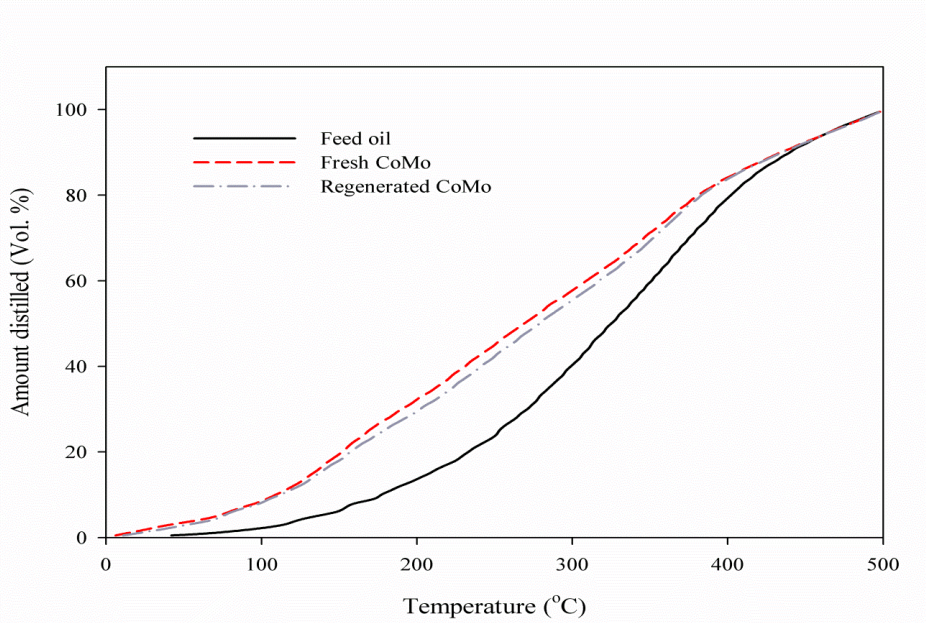

Figure D.2 TBP distribution curves for feed and upgraded oils obtained from using fresh Co-Mo catalyst and oxidative-regenerated spent Co-Mo catalyst from the nitrogen atmosphere experiment at reaction temperature of 425 ^{o}C, pressure 10 barg, and nitrogen-to-oil ratio 50mL.mL^{-1}.

This is concluded to be because some of the catalyst active sites may have been fouled and poisoned by coke and metal during the first experimental run, as the deposited coke and metals on the spent catalyst were not completely removed by oxidative-regeneration (see Chapter 5 and Figures 5.9 & 5.10). The catalytic upgrading reaction is a complicated process where molecules in the feedstock become adsorbed onto the catalyst acid sites first before reaction proceeds. Therefore, the strength of the acid sites of the oxidative-regenerated Co-Mo/alumina could have been weakened by the deposits after the first experimental use (Ho, et

al., 1992). This can limit the cracking ability of the regenerated Co-Mo/alumina catalyst leading to the observed low conversion and yield of low-boiling distillates. Also, the narrower pore size of the regenerated Co-Mo catalyst as revealed by the adsorption-desorption isotherm presented in Figure 5.9 does not grant the large molecules access to the acid sites.

D.3 Fresh vs. Regenerated: Spent Catalyst Coke Content

A comparison between the TG and DTG curves of the spent Co-Mo catalyst obtained with the nitrogen reaction medium before and after oxidative-regenerated was conducted are presented in Figure D.3 after 6 hours time-on-stream experiment. The coke contents of the fresh and regenerated catalysts were 23.48 and 24.73 %, respectively. It was noted that the coke content of the rejuvenated sample after reaction was 1.25 % higher than the catalyst used only once, which indicates that regeneration promotes the propensity of the catalyst to support the formation of coke.

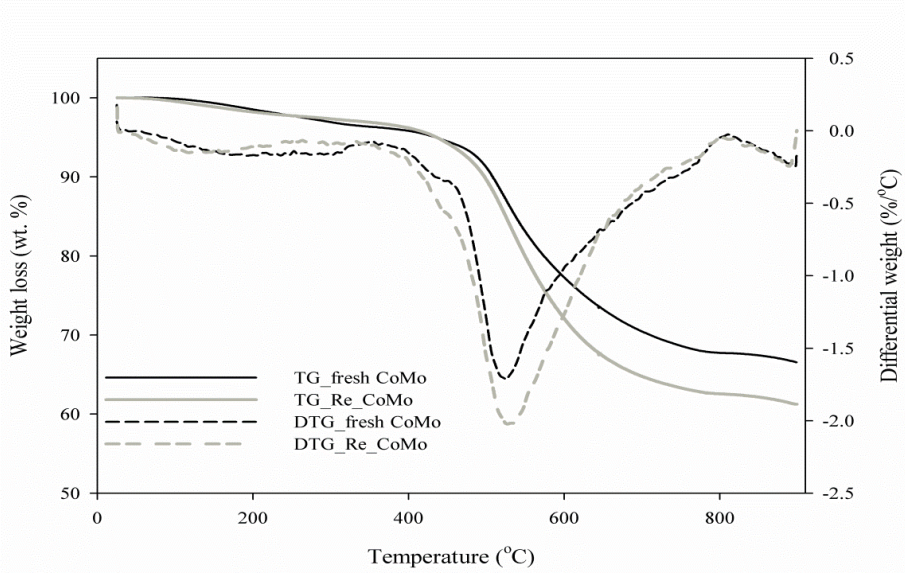

Figure D.3 TG and DTG curves of the spent Co-Mo catalyst obtained with the nitrogen reaction medium before and after oxidative-regenerated was conducted after 6 hours time-on-stream reaction at temperature of 425 ^{o}C, pressure 10 barg, and nitrogen-to-oil ratio 50mL.mL^{-1}.

The elevated yield of highly poly-aromatic coke corresponds to faster catalyst deactivation (Greaves, et al., 2012), with lower yield of liquid hydrocarbons of low boiling points upon the use of regenerated relative to fresh catalyst as reflected by the data shown in Figure D.2 and also by the SEM photomicrograph of the fresh and regenerated Co-Mo/alumina catalysts shown in Chapter 5, Figure 5.10. Additionally, the narrow pore structure of the regenerated catalyst could have to high coking.

Appendix E

Hydrocracking of Anthracene

E.1 Results and Discussion

The conversion of anthracene as a function of time-on-stream and temperature are shown in Figure E.1. It is clear that the conversion of anthracene increased as reaction temperature increases from 350 to 400 ^{o}C. This result is in line with that reported by Zhang et al. (1998) on the hydrogenation of anthracene over active carbon-supported nickel catalyst and Chareonpanich et al. (1996) on HDC of anthracene using USY-zeolite.

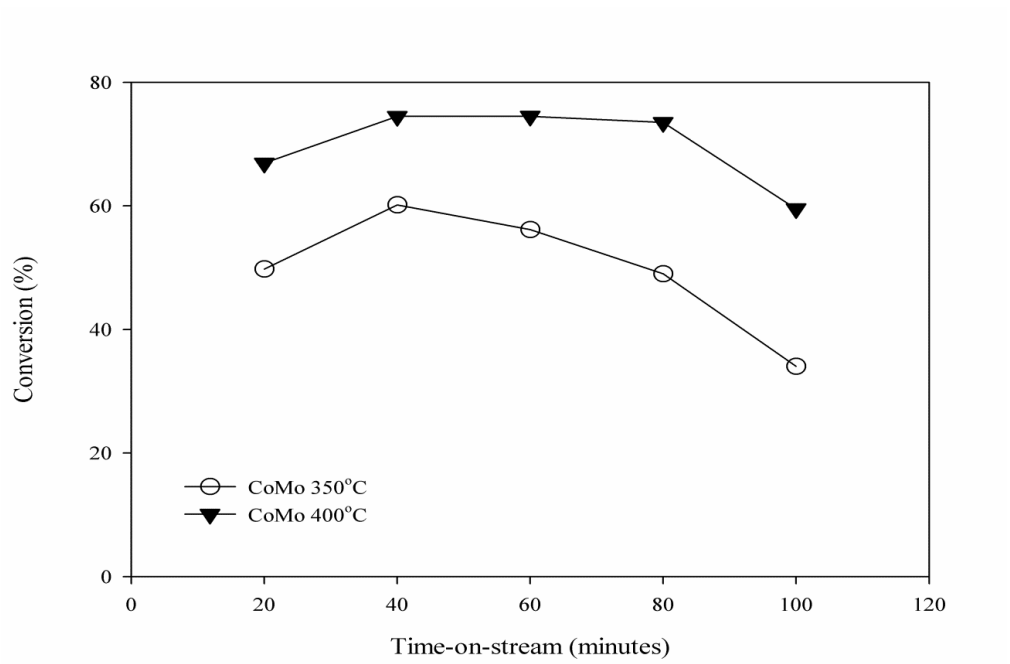

Figure E.1 Hydroconversion of anthracene with time at 350 and 400^{o}C, using Co-Mo/Al_2O_3 catalyst.

Consequently, the hydroconversion of the anthracene could follow the sequence three-fused-ring aromatic (i.e., anthracene) → two-fused-ring aromatics (e.g., naphthalene) →

monoaromatics (e.g., benzene) → olefins → paraffin. The presence of olefins and paraffin in the produced gas presented in Table E.1 confirmed the above mentioned sequence, which consists of hydrogenation of aromatic ring to naphthenic ring, followed by ring-opening and subsequently, side chain splitting.

Table E.1 Gas yield during the hydrocracking of anthracene.

	350 ^{o}C	**400 ^{o}C**
Gas component	**Yield (vol.%)**	**Yield (vol.%)**
Methane (CH_4)	0.16	0.09
Ethane (C_2H_6)	0.16	0.21
Ethene (C_2H_4)	0.12	0.17
Propene (C_3H_6)	0.23	0.27
i-butane (C_4H_{10})		0.04
Trans-2-butene (C_4H_8)	0.032	0.037

Moreover, analyses of collected liquid samples using GC connected to mass spectrometer (GC-MS) indicate the presence of the following: (a) 1,4-diethyl-benzene, (b) 1-propenylbenzene, (c) 9,10-dihydroanthracene, (d) 2-methylnaphthalene, and (e) 1-ethyl-benzene as shown in Figure E.2. Pinilla et al. (2013a,b) also reported the formation of these products upon anthracene catalytic cracking with steam as hydrogen-donor.

The hydroconversion reaction could have occurred through two possible pathways: one is the hydrogenation of the middle ring and the other is the outer ring leading to the formation of naphthenic ring (Chareonpanich, et al., 1996; Guan, et al., 2003). The naphthenic ring undergoes ring opening to aliphatic hydrocarbon substitute and subsequent dealkylation (i.e., cleavage of side chain). The formation of C_1-C_4 gases confirms the dealkylation reactions. Therefore, the anthracene being a tricyclic aromatic compound has been converted

to mono- (e.g., benzene, toluene, etc.) and di-aromatic (e.g., naphthalene, etc.) compounds along with their alkylated derivatives and cracked to C_1-C_4 hydrocarbons (see Table E.1). Based on the identified products from the conversion of anthracene, the proposed reaction pathway for hydroconversion of anthracene, therefore, is presented in Figure E.3.

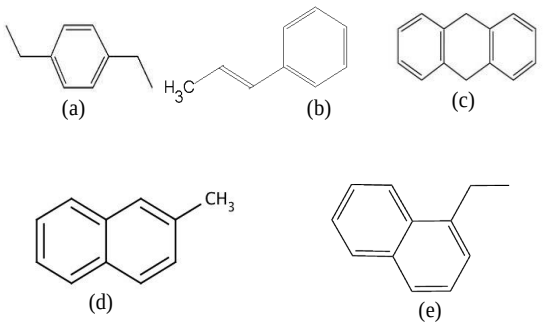

Figure E.2 Identified products of the catalytic cracking of anthracene at 400 ^{o}C using Co-Mo/Al_2O_3 catalyst in hydrogen atmosphere: (a) 1,4-diethyl-benzene, (b) 1-propenylbenzene, (c) 9,10-dihydroanthracene, (d) 2-methylnaphthalene, and (e) 1-ethyl-benzene.

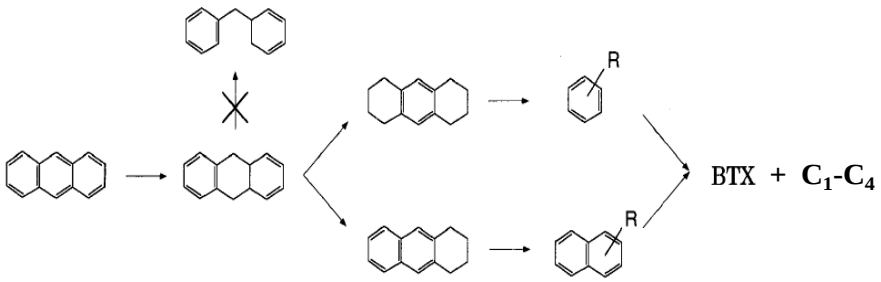

Figure E.3 Modified reaction pathway for hydrogenation and hydrocracking of anthracene using Co-Mo/Al_2O_3 catalyst, where BTX (i.e., benzene, toluene, and xylene derivatives) and R is alkyl hydrocarbon.

Pinilla et al. (2013a) pointed out that the formation of naphthalene from anthracene is commonly recognized as the key reaction pathway in the hydroconversion reaction through an orderly occurrence of hydrogenation, isomerisation, and cracking reactions. They also found that the opening of the central ring leads to the formation valuable intermediates such as monocyclic products.

Appendix F

Fixed-Bed and Dispersed Catalyst

F.1 Catalysts characterisation

The nitrogen adsorption-desorption isotherm of the pellets and crushed Co-Mo/γ-Al_2O_3 is presented in Figure F.1. Though the pore volume has decreased after pulverisation, the isotherm revealed that the shape of the hysteresis loop are identical and almost matches the values of the pelleted catalyst. This indicates there is not much modification to the pore and microstructures of the catalyst upon pulverisation.

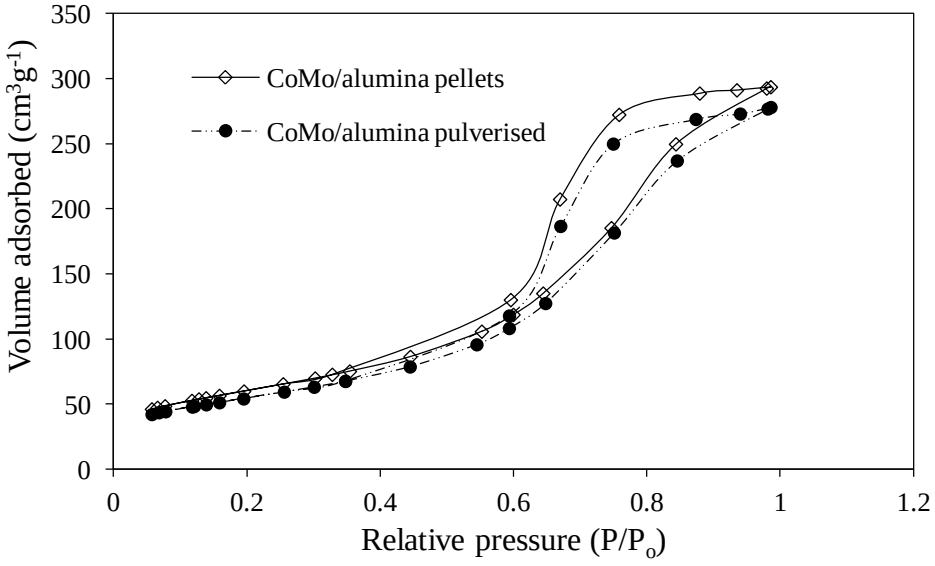

Figure F.1 Nitrogen adsorption-desorption isotherm of pulverised and pellets Co-Mo/Al_2O_3.

F.2 Reynolds Number of Fixed-Bed and Batch Reactors

In Table F.1, the heavy oil, fixed-bed and batch reactors properties are presented. Equations 1 and 2 were used to calculate the Reynolds number of the fixed-bed and batch reactors, respectively.

Table F.1 Characteristics of heavy oil, fixed-bed and batch reactors.

Parameter	**Value**
Density of heavy oil, ρ (kg.m^{-3})	974.5
Velocity of oil, v_s (m.s^{-1})	0.0032
Viscosity of heavy oil, μ (Pa.s)	1.091
Porosity of the fixed-bed, ε	0.48
Diameter of impeller, D (m)	0.01
Equivalent particle diameter, d_p (m)	0.035

$$Re\ (Fixed-bed) = \frac{\rho\, v_s d_p}{\mu\,(1-\varepsilon)} \quad (1)$$

$$Re\ (Batch) = \frac{\rho\, N\, D^2}{\mu} \quad (2)$$

where; N number of revolution per second

From eq. (1), the Reynolds number of the fixed-bed reactor is 0.1951. Therefore, the stirring speed of the batch reactor impeller that will give the same Reynolds number can be calculated using eq. 2. This gives 2.2 revolutions per second (i.e., 132 rpm).

Appendix G

Publications and Conferences

G.1 Publications (available upon request)

G.1.1 Journal Papers

1. Hart Abarasi, Leeke Gary, Greaves Malcolm, Wood Joseph, (2014) Downhole Heavy Crude Oil Upgrading Using-CAPRI: Effect of Steam upon Upgrading and Coke Formation, *Energy & Fuels*, 28 (3), 1811-1819.

2. Hart Abarasi, Leeke Gary, Greaves Malcolm, Wood Joseph, (2014) Down-hole heavy crude oil upgrading by CAPRI: Effect of hydrogen and methane gases upon upgrading and coke formation, *Fuel*, 119, 226-235.

3. Hart Abarasi, Shah Amjad, Leeke Gary, Greaves Malcolm, Wood Joseph, (2013) Optimization of the CAPRI process for heavy oil upgrading: Effect of hydrogen and guard bed, *Industrial & Engineering Chemistry Research*, 52 (44), 15394-15406.

G.1.2 Conferences Papers and Presentations

1. Hart Abarasi, Leeke Gary, Greaves Malcolm, Wood Joseph, (2013) Will heavy oil and bitumen be a significant source of energy in the next decades? *Poster presented at the MEGS IV Annual Conference, Public Engagement with Energy,* Loughborough, 12-13 September.

2. Hart Abarasi, Abdullah Al-Marshed, Amjad Shah, Gary Leeke, Malcolm Greaves and Joseph Wood, (2013) Prolonging Catalyst Lifetime in the THAI-CAPRI Process for Enhanced Oil Recovery, *34th International Energy Agency (IEA)-Enhanced Oil Recovery (EOR) Annual Workshop & Symposium*, Stavanger, Norway, September 8-13 (oral presentation).

3. Hart Abarasi, Leeke Gary, Greaves Malcolm, Wood Joseph, (2013) Laboratory Scale Investigation of CAPRI Upgrading of Heavy oil and Bitumen, *Poster presented at Catalysis and Chemical Engineering (IChemE)*, Institute of Physics, London, 4 June.

4. Hart Abarasi, Leeke Gary, Greaves Malcolm, Wood Joseph, (2013) Down-hole catalytic upgrading of heavy oil and bitumen to meet tomorrow's energy needs: the THAI-CAPRI process, *Proceedings of the 3rd North American Symposium on Chemical Reaction Engineering*, Houston, Texas, March 17-20 (oral presentation and paper on CDROM).

5. Hart Abarasi, Leeke Gary, Greaves Malcolm, Wood Joseph, (2012) Sustaining Petroleum-based Energy Source through the Recovery and Upgrading of Heavy oil and Bitumen using THAI-CAPRI, *Poster presented at MEGS III Annual Conference; Systems Thinking in Energy*,Available:http://www.megs.ac.uk/megs/imagesmultimedia/documents/abarasihart.pdf, Birmingham, 18-19 September.

6. Hart Abarasi, Leeke Gary, Greaves Malcolm, Wood Joseph, (2012) Control of Catalyst Deactivation in THAI-CAPRI Process for In-Situ Oilsand Recovery and Upgrading, *Paper presented at the World Heavy Oil Congress Conference*, Aberdeen, 10-13 September, 2012 (oral presentation and paper on CDROM).

7. Hart Abarasi, Leeke Gary, Greaves Malcolm, Wood Joseph, (2012) Minimising Catalyst Deactivation in THAI-CAPRI Process for Heavy Oil Recovery and Upgrading by using

Guard Bed, *Paper presented at the IChemE-RSC Applied Catalysis and Reaction Engineering Young Researchers Focus Conference*, Warwick, 19-20 April, 2012 (oral presentation).

8. Hart Abarasi, Leeke Gary, Greaves Malcolm, Wood Joseph, (2011) Laboratory Scale Investigation of the CAPRI Add-on to the THAI Process of Heavy Oil Recovery and Upgrading In-situ, *A Poster Presented at the Midlands Energy Graduate School II Christmas Event and MEGS Inaugural Lecture*, Loughborough, 13 December, 2011.

References

Abuhesa, B. M., Hughes R., (2009). Comparison of conventional and catalytic in situ combustion processes for oil recovery, *Energy Fuels*, 23, 186-192.

Absi-Halabi, M., Stanislaus, A., Al-Mughni, T., (1995). Hydroprocessing of vacuum residues: relation between catalyst activity, deactivation and pore size distribution, *Fuel*, 74 (8), 1211-1215.

Absi-Halabi, M., Stanislaus, A., Trimm, D. L., (1991). Coke formation on catalysts during the hydroprocessing of heavy oils, *Applied Catalysis*, 72, 193-215.

Abuhesa, B. M., Hughes, R., (2009). Comparison of conventional and catalytic in situ combustion processes for oil recovery, *Energy Fuels*, 23, 186-192.

Alemán-Vázquez, L. O., Cano-Domínguez, J. L., García-Gutiérrez, J. L., (2012). Effect of tetralin, decalin and naphthalene as hydrogen donors in the upgrading of heavy oils. *Procedia Engineering*, 42, 532 – 539.

Alfi, M., Barrufet, A. M., Paulo, D. F. S., Rosana, G. M., (2013). Simultaneous application of heat and electron particles to effectively reduce the viscosity of heavy deasphalted petroleum fluids, *Energy Fuels*, dx.doi.org/10.1021/ef400883z.

Ali, A. F., Hauser, A., Abdullah, H. A., Al-adwani, A., (2006). Accelerated solvent extraction of spent hydrotreating catalysts: A study on oil and coke fractions, *Energy Fuels*, *20*, 45-53.

Alkhaldi, S., Husein M. M., (2014). Hydrocracking of heavy oil by means of in situ prepared ultradispersed nickel nanocatalyst, *Energy Fuels*, 28, 643-649.

Al-Mutairi Adel and Marafi Abdulazim, (2012). Effect of the operating pressure on residual oil hydroprocessing, *Energy Fuels*, dx.doi.org/10.1021/ef3011228.

Alpak, O. F., Vink, C. J., Gao, G., Mo, W., (2013). Techniques for effective simulation, optimization, and uncertainty quantification of the in-situ upgrading process, *Journal of Unconventional Oil and Gas Resources*, http://dx.doi.org/10.1016/j.juogr.2013.09.001.

Al-Saleh, M. A., Hossain, M. M., Shalabi, M. A., Kimura, T., Inui, T., (2003). Hydrogen spillover effects on Pt-Rh modified Co-clay catalysts for heavy oil upgrading, *Applied Catalysis A: General*, 253, 453-459.

Alvarez-Ramirez, F., Edgar, R.-J., Yosadara, R. -M., (2006). Calculation of the interaction potential curve between asphaltene-asphaltene, asphaltene-resin, and resin-resin systems using density functional theory, *Energy Fuels*, 20 (1), 195-204.

Ancheyta, J., (2011). Modeling and simulation of catalytic reactors for petroleum refining, John Wiley & Sons, Inc., New Jersey, pp.2-8.

Ancheyta, J., Betancourt, G., Marroquin, G., Centeno, G., Castaneda, L.C., Alonso, F., Munoz, J. A., Gomez, T. M., Rayo, P., (2002). Hydroprocessing of Maya heavy crude oil in two reaction stages, *Applied Catalysis A: General*, 233, 159-170.

Ancheyta, J., Rana, M. S., (2007). Petroleum Engineering-Downstream, Eolss Publishers, Oxford, UK.

Ancheyta, J., Rana, S. M., Furimsky, E., (2005). Hydroprocessing of heavy petroleum feeds: Tutorial, *Catalysis Today*, 109, 3-15.

Angeles, M. J., Leyva, C., Ancheyta, J., Ramirez, S. A., (2013). A review of experimental procedures for heavy oil hydrocracking with dispersed catalyst, *Catalysis Today*, http://dx.doi.org/10.1016/j.cattod.2013.08.016.

Atkins, L., (2011). Heavy crude oil: A global analysis and outlook, available at www.heavyoilinfo.com/feature-items/heavy-crude-oil-a-global-analysis-and-outlook, accessed 23/08/2011.

Aysar, J. T., Mujtaba, I. M., Wood, A. S., (2011). Improvement of the middle distillate yields during crude oil hydrotreatment in a trickle-bed reactor, *Energy Fuels*, 25, 773-781.

Babich, V. I. and Moulijn, A. J., (2003). Science and technology of novel processes for deep desulfurization of oil refinery streams: a review, *Fuel*, 82, 607-631.

Bagci, S., Turna, E. P., Altmos, U., (1998). Steamflooding of medium and light oils in limestone using 3-D laboratory model, *Trans IChemE*, Part A, Vol.76, pp. 604-611.

Bagheri, S. R., Gray, R. M., Shaw, M. J., and McCaffrey, C. W., (2012). In situ observation of mesophase formation and coalescence in catalytic hydroconversion of vacuum residue using a stirred hot-stage reactor, *Energy Fuels*, 26, 3167-3178.

Barman, N. B., Leonidas, S., David, J. K., (1997). Simultaneous determination of oil and coke contents in spent hydroprocessing catalyst by thermogravimetry, *Energy Fuels*, 11 (3), 593-595.

Batholomew, C. H., (1993). Catalytic hydroprocessing of petroleum and distillates, *Proceedings of the AIChE Spring National Meeting*, Houston, TX, March 29 – April 1.

Batycky, J., (1997). An assessment of in-situ oil sands recovery processes, *J. Can. Petrol. Technol*., 36 (9), 15-19.

Bej, K. S., Dalai, K. A. and Adjaye, J., (2001). Comparison of hydrodehydrogenation of basic and nonbasic nitrogen compounds present in oil sands derived heavy gas oil, *Energy & Fuels*, 15, 377-383

Benito, A. M., Martinez, M. T., (1996). Catalytic hydrocracking of an asphaltenic coal residue, *Energy Fuels, 10* (6), 1235-1240.

Biswas, P., Narayanasarma, P., Kotikalapudi, M. C., Ajay, K. D., John, A., (2011). Characterization and activity of ZrO_2 doped SBA-15 supported NiMo catalysts for HDS and HDN of bitumen derived heavy gas oil, *Ind. Eng. Chem. Res.*, 50, 7882-7895.

Boahene, E. P., Kapil, K. S., Ajay K. D., John, A., (2011). Application of different pore diameter SBA-15 supports for heavy gas oil hydrotreatment using FeW catalyst, *Applied Catalysis A: General*, 402, 31-40.

Brown, R. L., (2010). Microbial enhanced oil recovery (MEOR), *Current Opinion on Microbiology*, 13, 316-320.

Bryan, J., Kantzas, A., (2007). Enhanced heavy-oil recover by alkali-surfactant flooding [c], *SPE 110738*, Anaheim, California, USA, 462-468.

Butler, R. M., (1985). A new approach to the modelling of steam-assisted gravity drainage, *J. Can. Petrol. Technol*., 42-50.

Butler, R. M., Jiang, Q., Yee, C. T., (1999). Steam and gas push (SAGP) 3: recent theoretical developments and laboratory results, Presented at *the 48th and 49th Annual Technical Meeting of the Petroleum Society of Canada*, Calgary, Alberta, Canada, June 14-18.

Butler, R. M.., Mokrys, I. J., (1989). Solvent analogue model of steam-assisted gravity drainage, *AOSTRA J. Res*., 5 (1), 17-32.

Butler, R. M., Mokrys, I. J., (1991). A new approach (VAPEX) for recovery heavy oil using hot water and hydrocarbon vapour, *J. Canadian Petrol. Technol.*, 30 (1), 97-106.

Butler, R. M., Stephens, D. J., (1980). The gravity-drainage of steamheated heavy-oil to parallel horizontal wells, Paper presented at *31st Annual Technical Meeting of the Petroleum Society of CIM in Calgary*, Canada, May 25-28.

Cai, H. -Y., Shaw, J. M. and Chung, K. H., (2001). Hydrogen solubility measurements in heavy oil and bitumen cuts, *Fuel*, 80, 1055-1063.

Carrillo, A. J., Corredor, M. L., (2012). Upgrading of heavy crude oils: Castilla. *Fuel Process. Technol.*, http://dx.doi.org/10.1016/j.fuproc.2012.09.059.

Castañeda, L. C., Muñoz, J. A., Ancheyta, J., (2012). Combined process schemes for upgrading of heavy petroleum, *Fuel*, 100, 110-127.

Castanier, L. M., Brigham, W. E., (2003). Upgrading of crude oil via in situ combustion, *Journal of Petroleum Science and Engineering*, 39, 125-136.

Cerqueira, S. H., Evaristo, C. B. Jr., Eduardo, F. S. –A., (1997). Mathematical modelling and simulation of catalytic cracking of gasoil in a fixed bed: coke formation, *Applied Catalysis A: General*, 164, 35-45.

Chareonpanich, M., Zhang, Z. –G., and Tomita, A., (1996). Hydrocracking of aromatic hydrocarbons over USY-zeolite, *Energy Fuels*, 10, 927-931.

Chen, J. W., Cao, H. C., (1994). Heavy oil upgrading and change of its chemical structure, *Pet. Ref. Eng.*, 24 (6), 1-9.

Chen, L., Zhang, G., Ge, J., Jiang, P., Tang, J., Liu, Y., (2013). Research of the heavy oil displacement mechanism by using alkaline/surfactant flooding system, *Colloids and Surfaces A: Physicochemical and Engineering Aspects*, 434, 63-71.

Chen Shuo and Manos George, (2004). Study of coke and coke precursors during catalytic cracking of n-hexane and 1-hexene over ultrastable Y zeolite, *Catalysis Letters*, 96 (3-4), 195-200.

Chen, Y.W. and Hsu, W. C., (1997). Hydrodemetalation of residue oil over CoMo/alumina-aluminum-phosphate catalysts in a trickle bed reactor, *Ind. Eng. Chem. Res.*, 36, 2526-2532.

Chianelli, R. R., Rendina, D., Hauptmann, G. E., Lucchesi, J. P., Torres, B., (2013). Conversion of heavy tar sands with asphaltene chemical structures via catalytic coking using MoS_2 catalytic material, *Energy Fuels*, dx.doi.org/10.1021/ef4014532.

Chuan, W., Lei, G. -L., Yao, C., Sun, K., Ping-yuan, G., Yan-bin C., (2010). Mechanism for reducing the viscosity of extra-heavy oil by aquathermolysis with an amphiphilic catalyst, *J. Fuel Chem. Technol.*, 38 (6), 684-690.

Clark, P. D., Hyne, J. B., (1990). Studies on the chemical reactions of heavy oils under steam stimulation condition, *AOSTRA J. Res.*, 29, 29-39.

Dai-yin, Y., Hui, P., (2008). Numerical simulation study on surfactant flooding for permeability oilfield in the condition of threshold pressure, *Journal of Hydrodynamics*, 20 (4), 492-498.

Das, K., Butler, M. R., (1998). Mechanism of the vapour extraction process for heavy oil and bitumen, *Journal Petroleum Science & Engineering*, 21, 43-59.

Deng, S., Yu, G., Jiang, Z., Zhang, R., Ting, Y., (2005). Destabilization of oil droplets in produced water from ASP flooding, *Colloids Surf. A: Physicochem. Eng. Aspects*, 252, 113-119.

Dockner, T., (1988). Reduction and hydrogenation with the system hydrocarbon/carbon, *Angew Chem. Int. Ed.*, 27 (5), 679-82.

Dong, M., Shanzhou, M., Qiang, L., (2009). Enhanced heavy oil recovery through interfacial instability: A study of chemical flooding for Brintnell heavy oil, *Fuel*, 88, 1049-1056.

Douda, J., Llanos, M. E., Álvarez, R., López Franco, C., Montoya de la. Fuente, J. A., (2004). Pyrolysis applied to the study of a Maya asphaltenes, *Journal of Analytical and Applied Pyrolysis*, 71, 601-612.

Dupain, X., Makkee, M., Moulijn, J. A., (2006). Optimal conditions in fluid catalyst cracking: A mechanistic approach, *Applied Catalysis A: General*, 297, 198-219.

Eijsbouts, S., Battiston, A. A., Leerdam van, G. C., (2008). Life cycle of hydroprocessing catalysts and total catalyst management, *Catalysis Today*, 130, 361-373.

Elizalde, I., Rodriguez, A. M., Ancheyta, J., (2010). Modeling the effect of pressure and temperature on the hydrocracking of heavy crude oil by the continuous kinetic lumping approach, *Applied Catalysis A: General*, 382, 205-212.

ExxonMobil, (2009). Global experience in Enhanced and Improved Oil Recovery, available at http://www.exxonmobilchemical.comIOGCECTechnology-EOR-insert-en.pdf, accessed 10/04/2011.

Fainberg, V., Podorozhansky, M., Hetsroni, G., Brauch, R., Kalchouck, H., (1996). Changes in the composition and properties of the vacuum residues as a result of visbreaking, *Fuel Sci. Technol. Int.*, 14, 839.

Fanaritis, J. P., Chilingarian, V. G., (1989). Steam enhanced oil recovery, *Development in Petroleum Science*, 19 (2), 221-282.

Fan, H., Liu, Y., Zhao, X. A., (2001a). study on heavy oil recovery by in-situ catalytic aquathermal cracking, *Oilfield Chem.*, 8 (1), 13-16.

Fan, H. -F., Liu, Y. -J., Zhong, L. -G., (2001b). Studies of the synergetic effects of mineral and steam on the composition changes of heavy oils, *Energy Fuels*, 15, 1475-1479.

Fan, H.-F., Zhang, Y., Lin, Y., (2004). The catalytic effects of minerals on aquathermolysis of heavy oils, *Fuel*, 83, 2035-2039.

Farouq, A., (1997). Is there life after SAGD? *J. Can. Petrol. Technol.*, 36 (6), 20-23.

Fatemi, S. M., Jamaloei, Y. B., (2011). Preliminary considerations on the application of toe-to-heel steam flooding (THSF): Injection well-producer well configurations, *Chemical Engineering Research and Design*, doi:10.1016/j.cherd.2011.03.007.

Fathi, M. M. and Pereira-Almao, P., (2013). Kinetic modelling of Arab light vacuum residue upgrading by aquaprocessing at high space velocities, *Industrial & Engineering Chemistry Research*, 52, 612-623.

Ferreira C., Tayakout-Fayolle M., Guibard I., Lemos F., Toulhout H., Ramoa-Ribero, F., (2012). Hydrodesulfurisation and hydrodemetallization of different origin vacuum residues: characterization and reactivity, *Fuel*, 98, 218-228.

Fesharaki, J. M., Ghashghaee, M., Karimzadeh, R., (2013). Comparison of our nanoporous catalysts in thermocatalytic upgrading of vacuum residue, *Journal of Analytical and Applied Pyrolysis*, 102, 97-102.

Flores, E., (2010). Heavy oil upgrading, *Technology Today*, Spring, Available at www.swri.org, accessed 15/05/2011, pp.10-15.

Focus, (2006). Bitumen and heavy crudes: the energy security problem solved? *Oil and Energy Trends*, 31 (6), 3-6.

Froment, G. F., (1991). The modelling of catalyst deactivation by coke formation, *Rev. Chem. Eng.*, 6 (4), 295-328.

Fukuyama, H., Terai, S., Uchida, M., Cano, L. J., Ancheyta, J., (2004). Active carbon catalyst for heavy oil upgrading, *Catalysis Today*, 98, 207-215.

Fumoto, E., Akimitsu, M., Sato, S., Takanohashi, T., (2009). Recovery of lighter fuels by cracking heavy oil with zirconia-alumina-iron oxide catalysts in a steam atmosphere, *Energy Fuels*, 23, 1338-1341.

Fumoto, E., Matsumura, A., Sato, S., Takanohashi, T., (2009). Recovery of lighter fuels by cracking heavy oil with zirconia-alumina-iron oxide catalysts in a steam atmosphere, *Energy Fuels*, 23, 1338-1341.

Fumoto, E., Sato, S., Takanohashi, T., (2011). Production of light oil by oxidative cracking of oil sand bitumen using iron oxide catalysts in a steam atmosphere, *Energy Fuels*, 25, 524-527.

Furimsky, E., (2009). Lowered emissions schemes for upgrading ultra heavy petroleum feeds, *Ind. Eng. Chem. Res.*, 48, 2752-2769.

Furimsky, E., Massoth, F. E., (1999). Deactivation of hydroprocessing catalysts, *Catal. Today*, 52, 381.

Galarraga, E. C., Pereira-Almao, P., (2010). Hydrocracking of Athabasca bitumen using submicronic multimetallic catalysis at near in-reservoir conditions, *Energy Fuels*, 24, 2383-2389.

Galarraga, E. C., Scott, C., Loria, H., Pereira-Almao, P., (2012). Kinetic models for upgrading Athabasca bitumen using unsupported NiWMo catalyst at low severity conditions, *Ind. Eng. Chem. Res.*, 51, 140-146.

Gao, H., Wang, G., Li, R., Xu, C., Gao, J., (2012). Study on the catalytic cracking of heavy oil by proper cut for higher conversion and desirable products, *Energy Fuels*, 26, 1880-1891.

Gao, L., Liu, Y., Wen, L., Huang, W., Mu, X., Zong, B., Fan, H., Han, B., (2010). The effect of supercritical water on the hydroconversion of Tahe residue, *Environ. Energy Eng.*, 56 (12), 3236-3242.

Garcia-Dopico, M., Garcia, A., and Garcia, A. S., (2006). Modelling coke formation and deactivation in a FCCU, *Applied Catalysis A: General*, 303, 245-250.

Gates, D. I., (2007). Oil phase viscosity behaviour in expanding-solvent steam-assisted gravity drainage, *Journal of Petroleum Science and Engineering*, 59, 123-134.

Gates, D. I., (2010). Solvent-aided steam-assisted gravity drainage in thin oil sand reservoir, *Journal of Petroleum Science and Engineering*, 74, 138-146.

Gates, I. D., Chakrabarty, N., (2006). Optimization of steam assisted gravity drainage in McMurray reservoir. *J. Can. Petrol. Technol.*, *45*, 54–62.

Gogarty, W. B., Tosch W. C., (1968). Miscible-type waterflooding: Oil recovery with micellar solutions, *J. Petrol. Technol*., 1407-1414.

Govreau, B., Marcotte, B., Sheehy, A., Town, K., Zahner, B., Tapper, S., Akintunji, F., (2013). Field application of organic oil recovery-A new MEOR method, Enhanced Oil Recovery Field Case Studies, 581-614.

Graue, J. Dennis, (2001). Upgrading and recovery of heavy crude oils and natural bitumen by in situ hydrovisbreaking, US Patent No. 6,328,104 B1.

Gray, R. M., (1994). Heavy oil and residue properties and composition, in upgrading petroleum residue and heavy oils, Marcel Dekker, Inc., New York, NY, pp. 1-40.

Gray, R. Murray and Ayasse R. Alan, (1995). Kinectics of hydrodesulfurization of thiophenic and sulphide sulphur in Athabasca bitumen, *Energy Fuels*, 9, 500-506.

Gray, R. M. and McCaffrey, W., (2002). Role of chain reactions and olefin formation in cracking, hydroconversion, and coking of petroleum and bitumen fractions, *Energy Fuels*, 16, 756-766.

Gray, R. M., Zhao, Y., and McKnight, C. M., (2000). Coke and mineral removal from bitumen hydroconversion catalysts, *Fuel*, 79, 285-294.

Gray, R. M., Zhao, Y., McKnight, M. C., Komar, A. D., Carruthers, D. J., (1999). Coking of hydroprocessing catalyst by residue fractions of bitumen, *Energy Fuels*, 13, 1037-1045.

Greaves, M., (2004). Air injection-improved oil recovery strategy for the UK continental shelf, Business Briefing: *Exploration & Production: the Oil & Gas Review*, 118-121.

Greaves, M., Dong, L. L., Rigby, S. P., (2012). Simulation study of the Toe-to-Heel Air Injection three-dimensional combustion cell experiment and effect in the mobile oil zone, *Energy Fuels*, 26, 1656-1669.

Greaves, M., El-Saghr, A., Xia, T. X., (2000). CAPRI horizontal well reactor for catalytic upgrading of heavy oil, Preprints-ACS, *Division of Petroleum Chemistry*, 47 (4), 595-598.

Greaves, M., Xia, T. X., (2004). Downhole upgrading of Wolf Lake oil using THAI/CAPRI processes-tracer tests, *Prep. Pap.-Am. Chem. Soc., Div. Fuel Chem.*, 49 (1), 69-72.

Greaves, M., Xia, T. X., Turta, A. T., (2008). Stability of THAI^{TM} process – theoretical and experimental observation, *Journal of Canadian Petroleum Technology*, 47 (9), 65-73.

Greaves, M., Xia, T. X., Turta, A. T., Ayasse, C., (2000a). Recent laboratory results of THAI and its comparison with other IOR process, *SPE/DOE Improved Oil Recovery Symposium*, Tulsa, Oklahoma, 3-5 April.

Greaves, M., Young, T. J., El-Usta, S., Rathbone, R. R., Ren, S. R., Xia, T. X., (2000b). Air injection into light and medium heavy oil reservoirs: combustion tube studies on West of Shetland clair oil and light Australian oil, *Trans IChemE*, Vol.78, Part A, pp. 721-730.

Groenzin, H. G., Mullins, O. C., (2000). Molecular size and structure of asphaltenes from various sources, *Energy Fuels*, 14 (3), 677-684.

Guan, C., Wang, Z., Yu, S., Guo, A., and Que, G., (2003). Upgrading petroleum residue by two-stage hydrocracking, *Fuel Processing Technology*, 85, 165-172.

Guangshou, S., Zhou, T., Cheng, L., Wang, Y., Tian, G., Pi, J., Zhang, Z., (2009). Aquathermolysis of conventional heavy oil with superheated steam, *Pet. Sci.*, 6, 289-293.

Habib, K. F., Diner, C., Stryker, M. J., Semagina, N., Gray, R. M., (2013). Suppression of addition reactions during thermal cracking using hydrogen and sulfided iron catalyst, *Energy Fuels*, dx.doi.org/10.1021/ef401904q.

Hart, A., (2013). A review of technologies for transporting heavy crude oil and bitumen via pipeline, *Journal of Petroleum Exploration and Production Technology*, DOI: 10.1007/s13202-013-0086-6.

Hart, A., Leeke, G., Greaves, M., and Wood, J., (2012). Control of Catalyst Deactivation in THAI-CAPRI Process for In-Situ Oilsand Recovery and Upgrading, *Proceedings of the World Heavy Oil Congress Conference*, Aberdeen, Scotland, 10-13 September.

Hart, A., Leeke, G., Greaves, M., and Wood, J., (2013b). Down-hole catalytic upgrading of heavy oil and bitumen to meet tomorrow's energy needs: the THAI-CAPRI process, *P. of the 3rd North Am. Symp. Chem. React. Eng.*, Houston, Texas, March 17-20.

Hart, A., Leeke, G., Greaves, M., Wood, J., (2014a). Down-hole heavy crude oil upgrading by CAPRI: Effect of hydrogen and methane gases upon upgrading and coke formation, *Fuel*, 119, 226-235.

Hart, A., Leeke, G., Greaves, M., Wood, J., (2014b). Downhole Heavy Crude Oil Upgrading Using-CAPRI: Effect of Steam upon Upgrading and Coke Formation, *Energy Fuels*, 28 (3), 1811-1819.

Hart, A., Shah, A., Leeke, G., Greaves, M., and Wood, J., (2013a). Optimization of the CAPRI process for heavy oil upgrading: Effect of hydrogen and guard bed, *Ind. Eng. Chem. Res.*, 52 (44), 15394-15406.

Hashemi, R., Nassar, N. N., Pereira-Almao, P., (2013). Enhanced heavy oil recovery by in situ prepared ultradispersed multimetallic nanoparticles: A study of hot fluid flooding for Athabasca bitumen recovery, *Energy Fuels*, dx.doi.org/10.1021/ef3020537.

Hashemi, R., Nassar, N. N., Pereira-Almao, P., (2013). In situ upgrading of Athabasca bitumen using multimetallic ultradispersed nanocatalysts in an oil sands packed-bed column: Part 1. Produced liquid quality enhancement, *Energy Fuels*, dx.doi.org/10.1021/ef401716h.

Hassanzadeh Hassan, Abedi Jalal, (2010). Modelling and parameter estimation of ultra-dispersed in situ catalytic upgrading experiments in a batch reactor, *Fuel*, 89, 2822-2828.

Heck, R. H., Diguiseppi, F. T., (1994). Kinetic effects in resid hydrocracking, *Energy Fuels*, 8, 557-560.

Hedrick, B. W., Seibert, K. D., Crewe, C., (2006). A new approach to heavy oil and bitumen upgrading, Report No. AM-06-29, UOP LLC, Des Plaines, Illinois.

Hein, F. J., (2006). Heavy oil and oil (tar) sands in North America: An overview & summary of contributions, *Nat. Resour. Res.*, 15 (2), 67-84.

Hirsch, L. R., Bezdek, R., and Wendling, R., (2006). Peaking of world oil production and its mitigation, *Perspective*, 52 (1), 2-8.

Ho, T. C., Katritzky, A. R., Cato, S. J., (1992). Effect of nitrogen compounds on cracking catalysts, *Ind. Eng. Chem. Res.*, 31, 1589-1597.

Hollander, dM. A., Makkee, M., Moulijn, J. A., (1998). Coke formation in fluid catalysic cracking studies with the microriser, *Catalysis Today*, 46, 27-35.

Hong, Y. W., Cao, X., Zhang, J., Zhang, A., (2009). Development and application of dilute surfactant-polymer flooding system for Shengli oilfield, *Journal of Petroleum Science and Engineering*, 65, 45-50.

Hongfu, F., Yongjian, L., Liying, Z., Xiaofei, Z., (2002). The study on composition changes of heavy oils during steam stimulation processes, *Fuel*, 81, 1733-1738.

Hossain, M. M., Al-Saleh, M. A., Shalabi, M. A., Kimura, T., Inui, T., (2004). Pd-Rh promoted Co/HPS catalysts for heavy oil upgrading, *Applied Catalysis A: General*, 278, 65-71.

Hou, J., (2007). Network modelling of residual oil displacement after polymer flooding, *Journal of Petroleum Science and Engineering*, 59, 321-332.

Hsu, C., Robinson, P., (2006). Practical advances in petroleum processing, Vol. 1, Springer Science + Business Media, Inc, p.22.

Hudgins, D. A., Llave, F. M., Chung F. T. H., (1990). Nitrogen miscible displacement of light crude oil: A laboratory study, *SPE Reservoir Engineering*, 5 (1), 100-106.

Hyne, J. B., Greidanus, J. W., Tyrer, J. D., Verona, D., Rizek, C., Clark, P. D., Clarke, R. A., Koo, J., (1982). Aquathermolysis of heavy oil, *Proceedings of the 2nd International Conference on Heavy Crude and Tar Sands*, Caracas, Venezuela, 25-30.

Ivanova, A. S., Korneeva, E. V., Bukhtiyarova, G. A., Nuzhdin, A. L., Budneva, A. A., Prosvirin, I. P., Zaikovskii, V. I., and Noskov, A. S., (2011). Hydrocracking of vacuum gas oil in the presence of supported nickel-tungsten catalysts, *Kinetics and Catalysis*, 52 (3), 446-458.

Jabbour, C., Quintard, M., Bertin, H., Robin, M., (1996). Oil recovery by steam injection: three-phase flow effects, *Journal of Petroleum Science and Engineering*, 16, 109-130.

Jacob, R. R., (1971). Coke quality and how to make it, *Hydrocarbon Process*, 9, 132-136.

Jamaloei, B., Yadali, R. K., Koorosh, A., Farshid, T., (2011). The influence of pore wettability on the microstructure of residual oil in surfactant-enhanced water flooding in heavy oil reservoirs:Implications for pore-scale flow characterization, *Journal of Petroleum Science and Engineering*, 77, 121-134.

Jarullah, T. A., Mujtaba, M. I., Wood, S. A., (2011). Improvement of the middle distillate yields during crude oil hydrotreatment in a trickle-bed reactor, *Energy Fuels*, 25, 773-781.

Javadli Rashad and Klerk de Arno, (2012). Desulfurization of heavy oil – oxidative desulfurization (ODS) as potential upgrading pathway for oil sands derived bitumen, *Energy Fuels*, 26, 594-602.

Javadli, R., Klerk, de A., (2012). Desulfurization of heavy crude oil, *Appl. Petrolchem. Res.*, 1, 3-19.

Jeon, G. S., Na, J. -G., Ko, H. C., Yi, B. K., Rho, S. N., Park, B. S., (2011). Preparation and application of an oil-soluble CoMo bimetallic catalyst for the hydrocracking of oil sands bitumen, *Energy & Fuels*, 25, 4256-4260.

Jian-hong, G., Long, J., Xu, Y., (2008). Protolytic cracking in daqing VGO catalytic cracking process, *Journal of Fuel Chemistry and Technology*, 36 (6), 691-695.

Jinzhong, L., Wenlong, G., Youwei, J., Changfeng, X., Bojun, W., Xiaoling, L., (2012). Propagation and control of fire front in the combustion assisted gravity drainage using horizontal wells, *Petrol. Explor. Dev.*, 39 (6), 764-772.

Joshi, B. J., Pandit, B. A., Kataria, L. K., Kulkarni, P. R., Sawarkar, N. A., Tandon, D., Ram, Y., Kumar, M. M., (2008). Petroleum residue upgradation via visbreaking: A review, *Ind. Eng. Chem. Res.*, 47, 8960-8988.

Junaid, A. S. M., Street, C., Wang, W., Rahman, M. M., An, W., McCaffrey, W. C., Kuznicki, S. M., (2012). Integrated extraction and low severity upgrading of oilsands bitumen by activated natural zeolite catalysts, *Fuel*, 94, 457-464.

Kang, W., (2001). Mechanism of the alkaline-surfactant-polymer flooding chemicals in Daqing oilfield, Vol.1, Petroleum Industry Publishers, Inc., Beijing, Pp.4-15.

Kapadia, R. P., Michael, S., Ian, D. G., (2011). Potential for hydrogen generation from in situ combustion of Athabasca bitumen, *Fuel*, 90, 2254-2265.

Kataria, L. K., Rohit, P. K., Aniruddha, B. P., Jyeshtharaj, B. J., Kumar, M. M., (2004). Kinetic studies of low severity visbreaking, *Ind. Eng. Chem. Res.*, 43, 1373-1387.

Kessick, M. A., (1982). Pipeline transportation of heavy crude oil, US Patent 4, 343, 323.

Kim, J. –W., Longstaff, C. D., Hanson, V. F., (1997). Upgrading of bitumen-derived heavy oils over a commercial HDN catalyst, *Fuel*, 76 (12), 1143-1150.

Kim, J. –W., Longstaff, C. D., Hanson, V. F., (1998). Catalytic and thermal effects during hydrotreating of bitumen-derived heavy oil, *Fuel*, 77 (15), 1815-1998.

Kisman, K. E., Lau, E. C., (1993). A new combustion process utilizing horizontal wells and gravity drainage, *The CIM 1993 Annual Technical Conference*, Calgary, Canada, 9-12 May.

Klerk, d. A., Gray, R. M., Zerpa, N., (2014). Chapter 5 – Unconventional oil and gas: Oilsands, Future Energy (Second Edition), pp. 95-116.

Korre, C. S. and Klein, T. M., (1995). Polynuclear aromatic hydrocarbons hydrogenation, 1. Experimental reaction pathways and kinetics, *Ind. Eng. Chem. Res.*, 34, 101-117.

Koshka, E., Kuhach, J., Veith, E., (2008). Improving Athabasca bitumen development economics through integration with HTL upgrading, *World Heavy Oil Congress*, Edmonton, March 2008.

Kressmann, S., More, F., Harle, V., Kasztelan, S., (1998). Recent development in fixed-bed catalytic residue upgrading, *Catalysis Today*, 43, 203-215.

Krumm, L. R., Milind, D., and Petrick, M., (2011). Direct thermal and catalytic Treatment of Paraffinic crude oils and heavy fractions, *Energy Fuels*, 26, 2663-2671.

Krumrine, P. H., Falcone Jr., J. S., (1983). Surfactant, polymer and alkaline interactions in chemical flooding processes, Paper SPE 11778, *Proceeding of the SPE International Symposium on Oilfield and Geothermal Chemistry*, Denver, Co, June 1-3, Pp. 79-86.

Lababidi, M. S. H., AlHumaidan, S. F., (2011). Modeling the hydrocracking kinetics of atmospheric residue in hydrotreating processes by the continuous lumping approach, *Energy Fuels*, 25, 1939-1949.

Label, J. P., Moriyama, R. T., (1997). History match of a mature cyclic steam stimulation process at Cold Lake, Presented at the *SPE International Thermal Operations & Heavy Oil Symposium*, held in Bakersfield, California, 10-12 February.

Lau, E. C., Kisman, K. E., (1994). Attractive control features of the combustion override split-production horizontal well process in a heavy oil reservoir, *Presented at the 45th Annual Technical Meeting of the Petroleum Society of CIM and AOSTRA*, Calgary, June 12-15.

Lazar, I., Petrisor, I. G., Yen, T. F., (2007). Microbial Enhanced Oil Recovery (MEOR), *Petroleum Science and Technology*, 25, 1353-1366.

Lee, H. J., Kang, S., Kim, Y., Park, S., (2011). New approach for kinetic modelling of catalytic cracking of paraffinic naphtha, *Industrial & Engineering Chemistry Research*, 50, 4264-4279.

Lee, J., Hwang, S., Lee, S. -B., and Song, K. I., (2010). Production of middle distillate through hydrocracking of paraffin wax over NiMo/TiO_2-SiO_2 catalysts, *Korean J. Chem. Eng.*, 27 (6), 1755-1759.

Le Perchec, P., Fixari, B., Elmouchnino, J., Peureux, S., Vrinat, M., Morel, F., (1993). New developments in deep hydroconversion of heavy oil residues with dispersed catalysts. Part 1: Thermocatalytic analysis of the transformation with various catalysts precursors, *Prepr. –Am. Chem. Soc., Div. Pet. Chem.*, 38, 401.

Leyva, C., Rana, S. M., Trejo, F., Ancheyta, A., (2007). On the use of acid-base-support catalysts for hydroprocessing of heavy petroleum, *Ind. Eng. Chem. Res.*, 46 (23), 7448-7466.

Li, J., Chen, Y., Liu, H., Wang, P., Liu, F., (2013). Influences on the aquathermolysis of heavy oil catalyzed by two different catalytic ions: Cu^{2+} and Fe^{3+}, *Energy Fuels*, 27, 2555-2562.

Li, Z., Wang, G., Liu, Y., Gao, J., Xu, C., Liang, Y., Wang, X., (2013). Study on reaction performance and competitive adsorption effect during coker gas oil catalytic cracking, *Fuel Processing Technology*, 115, 1-10.

Li, Z., Wang, G., Liu, Y., Wang, H., Liang, Y., Xu, C., Gao, J., (2012). Catalytic cracking constrainsts analysis and divisional fluid catalytic cracking process for coker gas oil, *Energy Fuels*, 26, 2281-2291.

Liu, D., Li, Z., Fu, Y., Zhang, Y., Gao, P., Dai, C., Zheng, K., (2013). Investigation on asphaltene structures during Venezuela heavy oil hydrocracking under various hydrogen pressures, *Energy Fuels*, 27, 3692-3698.

Liu, K., Fung, C. S., Ho, C. T., Rumschitzki, S. D., (2003). Hydrogasification of coke in heptane reforming over Pt – Re/Al_2O_3, *Ind. Eng. Chem. Res.*, 42, 1543-1550.

Liu, Q., Mingzhe, D., Shanzhou, M., Yun, T., (2007). Surfactant enhanced alkaline flooding for Western Canadian heavy oil recovery, *Colloids and Surfaces A: Physicochem. Eng. Aspects*, 293, 63-71.

Liu, W., Fred, R. W., (1994). Optimal control of three-dimensional steamflooding processes, *Journal of Petroleum Science and Engineering*, 11, 137-154.

Liu, Y., Fan, H., (2002). The effect of hydrogen donor additive on the viscosity of heavy oil during steam stimulation, *Energy Fuels*, *16* (4), 842-846.

Liu, Z., Cheng, L., Ji, Y., Liu, Q., (2011). Production features of steam and gas push: comparative analysis with steam assisted gravity drainage, *Petroleum Exploration and Development*, 38 (1), 79-83.

Longstaff, D. C., Deo, M. D., Hanson, F. V., (1994). Hydrotreatment of bitumen from the Whiterocks oil sands deposit, *Fuel*, 73 (9), 1523-1530.

Macquarie, R., (2010). The "In situ"-ation Report, available at www.macquarie.com.au/research/disclosures, accessed 23/04/2011.

Maity, S. K., Ancheyta, J., Marroquin, G., (2010). Catalytic aquathermolysis used for viscosity reduction of heavy crude oils: A review, *Energy Fuels*, 24, 2809-281.

Maity, S. K., Blanco, E., Ancheyta, J., Alonso, F., Fukuyama, H., (2012). Early stage deactivation of heavy crude oil hydroprocessing catalysts, *Fuel*, 100, 17-23.

Mansur, R. E., Claudia, M. R. de A., Lucas, F. E., (2012). Determination of asphaltene particle size: Influence of flocculant, additive, and temperature, *Energy Fuels*, dx.doi.org/10.1021/ef300365x.

Mapiour, M., Sundaramurthy, V., Dalai, A. K., and Adjaye, J., (2009). Effect of hydrogen purity on hydroprocessing of heavy gas oil derived from oil-sands bitumen, *Energy Fuels*, 23, 2129-2135.

Mapiour, M., Sundaramurthy, V., Dalai, A. K., and Adjaye, J., (2010). Effect of hydrogen partial pressure on hydrotreating of heavy gas oil derived from oil-sands bitumen: Experimental and kinetics, *Energy Fuels*, 24, 772-784.

Marafi, M., Stanilaus, A., (2001). Effect of catalyst acidity and feedstock quality on hydrotreaing catalyst deactivation by coke deposition, *Pet. Sci. Technol.*, 19 (5&6), 697-710.

Marafi, A., Kam, E., Stanislaus, A., (2008). A kinetic study on non-catalytic reactions in hydroprocessing Boscan crude oil, *Fuel*, 87, 2131-2140.

Marroquin-Sanchez, G., Ancheyta-Juarez, J., Ramirez-Zuniga, A., Farfan-Torres, E., (2001). Effect of crude oil properties on the hydrodesulphurisation of middle distillates over NiMo and CoMo catalysts, *Energy Fuels*, 15, 1213-1219.

Matsumura, A., Kondo, T., Sato, S., Saito, K., Ferraz de Souza, W., (2005). Hydrocracking Brazilian Marlin vacuum residue with natural limonite. Part I: catalytic activity of natural limonite, *Fuel*, 84, 411-416.

Matthews, C. S., (1989). Carbon dioxide flooding, *Developments in Petroleum Science*, 17 (2), 129-156.

Mayer, E. H., Breg, R. L., Carmichael, J. D., Weinbrandt, R. M., (1983). Alkaline injection for enhanced oil recovery-A status report, *Journal of Petroleum Technology*, 209-221.

McMillan, D. F., Manion, J. A., Tse, D. S., Malhotra, R., (1994). Hydrogen transfer promoted ring growth during catalytic resid hydroprocessing, *Symposium on Hydrogen Transfer in Hydrocarbon Processing presented at the Division of Petroleum Chemistry, Inc. at the 208th National Meeting, American Chemical Society*, 422-425.

Mehos, J. G. Ramirez, W. F., (1989). Use of optimal control theory to optimise carbon dioxide miscible-flooding enhanced oil recovery, *Journal of Petroleum Science and Engineering*, 2, 247-260.

Mehran, S., Ali, D., Dabir, H. T., Mahmoud, J., (2008). Microscopic mechanisms of oil recovery by near-miscible gas injection, *Transp. Porous Med.*, 72, 351-360.

Meng, X., Xu, C., Gao, J., (2007). Coking behaviour and catalyst deactivation for catalytic pyrolysis of heavy oil, *Fuel*, *86*, 1720-1726.

Meyer, R. F., Attanasi, E. D., (2003). Heavy oil and natural bitumen-strategic petroleum resources, USGS Fact Sheet 70-03, August. Available at http://pubs.usgs.gov/fs/fs070-03/fs070-03.html, Accessed April 26, 2011.

Meyer, F. R., Attanasi, E., (2004). Survey of Energy resources, 20th Edition, World Energy Council, 93-117.

Millan, M., Adell, C., Hinojosa, C., Herod, A.A., Kandiyoti, R., (2008). Mechanisms of catalytic activity in heavily coated hydrocracking catalysts, *Oil & Gas Science and Technology-Rev. IFP*, 63 (1), 69-78.

Ming, L., Wang, J., Deng, W., Que, G., (2007). Effects of Fe/carbon black, Ni/carbon black catalysts on hydrocracking reaction of residual oil, *Journal of Fuel Chemistry and Technology*, 35 (5), 558-562.

Mokrys, I. J., Butler, R. M., (1993). In-situ upgrading of heavy oils by propane deasphalting: the VAPEX process, *SPE 25452*, March 21.

Montel, V., Veronique, L., Benjamin, B., Honggang, Z., (2008). Asphaltene cake properties, *Energy Fuels*, 22 (6), 3970-3975.

Moore, R. G., Laureshen, C. J., Mehta, S. A., Ursenbach, M. G., Belgrave, J. D. M., Weissman, J. G., Kessler, R. V., (1999). A downhole catalytic upgrading process for heavy oil using in situ combustion, *Journal of Canadian Petroleum Technology*, 38(13), Pp. 1-8.

Moore, R. G., Laureshen, C. J., Belgrave, J. D. M., Ursenbach, M. G., and Mehta, S. A., (1997). In-Situ combustion heavy oil reservoirs: problems and perspectives, *In Situ*, 21(1), 1-26.

Mouli, C. K., Kapil, S., Ajay, D., John, A., (2011). Effect of pore diameter of Ni-Mo/Al-SBA-15 catalysts on the hydrotreating of heavy gas oil, *Applied Catalysis A: General*, 404, 21-29.

Murgich, J., Rodriguez, J., Aray, Y., (1996). Molecular recognition and molecular mechanics of micelles of some model asphaltenes and resins, *Energy Fuels*, 10, 68-76.

Murugan, P., Mahinpey, N., Thilakavathi, M., (2009). Thermal cracking and combustion kinetics of asphaltenes derived from Fosterton oil, *Fuel Processing Technology*, 90, 1286-1291.

Murugan, P., Thilakavathi, M., Mahinpey, N., Dong, M., (2011). Pyrolysis kinetics of Athabasca bitumen using a TGA under the influence of reservoir sand, *The Canadian Journal of Chemical Engineering*, 9999, 1-5.

Nares, H. R., Schacht-Hernandez, P., Ramirez-Garnica, M. A., Cabrera-Reyes, M. C., (2007). Heavy-crude-oil upgrading with transition metals, *Presented at SPE Latin American and Caribbean Petroleum Engineering Conference*, Buenos Aires, 15-18 April.

Nasr, T. and Isaac, E., (2001). Process for enhancing hydrocarbon mobility using a steam additive, U.S. Patent 6230814.

Noguera, G., Araujo, S., Hernandez, J., Rivas, A., Mendoza, D., Castellano, O., (2012). A comparative activity study of a new ultra-dispersed catalyst system for a hydrocracking/hydrotreating technology using residue oil: Merey/Mesa, *Chemical Engineering Research and Design*, 90, 1979-1988.

OECD/IEA, (2005). World Energy Outlook 2005, available at http://www.worldenergyoutlook.org/docs/weo2005/WEO2005.pdf, Accessed 20/06/2011.

Ogbuneke, U.K., Snape, E.C., Andresen, M.J., Crozier, S., Russell, C., and Sharpe, R., (2009). Identification of a polycyclic aromatic hydrocarbon indicator for the onset of coke formation during visbreaking of a vacuum residue, *Energy Fuels*, 23, 2157-2163.

Ortiz-Moreno, H., Ramirez, J., Cuevas, R., Marroquin, G., Ancheyta, J., (2012). Heavy oil upgrading at moderate pressure using dispersed catalysts: Effects of temperature, pressure and catalytic precursor, *Fuel*, 100, 186-192.

Ovalles, C., Filgueiras, E., Morales, A., Scott, E. C., Gonzalez, G. F., Pierre, E. B., (2003). Use of a dispersed iron catalyst for upgrading extra-heavy crude oil using methane as source of hydrogen, *Fuel*, 82, 887-892.

Ovalles, C., Filgueiras, E., Morales, A., Rojas, I., Jesus, de J. C., Berrios, I., (1998). Use of a dispersed molybdenum catalyst and mechanistic studies for upgrading extra-heavy crude oil using methane as source of hydrogen, *Energy Fuels*, 12, 379-385.

Ovalles, C. and Rodriguez, H., (2008). Extra heavy crude oil downhole upgrading using hydrogen donors under cyclic steam injection conditions: physical and numerical simulation studies, *Journal of Canadian Petroleum Technology*, 47 (1), 43-50.

Pacheco-Sanchez, J. H., Alvarez-Ramirez, F., Martinez-Magadan, J. M., (2004). Morphology of aggregated asphaltene structure model, *Energy Fuels*, 18, 1676-1686.

Panariti, N., Bianco, D. A., Piero, D G., Marchionna, M., (2000a). Petroleum residue upgrading with dispersed catalysts Part 1. Catalysts activity and selectivity, *Applied Catalysis A: General*, 204, 203-213.

Panariti, N., Bianco, D. A., Piero, D G., Marchionna, M., (2000b). Petroleum residue upgrading with dispersed catalysts Part 2. Effect of operating conditions, *Applied Catalysis A: General*, 204, 215-222.

Pashikanti, K. and Liu, Y. A., (2011). Predictive modelling of large-scale integrated refinery reaction and fractionation systems from plant data, Part2: fluid catalytic cracking (FCC) process, *Energy Fuels*, 25, 5298-5319.

Petrobank (2008) announces first THAI-CAPRI^{TM} Production, available at http://www.marketwire.com/press-release/Petrobank-Announces-First-THAI-CAPRI-Production-TSX-PBG-902105.htm, accessed 19/04/2011.

Petrobank Energy and Resources Ltd., (2010). CAPRI/THAI Processes for Upgrading and Recovering Getting Closer. http://nextbigfuture.com/2009/01/petrobank-caprithai-processes-for.html. Accessed 8/1/2010.

PingPing, S., Chen, X., Qin, J., (2010). Pressure characteristics in CO_2 flooding experiments, *Petroleum Exploration and Development*, 37 (2), 211-215.

Pinilla, J. L., Arcelus-Arrillaga, P., Puron, H., Millan, M., (2013a). Reaction pathways of anthracene selective catalytic steam cracking using a NiK/Al_2O_3 catalyst, *Fuel*, 109, 303-308.

Pinilla, J. L., Arcelus-Arrillaga, P., Puron, H., Millan, M., (2013b). Selective catalytic steam cracking of anthracene using mesoporous Al_2O_3 supported Ni-based catalysts doped with Na, Ca, or K, *Applied Catalysis A: General*, 459, 17-25.

Puron, H., Arcelus-Arrillaga, P., Chin, K. K., Pinilla, J. L., Fidalgo, B., Millan, M., (2014). Kinetic analysis of vacuum residue hydrocracking in early reaction stages, *Fuel*, 117, 408-414.

Puron, H., Pinilla, L. J., Berrueco, C., Fuente, de la M. J. A, Millan, M., (2013). Hydrocracking of Maya vacuum residue with NiMo catalysts supported on mesoporous alumina and silica-alumina, *Energy Fuel*, 27, 3952-3960.

Qi, W., Lei, G., Zong-xian, W., Bao-quan, M., Ai-jun, G., He, L., (2012). Hydrogen donor visbreaking of Venezuela vacuum residue, *J. Fuel Chem. Technol.*, 40 (11), 1317-1322.

Rahimi, M. P., Gentzis, T., (2006). The chemistry of bitumen and heavy oil processing, Practical Advances in Petroleum Processing, Vol.1, Springer Science + Business Media, Inc., 149-186.

Ramachandran, P. A., Chaudhari, R. V., (1983). Three phase catalytic reactor, Gordon and Breach, Science Publishers, S. A.

Rana, M. S., Ancheyta, J., Maity, S. K., Rayo, P., (2008). Heavy crude oil hydroprocessing: A zeolite-based CoMo catalyst and its spent catalyst characterisation, *Catalysis Today*, 130, 411-420.

Rana, M. S., Sa´mano, V., Ancheyta, J., Diaz, J. A. I., (2007). A review of recent advances on process technologies for upgrading of heavy oils and residua, *Fuel*, *86*, 1216–1231.

Razavi, S. D., Kharrat, R., (2009). Application of cyclic steam stimulation by horizontal wells in Irranian heavy oil reservoirs, Transactions C: *Chemistry and Chemical Engineering*, 16 (2), pp. 125-139.

Ren, Y., Mahinpey, N., Freitag, N., (2007). Kinetic model for the combustion of coke derived at different coking temperature, *Energy & Fuels*, 21, 82-87.

Reyniers, C. G., Froment, F. G., Kopinke, F. -D., Zimmermann, G., (1994). Coke formation in thermal cracking of hydrocarbons. 4 Modeling of coke formation in naphtha cracking, *Ind. Eng. Chem. Res.*, 33, 2584-2590.

Rezaei, H., Ardakani, J. S., and Smith, J. K., (2012). Comparison of MoS_2 catalysts prepared from Mo-micelle and Mo-octoate precursors for hydroconversion of Cold Lake vacuum residue: catalyst activity, coke properties and catalyst recycle, *Energy Fuels*, 26, 2768-2778.

Rezaei, H., Liu, X., Ardakani, J. S., Smith, J. K., Bricker, M., (2010). A study of Cold Lake vacuum residue hydroconversion in batch and semi-batch reactors using unsupported MoS_2 catalysts, *Catalysis Today*, 150, 244-254.

Rezaei Mehdi, Schaffie Mahin, Ranjbar Mohammad, (2013). Thermocatalytic in situ combustion: Influence of nanoparticles on crude oil pyrolysis and oxidation, *Fuel*, 113, 516-521.

Robinson, R. P., (2006). Petroleum processing overview Chapter 1 in Practical Advances in Petroleum Processing, Vol. 1, Springer, Science + Business Media, Inc. New York, 31-42.

Rodger, A., Chmel, P. N., Razmkhah, K., et al., (2008). Rheology study, http://www2.warwick.ac.uk/fac/sci/chemistry/research/arodger/arodgergroup/people/msrhab/collaborators/rheologystudy/ (Accessed, 24/10/2013).

Rogel, E., Ovalles, C., Pradhan, A., Leung, P., Chen, N., (2013). Sediment formation in residue hydroconversion processes and its correlation to asphaltene behavior, *Energy Fuels*, dx.doi.org/10.1021/ef401614a.

Salama, D., Kantzas, A., (2006). Experiment observation of miscible displacement of heavy oil with hydrocarbon solvent, *Journal of Petroleum Technology*, SPE 97854, 102-104.

Sambi, I. S., Khulbe, K. C., Mann, and Ranveer, S., (1982). Catalytic hydrotreatment of heavy gas oil, *Ind. Eng. Chem. Pro. Dev.*, 21 (4), 575-580.

Sanchez, S., Ancheyta, J., (2007). Effect of pressure on the kinetics of moderate hydrocracking of Maya crude oil, *Energy Fuels*, 21 (2), 653-661.

Sanford, E. C., (1994). Molecular approach to understanding residue conversion, *Ind. Eng. Chem. Res.*, *33* (1), 109-117.

Sato, T., Tomita, T., Trung, H. P., Itoh N., Sat, S., Takanohashi, T., (2013). Upgrading of bitumen in the presence of hydrogen and carbon dioxide in supercritical water, *Energy Fuels*, 27, 646-653.

Savage, P., Klein, M., Kukes, S., (1988). Asphaltenes reaction pathways 3. Effect of reaction environment, *Energy Fuels*, 2, 619-628.

Sawarkar, A. N., Pandit, A. B., Joshi, J. B., (2007). Studies in coking of Arabian mix vacuum residue, *Trans IChemE, Part A, Chemical Engineering Research and Design*, 85 (A4), 481-491.

Sawarkar, A. N., Pandit, A. B., Shriniwas, D. S., Jyeshtharaj, J. B., (2007). Petroleum residue upgrading via delayed coking: A review, *The Canadian Journal of Chemical Engineering*, 85, 1-24.

Scherzer, J., Gruia, A. J., (1996). Hydrocracking science and technology, Marcel Dekker, New York.

Sen, R. K., (2008). Biotechnology in petroleum recovery: the microbial EOR, *Progress in Energy and Combustion Science*, 34, 714-724.

Shah A., Fishwick, R. P., Wood, J., Leeke, G., Rigby, S., Greaves, M., (2010). A review of novel techniques for heavy oil and bitumen extraction and upgrading, *Energy & Environmental Science*, 3, 700-714.

Shah, A., Fishwick, R. P., Leeke, A. G., Wood, J., Rigby, S. P., Greaves, M., (2011). Experimental optimisation of catalytic process in situ for heavy-oil and bitumen upgrading, *J. Can. Petrol. Technol.*, 50 (11-12), 33-47.

Sheng, J. J., (2011). Modern Chemical Enhanced Oil Recovery, Elsevier Inc, DOI: 10.1016/B978-1-85617-745-0.00010-3, pp.389-460.

Sheng, J. J., (2013). Enhanced Oil Recovery Field Cases Studies, pp. 63-167.

Shen Z., Cao Z., Zhu X., Li, X., (2008). Visbreaking of Chinese oilsands bitumen, *Pet. Sci. Technol.*, 26, 1676-1683.

Shuyi, Z., Deng, W., Luo, H., Liu, D., Que, G., (2008). Slurry-phase residue hydrocracking with dispersed nickel catalyst, *Energy Fuels*, 22, 3583-3586.

Shuyi, Z., Liu, D., Deng, W., Que, G., (2007). A review of slurry-phase hydrocracking heavy oil technology, *Energy Fuels*, 21 (6), 3057-3062.

Silverman, M. A., Pavel, S. K., Hillerman, M. D., (2011). HTL heavy oil upgrading: A key solution for heavy oil upstream and midstream operations, *World Heavy Oil Congress* [WHOC11-419], Edmonton, Alberta, Canada.

Smalley, C., (2000). Heavy oil and viscous oil, Chapter from Modern Petroleum Technology, R. A. Dawe, ed., John Wiley and Sons Ltd.

Solar, J. M., Derbyshire, F. J., Radovic, L. R., (1991). Effects of surface and structural properties of carbon on the behaviour of carbon-supported molybdenum catalysts, *J. Catal.*, 129 (2), 330-342.

Smith, B. R. J., Loganathan, M., Murthy, S. S., (2010). A review of the water gas shift reaction kinetic, *Int. J. of Chem. Reactor Eng.*, 8, 1-32.

Speight, J. G., (1998). The chemistry and physics of coking, *Korean J. Chem. Eng.*, 15 (1), 1-8.

Speight, J. G., (2009). Enhanced recovery methods for heavy oil and tar sands, Gulf Publishing Co., Houston, Texas, 261-291.

Speight, J. G., (2011). The refinery of the future, Gulf Professional Publishing, London, 81-116.

Speight, J. G., (2013). Oil sand and tar production processes, Gulf Professional Publishing, Elsevier, Oxford, 139-153.

Speight, J. G. and Moschopedis, S. E., (1979). Some observations on the molecular nature of petroleum asphaletnes, *Prepr.-Am. Chem. Soc., Div. Pet. Chem.*, 24, 910-923.

Stanislaus, A., Absi-Halabi, M., and Khan, Z., (1996). Influence of catalyst pore size on asphaltenes conversion and coke-like sediments formation during catalytic hydrocracking of Kuwait vacuum residues, *Studies in Surface Science and Catalysis*, 100, 189-197.

Stoyanov, R. S., Gusarov, S., Kuznicki, M. S., Kovalenko, A., (2008). Theoretical modelling of zeolite nanoparticle surface acidity for heavy oil upgrading, *J. Phys. Chem. C.*, 112 (17), 6794-6810.

Strauz, O. P., Lown, E. M., (2003). The chemistry of Alberta oil sands, bitumen and heavy oils, Book Published by the Alberta Energy Research Institute, Calgary, AB, Canada.

Sun, L.-B, Zong, Z.-M, Kou, J.-H, Zhang, L.-F, Ni, Z.-H, Yu, G.-Y, Chen, H., Wei, X.-Y, and Lee, C.W., (2004). Activated carbon-catalyzed hydrogenation of polycyclic arenes, *Energy Fuels*, 18, 1500-1504.

Sun, Y., Yang, C., Zhao, H., Shan, H., and Shen, B., (2010). Influence of asphaltene on the residue hydrotreating reaction, *Energy Fuels*, 24, 5008-5011.

Swapan, K. D., Butler, R. M., (1997). Mechanism of the vapour extraction process for heavy oil and bitumen, *Journal of Petroleum Science and Engineering*, 21, 43-59.

Terai, S., Fukuyama, H., Uehara, K., (2000). Hydrocracking of heavy oil using iron-active carbon catalyst, *Sekiyu Gakkaishi*, 43 (1), 17-24.

Thomas, S., (2008). Enhanced oil recovery – An overview, *Oil & Gas Science and Technology – Rev-IFP*, 68 (1), 9-19.

Thomas, S., Farouq Ali S. M., (1999). Status and assessment of chemical oil recovery methods, *Energy Sources*, 21, 177-189.

Trejo, F., Rana, S. M., Ancheyta, J., (2010). Thermogravimetric determination of coke from asphaltenes, resins and sediments and coking kinetics of heavy crude asphaltenes, *Catalysis Today*, 150, 272-278.

Tuzunoglu, E. and Bagci, S., (2000). Scaled 3-D mode studies of immiscible CO_2 flooding using horizontal wells, *Journal of Petroleum Science and Engineering*, 26, 67-81.

US. Department of Energy, Energy Information Administration, EIA (2005) Int. Energy Outlook, July.

Veith, E. J., (2007). Performance of Heavy-to-Light-Crude-Oil upgrading Process, presented at 2007 *SPE International Oil Conference and Exhibition*, Veracruz, Mexico, 27-30 June.

Viet, T. T., Lee, H. J., Ma, F., Kim, R. G., Ahn, I. –S., Lee, C. –H., (2013). Hydrocracking of petroleum vacuum residue with activated carbon and metal additives in a supercritical m-xylene solvent, *Fuel*, 103, 553-561.

Viet, T. T., Lee, H. J., Ryu, W. J., Ahn, I.-S., Lee, C. –H., (2012). Hydrocracking of vacuum residue with activated carbon in supercritical hydrocarbon solvents, *Fuel*, 94, 556-562.

Vishwakarma, K. S., Sundaramurthy, V., and Ajay, K. D., (2007). Performances of Co-W/γ-Al_2O_3 catalysts on hydrotreatment of light gas oil derived from Athabasca bitumen, *Ind. Eng. Chem. Res.*, 46, 4778-4786.

Voorhies, A., (1945). Carbon formation in catalytic cracking, *Ind. Eng. Chem. Res.*, 37, 318-22.

Wang Baodong and Manos George, (2007). A novel thermogravimetric method for coke precursor characterisation, *Journal of Catalysis*, 250, 121-127.

Wang, B., Tao, W., Yujiang, L., Dejun, S., Min, Y., Yingxin, G., Fengjuan, L., Xia, L., (2011). The effects of oil displacement agents on the stability of water produced from ASP (Alkaline/Surfactant/Polymer) flooding, *Colloids and Surface A: Physicochem. Eng. Aspects*, 379,121-126.

Wang, G., Li, Z. K., Liu, Y. D., Gao, J. S., Xu, C. M., Lan, X. Y., Ning, G. Q., Liang, Y. M., (2012). FCC-catalyst coking: sources and estimation of their contribution during coke gas oil cracking process, *Ind. Eng. Chem. Res.*, 51, 2247-2256.

Wang, G., Liu, Y., Wang, X., Xu, C., and Gao, J., (2009). Studies on the catalytic cracking performance of coker gas oil, *Energy Fuels*, 23, 1942-1949.

Wang, H., Wu, Y., Li, H., Liu, Z., (2012). Supporting tungsten oxide on zirconia by hydrothermal and impregnation methods and its use as a catalyst to reduce the viscosity of heavy crude oil, *Energy Fuels*, 26, 6518-6527.

Wang, J., Dong, M., (2009). Optimum effective viscosity of polymer solution for improving heavy oil recovery, *Journal of Petroleum Science and Engineering*, 67, 155-158.

Wang, J., Reyniers, M. -F., Marin B. G., (2007). Influence of dimethyl disulfide on coke formation during steam cracking of hydrocarbons, *Ind. Eng. Chem. Res.*, 46, 4134-4148.

Wang, Y., Chen, Y., He, J., Li, P., and Yang, C., (2010). Mechanism of catalytic aquathermolysis: Influences on heavy oil by two types of efficient catalytic ions: Fe^{3+} and Mo^{6+}, *Energy Fuels*, 24, 1502-1510.

Wei, L., Zhu, J., Qi, J., (2007). Application of nano-nickel catalyst in the viscosity reduction of Liaohe extra-heavy oil by aqua-thermolysis, *Journal of Fuel Chemistry and Technology*, 35 (2), 176-180.

Weissman, J. G., Kessler, R. V., (1996). Downhole heavy crude oil hydroprocessing, *Applied Catalysis A: General*, 140 (1), 1-16.

Weissman, J. G., Kessler, R. V., Sawicki, R. A., Belgrave, J. D. M., Laureshen, C. J., Mehta, S. A., Moore, R. G., Ursenbach, M. G., (1996). Downhole catalytic upgrading of heavy crude oil, *Energy Fuel*, 10 (4), 883-889.

Wenlong, G., Xi, C., Chen, Y., Zhang, X. M., Jinzhong, L., Jihong, H., Jian, W., (2011). Fire-flooding technoloies in post-steam-injected heavy oil reservoirs, *Petrol. Explor. Dev.*, 38 (4), 452-462.

Wiehe, I. A., (1999). Tutorial on resid conversion and coking, *Proceedings 2nd International Conference on Refinery Processing*, AIChE 1999 Spring National Meeting, Houston, TX, March 14-18, 499-505.

Wiehe, I. A. and Liang, K. S., (1996). Asphaltenes, resins, and other petroleum macromolecules, *Fluid Phase Equilibrium*, 117, 201-210.

Wilson R. Geoffrey, (1975). Heavy oil demetallization and desulfurization process, United States Patent, No. 3,898,155.

Xia, T. X. and Greaves, M., (2000). Upgrading Athabasca tar sand using toe-to-heel air injection, SPE/Petroleum Society of CIM 65524, *International Conference on Horizontal Well Technology*, Calgary, Alberta, Canada, 6-8 November.

Xia, T. X., Greaves, M., (2001). Downhole upgrading Athabasca tar sand bitumen using THAI-SARA analysis, SPE 69693, *SPE International Thermal Operations and Heavy Oil Symposium held in Portlamar*, Margarita Island, Venezuela, 12 March.

Xia, T. X., Greaves, M., (2001b). 3-D physical model studies of downhole catalytic upgrading of Wolf-Lake heavy oil using THAI, *Petroleum Society's Canadian International Petroleum Conference*, Calgary, Alberta, Canada, June 12-14, Paper 2001-17.

Xia, T. X., Greaves, M., (2006). In situ upgrading of Athabasca tar sand bitumen using THAI, *Chemical Engineering Research and Design*, 84 (A9), pp. 856-864.

Xia, T. X., Greaves, M., Turta, A. T., Ayasse, C., (2003). THAI-A short-distance displacement in situ combustion process for the recovery and upgrading of heavy oil, *Institute of Chemical Engineers*, Vol.18, Part A, pp. 295-304.

Xia, T. X., Greaves, M., Werfilli, W.S., Rathbone, R. R., (2002). Downhole conversion of Lloydminster heavy oil using THAI-CAPRI process, *SPE/Petroleum Society of CIM/CHOA 78998 International Thermal Operations and Heavy Oil Symposium and International Horizontal Well Technology Conference*, Calgary, Alberta, Canada, 4-7 November.

Xuhong, M., Dianzhong, W., Yongrui, W., Min, L., Shibiao, C., Xingtian, S., (2013). Nanosized molecular sieves as petroleum refining and petrochemical catalysts, *Chinese Journal of Catalysis*, 34, 69-79.

Yan, T. Y., (1980). Dynamics of a trickle-bed hydrocracker with a quenching system, *Can. J. Chem. Eng.*, 58, 259.

Yin, C.-X., Jeffrey, M. S., and Gray, R. M., (2009). Separation of petroporphyrins from asphaltenes by chemical modification and selective affinity chromatography, *Energy Fuels*, 23, 2600-2605.

Zachariah, A., Wang, L., Yang, S., Prasad, V., Klerk, d. A., (2013). Suppression of coke formation during bitumen pyrolysis, *Energy Fuels*, 27, 3061 – 3070.

Zajac, G. W., Sethi, N. K., and Joseph, J. T., (1994). Maya petroleum asphaltene imaging by scanning tunnelling microscopy: verification of structure from ^{13}C and proton nuclear magnetic resonance, *Scanning Microsc*., 8, 463-470.

Zhang, H. Q., Sarica, C., and Pereyra, E., (2012). Review of high-viscosity oil multiphase pipe flow, *Energy Fuel*, dx.doi.org/10.1021/ef300179s.

Zhang, J., Shan, H., Liu, W., Chen, X., Li, C., and Yang, C., (2013). Synergistic process for coker gas oil catalytic cracking and gasoline reformation, *Energy Fuels*, 27, 654-665.

Zhang Xiaohui and Shaw M. John, (2006). Impact of multiphase behaviour on coke deposition in heavy oils hydroprocessing catalysts, *Energy Fuels*, 20, 473-480.

Zhang, Z. -G., Okada, K., Yamamoto, M. and Yoshida, T., (1998). Hydrogenation of anthracene over active carbon-supported nickel catalyst, *Catalysis Today*, 45, 361-366.

Zhao, S., Kotlyar, S. L., Woods, R. J., Sparks, D. B., Chung, H. K., (2001). Effect of thermal and hydro-catalytic treatment on the molecular chemistry of narrow fractions of Athabasca bitumen pitch, *Energy Fuels*, 15, 113-119.

Zhao, S., Sparks, B. D., Kotlyar, L. S., Chung, K. H., (2007). Correlation of processability and reactivity data for residua from bitumen, heavy oils and conventional crudes:

characterization of fractions from super-critical pentane separation as a guide to process selection, *Catalysis Today*, 125, 122-136.

Zhao, Y., Gray, R. M., Chung, K. H., (2001). Molar kinetics and selectivity in cracking of Athabasca asphaltenes, *Energy Fuels, 15*, 751-755.

Zhicheng, L., Wang, Y., Xie, Z., (2012). Thoughts on the future development of Zeolite catalysts from an industrial point of view, *Chinese Journal of Catalysis*, 33 (1), 22-38.

Zobell, C., (1947). Bacterial release of oil from sedimentary metrials, *Oil & Gas Journal*, 46, 62-65.

Zuo, Y. –X., Ji-Zheng, C., Shui-lin, K. and Tian-Min, G., (1993). A study on the minimum miscibility pressure for miscible flooding systems, *Journal of Petroleum Science and Engineering*, 8, 315-328.